Εθνικό Μετσόβιο Πολυτεχνείο
Σχολή Πολιτικών Μηχανικών
Τομέας Γεωτεχνικής

National Technical University of Athens
School of Civil Engineering
Geotechnical Division

Διπλωματική Εργασία

Θεοφίλου Μιχαήλ

Επιβλέποντες

Καθηγητές Γ. Γκαζέτας, Ι. Αναστασόπουλος

Αθήνα, Δεκέμβριος 2013

ΝΕΑ ΥΒΡΙΔΙΚΗ ΘΕΜΕΛΙΩΣΗ ΓΙΑ ΘΑΛΑΣΣΙΕΣ ΑΝΕΜΟΓΕΝΝΗΤΡΙΕΣ

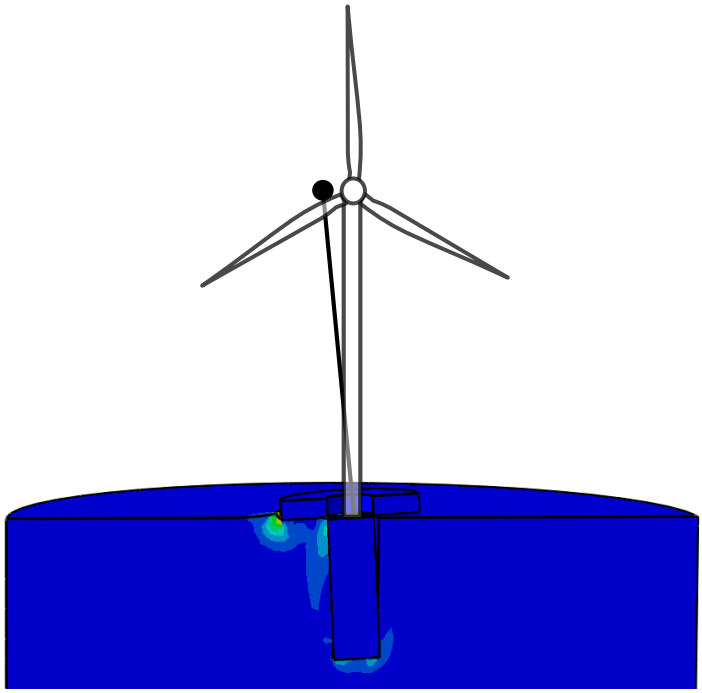

A HYBRID FOUNDATION FOR OFFSHORE WIND TURBINES

Diploma Thesis

Theofilou Michail

Supervisors

Professors G. Gazetas, I. Anastasopoulos

Athens, December 2013

Ευχαριστίες

Η εργασία αυτή πραγματοποιήθηκε χάρη στη συμβολή πολλών ανθρώπων στους οποίους θέλω να εκφράσω τις ευχαριστίες μου.

Αρχικά θα ήθελα να εκφράσω την ευγνωμοσύνη μου στον καθηγητή Γ. Γκαζέτα που μέσα από τις γνώσεις του, τις παροτρύνσεις και την ευχάριστη παρουσία του υπήρξε η πηγή έμπνευσης που μου έδωσε το κίνητρο και τη διάθεση για την επίτευξη αυτού του στόχου.

Ιδιαίτερες ευχαριστίες οφείλω και στον καθηγητή Ι. Αναστασόπουλο ο οποίος μου προσέφερε συνεχή καθοδήγηση και υποστήριξη καθ' όλη τη διάρκεια της εργασίας, καθώς και πολύτιμες και εύστοχες συμβουλές για την λύση προβλημάτων που προέκυψαν στην πορεία.

Ακόμα, θέλω να ευχαριστήσω όλα τα μέλη του εργαστηρίου και τους συμφοιτητές μου που εργάστηκαν εκεί, επειδή δημιούργησαν τις κατάλληλες συνθήκες για παραγωγική και ευχάριστη δουλεία.

Τέλος, δεν θα μπορούσα να παραλείψω τους φίλους και την οικογένειά μου, που στάθηκαν δίπλα μου και με υποστήριξαν με τον καλύτερο τρόπο όλον αυτόν τον καιρό και για αυτόν το λόγο τους ευχαριστώ εκ βαθέων.

Table of Contents

Νέα υβριδική θεμελίωση για θαλάσσιες ανεμογεννήτριες – Σύντομη περίληψη

Λέξεις κλειδιά: Ενεργειακή γεωτεχνική, αλληλεπίδραση εδάφους – κατασκευής, επιφανειακές και βαθιές θεμελιώσεις

Ο κλάδος των θαλάσσιων ανεμογεννητριών ήδη γνωρίζει μεγάλη άνθιση, στα πλαίσια της γενικότερης στροφής της κοινωνίας προς ανανεώσιμες πηγές ενέργειας. Το θαλάσσιο περιβάλλον είναι δυσμενές για τέτοιες ελαφριές κατασκευές, οι οποίες δέχονται δυσανάλογα μεγάλα φορτία στην οριζόντια διεύθυνση και υποβάλλονται σε μεγάλο αριθμό κύκλων φόρτισης. Η συνηθέστερη μορφή θεμελίωσης είναι ο μονοπάσσαλος, ο οποίος όμως μπορεί να αποδειχτεί μη – οικονομική λύση, κυρίως λόγο του αυξημένου κόστους έμπηξης. Προτείνεται λοιπόν μια νέα υβριδική λύση θεμελίωσης, που συνδυάζει το μονοπάσσαλο με ένα επιφανειακό κυκλικό θεμέλιο, τοποθετημένο στην κεφαλή. Στην εργασία ερευνάται η απόδοση της υβριδικής θεμελίωσης, μέσω παραμετροποίησης της διαμέτρου του πεδίλου (D) και του μήκους έμπηξης του πασσάλου (L). Εξετάζονται δυο προφίλ συνεκτικού εδάφους: ένα ομοιογενές και ένα ανομοιογενές με γραμμικώς αυξανόμενη αντοχή με το βάθος. Λαμβάνονται υπόψιν μη – γραμμικότητες στις διεπιφάνειες εδάφους - θεμελίου.

Οι γεωμετρικές παράμετροι συσχετίζονται με τη φέρουσα ικανότητα του θεμελίου, υπό μονοαξονική και συνδυασμένη φόρτιση (περιβάλλουσα αστοχίας M – Q – N). Μελετάται ακόμα η επίδρασή τους στην αρχική δυσκαμψία του συστήματος εδάφους – θεμελίου. Επιπρόσθετα, εξετάζεται η απόκριση του συστήματος ανωδομή – θεμέλιο – έδαφος υπό ανακυκλική φόρτιση, μέσω δύο σεναρίων φόρτισης ανέμου και κυμάτων. Με κριτήριο τον περιορισμό των στροφών και καθιζήσεων, καθώς και την απομείωση της δυσκαμψίας με την πάροδο των κύκλων φόρτισης, επιλέγεται κατάλληλο θεμέλιο για τρία χαρακτηριστικά μεγέθη ανεμογεννητριών. Πραγματοποιείται και λογαριθμική προεκβολή των αποτελεσμάτων στα εκατομμύρια κύκλων που αντιστοιχούν στο χρόνο ζωής τέτοιων έργων. Η ακρίβεια των προβλέψεων επαληθεύεται με ανάλυση πολλών κύκλων και η σύγκριση με τα αποτελέσματα από τους πρώτους 9 κύκλους είναι αρκετά ικανοποιητική. Επιχειρείται ακόμα αποτίμηση της δυναμικής απόκρισης μιας ανεμογεννήτριας 3.5 MW στο σεισμό του Takatori (1995). Η απόδοση των υβριδικών θεμελίων συγκρίνεται σε κάθε σημείο με μονοπάσσαλο μήκους 30 m και 35 m. Αποδεικνύεται ότι υπάρχουν σημαντικές δυνατότητες μείωσης του μήκους έμπηξης όταν ο μονοπάσσαλος συνδυάζεται με επιφανειακό πέδιλο.

Συμπεραίνεται ότι η υβριδική θεμελίωση αποτελεί αποδοτική εναλλακτική του μονοπασσάλου. Επισημαίνεται δε και η ευελιξία που προσφέρει η υβριδική λύση, καθώς μπορεί να προσαρμοστεί σε διάφορα εδαφικά προφίλ. Ενδέχεται να υπάρχουν και οικονομικά οφέλη, καθώς υπό προϋποθέσεις το μήκος έμπηξης μπορεί να μειωθεί αρκετά.

CHAPTER 1

Literature review

1.1 Introduction
1.2 Loads of Offshore Wind Turbines
1.3 Bearing Capacity
1.4 Elastic and Nonlinear Stiffness of foundations

1.1 Introduction

1.1.1 Scope of study

In recent times, concerns are being raised regarding energy produced by fossil fuels; fears of their possible exhaustion, as well as increased awareness of the environmental harm caused by their combustion products, are leading the energy industry towards exploitation of renewable sources. Moreover, breaking the dependence on fossil fuels incites technological and scientific progress, and can offer a significant boost to the international economy. Within this framework, the EU has set as a target 20 % of its energy to derive from renewable energy sources by 2020; many other countries, including the USA, have set similar targets. One of the most promising and rapidly growing fields in renewable energy has to do with the exploitation of wind power.

Wind energy has been harvested by mankind from the early years and is used in sailing and windmills ever since. Only recently though, it has become a financially competitive source of energy through the use of wind turbines. The latter are devices that convert mechanical energy from the wind into electrical power. So far, the majority of wind turbines have been installed onshore, however offshore wind turbines are increasingly being adopted by the wind energy industry, due to the significant advantages they demonstrate. First of all, the potential of wind exploitation is higher, as better wind speeds are available offshore compared to on land (source: en.wikipedia.org/wiki/Offshore_wind_power). In addition, the lack of topography allows offshore wind turbines to operate in steadier conditions without wind turbulence; therefore, electricity output can be maximized. Furthermore, space is more abundant offshore and larger wind farms can be constructed. Besides that, aesthetic criteria can easily be met as complaints and objections from nearby residents are minimized; many such projects have been delayed or cancelled onshore, due to “not in my back yard” (NIMBY) types of attitude.

The benefits of offshore wind turbines are limited due to their significantly increased cost, compared to turbines installed in land. The installation procedure is quite more expensive as it involves the implementation of vessels to transport the turbines at the site and special machinery to perform the positioning. Moreover, there is no existing grid in most offshore installation sites, so an extra cost is arising because of the need to construct and connect the grid. Additionally, maintenance is harder and more expensive, especially for the submerged parts. A cost breakdown for offshore and onshore wind turbines is provided in **figure 1.1** [Kuhn *et al*., 1998]. The cost of foundations for offshore wind turbines is higher than in – land and can reach up to 25 % of the total cost. This is a key aspect of the reduction of the overall cost of such projects, which is currently of high interest to geotechnical engineers. Extensive research has already been conducted in order to assess a foundation solution of reduced cost, which will make large scale exploitation of offshore wind more viable [i.e. Bransby & Randolph, 1998; Byrne 2000, ;Byrne & Houlsby, 2003; Gourvenec, 2007;]

Offshore wind turbines are tall and slender structures that are subjected to millions of horizontal load cycles during their lifetime due to wind and waves. The weight of such structures is relatively low, so the vertical load acting on the foundation is small compared to

the horizontal load and overturning moment. Given that most design practices for offshore foundations to date concern jack – up platforms, which transfer large vertical loads to the foundations, the problem is quite challenging and novel foundation designs are required. Furthermore, lightweight structures are more exposed to dynamic excitation. Comparison of a jack – up platform to a typical 3.5 MW offshore wind turbine is depicted in **figure 1.2** [Byrne, 2011]. Since the number of turbines installed in an offshore wind farm is quite large, it is crucial to design the foundation to be easily transported and mass – produced.

Concepts of floating wind turbines have been proposed, however they are not likely to be applied in the near future; all wind turbines installed up to date are bottom – mounted. Foundations for offshore wind turbines are generally divided into two main categories: monopod foundations, which have a single soil – foundation interface and multipod foundations, which have multiple soil – foundation interfaces. The load transfer mechanisms are significantly different in the two cases; while monopod foundations transfer the loads mainly via the generation of lateral stresses on the interface, multipod foundations sustain the loads via pull – push axial forces. Monopod foundations are already widely applied in case of small and medium depths but as the water depth increases multipod solutions are considered more effective.

Typical foundations for offshore wind turbines are depicted in **figure 1.3** [Byrne, 2011]. For shallow waters, gravity base foundations have been used. This is the first type of foundation applied on offshore wind turbines, which consists of a concrete base that is usually made hollow and filled in – situ in order to sink into place. It is a rather simple design that can be easily constructed, however feasibility in deeper waters or in case of larger wind turbines is questionable. As implied by their name, these foundations require large vertical loads in order to sustain overturning moments; therefore, a very large size is required for large wind turbines, which can be difficult to handle and uneconomical. A novel foundation concept is the suction caisson; a skirted foundation that resembles an upside – down bucket, made of steel. During installation, excess water is removed from the interior of the bucket, allowing the pressure differential to assist penetration along with self – weight [Houlsby & Byrne, 2000]. Despite this advantage, suction caissons remain an unproven technology and can be seriously affected by the underlying soil; the presence of even a small layer of rock in softer soils would result in buckling failure during installation, causing severe economic loss.

The most popular foundation to this day is the monopile; a large cylindrical tube typically made of steel. The usual diameter is 4 m or larger, while the required embedment length is 4 – 8 times the diameter. The industry has developed confidence on the monopile, which has proven its reliability as it has been used for many years. As can be seen in **figure 1.4**, monopile foundations dominate the industry, since they are used in at least 60% of both operating and under construction wind farms. The manufacturing process is quite simple and consists of rolling steel layers and welding them together to form the tube. It has been used in water depths of up to 35 m, but larger monopiles can perform in deeper waters. However, its feasibility in larger depths is limited, as the amount of steel needed will make it really heavy and expensive. Installation is most commonly performed by large hydraulic hammers, which drive the monopile in place. Driving of the pile is an expensive procedure that, along with

material cost, limit the use of monopiles in larger wind turbines or deeper waters. Given that the offshore wind industry is expanding rapidly, with larger turbine models already being put in use, it is certain that the monopile needs to be improved.

1.1.2 The Hybrid Monopile – Footing Foundation

Based on the above, the need to develop novel foundation concepts is apparent. Cost – effectiveness and efficiency are the two key factors that should be taken into consideration. This study investigates the combination of a monopile and a circular footing in order to create a hybrid foundation which will integrate the assets of both surface and deep foundations. Adding a footing to the top of a monopile provides a lateral restraint that can increase the moment capacity. This enhanced performance can lead to a reduction of the monopile length, which offers significant cost savings. Additionally, the use of a monopile as the basic component of the hybrid foundation makes it a trustworthy solution compared to new and untested concepts; the industry has gained substantial experience with monopiles throughout their use.

Since this is a new concept, the amount of existing information in literature is limited. However, recently conducted research suggests that such hybrid configurations demonstrate an increased lateral resistance compared to monopiles. [Stone & Newson, 2007; El – Marassi *et al*., 2008; El – Marassi, 2011; Arshi, 2011, 2012; Arshi & Stone, 2012]. On the other hand, extensive research has been carried out concerning the individual components. Specifically, several methods have been developed over the years for the analysis of piles; their response to lateral loads is a topic of particular interest when it comes to their application in offshore projects and has been extensively investigated [i.e. Matlock & Reese, 1960; Broms, 1964; Poulos, 1971; Reese *et al.,* 1974; Randolph, 1981; Murff & Hamilton, 1993; Duncan *et al.,* 1994; Zhang *et al.,* 2005, Fleming *et al., 2009*]. The response of shallow footings has also been thoroughly examined; innovative solutions for the behavior of footings under combined loading have been developed [i.e. Bransby & Randolph, 1998; Houlsby & Puzrin, 1999; Taiebat & Carter, 2000; Gourvenec & Randolph, 2003; Yun & Bransby, 2007; Gourvenec, 2007, 2008], along with the classical bearing capacity solutions [Prandtl, 1921, Meyerhoff, 1953; Cox *et al.,* 1961, Vesic, 1975].

A schematic illustration of the hybrid monopile – footing system examined by Stone et al. is shown in **figure 1.5**. Arshi (2011), and Arshi & Stone (2012) conducted a series of single gravity experimental tests concerning the same hybrid system, and reported the significant effect of the size of the footing on the overall horizontal bearing capacity. The increase in moment capacity ranged from 50 to 100%. They also indicated the importance of the vertical to horizontal load ratio, which seems to have an important effect on the lateral performance of the system; larger vertical loads tend to improve the overall lateral resistance of the hybrid foundation. Furthermore, they suggested that the hybrid foundation tends to be more effective when vertical movements are allowed at the pile – footing connection, permitting the footing to act independently from the pile; hence, the beneficial contact between the footing and the underlying soil is controlled by the vertical load acting on the footing. Using

analytical and numerical methods, they concluded to simple design charts that provide the normalized moment capacity of the hybrid foundation in relation to their pile length to footing diameter ratio (L/D), as well as to the footing to pile diameter ratio (D/d). An example of such a design chart is shown in **figure 1.6**. Finally, they introduced the idea of adding skirts to the footing, which have been proven to further increase the lateral resistance.

The hybrid foundation examined in this thesis also adopts the concept of decoupling the two components in the vertical sense, however with a significant difference to the arrangement presented in **figure 1.5**; the wind turbine tower is connected onto the footing and not to the monopile. In this way, the vertical load acting on the footing is further increased, by taking advantage of the turbine's weight, making the hybrid system even more effective. While the pile remains uncharged in the vertical direction, the shear forces and bending moments can be transferred to the pile via a simple configuration; the footing has a hole in the middle, allowing the pile to penetrate it. Hence, lateral resistance of the pile will be mobilized via the generation of stresses in the internal pile - footing interface, resembling a shear key. This type of connection is of critical importance for various reasons; first of all, the beneficial contact between the footing and the underlying soil is ensured. In addition, long – term consolidation settlements can be effectively dealt with. Due to the axial stiffness of the pile, settlement of the footing would be prevented if the two components were rigidly connected, leading to deterioration of the interface contact conditions. By implementing the vertical decoupling, the footing is able to reposition itself and maintain good contact with the underlying soil. The hybrid foundation system proposed in this study is depicted in **figure 1.7**, while the load transfer mechanisms for vertical and lateral loading are illustrated in **figure 1.8**.

Moreover, this connectivity offers simplicity in the installation process: The footing can be installed first, along with a transition piece to connect the tower, and then used as a guide to drive the monopile in place. This study does not focus on the construction of the footing; reinforced concrete or steel can either be used. However, design practice from gravity base foundations suggests that such large structures should be constructed hollow, and filled with ballast material in situ.

The hybrid foundation examined in this thesis is based on the patent submitted by Anastasopoulos (2013). In fact, Anastasopoulos came up with a way of constructing the footing in order to realize the hybrid configuration described above, as well as the installation method. The footing proposed by Anastasopoulos is a lightweight steel structure, which can be filled in – situ with soil material, in order to gain more stabilizing weight. Internal stiffeners ensure the required bending stiffness and lateral loads are transmitted to the monopile via an internal bearing plate. A schematic illustration of this footing can be seen in **figure 1.9**. After preliminary numerical analysis, Anastasopoulos concluded that the hybrid system outperforms a conventional 30 m monopile; this performance is achieved with a 50% shorter monopile combined with a footing which has a 14 m diameter. Results in terms of moment – rotation for the two systems are depicted in **figure 1.10**. According to Anastasopoulos, this reduction on embedment length can lead to a reduction of the order of 30% of the total foundation/installation cost.

1.2 Loads of Offshore Wind Turbines

1.2.1 Preface

Offshore wind turbines are subjected to a variety of loads, most of which are dynamic in nature. The most evident source of excitation is the rotor. For a three – bladed rotor, the first excitation frequency corresponds to a full revolution and is commonly denoted as 1P, while the second excitation frequency is denoted as 3P and corresponds to the blade passing frequency. Typical value ranges for 1P and 3P excitation frequencies are 0.17-0.33 Hz and 0.5-1 Hz respectively, in case of wind turbines of nominal power up to 3.6 MW [LeBlanc, 2009]. Design of the wind turbine tower should avoid these frequencies, therefore three design options are available: a very stiff structure with its first natural frequency higher than 3P (Stiff – Stiff response), a very soft structure with its first natural frequency below 1P (Soft – Soft response) and a structure of intermediate stiffness with its first natural frequency being located between 1P and 3P (Soft – Stiff response).

Additional excitation frequencies that should be considered in the design is the frequency of waves, which is generally smaller than the 1P frequency and the frequency of wind that is even smaller. The effect of soil – foundation interaction will lead to a further decrease in the first natural frequency, therefore it is very important and should be taken into consideration. The above information concerning the frequencies of a wind turbine is summarized in **figure 1.11**. Avoidance of resonance is of very high importance in the design of offshore wind turbines. Frequency domain analysis is also crucial when it comes to fatigue assessment of offshore wind turbines; this subject is not addressed in the current study. Van der Tempel (2005) modelled a wind turbine as a flexible beam with a concentrated mass on the top and an equally distributed mass along the tower, and came up with the following approximate expression for its first natural frequency:

$$f_{nat} \cong \frac{D_{av}}{L^2}\left(\frac{E}{104(a+0.227)\rho_{steel}}\right)^{0.5} \qquad (1.1)$$

where:

$D_{av} = D - t_w$ the tower average diameter [m]

D: the tower section outer diameter [m]

t_w: the tower thickness [m]

L: the tower height [m]

E: the tower modulus of elasticity [Pa]

ρ: the tower steel density [kg/m^3]

the parameter α is given by:

$$a = \frac{m_{top}}{\rho_{steel}\,\pi\,D_{av}\,t_w\,L} \tag{1.2}$$

where:

m_{top}: the tower head mass [kg]

This thesis examines the problem from a geotechnical point of view, therefore an assumption is made, that no resonance will occur due to wave and wind loading. Hence, those loads are applied in a static manner, through force – controlled loading steps in order to approach their cyclic nature. An additional load case of earthquake is also examined. The seismic excitation, due to its strong dynamic and kinematic nature, is inevitably imposed in a dynamic manner as a ground acceleration. The loads examined in this thesis are schematically illustrated in **figure 1.12**.

1.2.2 Waves and Currents

Sea waves are mainly caused by wind; even small gusts of wind can cause changes in the sea surface and this is a random process. Sea wave periods are considerably smaller than wind periods, typically being of the order of 2 – 10 seconds. Measured time history data of sea elevation is often transformed into an energy spectrum, called the wave spectrum. Those spectrums represent a stochastic process and they can be approached by several models; the most common is the Pierson – Moskowitz wave spectrum, which originally used the average wind speed as the sole input parameter, but was later adjusted to have the significant wave height H_S and mean zero crossing period T_z as input parameters. An extended version is the JONSWAP spectrum, which represents sea states that are not fully developed under a certain wind condition, using a peak enhancement factor. Comparison of the two spectra, along with an example of a sea elevation time series are shown in **figures 1.14** and **1.13** respectively.

To calculate wave loads acting on a wind turbine, the Morison Equation can be used. It is a semi – empirical formula, which is used widely to calculate hydrodynamic loads on slender cylindrical submerged members per unit length, due to unbroken surface waves; a schematic illustration is shown in **figure 1.15**. The Morison equation is expressed below:

$$f_{Morison}(x,z,t) = f_d(x,z,t) + f_i(x,z,t) \tag{1.3}$$

$$f_d(x,z,t) = C_d \frac{1}{2}\,\rho_w D\,|u(x,z,t)|\,u(x,z,t) \tag{1.4}$$

$$f_i(x,z,t) = C_m \frac{\rho_w \pi D^2}{4}\,\dot{u}(x,z,t) \tag{1.5}$$

where:

$f_{Morison}$: Hydrodynamic load per unit length [N/m]

f_d: Hydrodynamic drag load per unit length [N/m]

f_i: Hydrodynamic inertia load per unit length [N/m]

C_d: Non – dimensional hydrodynamic drag coefficient

C_m: Non – dimensional hydrodynamic inertia coefficient

ρ_{water}: density of water [kg/m^3]

u: water particle velocity [m/s]

$\dot{u}$: water particle acceleration [m/s^2]

D: diameter of cylinder section [m]

The right choice of the drag and inertia coefficients is crucial in order to estimate the acting wave loads correctly. Both coefficients depend on the body shape and surface roughness, as well as to characteristic parameters of the flow (i.e. Reynolds number). The presence of marine growth should also be considered.

To take account for the action of currents, the current velocity can be inserted in the calculation of the total hydrodynamic force via a modification of the drag term:

$$f_d = C_d \cdot \tfrac{1}{2} \rho_{water} D \cdot \left(\left| (u + U_c) \right| (u + U_c) \right) \quad (1.6)$$

In the above expression, U_C is the current velocity, which is added to the wave particle velocity u. Both velocities are expressed in [m/s].

The basic assumption of the Morison equation is that the size of the submerged members is not large enough to interact with the waves; the diameter of the cylinder should be quite small, compared to the examined wave length. Otherwise, the inertia coefficient should be properly modified, to take account for diffraction effects. Should the size of the member be relatively large, the MacCamy – Fuchs correction is usually implemented to reduce the magnitude of the inertia coefficient. An example of corrected inertia coefficient due to diffraction is shown in **figure 1.16.** Another assumption of the formula is that the waves are not breaking. Thus, the probability of breaking waves at a specific wind farm site must be assessed.

1.2.3 Wind

Wind loading is cyclic in nature, however it can be considered as a monotonic load due to its large period, which can be of the order of minutes. The force acting on the rotor is related to the wind speed. The mean wind speed, which is generally averaged within a period of 10 minutes, increases with height; however, the actual wind speed is fluctuating around the mean value due to wind turbulence. An example of a measured time history of wind is show in **figure 1.17**. Within the atmospheric boundary layer, wind speed is affected by the earth's

surface and is reduced to zero near the ground. This distribution is usually approached via either a power law or a logarithmic law.

Most wind turbines operate within a wind speed range of 3 to 25 m/s. If the wind speed gets larger, the generated aerodynamic torques and rotational speeds will cause severe damage to the turbine. In order to withstand extreme wind events, wind turbines are designed with a cut – out speed, above which breaks force the turbine to slow down. The mechanisms implemented to deal with high wind can be generally categorized into pitch – regulated and stall – regulated. The difference between the two types of wind turbines mainly lies on the way they deal with high wind speeds; while pitch – regulated turbines use an active control system that varies the pitch angle of the blades, stall – regulated turbines rely on the aerodynamic design of the blades, so that they will perform worse in larger wind speeds. Hence, stall – regulated wind turbines experience a loss in power production after reaching the cut – out speed, while pitch – regulated turbines manage to maintain a constant output, as seen in **figure 1.18**.

The effect of wind is in reality quite complex, as it involves the generation of unsteady stresses in several parts of the rotor – nacelle assembly. A crucial aspect of wind loading has to do with the interference of the rotating blades with the tower; the passing blades generate a dynamic excitation which is likely to resonate and cause excessive damage to the tower. To simplify the problem and approach it in a geotechnical manner, the effect of wind in this study is translated into a concentrated thrust force acting on the rotor. As suggested by the American Petroleum Institute, the force of wind is calculated via the following expression:

$$F = \frac{w}{2g} V^2 C_g A \tag{1.5}$$

where:

F: concentrated thrust wind force [N]

w: unit weight of air [N/m^3]

V: wind speed [m/s]

A: rotor area [m^2]

g = 9.81 m/s^2

C_g: dimensionless thrust coefficient (approximately equal to 0.3 for wind turbines)

1.2.4 Seismic Loads

Seismic loading of wind turbines is generally not considered as a main driver of design, except for cases of high seismic hazard regions. This is attributed to the fact that wind turbines, especially larger models, are quite flexible and therefore are not expected to be heavily excited by earthquakes. However, smaller models such as turbines of 2 MW nominal capacity may be more affected, as their first natural frequency is higher. Existing codes that offer direct

guidance for seismic loading of wind turbines are provided by Risø (2001), Germanischer Lloyd (GL, 2003) and the IEC (2005). With few exceptions, these guidelines either refer to existing building codes or specify similar simplified approaches to assess the seismic risk of wind turbines. Commonly, the first natural period is used to extract the design response acceleration from a design response spectrum. The acceleration is then transformed into base shear and moment.

Seismic loading of wind turbines has been investigated by numerous researchers [i.e. Bazeos *et al.,* 2002; Lavassas *et al.,* 2003; Ritschel *et al.,* 2003; Witcher, 2005; Haenler *et al.,* 2006; Zhao and Maisser, 2006; Prowell *et al.,* 2009, 2010;]. Initially, the researchers had focused on the tower, using models that lumped the rotor – nacelle assembly into a pointed mass; Bazeos *et al.* (2002) suggested that beam – column models compare quite well with more sophisticated shell models for towers; the latter, however, are necessary to assess the possibility of local stress accumulation and buckling. Other models include beam elements that correspond to the turbine blades as well [Malcolm and Laird, 2003]. The effect of soil – structure interaction was examined through the incorporation of springs and dampers at the model base [Bazeos *et al.,* 2002; Zhao & Maisser; 2006]. Lavassas *et al.* (2003) conducted excessive numerical investigation of a 1 MW wind turbine and concluded that seismic stresses were 60% lower compared to those produced by extreme winds.

When it comes to offshore wind turbines, publications concerning seismic assessment are limited. An investigation of the performance of offshore wind turbines founded on suction caissons has been performed by Kourkoulis *et al.* (2012) and Lekkakis (2012); Kourkoulis *et al.* focused more on the effect of imperfect foundation – soil interfaces and concluded that interface non – linearities enable foundation rotation, which limits the tower bending but may lead to irrecoverable displacement on the nacelle level. They suggested that increasing the foundation diameter is more effective on limiting this rotation, compared to increasing the embedment length. Lekkakis (2012) also investigated the response of offshore wind turbines founded on suction caissons and concluded that serviceability limits can be met very early when a seismic event occurs. A crucial aspect of the problem is that seismic loads will act simultaneously with wave and wind loads, further increasing the rotation caused by the millions of loading cycles an offshore wind turbine is subjected to during its lifetime.

1.3 Bearing Capacity

1.3.1 Preface

The role of all foundations is to safely transfer the loads of the superstructure to the surrounding soil. In case of an offshore wind turbine, the transmitted loads are a combination of vertical force (N), horizontal force (Q) and moment (M); the maximum load that can be sustained by a foundation without failure is referred to as the foundation's bearing capacity. Bearing capacity of a foundation can be defined both for uniaxial and combined loads.

As discussed above, the components of the hybrid foundation examined in the current thesis are decoupled from each other; the entire vertical load, along with part of the horizontal load

is sustained by the footing, while the monopile is only mobilized by lateral loading. A brief presentation of the available literature concerning each component separately, as well as hybrid foundations is presented below.

1.3.2 Shallow Foundations Under Combined Loading

Loading of a shallow footing sustaining an offshore wind turbine consists of monotonic vertical load due to dead weights of the tower and footing, and of cyclic horizontal and moment loads, due to action of wind and waves. The ratio of moment to horizontal loading indicates whether the structure is prone to sliding or overturning. So far, design practices for calculation of bearing capacity of offshore shallow foundations [i.e. ISO, 2000; DNV, 1992; API, 2000] are based on classical bearing capacity equations [i.e. Terzaghi, 1943], combined with various coefficients that take account for load eccentricity and inclination, foundation shape and soil strength profile. The validity of these solutions to take account for combined M – Q – N loading was first questioned by Ukritchkon *et al.* (1998) for strip foundations and by Gourvenec & Randolph (2003a) for circular foundations. As seen in the following paragraphs, these classical solutions express the bearing capacity as a modified vertical limit load, rather than individual components; hence, they are not easily applicable for offshore foundations, where the ultimate moment and horizontal force need to be defined.

Traditional bearing capacity solutions are based on plasticity theory; the bound theorems are used to provide upper and lower bound solutions. Only when the two bound solutions coincide, the result is considered the exact solution. These plasticity solutions model the soil as elastic – perfectly plastic material, and do not take account for hardening or softening behaviors. Despite their simplicity in modelling the soil, plasticity solutions are the basis of bearing capacity solutions for both onshore and offshore foundations and are still used widely in a variety of problems.

The first to provide a solution concerning the bearing capacity of foundations was Prandtl (1921). His solution concerns a surface strip foundation lying on a homogeneous cohesive soil half – space, under vertical loading in undrained loading conditions. The soil was assumed perfectly plastic and weightless. Specifically, the following exact expression was extracted, as the result of both upper and lower bound approaches:

$$q_u = (\pi + 2)S_u = 5.14S_u \tag{1.6}$$

where:

q_u : the ultimate failure stress

S_u : the undrained soil shear strength

Based on Prandtl's theory, Terzaghi (1943) proposed an expression to estimate the bearing capacity of a surface strip foundation, which includes the effect of soil weight and overburden. Meyerhof (1951) further expanded Terzaghi's theory to take account for the

expansion of the failure surface into the overlying soil, as well as the foundation's side friction. Hence, the contribution of soil embedment consists of the generation of shear stresses onto the failure surface as well as onto the side interfaces of the foundation, not only of the overburden weight. Although these expressions were initially limited to strip foundations (plane strain conditions), they can be easily modified to take account for other footing shapes via the use of shape factors [Meyerhof, 1953; Hansen, 1970; Vesic, 1973]. The exact solution for the bearing capacity of a rough circular foundation ($q_u = 6.05S_U$) was provided by Cox *et al.* (1961)

Classical bearing capacity solutions deal with moment and horizontal loads via load eccentricity and inclination respectively. Methods have been developed that take account for these effects [i.e. Meyerhof, 1951; Brinch Hansen, 1970; Vesic, 1975]. A widely used expression up to date is the following expansion of Terzaghi's solution:

$$q_u = cN_c\zeta_c + qN_q\zeta_q + 0.5\gamma BN_\gamma\zeta_\gamma \quad (1.7)$$

where:

q_u : ultimate soil failure stress

B : the smaller dimension of the foundation (L is the larger)

c : soil cohesion

q : effective overburden at foundation base level

γ : specific weight of soil

N_c, N_q, N_γ : bearing capacity factors that depend on the soil's angle of friction ϕ

ζ_c, ζ_q, ζ_γ : factors that take account for the effect of foundation shape, loading inclination and eccentricity, soil surface inclination, foundation embedment and interface conditions etc.

Uniaxial undrained horizontal bearing capacity of a surface foundation is, on the other hand, independent of the foundation's shape; as failure occurs by sliding when the acting horizontal load is larger than the maximum interface shear stress that can be developed, bearing capacity solely depends on the interface conditions. For a rough foundation surface, $H_{ULT} = AS_{U,0.}$ Furthermore, undrained uniaxial moment bearing capacity of a strip or circular foundation with a tensionless interface is given by the effective area principle [Meyerhof, 1953]. The maximum moment capacity of $M_{ult}/ADS_{u0} = 0.64$ and 0.61 for strip and circular foundations respectively is mobilized under a vertical load of $0.5V_{ult}$.

The effect of soil strength inhomogeneity on the vertical bearing capacity is under predicted by traditional bearing capacity theory solutions. This effect is commonly incorporated via correction of the shape factors, produced by more advanced solutions. The current design guidelines adopt corrected factors based on rigorous solutions with the method of characteristics [Davis & Booker, 1973; Houlsby & Roth, 1983], concerning linearly increasing soil strength with depth. Soil inhomogeneity has a trivial effect on horizontal bearing capacity

due to the large role of interface conditions. Concerning undrained moment bearing capacity, the effect of soil shear strength heterogeneity has been determined by Gourvenec & Randolph (2003); they produced moment capacity factors as a function of heterogeneity factor κ, for strip and circular foundations with full – tension interface capacity. They observed that when the surface soil is weaker, the moment failure mechanism into the shallower layers, as seen in **figure 1.19**.

Embedment increases vertical, horizontal and moment capacity of shallow foundations, as the failure mechanisms are forced into deeper soil masses, and larger bodies of soil are mobilized. This effect is more intense for soils with increasing shear strength with depth. As discussed above, classical bearing capacity theory implements depth factors to modify the uniaxial vertical bearing capacity of foundations [Skempton, 1951; Brinch Hansen, 1970]. These depth factors were originally derived for smooth – sided circular foundations. More recent work has questioned the use of these traditional modification factors and revealed changes in the mode of failure with increasing embedment. The effect of embedment to the horizontal bearing capacity of a foundation lies to a change of the failure mechanism; a translational scoop mechanism is mobilized, rather than pure sliding. Depth factors for rough embedded strip foundations are related to the square of the embedment ratio [Yun & Bransby, 2007b; Gourvenec, 2008]. Undrained moment capacity is also affected by the embedment ratio; the scoop failure mechanism is similar to the one of surface foundations, but extends deeper, in order to intersect the edges of the foundation's base. It has been reported that an embedment ratio of 0.5 can increase the maximum moment capacity by up to 85% in homogeneous soil deposits [Bransby & Randolph, 1999].

An important effect of embedment in the lateral response of foundations is the development of coupling between the horizontal and rotational degrees of freedom. This means that imposing a rotation at the top of an embedded foundation will result in a horizontal displacement as well, and vice versa. This effect increases with the increase of the embedment ratio and leads to increased available moment and horizontal bearing capacity. However, for this extra bearing capacity to be mobilized, one of the coupled degrees of freedom must be constrained. In case none of the degrees of freedom is constrained, the actual capacity (H_{ult}, M_{ult}) will be smaller than the maximum available (H_{max}, Mmax). Failure mechanisms under horizontal and moment load resemble to each other due to this coupling. Such failure mechanisms are depicted in **figure 1.20** and **1.21** respectively [Gourvenec, 2008]. Classical bearing capacity theories do not take account for this effect.

Offshore foundations are subjected to large horizontal loads and moments, combined with vertical loads. As it is pointed out in the above paragraphs, implementing traditional bearing capacity theories in such problems can lead to a number of inaccuracies. Several advanced solutions exist in order to assess ultimate limit states under such complex loading regimes; the most convenient and straightforward among them is the extraction of failure envelopes. They can be expressed in planes of constant vertical, horizontal, or moment load, or as a three – dimensional surface in the M – Q – N loading space. Any load combination inside the failure envelope is considered safe while any load combination outside of the envelope results in failure. The size and shape of these interaction diagrams has been the subject of investigation

for numerous researchers [i.e. Martin, 1994; Ukritchkon *et al.*, 1998; Bransby & Randolph, 1998; Taiebat & Carter, 2000, 2002; Randolph & Puzrin, 2003; Gourvenec & Randolph, 2003; Gourvenec 2007a & b, 2008].

An example of a three – dimensional failure envelope for general loading of a circular surface foundation with a zero – tension foundation/soil interface is depicted in **figure 1.21**. An envelope of such form can be described by an ellipse in terms of normalized loads [Gourvenec, 2007]. i.e. $v = V/V_{ult}$, $h = H/H_{ult}$ and $m = M/M_{ult}$. Envelopes derived from finite element analyses of surface foundations with a zero – tension interface have been compared with results from traditional bearing capacity theory; the later seems to under predict the actual failure envelope, leading to conservative results. However, a large part of the research concerns full – tension interfaces [Tani & Craig, 1995; Bransby & Randolph, 1998; Taiebat & Carter, 2000; Gourvenec & Randolph, 2003]. The main difference is that maximum capacity is observed for zero vertical loads when a full – tension interface is considered, while tensionless interface approaches require a vertical load of $0.5V_{ult}$ to mobilize the peak moment resistance. Taiebat & Carter (2000) proposed the following closed – form expression to describe the failure envelope of a circular foundation with a full – tension interface resting on homogeneous soil.

$$f = \left(\frac{V}{V_{ult}}\right)^2 + \left[\left(\frac{M^*}{M_{ult}}\right)\left(1 - 0.3\frac{HM}{MH_{ult}}\right)^2\right] + \left(\frac{H}{H_{ult}}\right)^3 - 1 \qquad (1.8)$$

Concerning embedded foundations, they are commonly treated as surface foundations resting on the foundation base level. Therefore, it is assumed that the shape of the envelope is not affected by the foundation shape. This approach is increasingly being questioned, as it does not take account for the coupling of the rotational and translational degrees of freedom that is described above. Gourvenec (2008) proved that this coupling is directly reflected in the shape of the moment – horizontal force interaction diagram; constraining one coupled degree of freedom will cause extra capacity to be mobilized on the other one. Hence, an asymmetry is developed in these failure envelopes, which becomes more pronounced as the embedment ratio increases, as seen in **figure 1.22**. Fitting approximate expressions in such asymmetrical interaction diagrams can be quite challenging.

The footing used as a component of the hybrid foundation examined in the current study is not embedded, however the interaction diagrams of the hybrid system in the M – H load space are expected to demonstrate eccentricity, due to embedment of the pile. Footings with tensionless interfaces rely on the acting vertical load in order to mobilize their maximum lateral capacity, as seen in **figure 1.23**, which depicts interaction diagrams for a surface foundation in the M – V load space. The decoupling in the vertical degree of freedom utilized in the examined hybrid foundation takes advantage of this beneficial effect of vertical loads on the lateral capacity of footings.

1.3.3 Piled Foundations Under Lateral Loading

Offshore piles are commonly exposed to large horizontal loads and moments. In case of a monopile supporting offshore wind turbines, the dominant design load acts laterally. The hybrid foundation examined in this thesis implements a pile to sustain horizontal loads along with the footing, but remains uncharged vertically. Therefore, only the lateral bearing capacity of piles is discussed here.

Lateral loads are transmitted by piles via the generation of mainly normal stresses on the pile – soil interface. The effect of lateral loading is limited to the upper part of the pile (typically 10 – 15 pile diameters). This length is called the active length of the pile and is used to distinguish two types of lateral response; piles with embedment length smaller than the active length are characterized as short piles while piles with embedment length larger than the active length are characterized as long piles. The difference lies in the failure mechanisms due to lateral loading; short piles are lead to failure by rigid body rotation about a rotation point, while long piles develop a plastic hinge which limits the effect of lateral loads to the length above it, as seen in **figure 1.24**. Gazetas (1991) proposed the following expression to estimate the active length of a pile laying on a uniform elastic half – space:

$$l_c \approx 1.5d \left(\frac{E_p}{E_s}\right)^{0.25} \tag{1.9}$$

where:

l_c: pile's active length

d: pile's diameter

Ep: Elastic Modulus of the pile

Es: Elastic Modulus of the soil

Monopiles have diameters larger than 4 meters, which means that they generally behave as short piles. Short pile failure mechanisms involve the rotation of the pile as a rigid body about a center of rotation, usually located at 70 – 80% of the embedment length. The soil resistance will be positive above the center of rotation and negative below it. The actual pressure distribution is idealized by assuming a sharp transition, as seen in **figure 1.24**. The two resisting forces (P_{ab} and P_{bc}) are calculated by integrating the lateral stresses along their lengths of action. The lever arms L_{ab} and L_{bc} also need to be calculated. By considering moment and horizontal force equilibrium, two equations are formed:

$$H_{ult} = P_{ab} - P_{bc} \tag{1.10}$$

$$H_{ult}e = -P_{ab}L_{ab} + P_{bc}L_{bc} \tag{1.11}$$

By expressing the above forces and lever arms in terms of z_{crit}, the lateral bearing capacity of a pile H_{ult} can be calculated. It is reminded that e is the load eccentricity (e = M/H).

The short pile failure mechanism involves the formation of a wedge of soil in front of the pile, with a gap forming in the back of the pile, as seen in **figure 1.25**. According to Broms (1964a), the limiting soil resistance for piles in clayey soils is taken to increase with depth from a value of $2DS_u$ to a limiting value of $9DS_u$. These bounds correspond to passive failure of the wedge near the surface and failure due to soil flow near the pile tip, respectively. Other similar bound solutions are derived by several researchers [Matlock, 1970; Murff and Hamilton, 1993, 1995]. Design charts for piles under lateral loading have been developed, using the combination of equations presented above, along with different distributions of lateral stresses. Examples of such design charts for short piles can be seen in **figure 1.26.** An important observation is that the degree of rotational fixity at the pile head contributes to the ultimate lateral capacity; a restrained (fixed – head) pile can demonstrate a significantly increased bearing capacity than a free head pile.

1.3.3 Bearing Capacity of Hybrid Monopile – Footing Foundations

Investigation of hybrid foundations is still on its very early stages. Extensive numerical analyses have been carried out and the results are quite promising [El-Marassi *et al.*, 2008; Stone *et al.,* 2010; Arshi *et al.,* 2011; Arshi & Stone, 2012], but simple design practices are yet to be developed. Recently, Stone *et al.* (2013) proposed a simple analytical method to estimate to estimate the moment bearing capacity of such systems. This method utilizes conventional lateral pile analysis methodology in which the hybrid system is idealized as a lateral pile with a resisting moment applied at the mud line, to take account for the moment capacity of the footing. Conventional bearing capacity theory is utilized to provide the moment capacity of the footing, which is applied as a concentrated moment acting at the mud line, on the opposite direction to the loading. This approach only considers the ultimate state just before failure; in reality, the resisting moment generated by the footing is a function of the footing's angle of rotation ϑ. Results from this simplified analytical solution are presented in **figure 1.27**. A similar method was proposed by Mokwa & Duncan (2003) in order to estimate the contribution of pile caps to the lateral resistance of a single pile. In their work, Mokwa & Duncan incorporated the rotational restraint coefficient $K_{M\vartheta}$ which was introduced by Matlock & Reese (1961).

Furthermore, El-Marassi (2011) conducted extensive numerical analysis of hybrid foundations and came up with closed – form expressions for the M – V and H – V interaction diagrams of hybrid foundations with several pile to footing ratios. An example of these failure envelopes can be seen in **figure 1.28.** It is worth noting that in this work the special connectivity that allows relative vertical translation between the pile and the footing was not implemented, therefore there are no evidence of the beneficial contribution of vertical loads on the ultimate moment and horizontal capacities, in case of tensionless soil – foundation interfaces.

1.4 Elastic and Nonlinear Stiffness of Foundations

1.4.1 Preface

Stiffness of a foundation is a key design criterion in addition to bearing capacity. The effect of soil – structure interaction on the overall response can be taken into account by using a stiffness matrix, which can be expressed through the following relationship:

$$\{F\} = [K]\{u\} \tag{1.12}$$

where {F} the forces acting on the foundation, {u} the displacements and rotations and [K] the stiffness matrix. The latter contains all the stiffness components that correspond to the degrees of freedom of the problem. In the general case of a three – dimensional, six degree of freedom problem, the stiffness matrix is expressed as follows for a symmetrical foundation:

$$\begin{Bmatrix} V \\ H_1 \\ H_2 \\ M_1 \\ M_2 \\ T \end{Bmatrix} = \begin{bmatrix} K_V & & & & & \\ & K_{HH} & & & K_{HM} & \\ & & K_{HH} & K_{HM} & & \\ & & K_{MH} & K_{MM} & & \\ & K_{MH} & & & K_{MM} & \\ & & & & & K_T \end{bmatrix} \begin{Bmatrix} w \\ u_1 \\ u_2 \\ \theta_1 \\ \theta_2 \\ \omega \end{Bmatrix} \tag{1.13}$$

where:

KV: Vertical stiffness [kN/m]

KHH: Horizontal – translational stiffness [kN/m]

KMM: Rotational stiffness [kNm]

KHM, KMH: Coupled stiffness components (for embedded foundations) [kN]

KT: Torsional stiffness [kNm]

Assessing the stiffness matrix of a soil – foundation subsystem is crucial, as it can provide a simple way to estimate the response of the whole system in the small – strain domain; thus, approximately predicting serviceability deformations. The elastic stiffness components can also be used to approximately estimate the first natural period of a structure and deal with dynamic problems that incorporate soil – structure interaction. A simplified approach is to substitute the whole soil – foundation subsystem by a set of uncoupled springs, as in the Winkler method.

More complex methods involve the incorporation of coupled springs and dampers that are used to form a macro – element; these methods can accurately estimate the static and dynamic response of structures, and the components of the stiffness matrix as usually

required as input parameters. Recent methods also include non – linear stiffness components, which can usually be expressed as a function of deformations; an approximate method for the analysis of non – linear rocking systems is depicted in **figure 1.29**. As can be observed, the initial stiffness components need to be defined in order to calibrate the springs.

When it comes to offshore wind turbines, minimum foundation rotational stiffness is the most common foundation design specification, other than loads. Horizontal stiffness and the cross – coupled stiffness components are also very important, in case of embedded foundations. [Morgan & Ntambakwa, 2008].

1.4.2 Elastic Stiffness of Shallow Foundations

At very small values of deformation, linear elasticity can be used to describe the response of shallow foundations. In case of surface foundations, it is considered that tension can be sustained in the soil – foundation interface, due to action of vertical loads. For an arbitrarily – shaped surface foundation lying on a homogeneous half – space (G, v), the following expressions can be used to approximately estimate the linear stiffness components, after Gazetas (1991):

$$K_V = \frac{2GL}{1-v}(0.73 + 1.54\chi^{0.75}) \tag{1.14}$$

$$K_{HHy} = \frac{2GL}{2-v}(2 + 2.50\chi^{0.85}) \tag{1.15}$$

$$K_{HHx} = K_{HHy} - \frac{0.2GL}{0.75-v}\left(1 - \frac{B}{L}\right) \tag{1.16}$$

$$K_{MMx} = \frac{G}{1-v} I_{bx}^{0.75} \left(\frac{L}{B}\right)^{0.25} \left(2.4 + 0.5\frac{B}{L}\right) \tag{1.17}$$

$$K_{MMy} = \frac{3G}{1-v} I_{by}^{0.75} \left(\frac{L}{B}\right)^{0.15} \tag{1.18}$$

$$K_t = 3.5GI_{bz}^{0.75} \left(\frac{B}{L}\right)^{0.4} \left(\frac{I_{bz}}{B^4}\right)^{0.2} \tag{1.19}$$

where:

$$\chi = \frac{A_b}{4L^2}$$

Ab : the foundation area

Iby, Ibx, Ibz: moment of inertia about the axes y, x, z respectively

B,L: half – breadth and half – length of a corresponding orthogonal foundation (see **figure 1.30)**

G, v: Shear modulus and Poisson's ratio for the soil

The above equations concern the general case of a non – symmetrical arbitrarily – shaped surface foundation. They can be used to estimate deformations in the small – strain domain. In case of rectangular, strip or circle foundations the equations are simplified. It is worth noting that stiffness derived from accurate finite element analyses would present a deviation not larger than 20%, depending on the type of interfaces adopted.

For embedded foundations stiffness components tend to be larger, due to the action of two effects: the trench effect and the sidewall effect, as illustrated in **figure 1.31**. Concerning the trench effect, placing a surface foundation inside an open trench results in increasing its stiffness due to the generation normal and shear tractions from the overlying soil, which restrict the deformation. The sidewall effect is caused by contact of the vertical sidewalls with the surrounding soil, which helps transmit the applied load through normal and shear stresses generated there as well. In case of inhomogeneous soil deposits, which are commonly found at seabed areas, stiffness of embedded foundations is additionally increased due to the foundation's tip reaching deeper and stronger soil layers. Gazetas (1991) proposed the following modifications in the stiffness components of surface foundations, to take account for embedment:

$$\frac{K_{V,emb}}{K_{V,surf}} = \left[1 + \left(\frac{1}{21}\right)\left(\frac{D}{B}\right)(1 + 1.3\chi)\right]\left[1 + 0.2\left(\frac{A_w}{A_b}\right)\right] \quad (1.20)$$

$$\frac{K_{HHy,emb}}{K_{HHy}} = \left[1 + 0.15\left(\frac{D}{B}\right)^{0.5}\right]\left[1 + 0.52\left(\frac{h}{B}\frac{A_w}{L^2}\right)^{0.4}\right] \quad (1.21)$$

$$\frac{K_{HHx,emb}}{K_{HHx}} = \frac{K_{HHy,emb}}{K_{HHy}} \quad (1.22)$$

$$\frac{K_{MMx,emb}}{K_{MMx}} = \left[1 + 1.26\left(\frac{d}{B}\right)\left(1 + 0.52\frac{h}{B}\frac{A_w}{L^2}\right)^{0.4}\right] \quad (1.23)$$

$$\frac{K_{MMy,emb}}{K_{MMy}} = \left[1 + 0.92\left(\frac{d}{L}\right)^{0.6}\left(1.5 + \left(\frac{d}{L}\right)^{1.9}\left(\frac{d}{L}\right)^{-0.6}\right)\right] \quad (1.24)$$

$$K_{MHxy} = K_{HMxy} = \frac{1}{3}\, dK_{HHx,emb} \quad (1.25)$$

$$K_{MHyx} = K_{HMyx} = \frac{1}{3}\, dK_{HHy,emb} \quad (1.26)$$

where:

d: effective sidewall contact height

A_w: actual sidewall – soil contact area

h: trench depth

The above expressions are considerably simplified in case of circular, rectangular or strip foundations. Additionally, modification factors have been proposed to take account for a rocky substratum at the base of the homogeneous deposit.

1.4.3 Elastic Stiffness of Piles

The difference between piles and shallow embedded foundations is that piles have an embedment ratio larger than 1. As aforementioned, laterally loaded piles are divided into two main categories, long and short piles, according to their active length l_c. Gazetas (1991) came up with the following expressions to estimate the lateral stiffness of long piles for two types of soil, as depicted in **figure 1.31**.

For homogeneous soil deposits:

$$K_{HH} \approx E_s d \left(\frac{E_p}{E_s}\right)^{0.21} \tag{1.27}$$

$$K_{MM} \approx 0.15 E_s d^3 \left(\frac{E_p}{E_s}\right)^{0.75} \tag{1.28}$$

$$K_{HM} = K_{MH} \approx -0.22 E_s d^2 \left(\frac{E_p}{E_s}\right)^{0.50} \tag{1.29}$$

For inhomogeneous “Gibson” soils:

$$K_{HH} \approx 0.6 E_s' d \left(\frac{E_p}{E_s'}\right)^{0.35} \tag{1.30}$$

$$K_{MM} \approx 0.15 E_s' d \left(\frac{E_p}{E_s'}\right)^{0.80} \tag{1.31}$$

$$K_{HM} = K_{MH} \approx -0.17 E_s' d^2 \left(\frac{E_p}{E_s'}\right)^{0.60} \tag{1.32}$$

where:

E_s: Elastic modulus of soil

E_p: Elastic modulus of pile

d: pile diameter

1.4.4 Non – Linear Stiffness of Foundations

If the soil behavior was elastic – perfectly plastic, assessing the linear stiffness and failure load would be enough to fully predict its response to applied loading. However, soil non –

linearities start to develop significantly before the foundation – soil system reaches its ultimate bearing capacity; they can appear at relatively small strain levels γ, of the order of 10^{-4}. In addition, geometrical non – linearities such as uplifting take place, as no tension can be carried on the soil – foundation interfaces.

Based on the above, it is obvious that assessing the non – linear stiffness of foundations can lead to more accurate predictions of the overall response of a soil – foundation – superstructure system. Furthermore, recent study has proven that the generation of controlled non – linearities on the soil – foundation interfaces can offer significant energy dissipation during strong seismic events, thus improve the seismic response of structures.

Vertical loads play a very important role in the non – linear rocking response of a foundation. I turns out that lightly loaded footings tend to uplift while heavily loaded footings mobilize a strongly inelastic soil response underneath them, with minor uplifting. This effect can be seen in **figures 1.31 a** & **b**, which depict the results of numerical pushover analyses of shallow footings with different vertical factors of safety [Gazetas *et al.,* 2013]. Specifically, an important observation is that footings with a large factor of safety (F.S. = 20) exhibit a larger initial rocking stiffness, but smaller moment bearing capacity. This can be attributed to the fact that heavier loads cause inevitable non – linearities on the underlying soil, which cause the initial rocking stiffness to degrade. On the other hand, vertical loads are necessary for moment capacity of surface footings, as they counterbalance the inability of tension transition via the soil – foundation interface. The threshold beyond which soil inelasticity due to vertical loads begins to deteriorate the ultimate moment capacity is traditionally FS = 2.

A convenient way to present stiffness degradation of foundations, is to plot it against the angle of rotation for different values of FS, as seen in **figure 1.34**. Note that stiffness degradation begins earlier in foundations with high values of FS, due to the inability of the low vertical loads to prevent uplifting. Interestingly, the above remarks hold true for the hybrid foundation examined in this study, as can be seen in Chapter 4 of the thesis. The dependencies of the footing on the acting vertical load are adopted by the hybrid foundation, as a result of the vertical decoupling utilized which allows the footing to sustain the total vertical load and settle autonomously.

CHAPTER 1: FIGURES

Literature review

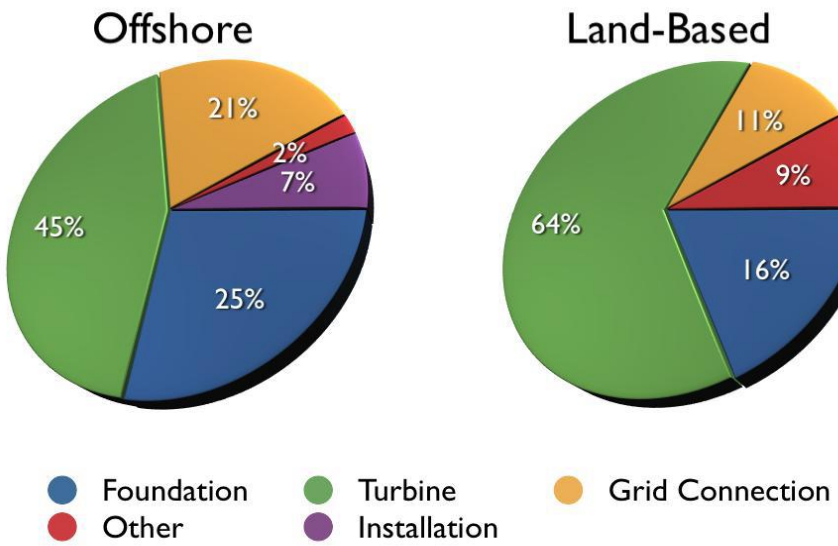

Figure 1.1. Typical cost comparison between onshore and offshore wind turbines [Kühn, et al., 1998]

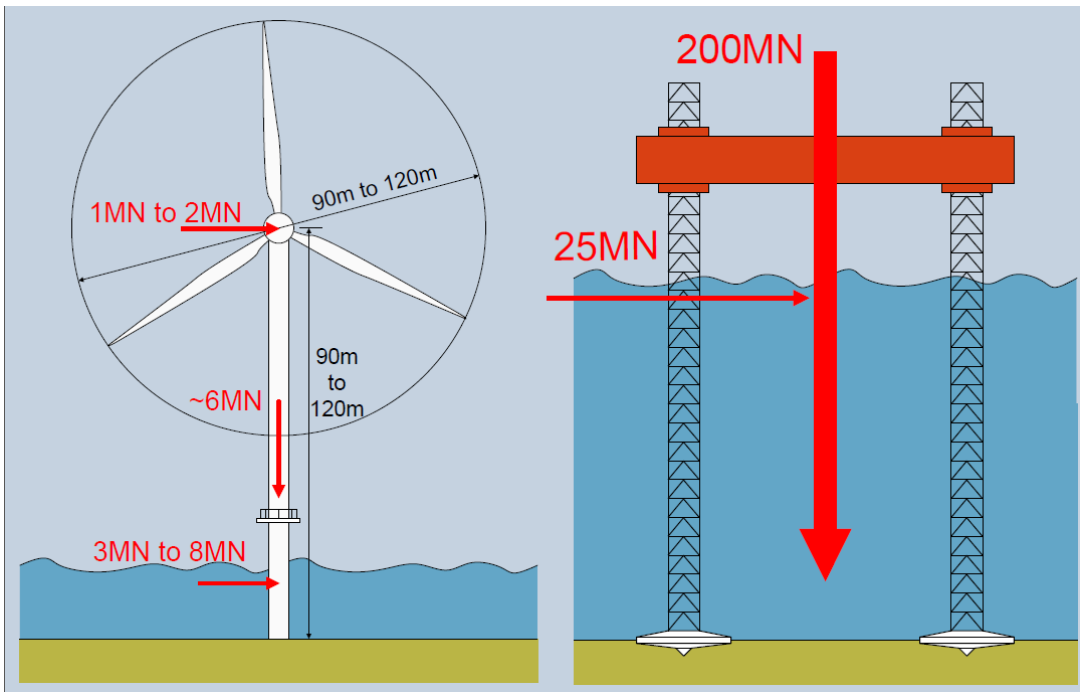

Figure 1.2. Comparison between a typical offshore wind turbine and a jack – up platform [Byrne, 2011]

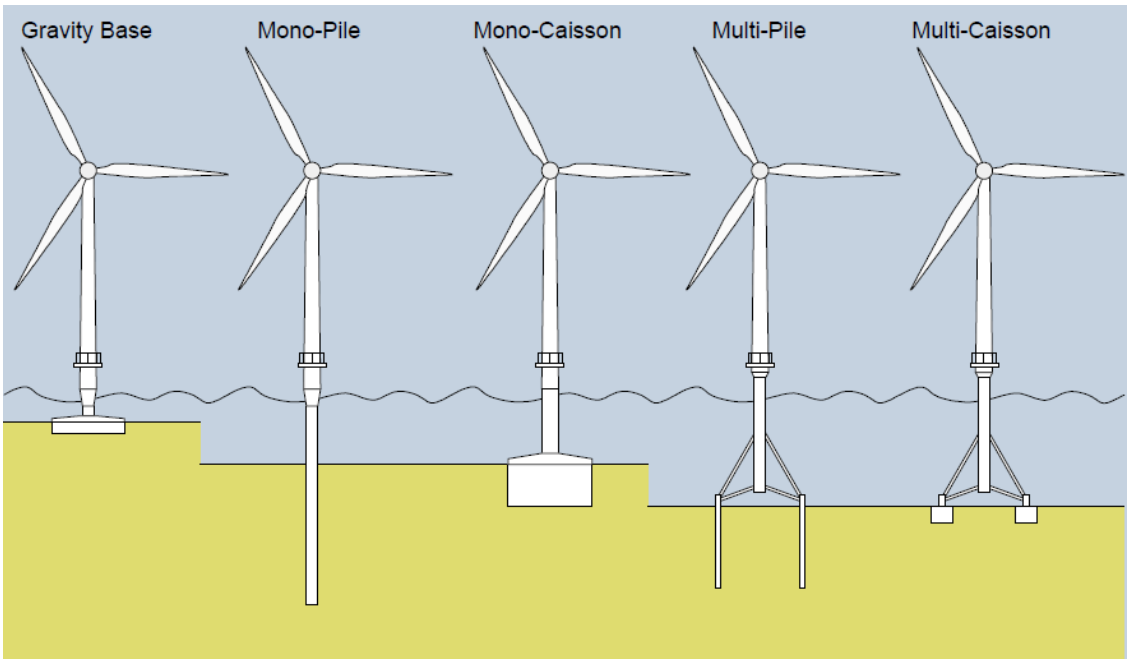

Figure 1.3. Typical foundations for offshore wind turbines. [Byrne, 2011]

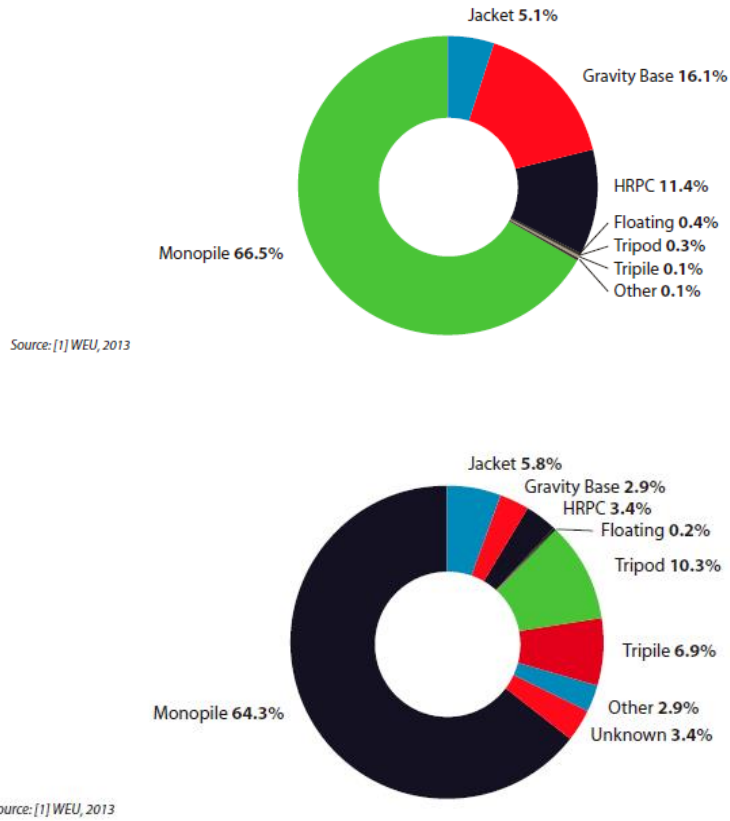

Figure 1.4. Market share of wind turbine foundations. Top: Operating turbines. Bottom: Under construction [Wind Offshore Foundations Report 2013]

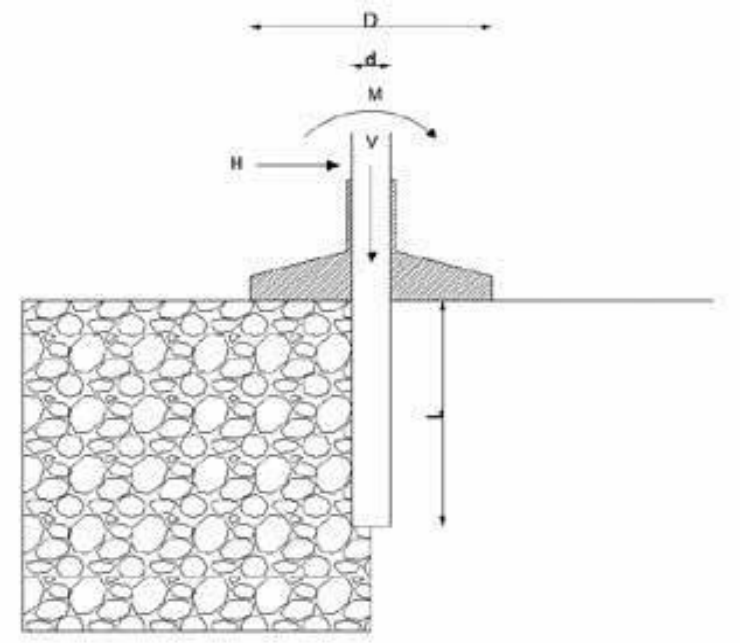

Figure 1.5. Schematic illustration of the hybrid monopile – footing system examined by Stone et al. (2013).

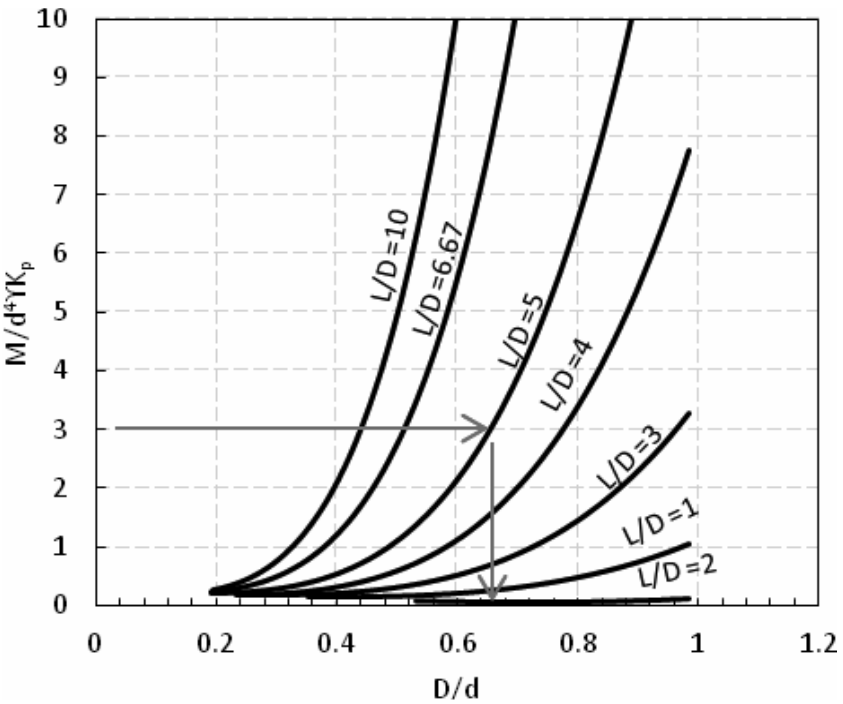

Figure 1.6. Example of a design chart for the hybrid system, developed using analytical and numerical methods. [Stone et al. 2013]

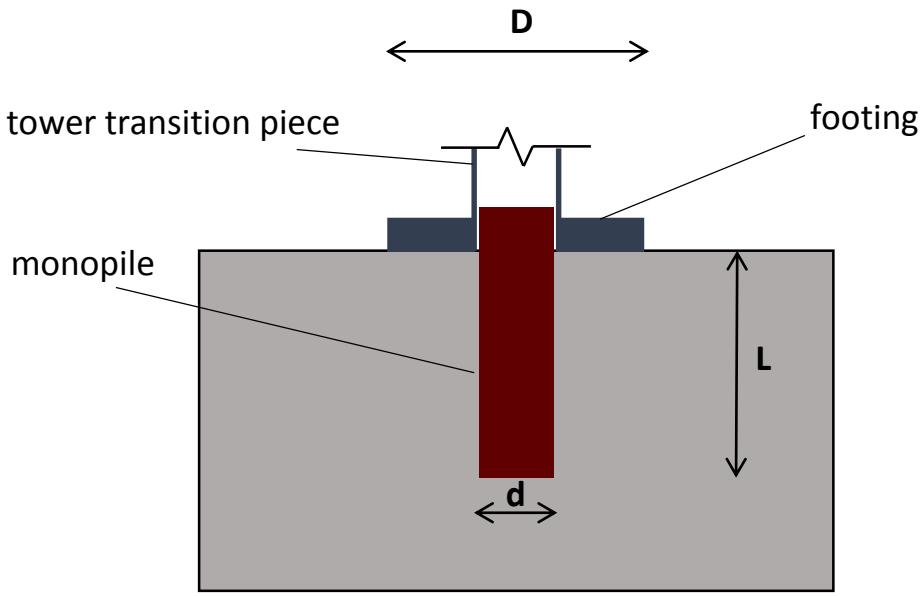

Figure 1.7. Schematic illustration of the hybrid monopile – footing system examined in the current thesis.

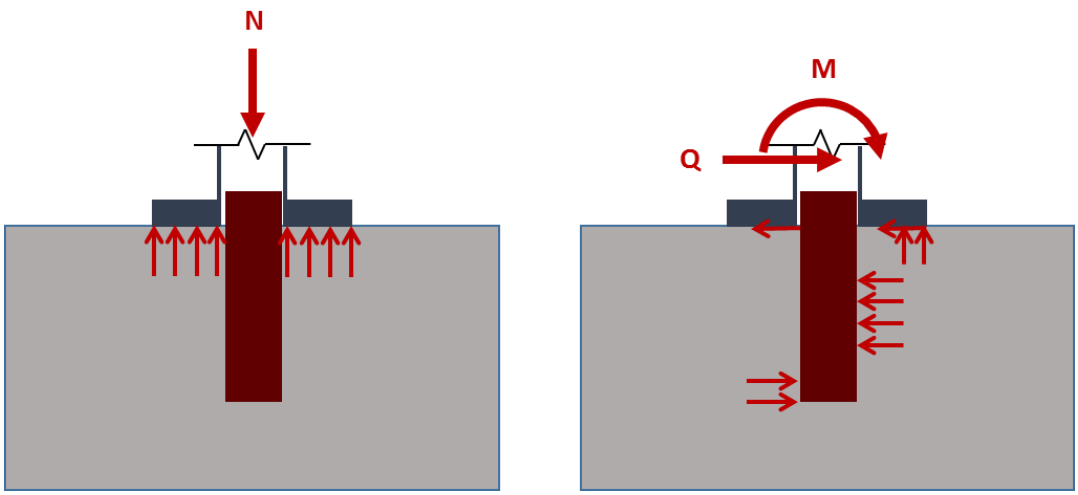

Figure 1.8. Schematic illustration of the load transfer mechanisms of the examined hybrid foundation system under vertical and lateral loading.

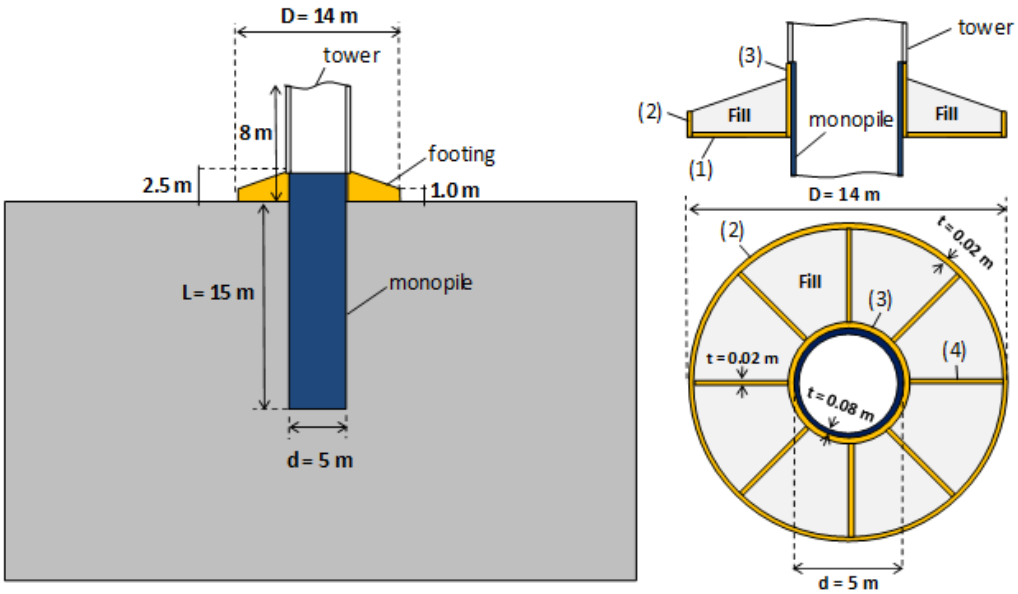

Figure 1.9. Schematic illustration of the hybrid monopile – footing foundation system invented by Anastasopoulos (2013).

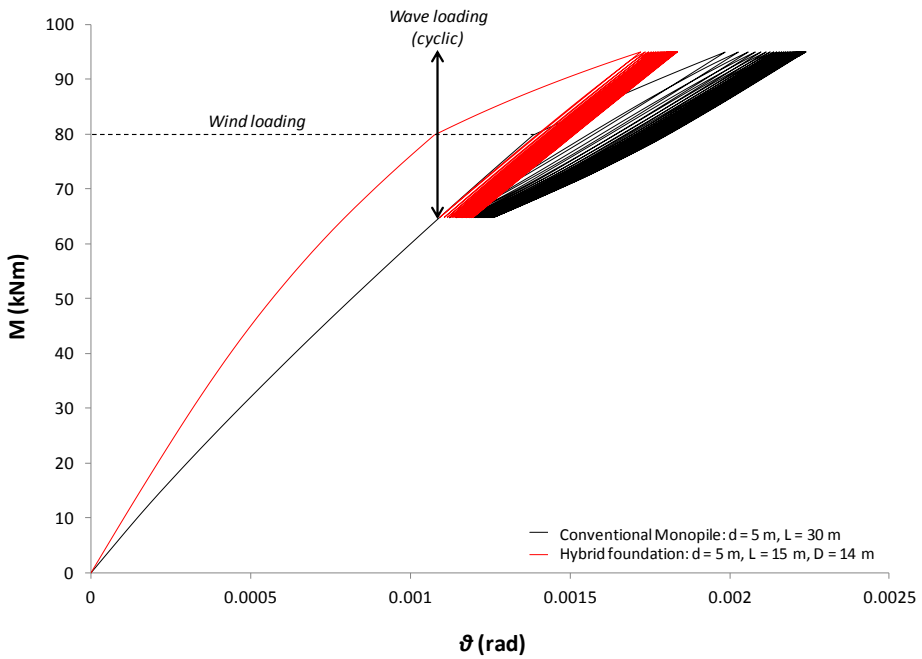

Figure 1.10. Comparison of conventional monopile foundation to the hybrid foundation invented by Anastasopoulos (2013). Performance in terms of moment – rotation due to wind and wave loading.

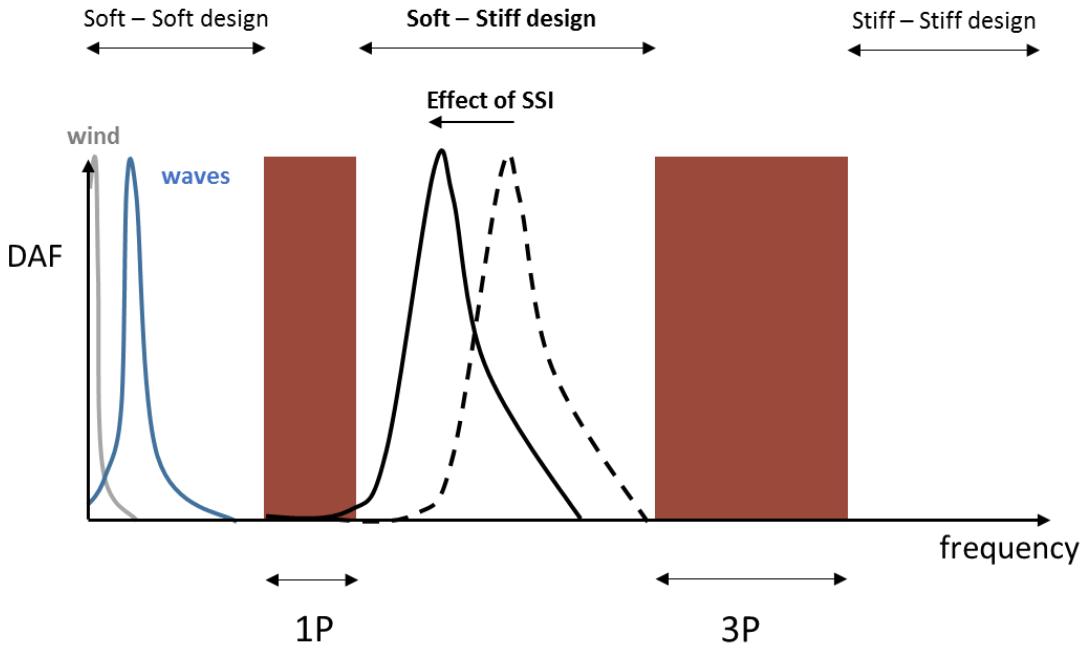

Figure 1.11. Schematic illustration of the main excitation frequencies of an offshore wind turbine, along with the effect of soil – structure interaction on the response of wind turbine designed as "soft – stiff".

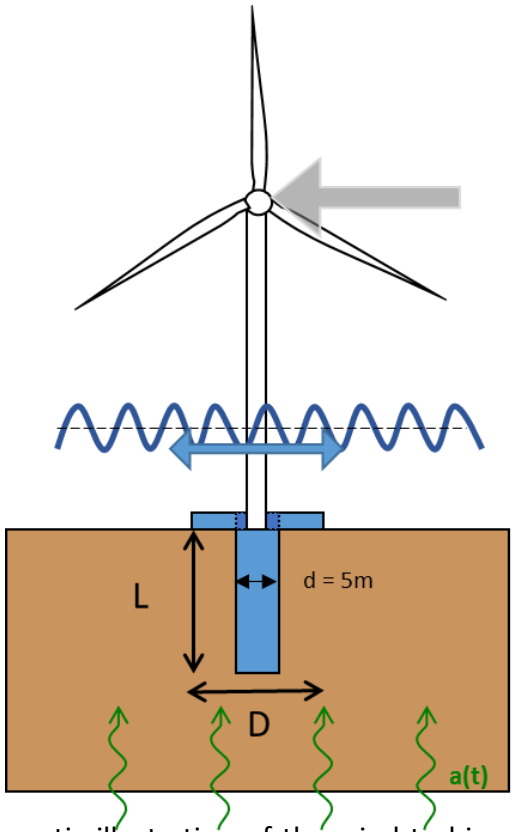

Figure 1.12. Schematic illustration of the wind turbine loads examined in the current thesis.

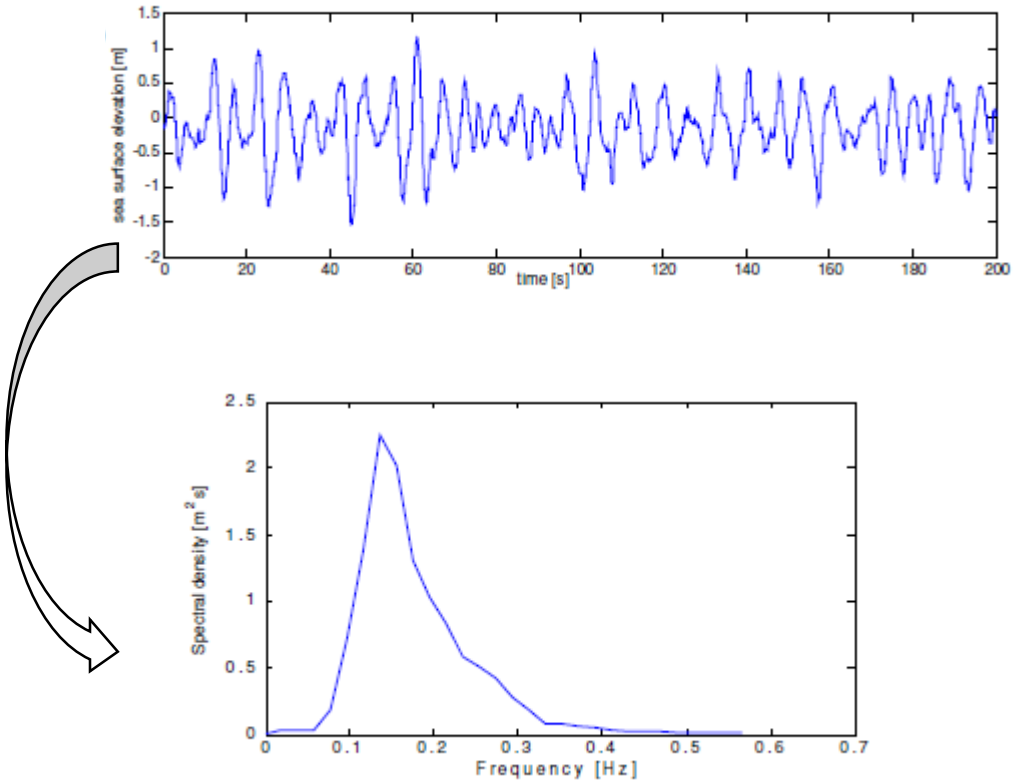

Figure 1.13. Transformation of a sea elevation time series (top) into a wave spectrum (bottom) [Van Der Tempel, 2005]

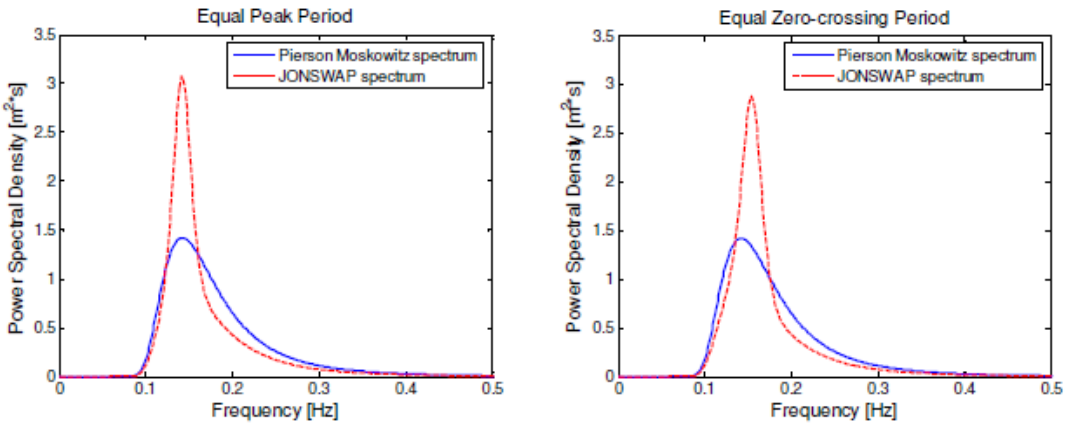

Figure 1.14. Pierson-Moskowitz (PM) and JONSWAP (JS) spectra for *Hs* = 1.5 m and *Tz* = 5 s. left: equal peak period, right: equal zero-crossing period. [Van Der Tempel, 2005]

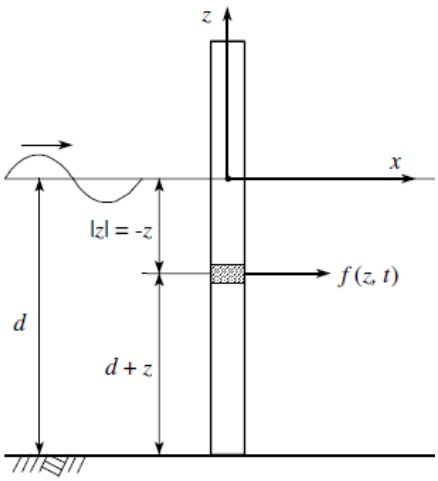

Figure 1.15. Schematic illustration of a slender cylindrical tube subjected to hydrodynamic loading [Van Der Tempel, 2005]

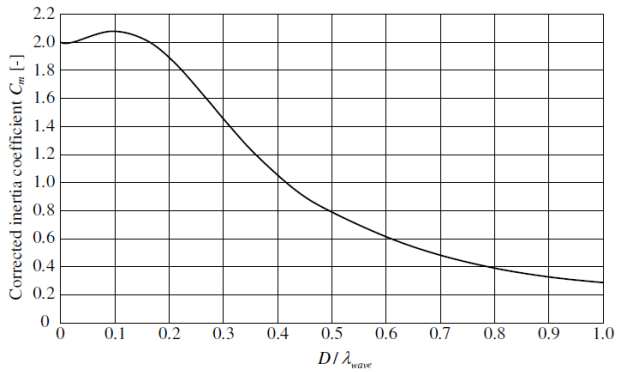

Figure 1.16. Corrected inertia coefficient due to diffraction. [Van Der Tempel, 2005]

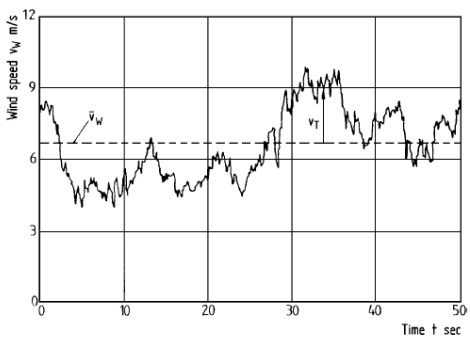

Figure 1.17. Example of measured wind speed .
time history [Hau, 2005]

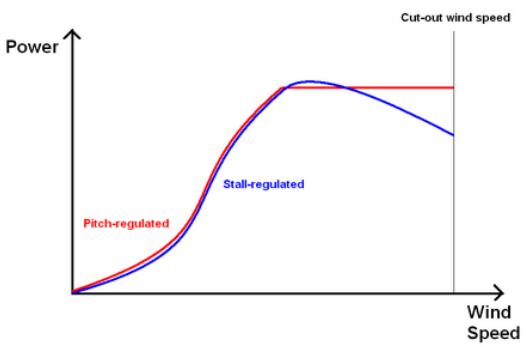

Figure 1.18. Power output of pitch – regulated and stall – regulated wind turbines. [WindSim]

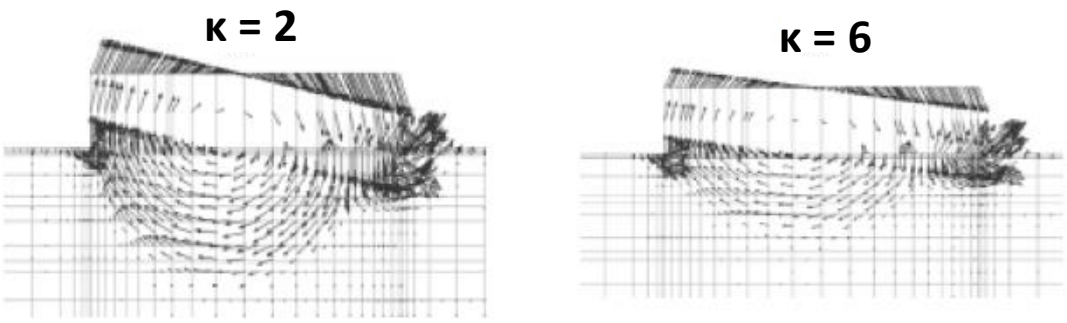

Figure 1.19. Effect of soil heterogeneity on the failure mechanisms under moment loading. ($V = 0.25V_{ult}$). [Gourvenec, 2007]

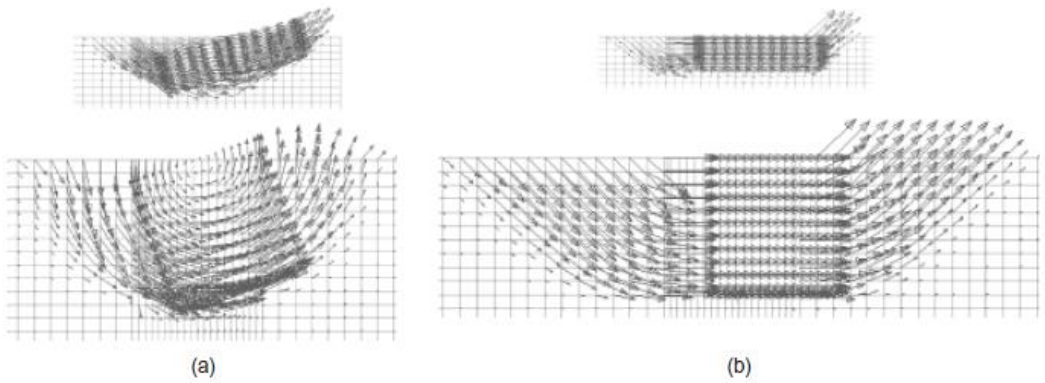

Figure 1.20. Failure mechanisms under horizontal load for D/B = 0.25 and 1. (a) H_{ult} (θ free) (b) H_{max} (θ constrained). [Gourvenec, 2008]

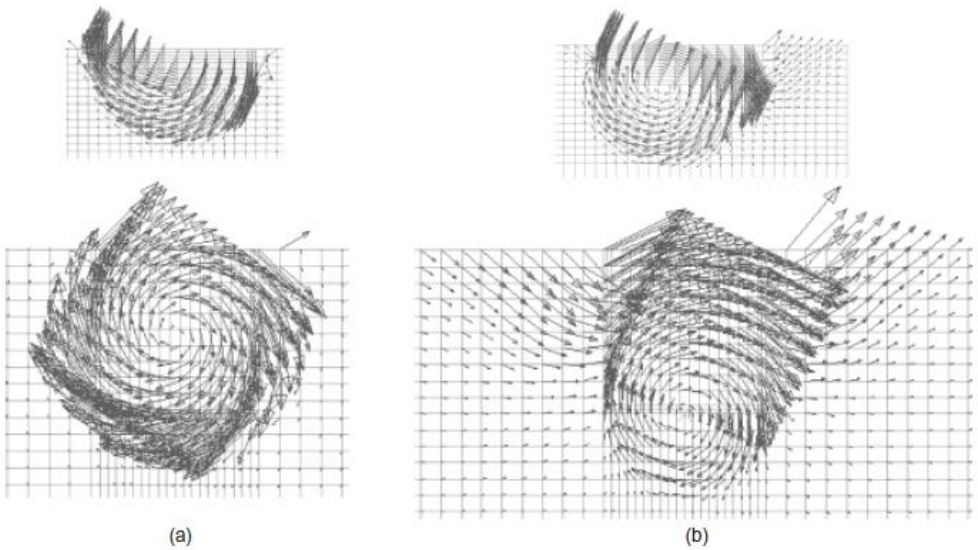

Figure 1.21. Failure mechanisms under moment load for D/B = 0.25 and 1. (a) M_{ult} (u free) (b) M_{max} (u constrained). [Gourvenec, 2008]

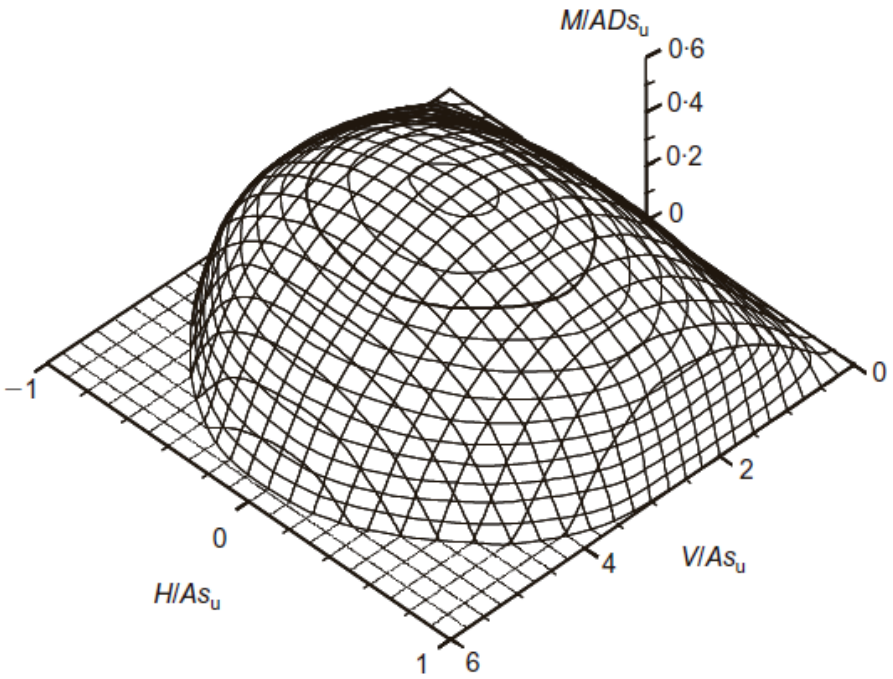

Figure 1.21. Three – dimensional failure envelope for general loading of a circular surface foundation with a zero – tension foundation/soil interface; ur

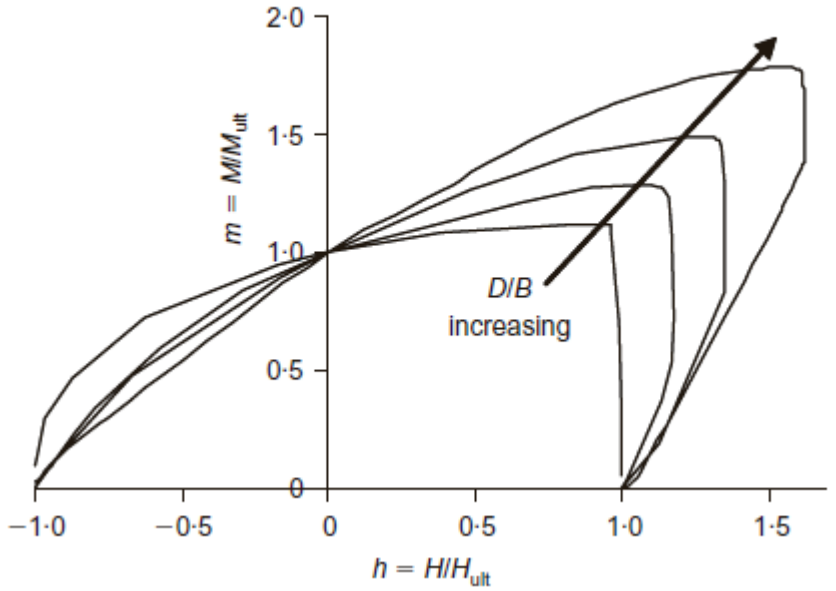

Figure 1.22. Effect of embedment on the failure envelope for horizontal and moment loading (V = 0). [Gourvenec, 2008]

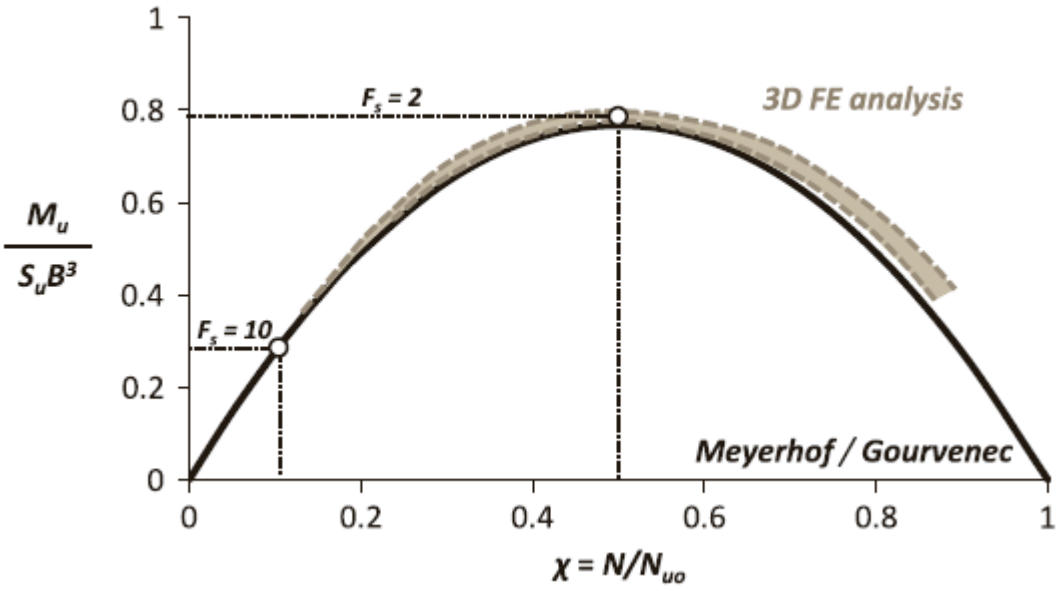

Figure 1.23. Moment – Vertical Load interaction for a surface foundation and comparison with previously published results. [Gazetas *et al.* 2013].

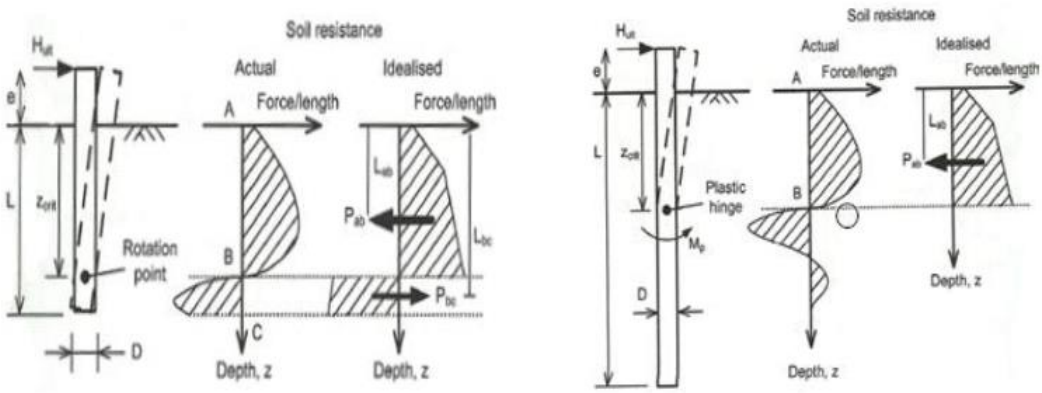

Figure 1.24. Failure mechanisms for short (left) and long (right) piles. [Randolph & Gourvenec, 2011]

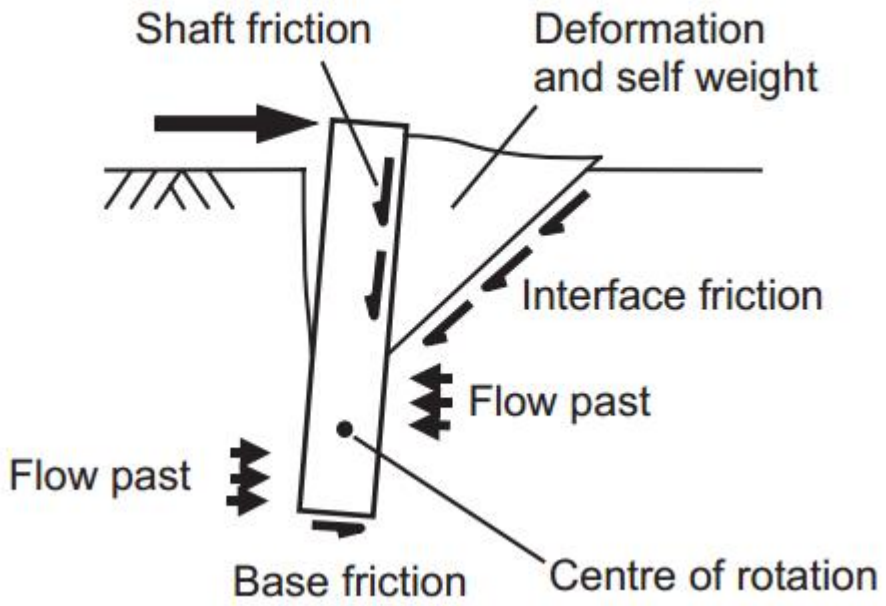

Figure 1.25. Short pile failure mechanism – components of resistance. [Fleming *et al.*, 2009]

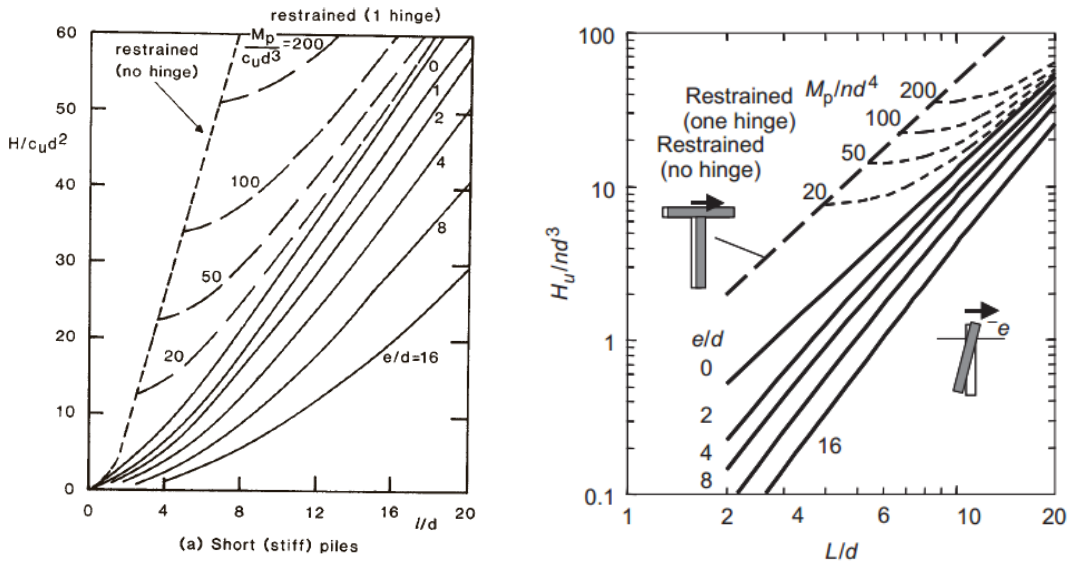

Figure 1.26. Short pile design charts for lateral capacity. Left: uniform clay. Right: Linearly increasing resistance with depth. [Fleming *et al.*, 2009]

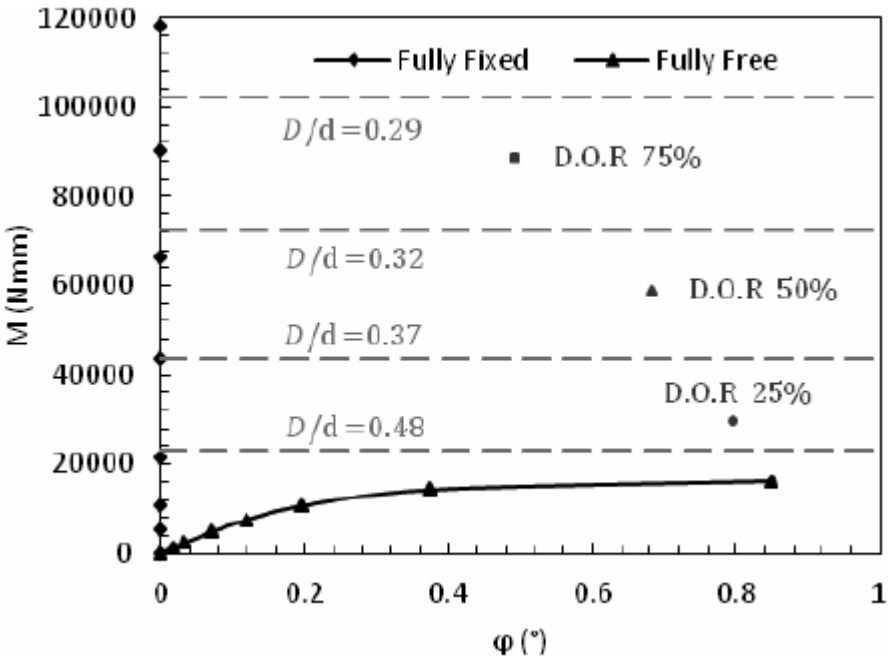

Figure 1.27. Moment – rotation plot for a hybrid system with different pile to footing ratios. The dashed lines represent the analytically calculated moment bearing capacity. [Stone *et al.,* 2013].

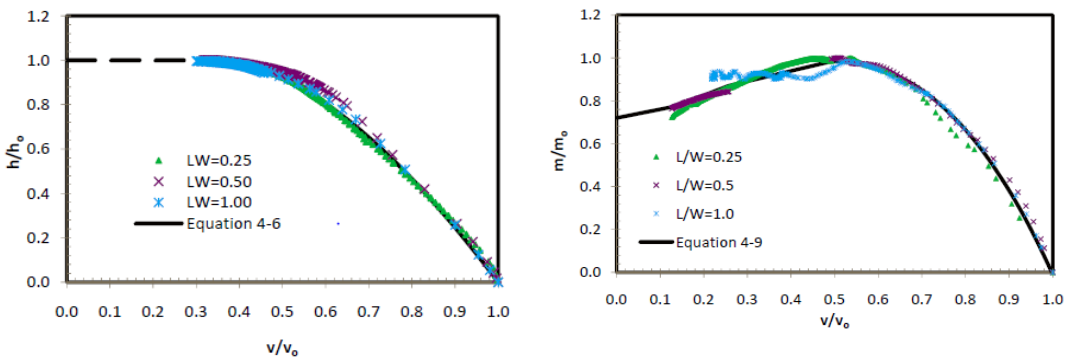

Figure 1.28. Curve fitting of horizontal force – vertical load (left) and moment – vertical load (right) interaction diagrams for hybrid foundations of several pile length to footing breadth ratios and tensionless (instant breakaway) conditions. [El – Marassi, 2011]

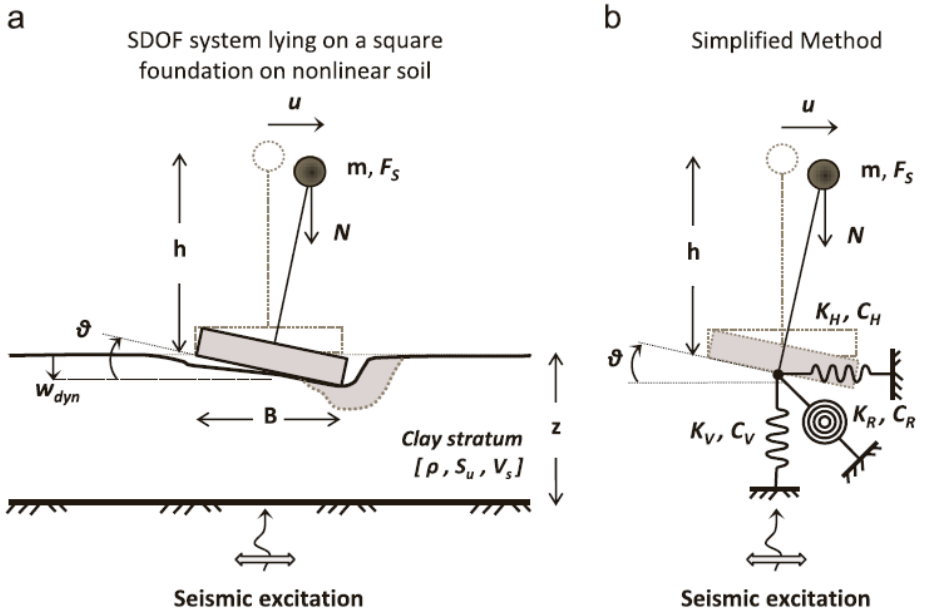

Figure 1.29. a) SDOF system lying on a square surface foundation on a homogeneous clay stratum; simplified method where the soil– foundation system Is replaced by a nonlinear rotational spring KR, accompanied by a linear dashpot CR, as well as linear vertical and horizontal springs and dashpots, KV and CV , and KH and CH, respectively [Anastasopoulos & Kontoroupi,2013]

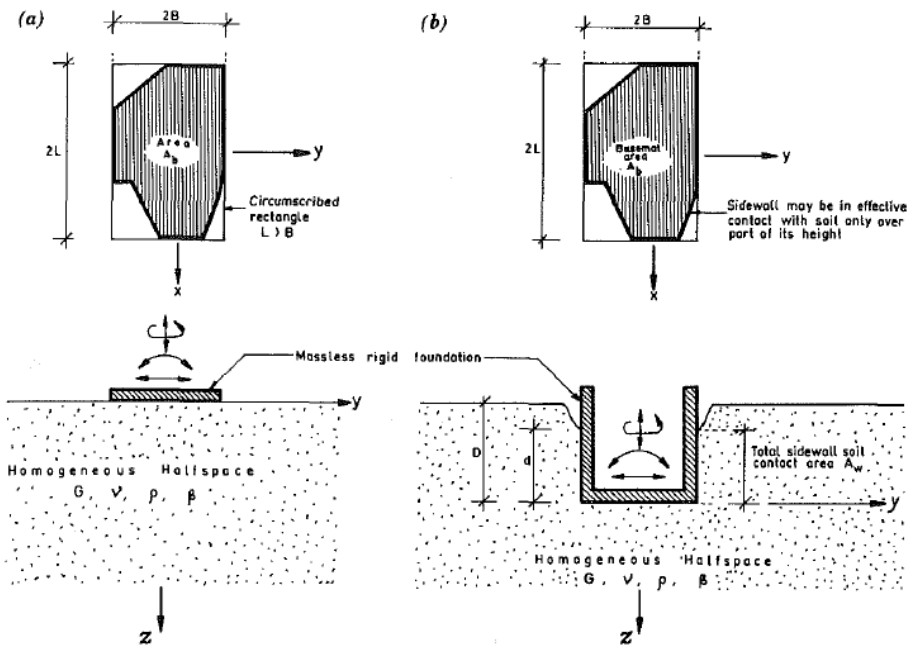

Figure 1.30. Surface and embedded foundation of arbitrary shape examined by Gazetas (1991)

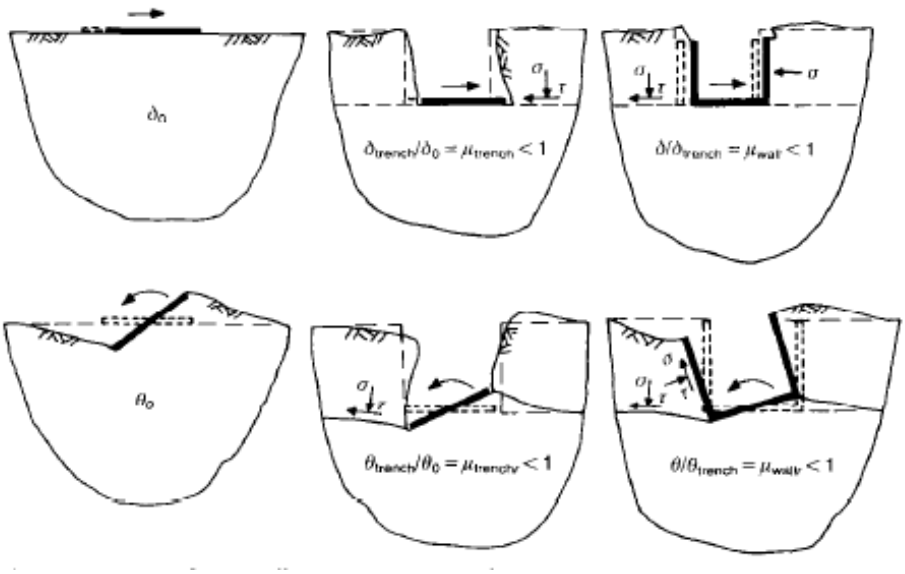

Figure 1.31. Illustration of trench and sidewall effects for embedded foundations. [Gazetas, 1988]

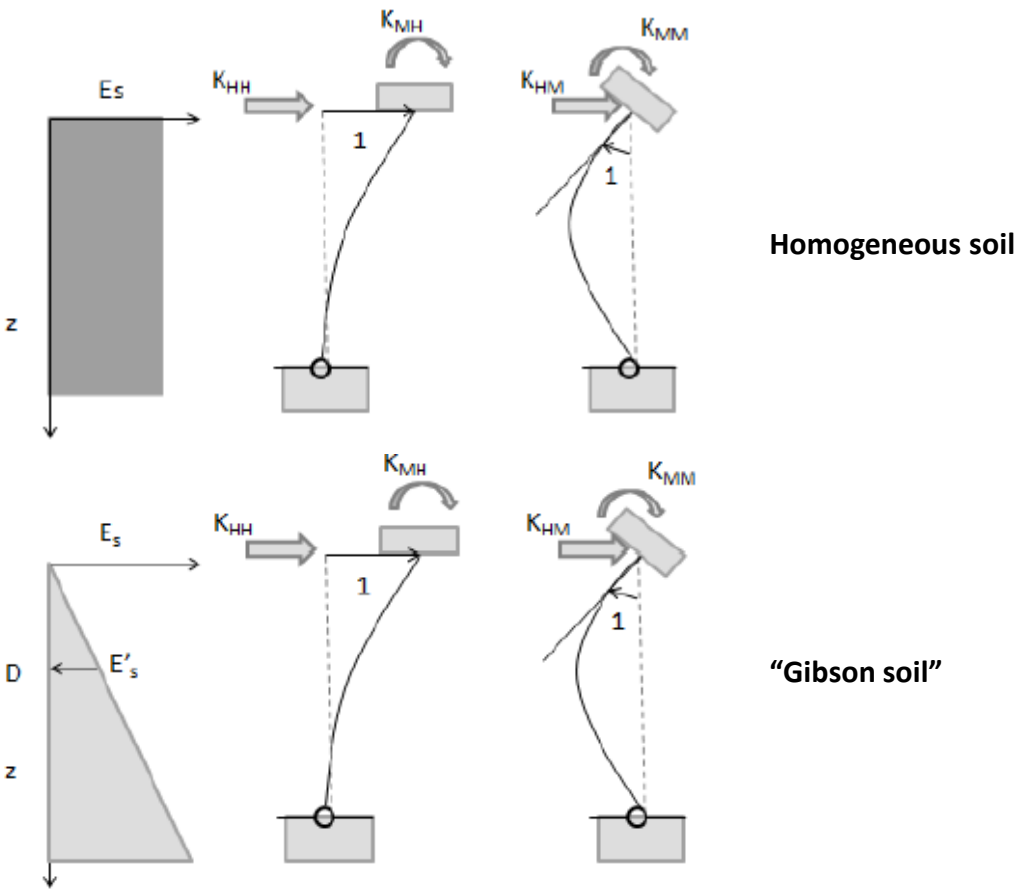

Figure 1.32. Definition of lateral stiffness components for long piles laying on two different soil types. [Gazetas, 1991]

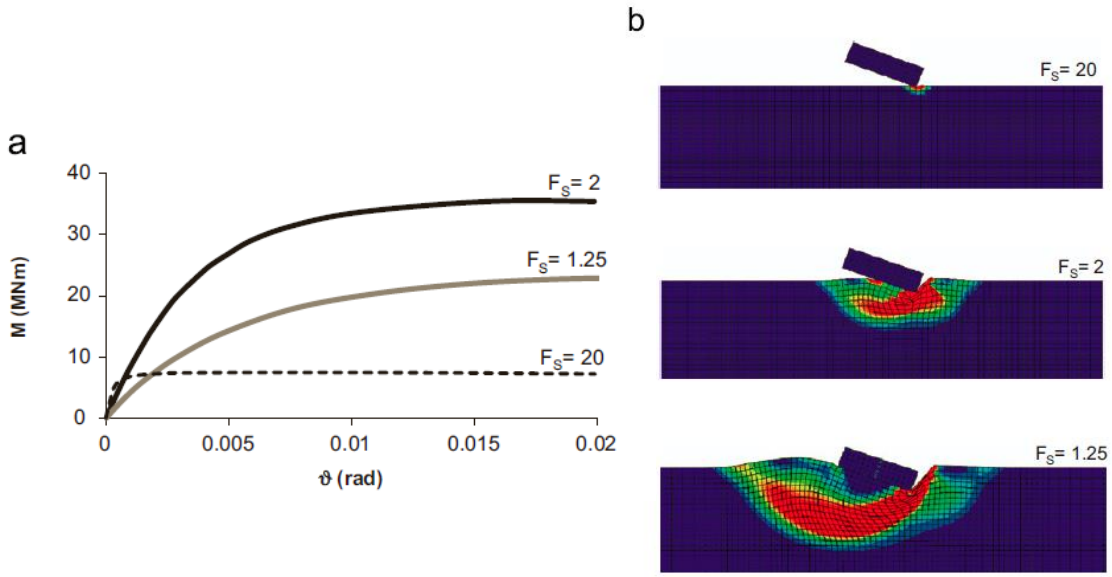

Figure 1.33. a) moment – rotation diagrams for surface footings with different factors of safety against vertical loads. **b)** failure mechanisms in terms of plastic strain contours. [Gazetas *et al.,* 2013].

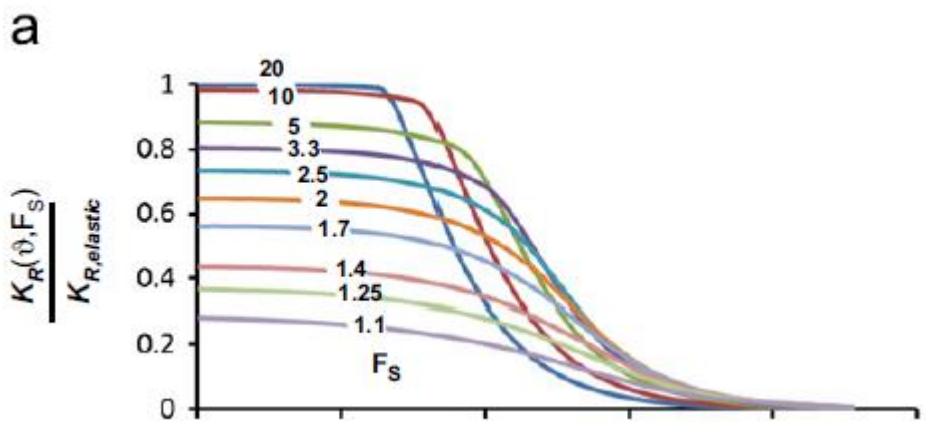

Figure 1.34. Rocking stiffness of a strip footing with respect to rotation amplitude and safety factor against vertical loading. [Gazetas et al., 2013]

CHAPTER 2

Problem Definition, Model and Method of Analysis

2.1 Problem Definition
2.2 Finite Element Model
2.3 Soil Behavior
2.4 Method of Analysis

2.1 Problem Definition

The current thesis deals with numerical analysis of a novel hybrid foundation for offshore wind turbines. The concept is to combine a monopile with a surface foundation as can be seen in **figure 2.1**. As aforementioned, a limited number of researchers has worked in this direction, investigating the performance of such configurations [El-Marassi, 2011; Stone & Newson, 2007; Arshi & Stone, 2011]. It is proven that adding a surface footing to the top of a monopile can enhance its capacity. Considering that monopiles are a widely – applied solution to founding offshore wind turbines at medium depths, the analysis of a conventional monopile is also included in this study as a benchmark.

As reported in chapter 1, when including interface non-linearities in the analysis of shallow footings dead loads play a major role both in moment and horizontal capacities. This beneficial effect is diminished when the footing is rigidly connected to a monopile. The latter has a vertical stiffness quite larger than the one of the footing, so the biggest part of the vertical load is transferred to the pile. In addition, consolidation of clays may lead to the same effect. In order to overcome these obstacles the hybrid foundation of this study is disconnected from the pile in the vertical sense, as shown in **figure 2.2**. This release of the vertical degree of freedom allows relative translation of the footing through the pile, forcing it to carry the total vertical load while the pile remains uncharged. The connection of the two components in the remaining degrees of freedom (lateral and rotational) is rigid. Exact modelling of this connection in the numerical analysis is described later on this chapter.

The scope of this study is to investigate the performance of such hybrid foundations and directly compare them against the monopile. Response of the foundations is examined in undrained conditions, on two different cohesive soil profiles: A homogeneous soil with a constant undrained shear straight of Su = 60 kPa and an inhomogeneous soil with linearly increasing shear strength, as shown in **figure 2.3**. The soil – foundation interface is modelled non – linear, cannot carry tension and follows a frictional coulomb law.

Figure 2.4 depicts the geometrical parameters of the problem as well as the sign convention. Various hybrid foundations are examined, in an effort to relate their geometry and design to the system's bearing capacity and stiffness. Varied parameters are the length of the monopile L and the diameter of the footing D. Diameter of the monopile d and height of the footing h are kept constant at 5m and 2m respectively throughout the whole thesis.

In the first part of the study (chapters 3 & 4) the results are presented separately for various monopile lengths and footing diameters, so that contribution of each component to the total hybrid response is better comprehended. In the second part (chapters 5 & 6) the whole superstructure-foundation-soil system is examined and foundation geometries are presented in a more standardized manner (i.e. D15 - L15 stands for a hybrid foundation with monopile length L = 15 m and footing diameter D = 15 m).

To begin with, a set of analyses, presented in chapter 3, investigates the bearing capacity of the soil – foundation system. Both one-dimensional and combined loading are examined, in an attempt to understand the response of the system under the complex M-Q-N regime imposed by the superstructure and extract the basic physical mechanisms behind it. Chapter

4 deals with stiffness of the soil – foundation system. The initial (elastic) stiffnesses, as well as non-linear stiffness degradation with increasing deformations are extracted and depicted in charts. Preliminary quantitative correlations are produced between the stiffness components and the basic geometrical parameters of the problem (D, L). The second part of the thesis addresses the response of the total soil-foundation-superstructure system under environmental excitations, taking account for P – δ effects. Chapter 5 includes monotonic and slow-cyclic loading of wind turbines due to waves and wind. Three wind turbines of 2 MW, 3.5 MW and 5 MW are examined here (**figure 2.5**), and their dimensions are shown in **table 2.1**. Finally, chapter 6 deals with the dynamic analysis of 3.5 MW wind turbine, subjected to the Takatori seismic motion. More details are provided in each chapter.

2.2 Finite Element Model

All of the analyses are three –dimensional and were conducted using the commercially available finite element code ABAQUS, v. 6.11 and 6.13 (2013). Due to the symmetrical nature of the problem, only half of the soil, superstructure and foundation needs to be modeled.

The mesh is semi- cylindrical and its radius in polar coordinates is equal to 37.5 m, 3.75 times the radius of the largest footing used. The soil height is 40 m for all models except the 35 m monopile benchmark, for which it is 45m. The mesh is divided into 26 sectors and the total number of finite elements is of the order of 35000.Two of the models used are depicted in **figure 2.6**.

The clay stratum is modelled using 8-node hexahedral continuum elements (C3D8), with a corresponding constitutive model. Undrained shear straight is equal to S_U = 60 kPa for the homogenous soil stratum and for the inhomogeneous S_{U0} = 30 kPa at the seabed level with a linear increase of 5 kPa per meter of depth. The soil density is taken ρ’ = 1 t / m^3 which corresponds to a submerged specific weight of 10 kN / m^3.

The monopile is considered driven and has a pipe cross section with a diameter d = 5m and wall thickness t = 0.08m in order to validate the model against previous work [Christou L. 2012]. In fact, Christou conducted parametric analyses and assessed the chosen ratio d / t = 62.7 as quite reasonable, considering capacity and structural steel cost. Assuming that the pile is filled with soil during pile driving, it has a rather large moment capacity. Thus, and to focus on the soil failure mechanisms, the pile is considered linear elastic. To model the pile, linear beam elements (B31) are used, to form a central beam on which the full cross section is assigned. Discretization is 1m. For the soil fill, a 5m diameter semi-cylinder of soil is defined, with the nodes on each meter of depth z rigidly connected to the pile beam element node on that depth, using TIE constraints (**figure 2.7**). Since the full cross section is assigned, elastic modulus and density of the pile steel have half the actual values; Es =105 GPa and ρs = 6.85/2 = 3.425 t /m^3. 6 monopile lengths are examined for the hybrid foundation; L = 10 m, 15 m, 20 m, 25 m & 30 m. For the benchmark monopile, lengths of 30m and 35m were considered.

Height of the footing is h = 2m and the diameters examined are three; D = 11m, 15 m and 20 m. To model the footing, linear elastic 8-node hexahedral continuum elements (C3D8) are

used. The footing is circular with a circular hole in its center, with the examined outside diameter D and an inside diameter d = 5 m so that the pile can slide through it. It is assumed that the footing is fully rigid and it has an elastic modulus of E = 105 GPa. Unless otherwise stated, density is taken $\rho' = 1.5$ t/m^3 which corresponds to the submerged unit weight of reinforced concrete, $\gamma' = 15$ kN/m^3. The exact type of the shallow footing is not prescribed in this thesis, as it concerns any type of stiff pile cap. However, investigation of influence of the footing weight in the total performance of the foundation is interesting, and is conducted in parts of chapters 3 & 5. In fact, it is proven that the heavier footings respond better to the cyclic wave loads that excite the wind turbine throughout its lifetime and tend to accumulate smaller rotations.

The tower is modeled by using linear elastic beam elements (B31). Its elastic modulus is taken half of the modulus of steel (E'=105 GPa), and its section inertia as the one of the full section, so that the corresponding bending stiffness is (EI)' = EI/2. For the same reason the tower's distributed mass is taken half of the normally disturbed mass ($\mu' = \mu/2 = 4.25$ t/m). Steel density for the tower is increased from its normal value ($\rho's = 8.5$ t/m^3) to take account for the extra weight due to welds and other equipment of the tower. Tower head mass is different for each wind turbine examined.

The hybrid foundation is realized by connecting the two components with a spring array. The tower is based on the footing and the whole system is originally unconnected to the pile. The central node of the pile head is connected to the footing with five spring elements (SPRING2), one on each degree of freedom except the vertical translation w. The springs have infinite stiffness, so a rigid connection is ensured and the horizontal forces and moments are fully transferred to the pile top, while the vertical force is carried exclusively by the footing. The connection is sketched in **figure 2.8**.

Boundary conditions imposed at the model edges are constraint of the horizontal displacement towards any direction for the periphery faces of the model, constraint of out-of-plane movements for the nodes of the plane of symmetry (x-z face) and fully fixed displacements for the nodes at the model base. For the seismic problem in chapter 6, it was necessary to remove all boundary conditions from the peripheral nodes of the model, and tie them to a central node in the same depth z, in order to minimize wave reflections at boundaries (**figure 2.9**).

Each component of the hybrid foundation has a different contact surface with the soil. Interfaces are modelled using no - tension contact elements. They are both governed by a Coulomb friction law, which dictates that the maximum shear stress that can be developed is equal to the normal effective stress reduced by the friction coefficient as described by the expression:

$$\tau_{max} = K\tan\delta\sigma'_v = \mu\,\sigma'_v$$

The effective stress may not be directly correlated to the undrained shear strength in undrained conditions, but this type of frictional interface is deemed reasonable considering the pile is driven. The value of μ is taken 0.5 both for the footing and pile surfaces; this is a

rather unfavorable value which is chosen in order to minimize any doubts rising from the fact that the real contact conditions are hard to define.

Second order effects are taken into account for the analysis in chapters 4, 5 & 6.

2.3 Soil Behavior

The constitutive model used in the current thesis has a Von Mises failure criterion with combined kinematic-isotropic hardening law and associated plastic flow rule. This type of constitutive model is deemed appropriate to model the elastoplastic behavior of clays under undrained conditions, which is considered independent of the mean effective stress. A similar constitutive model is validated against laboratory tests for simulation of cyclic response of shallow foundations by Anastasopoulos et al. (2010).

The evolution of stresses is defined as:

$$\sigma = \sigma_0 + \alpha \qquad (2.1)$$

where σ_0 = the stress at zero plastic strain and α the "backstress", which defines the kinematic evolution of the yield surface in the stress space. The yield surface is defined by a function F:

$$F = f(\sigma - \alpha) - \sigma_0 \qquad (2.2)$$

f (σ – α) stands for the equivalent Mises stress with respect to the backstress.

The associated plastic flow rule determines the plastic flow rate

$$\dot{\varepsilon}^{pl} = \dot{\bar{\varepsilon}}^{pl} \frac{\partial F}{\partial \sigma} \qquad (2.3)$$

where $\dot{\bar{\varepsilon}}^{pl}$ = equivalent plastic rate. The meaning of the associated plastic flow rule is that the plastic strain vectors are perpendicular to the failure curve.

Two components are included in the evolution of stress:

1. An isotropic hardening component, which defines the evolution of the size of the yield surface as a function of the equivalent plastic strain $\dot{\bar{\varepsilon}}^{pl}$

   $$\sigma = \sigma_0 + Q_\infty (1 - e^{-b \dot{\bar{\varepsilon}}^{pl}}) \qquad (2.4)$$

   where Q_∞ and b define the maximum change of size of the yield surface and the rate of change with $\dot{\bar{\varepsilon}}^{pl}$ respectively. For Q_∞ = 0, size of the yield surface remains constant and the combined model is reduced to a kinematic hardening model.

2. A kinematic hardening component, the evolution of which is described by the following equation:

$$\dot{\alpha} = C\frac{1}{\sigma_0}(\sigma - \alpha)\dot{\bar{\varepsilon}}^{pl} - \gamma a\dot{\bar{\varepsilon}}^{pl} \qquad (2.5)$$

Where C stands for the initial kinematic hardening modulus ($C = \sigma_y\varepsilon_y = E$) and γ is a parameter determining the rate of decrease of kinematic hardening with increase of plastic strain. The first term of the equation represents Ziegler's (1959) kinematic hardening law and the second term with γ is introduced to take account for the nonlinearity of the evolution law.

Figure 2.10 illustrates the evolution of the two hardening components for uniaxial and multiaxial loading. The parameter α of the kinematic hardening component remains bounded in a cylinder with radius:

$$\sqrt{\frac{2}{3}\frac{C}{\gamma}} = \sqrt{\frac{2}{3}\,\alpha_s} \qquad (2.6)$$

where α_s is the value of α at saturation. The bounding of the yield surface demands that all stress points are enclosed in a circle of radius of $\sqrt{\frac{2}{3}\,\sigma_\gamma}$, where σ_γ is the maximum yield stress at saturation. At large plastic strains when σ approaches σ_γ, the magnitude of α becomes equal to $\alpha_s = C / \gamma$, $(\sigma - \alpha)$ approaches σ_0 and $\dot{\alpha}$ tends to zero.

The maximum yield stress is defined according to the Von Mises criterion:

$$\sigma_y = \sqrt{3}\,S_U \qquad (2.7)$$

Finally, since $\sigma_\gamma = c/\gamma + \sigma_0$, parameter γ is defined

$$\gamma = \frac{C}{\sqrt{3}S_U - \sigma_0} \qquad (2.8)$$

The parameter C is the Young's modulus for very small strains and is taken $C = E = 1800S_U$, a value corresponding to a rather stiff clay. For the inhomogeneous soil, the stratum is divided into layers of 2.5 m each, and the parameters C, σ_γ and γ are calibrated for each layer according to the shear strength profile.

2.4 Methods of Analysis

2.4.1 Sign Convention & Symbols

Sign convention followed in the current study is shown at **figure 2.4**. The basic symbols used are N for vertical (axial) force, Q for horizontal (shear) force and M for moment. Correspondingly, *w*, *u* and ϑ stand for settlement, horizontal displacement and rotation respectively. It is worth noting that settlements are positive and uplift is negative, as the Z axis is faced downwards.

2.4.2 Bearing Capacity & Interaction Diagrams

To extract bearing capacity curves for uniaxial loading, a prescribed displacement is imposed at the center of the foundation lid and the reaction forces are given by ABAQUS at the same

point. The analyses are carried out in steps, where in the first step the dead loads of soil are imposed in a geostatic manner, in the second step dead loads of the hybrid foundation and of a typical superstructure are imposed and in the third step the prescribed displacement until failure. It was chosen to conduct the analyses for a typical 3.5 MW superstructure dead load, in order to obtain results that are relevant to the wind turbine problem. This is not the case for the vertical load – settlement curves, which were extracted without any dead load. P – δ effects are not taken into account.

The interaction diagrams under combined loading are produced by a displacement – controlled method, first introduced by Bransby & Randolph (1997) and is believed to extract quite accurately the failure envelopes. Fixed displacement ratios of u/w, u/θd and w/θδ was imposed to extract the Q-N, Q-M and N-M interaction diagrams respectively. For each failure envelope, many displacement probes are examined, each terminating on the failure envelope. Finally the termination points during failure of each displacement probe are connected to form the failure envelope. The weight load of a 3.5 MW wind turbine is first imposed, only for the M-Q interaction diagram. The analyses in the Q-N and N-M loading planes are conducted without any dead load. P – δ effects are not taken into account.

2.4.3 Foundation Stiffness

To define the foundation stiffness a series of analyses were conducted, imposing a gradually increasing displacement at the center of the foundation lid while keeping the other degree of freedom constrained. A 3.5 MW superstructure is also considered here, in an effort to produce results one step closer to practical design. At the end of the chapter, the same analyses were conducted for each component of the hybrid foundation separately in order to examine their contribution to the elastic stiffnesses as well as to stiffness degradation. More details are provided in chapter 4.

2.4.3 Monotonic & Cyclic Loading

Three turbine towers are examined against both monotonic and cyclic loading (2 MW, 3.5 MW & 5 MW). For monotonic loading analyses the tower is modelled with infinite stiffness, so that deformations are concentrated at the foundation. The loading consists of a typical pushover analysis, imposing a horizontal displacement at the top of the tower until failure. The bending moment at the tower base is reported, taking account for the P – δ effects. In addition, a pushover analysis is conducted by imposing a horizontal displacement until failure at +8m above mud line, which is considered the wave load application point.

Concerning cyclic loading, two cases are examined as can be seen in **figure 2.11**. The first case involves force – controlled wind cyclic load imposed at the top of each tower. This type of loading may represent total direction change of the turbine's rotor – nacelle assembly, which is possible in some wind turbine models and aims in capturing the direction of the prevailing wind. The second scenario is monotonic wind loading and cyclic loading induced by waves; the cyclic wave force is imposed at the wave load application point, which is located

approximately 8 m from the mud line for a mean sea level of 15 m. This is considered a typical load scenario for offshore wind turbines, as they are subjected to numerous wave cycles during their lifetime. In addition, wave periods of approximately 2-10 sec are way smaller than wind periods which are of the order of minutes, so it is deemed realistic to keep the direction of wind load constant while the waves are cycling. In reality, the nature of these loads is dynamic but in this study it is assumed that their excitation frequencies are not close to the eigenfrequencies of the system, so they can be imposed in a static manner. Most of the cyclic analyses are conducted for a limited (8-9) number of load cycles, in order to reduce the computational effort. Logarithmic extrapolations are provided and their validity is checked by a 40-cycle analysis presented in the end of chapter 5. More details, as well as the results from the analyses in terms of moment-rotation, settlement-rotation, accumulated rotations and settlements as well as logarithmic predictions for the wind turbine's lifetime are discussed in chapter 5. The lifetime of such projects is considered approximately 20 years.

2.4.4 Seismic Loading

For seismic assessment of hybrid foundations, the Takatori_090 (1995) record was used as an input ground motion. This is one of the most adverse motions ever recorded and is used clearly for comparing the response of two hybrid foundations to the conventional monopile, not to conduct a full dynamic – seismic analysis of a wind turbine. All the results in chapter 6 concern a 3.5 MW wind turbine lying on homogeneous soil.

CHAPTER 2: FIGURES

Problem Definition, Model and Method of Analysis

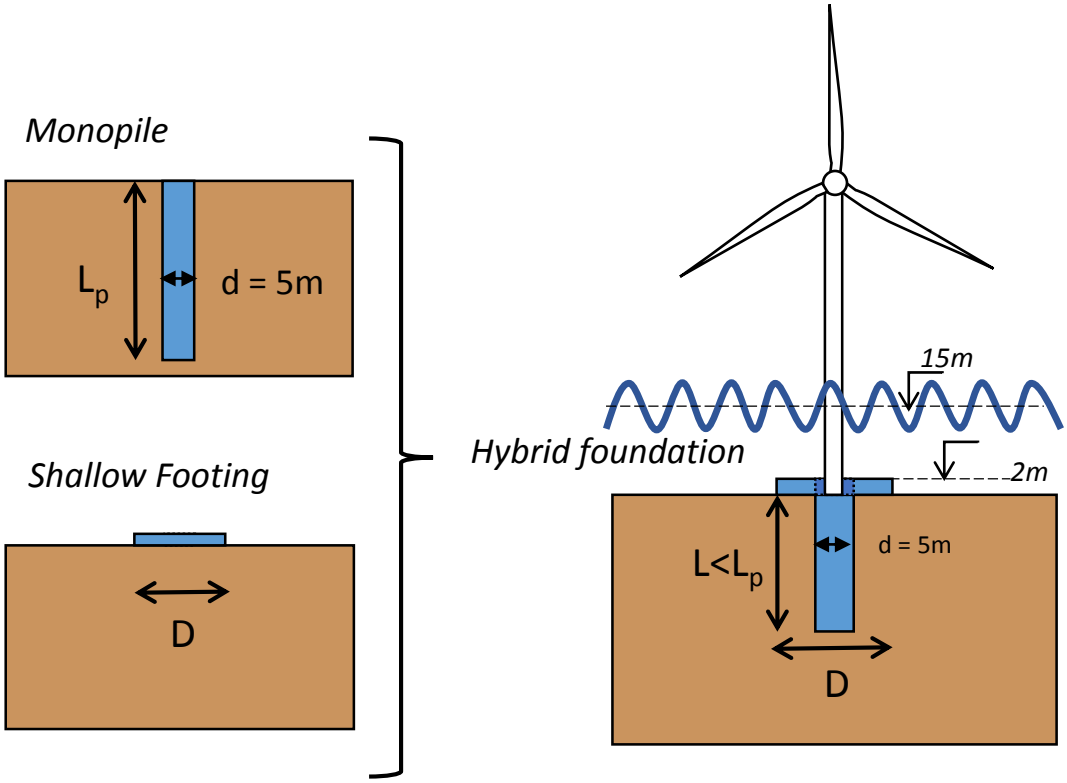

Figure 2.1. The hybrid foundation concept investigated in the current thesis.

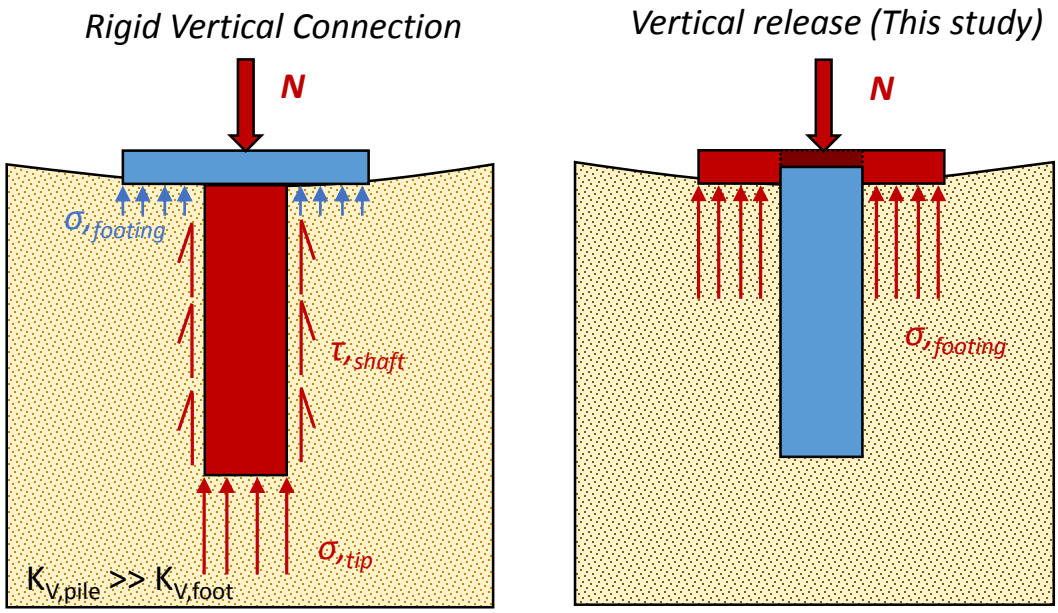

Figure 2.2. Sketch illustrating the vertical release implemented in this study, allowing the footing to fully carry the vertical loads, in order to ensure better interface contact and performance, by taking advantage of the dead loads.

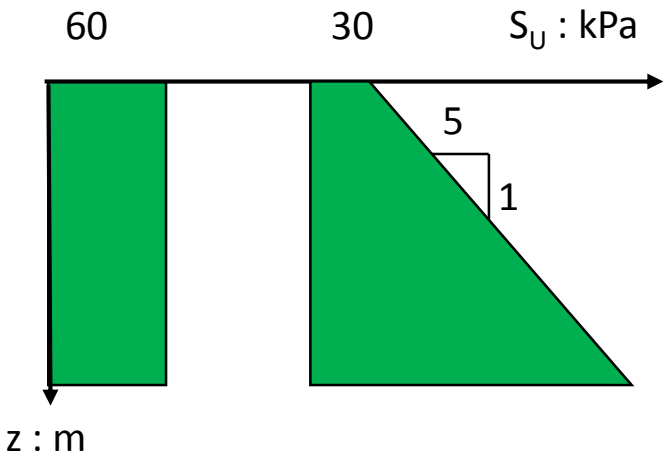

Figure 2.3. Undrained shear strength distribution for the two soil profiles examined.

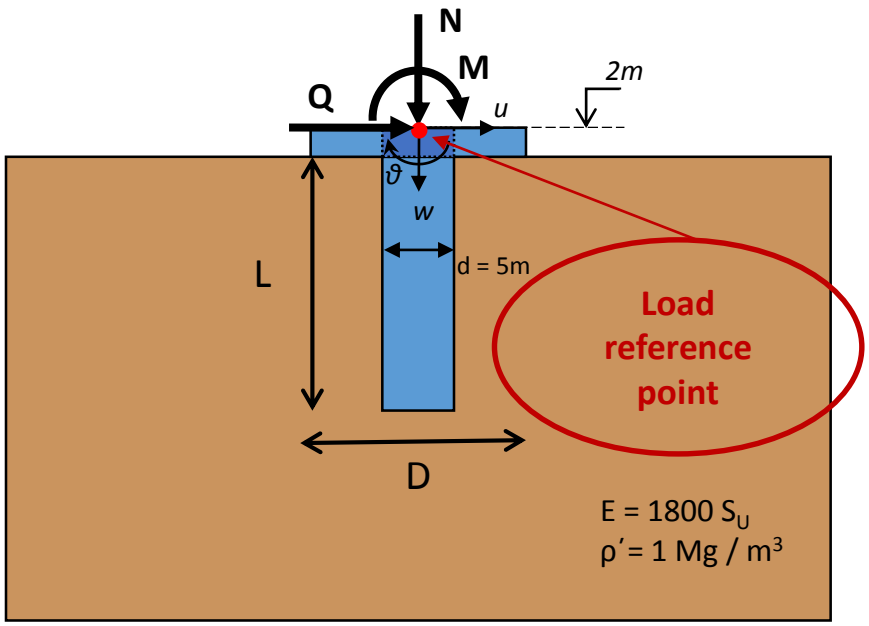

Figure 2.4. Load reference point, varying and constant parameters, and basic nomenclature.

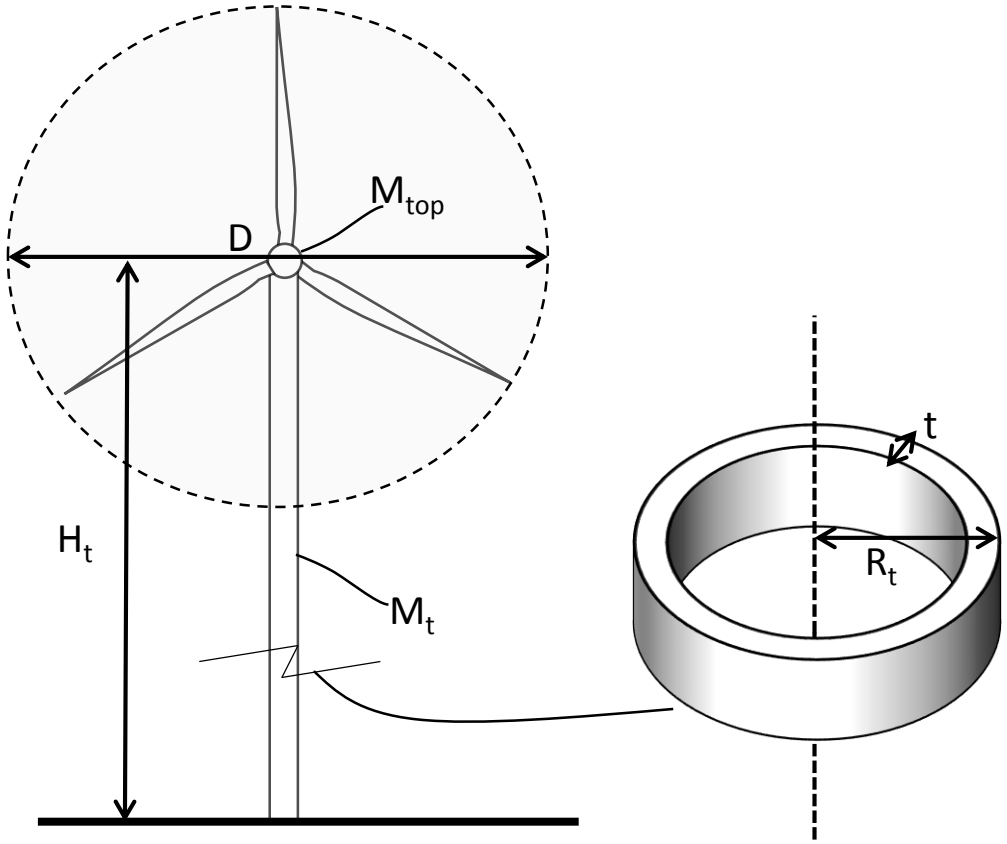

Figure 2.5. A typical wind turbine tower and cross section.

	D : m	H_t : m	R_t : m	t : m	M_{top} : Mg	Mt : Mg	I : m^4	E : GPa
2 MW	65	60	2	0.02	200	128	0.495	210
3.5 MW	90	80	2	0.023	220	195	0.568	210
5 MW	110	90	2.46	0.023	350	271	1.071	210

Table 2.1. Tower characteristics of the three wind turbines examined.

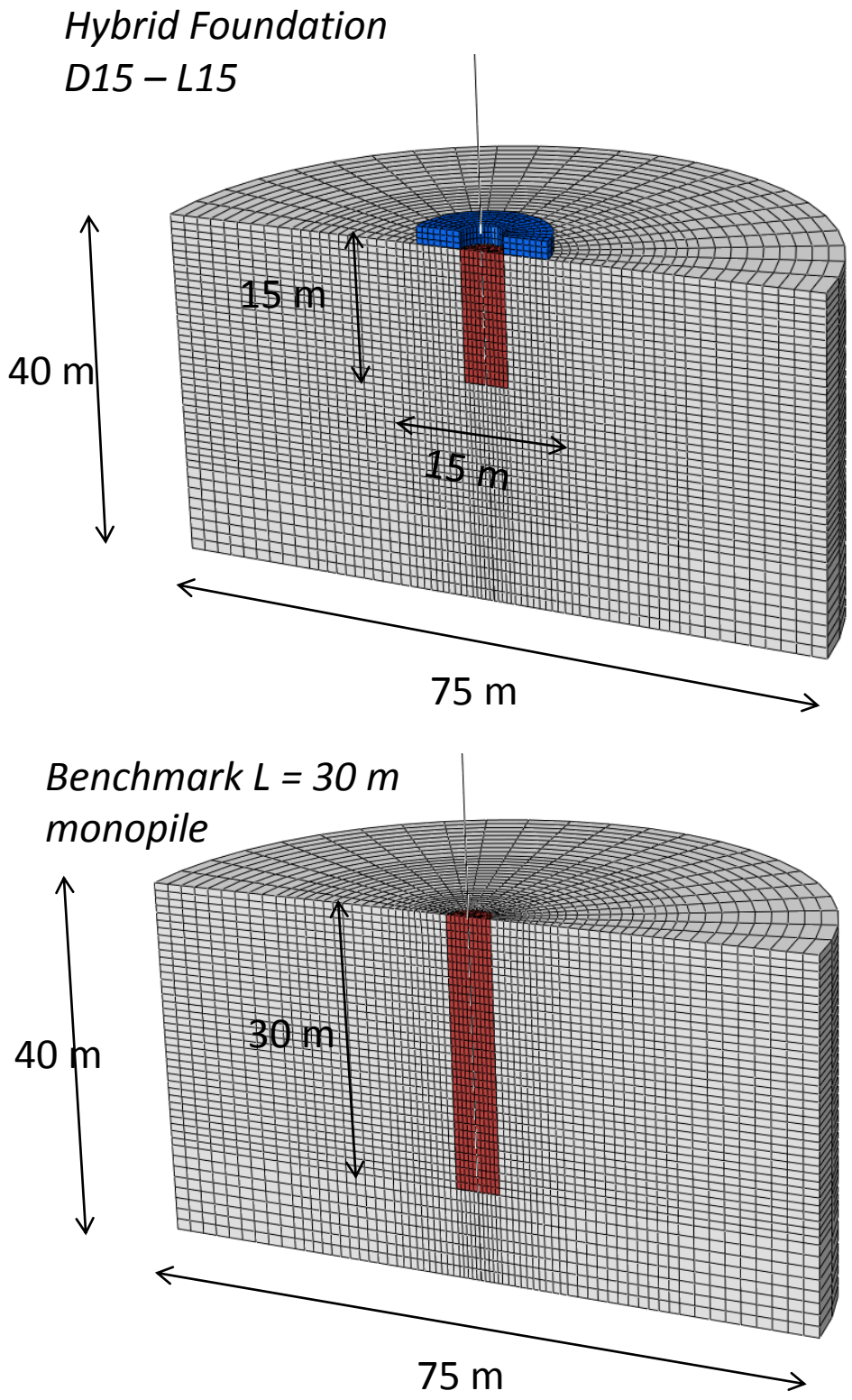

Figure 2.6. Two of the ABAQUS finite element models used in the current study. Top: Hybrid foundation with monopile length L = 15m and footing diameter D = 15m. Bottom: 30m monopile used for comparison. Diameter of the monopile is kept constant ar 5m for all analyses.

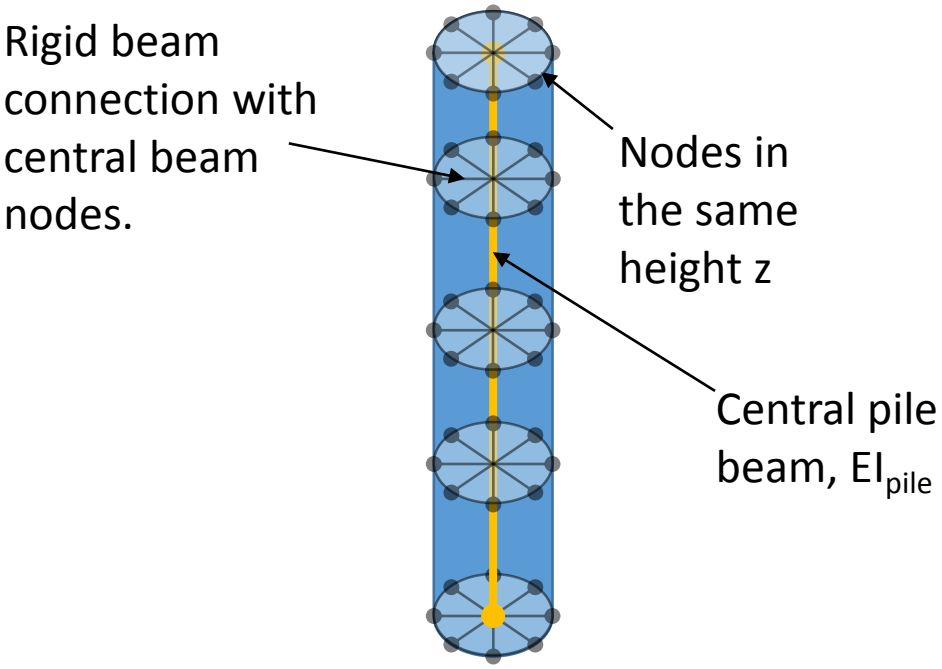

Figure 2.7. Modeling the 3D geometry of the pile using beam elements to form a central beam and rigid MPC connections to tie together all the same-height nodes of the surrounding soil.

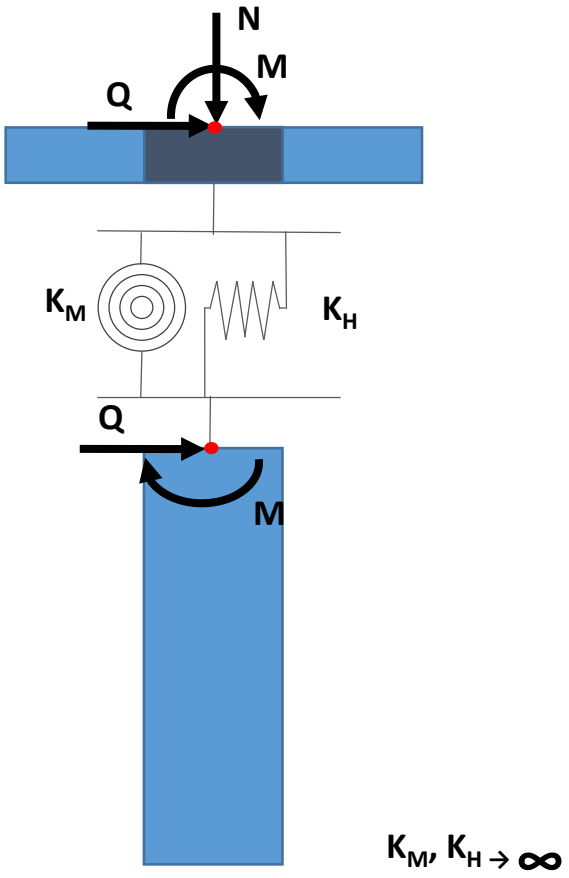

Figure 2.8. 2-D sketch of the connection between the footing and the pile, allowing relative vertical translation of the two components, while horizontal loads and moments are carried by the hybrid foundation.

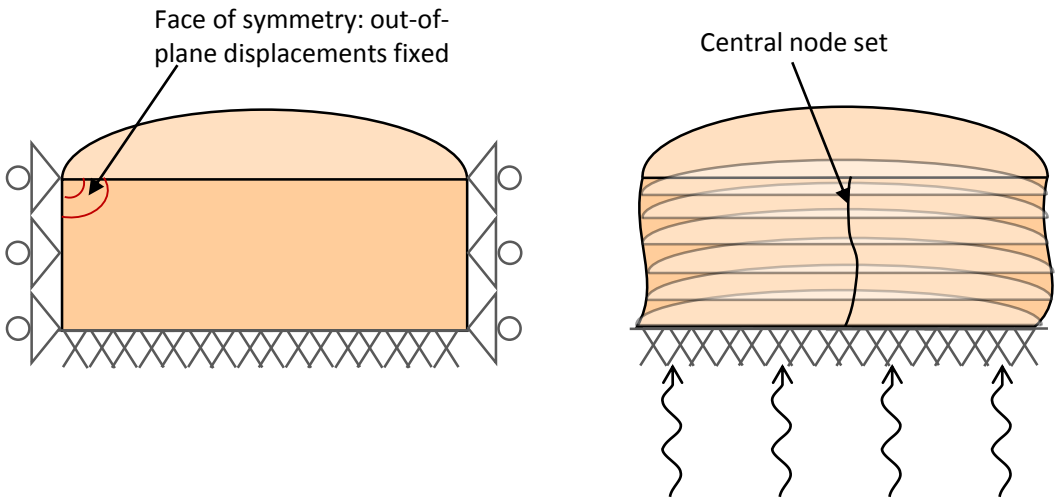

Figure 2.9. Left: Boundary conditions for the static problem. Right: Boundary conditions for the dynamic problem, where the periphery nodes are all tied to a central node set.

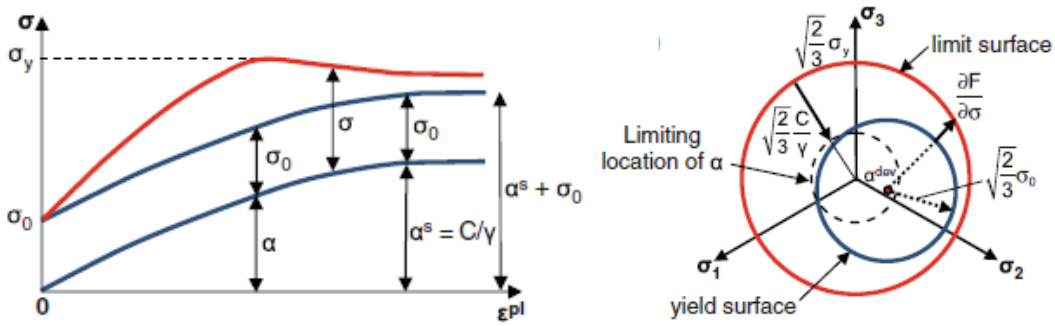

Figure 2.10. Evolution of the kinematic and isotropic hardening components for uniaxial (left) and multiaxial (right) loading, for the soil constitutive model used.

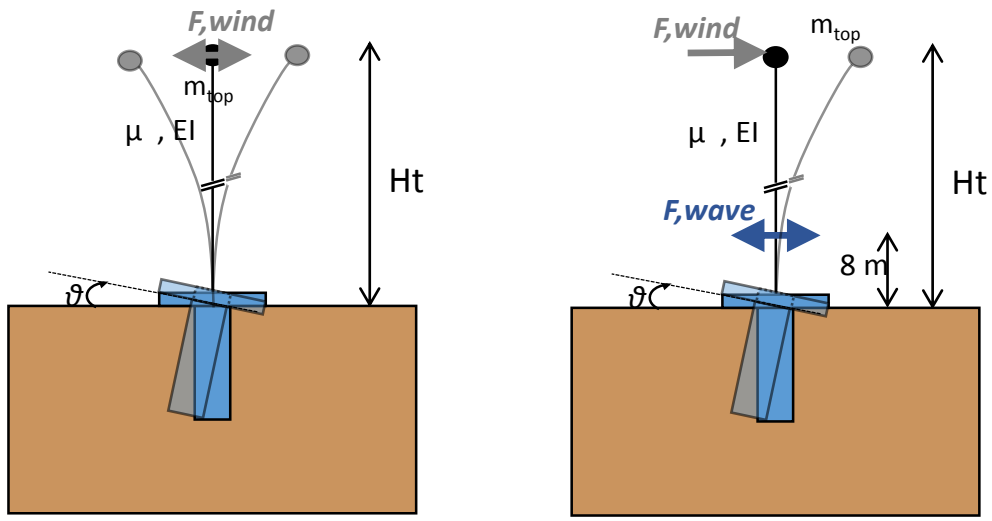

Figure 2.11. Sketch illustrating the two cyclic loading scenarios considered: i) Wind cyclic load on the left and ii) wave cyclic load and wind monotonic load on the right

CHAPTER 3

Bearing Capacity of Hybrid Foundations

3.1 Prologue

Bearing capacity of foundations is one of the most important aspects of geotechnical engineering, as it concerns transferring loads from the superstructure to the supporting soil in a safe manner. The factor of safety is perhaps the most straightforward way to describe the reliability of a structure and is defined as the loads acting on the structure divided by the corresponding bearing capacity. The transfer of loads is accomplished by development of normal and shear stresses acting on the soil-foundation interfaces. Interface non-linearities play an important role and are taken into account in the current thesis, while most publications so far assume a fully bonded interface [e.g. Bransby & Randolph, 1998; Gourvenec & Randolph, 2003; Gourvenec, 2007; Bransby & Yun, 2009].

Offshore wind turbines are tall and slender structures with a relatively low self-weight of the order of 4-6 MN. Environmental conditions (wind and wave loading) impose a complex loading regime, characterized by high horizontal and even higher overturning moment loading (about 4 MN and 80 MNm respectively), while vertical loads remain relatively low (4 – 6 MN). This is a rather unfavorable load combination and the trend in the offshore foundation research field is to examine the bearing capacity of such foundations in the three-dimensional M-Q-N load space [i.e. Martin, 1994; Ukritchkon *et al.*, 1998; Bransby & Randolph, 1998; Taiebat & Carter, 2000, 2002; Randolph & Puzrin, 2003; Gourvenec & Randolph, 2003; Gourvenec 2007a & b, 2008], rather than adopt uniaxial solutions for vertical loading with eccentricity factors, used in the past [Meyerhof, 1951, 1953; Hansen, 1961, 1970; Vesic, 1975].

The foundation examined in this study is hybrid, composed of a monopile and a surface footing which are unconnected to each other in the vertical degree of freedom. As a result, vertical loads are carried and transferred to the soil exclusively by the footing, while horizontal and moment loads are carried by both components. Surface footings carrying vertical loads is the most common problem of geotechnical engineering and has been studied extensively in the past [Prandtl, 1921; Terzaghi, 1953]. Furthermore, the behavior of both surface and embedded foundations under lateral loading is more complex, but extensive research has also been conducted for each component of the hybrid foundation, part of it presented in chapter 1. The basic lateral load-transfer mechanisms are shown in **figure 3.1.a** for surface and embedded foundations and in **figure 3.1.b** for the hybrid foundation.

To investigate the bearing capacity of the foundation examined in the current study, a series of 3-D finite element analyses is conducted, the basic parameters of which are depicted in **figure 3.2**. The load reference point for this chapter is taken at the middle of the foundation lid (2m above mud line), and the soil – foundation interface is considered frictional, for both the footing and the (driven) pile, with the friction coefficient μ taken 0.5, as described in the previous chapters. Both the diameter of the footing and the length of the monopile are varied, in order to point out the effect of each component on the bearing capacity. The diameter of the pile is kept constant at 5 m. Two soil profiles are examined, as seen in **figure 3.3**; a uniform clay soil with an undrained shear strength of S_U=60 kPa and an inhomogeneous soil body, with S_U = 30 kPa at the surface and linearly increasing strength with depth.

All the analyses conducted to estimate bearing capacity are displacement-controlled. Details are provided in each subsection of this chapter. The impact of the pile length and footing diameter on the results of this chapter is presented separately, in an effort to estimate the contribution of each component to the total hybrid response.

3.2 Uniaxial Bearing Capacity

3.2.1 Vertical Loading

To begin with, capacity under vertical loading is examined. It is reminded that vertical loads are carried exclusively by the footing, as seen in **figure 3.4**. Three footing diameters are examined; D = 11 m, 15 m and 20 m. The bearing capacity is estimated by imposing vertical displacement at the load reference point and extracting the resisting force at the same point from ABAQUS.

Figure 3.5 demonstrates vertical load – settlement curves for each foundation, for homogenous and inhomogeneous soil. It is obvious that increasing the diameter of the footing directly increases the vertical bearing capacity for both cases. For the uniform clay, vertical bearing capacity can reach the value of 110 MN for the 20 m footing, 50 MN for the 15 m footing and approximately 30 MN for the 11 m footing. All the footings offer a satisfactory safety factor against the typical value of dead weights of 6 MN. For the inhomogeneous soil vertical resistance is decreased, as it depends on the surface layers of clay which have half the undrained shear strength of the uniform soil. To be specific, the capacity is 37% lower for the 20 m footing, 34 % lower for D = 15 m and 44 % for D = 11m. The initial vertical stiffness of the foundations for very small settlements is represented by the tangent of each curve.

Failure mechanisms under vertical loading are presented in **figure 3.6**. The mechanisms resemble the typical failure mechanism of a surface footing under vertical loading, with the difference being that the monopile cuts through the plastic shear zones, forming two smaller wedges on each side. It is worth noting that, despite the fact that vertical loads are not transferred to the pile directly, it also tends to settle in a smaller rate. This is caused by the frictional interface, which allows shear stresses to develop on the pile shaft. While the vertical load is transferred to the soil via bearing stresses on the footing interface, the soil surrounding the pile settles and inflicts shear stresses on the pile shaft, causing it to settle too. This effect is more obvious for the larger footings, which mobilize a larger soil body. For the inhomogeneous soil the shear zones are isolated on the top weaker layers, while the pile remains intact because the maximum shear stress that can be developed depends on the pressure acting on the interface which is smaller than the one in the homogeneous case, so the interface “breaks” before the pile starts to settle.

The effect of the diameter of the footing on vertical bearing capacity is better illustrated in **figure 3.7.a**. In particular, the vertical bearing capacity seems to be directly proportional to the square of the footing diameter, as implied by most empirical formulae available. In fact,

the results compare quite well to the empirical formula proposed by Vesic (1963), which is expressed by the following equation for a circular footing:

$$V_{ULT} \approx 6.17\ A\ S_U$$

As seen in **figure 3.7.b**, vertical bearing capacity is practically unaffected by the monopile, because of the vertical release implemented.

For the case of offshore wind turbines vertical bearing capacity is not critical, as they are rather light-weighted structures. It is nevertheless important to note that the footing weight must not be neglected, as for a 15 m diameter footing it is

$$W_{D15} = (2m)\ \pi\ (15m)^2/4\ (15\ kN/m^3) = 5302\ kN = 5.3\ MN$$

which is rather considerable, as it is heavier than the superstructure (4 MN). A submerged unit weight of 15 kN / m^3 is deemed representative, as it stands for a reinforced concrete footing. It is proven later on (Chapter 5) that the weight of the footing can be of significant importance for the design of the foundation, as heavier footings present a stiffer response.

3.2.2 Horizontal Loading

This type of loading is dominant for offshore wind turbine foundations, as it is imposed by wind and waves acting on the superstructure. Both the footing diameter D and monopile length L are varied, to examine their influence on the hybrid behavior. The footing diameters examined are 11 m, 15 m and 20 m, while the monopile lengths 10 m, 15 m, 20 m and 25m. In addition, a 15 m monopile and a 15 m footing are examined separately, to better understand their behavior and relate their capacity to the one of the hybrid foundation. The procedure followed is imposing a horizontal displacement at the load reference point until failure, without restriction of rotation, and extracting the reaction force at the same point. For all the analyses here, the weight of a typical 3.5 MW wind turbine is considered and imposed before the horizontal displacement.

As reported in chapter 1, embedded foundations such as monopiles develop a significant coupling between the rotational and translational degree of freedom. This means that imposing a horizontal displacement at the top of a monopile causes it to rotate too. It is shown later on that this type of behavior is adopted by the hybrid foundation. Horizontal load – displacement curves are shown in **figure 3.8.a**, for hybrid foundations with a 15 m monopile and various footings, as well as for a 15 m monopile without a footing, for homogeneous and inhomogeneous soil. It is evident that adding a footing on top a monopile increases its horizontal capacity by up to 74 % (20 m footing). The addition of a 15 m footing gives an increase of approximately 35 % and the addition of an 11 m footing gives an increase of 15 %. For the inhomogeneous soil, the influence of the footing is decreased. The 20 m footing diameter increases the horizontal resistance of a 15 m monopile by 62 %, the 15 m footing increases the resistance by 25 %, while the influence of the 11 m footing seems to totally diminish.

The same curves are presented in **figure 3.8.b**, for hybrid foundations with a 15 m footing and various monopile lengths. Bearing capacity of a 15 m footing alone is also depicted. Addition of a monopile to a footing also increases its horizontal bearing capacity to a significant extent. Even a short 10 m monopile increases the capacity of the footing by 140 %, while a larger monopile (L = 20 m) can increase it by 325 %. To avoid confusion, it is noted at this point that the 15 m footing has a smaller bearing capacity than a 15 m monopile when they are used alone, so the percentage of increase is not to be compared with the above paragraph. To clear things out, we can say that the contribution of each component to the hybrid foundation's horizontal capacity is almost the same. A rational comparison is that the D15-L20 and the D20-L15 hybrid foundations have approximately the same horizontal bearing capacity. For the inhomogeneous soil, the hybrid foundations with various monopile lengths have a slightly diminished horizontal capacity, especially for the shorter monopiles due to the fact that the mean soil strength is about 60 kPa for the first 15 m of soil depth. It is worth noting that the behavior of the footing alone is the same for the two soil profiles, as it depends solely on the overlying weight and the coefficient of friction μ. This is the reason the shape of the capacity curve is nearly elastic – perfectly plastic. In fact, horizontal capacity of the footing alone can be easily computed as a sliding body:

$Q_{ULT,\,D15} = \mu N = 0.5\,(5.3 + 4) = 4.15\ MN \cong 4.3\ MN$ (F.E.A.)

However, the contribution of the footing is not limited to its horizontal capacity. It also offers a certain degree of rotational fixity to the pile head, improving the pile's capacity as well [Fleming et al. 2009].

Failure mechanisms under horizontal loading are shown in **figure 3.9.a** for a hybrid foundation with a 15 m monopile and increasing footing diameter, for homogeneous and inhomogeneous soil. Rotation caused by the coupling of the two degrees of freedom is obvious, as all the mechanisms have an "inverted pendulum" shape. The rotation point is located near the pile base. A soil wedge is formed, resembling the failure mechanism of a short pile. However, the presence of the footing forces the wedge to expand deeper and wider, mobilizing a larger part of the soil. For the small footing, the wedge is located near the surface but as the footing diameter increases, the wedge is also forced to start deeper, even at the pile base. Moreover, heave of soil near the footing edge can be observed, implying that an extra capacity from the mobilization of passive soil strength can be accomplished. Detachment on the other side of the pile is visible, as well as footing uplift. For the inhomogeneous case, where the surface soil is softer, uplift is substituted by sinking of the footing into the soil, forcing the wedge to expand deeper.

Figure 3.9.b shows the same failure mechanisms for a hybrid foundation with D = 15 m and an increasing pile length. A first observation is that the L = 10 m hybrid foundation is located completely inside the plastic shear zone, as the soil wedge covers the whole pile. On the other hand, for the foundations with 20m and 25 m pile, the wedge is limited at the top 15 m and a separate plastic zone is developed at the pile base, due to base shear. Soil inhomogeneity mainly affects the footing, making sinking more dominant over uplift, as mentioned above.

Figure 3.10.a shows the contribution of the monopile to the total horizontal bearing capacity of a hybrid foundation with D = 15 m. It is obvious that the addition of a monopile to a footing significantly increases the horizontal capacity of the system. With increase of pile length, the effect of inhomogeneous soil tends to diminish, due to the pile reaching deeper and stronger soil layers.

Contribution of various footings to the horizontal capacity of a 15 m monopile is presented in **figure 3.10.b**. The rate of capacity increase per meter of footing diameter seems to be approximately the same as the rate per meter of monopile length. For linearly increasing S_U with depth, the loss is the same for all footings because, as mentioned before, the footing transfers shear loads to the soil only via pure friction on the interface, and its horizontal capacity is practically independent of the soil profile, since the friction coefficient is pre-determined. The loss is caused by softer response of the pile, due to smaller degree of rotation fixity at the pile head.

3.2.3 Overturning Moment

Moment capacity is definitely a key design criterion for offshore wind turbine foundations. Wind loading acts at the rotor level, typically at 60 – 90 m above the seabed. With the force being on the order of 1 MN, extremely large moments (that can reach up to 80 - 140 MNm) develop and need to be transferred safely into the soil. All the foundations are examined considering the weight of a typical 3.5 MW superstructure.

The results are presented in the same manner as for the horizontal bearing capacity. Moment – rotation curves presented in **figure 3.10** reveal the dominant role of the monopile length in moment bearing capacity of the hybrid foundation. Specifically, while for the largest footing (D = 20 m) combined with a 15 m monopile the moment capacity is about 270 MNm, for the D15 – L25 hybrid foundation the capacity is over 450 MNm. The effect of inhomogeneity is a small capacity decrease because of the footing laying on softer soil which is compensated as the monopile embedment length increases. In fact, because the center of rotation of the monopile is higher for moment loading than for horizontal, passive soil earth pressure is acting on a larger area of the pile below the center. This causes the 25 m monopile to develop higher capacity on the inhomogeneous soil profile, where it mobilizes stiffer layers of soil.

Failure mechanisms under pure moment loading are depicted in **figure 3.12.a & b,** for hybrid foundations with constant footing diameter and increasing pile length, and vice versa. All the observations made for the horizontal failure mechanisms apply here, with the difference being that the pile center of rotation is located higher and yielding of the soil is also taking place at the bottom of the pile, where a “scoop” mechanism develops.

Figure 3.13.a shows the contribution of the monopile to moment capacity of a hybrid foundation with D = 15 m and **Figure 3.13.b** the contribution of the footing to a hybrid foundation with L =15 m. The rate of capacity increase per meter of monopile length is significantly larger than per meter of footing diameter. However, adding a 15 m footing to a 15 m monopile almost doubles its capacity, which is still a quite satisfying increase.

To sum up, the monopile carries moment loads by mobilizing lateral earth pressure as it rotates around a fixed point, while the role of the footing is dual; it mobilizes bearing soil stresses during its rotation and it offers a degree of fixity at the pile head, making its response stiffer as well, compared to a free – head pile. It is important to stress out that the hybrid foundation is an embedded foundation and as a result develops coupling between the rotational and horizontal degree of freedom, which means that applying pure moment of the foundation load reference point will also cause it to translate horizontally. This is better pointed out later on, in the investigation of M – Q interaction.

3.3 Bearing Capacity Under Combined Loading

Uniaxial bearing capacity is important to understand the basic physical mechanisms behind the transfer of loads from the superstructure to the soil via the hybrid foundation, however this is probably never the case in reality. An offshore wind turbine is subjected to a complex combined M-Q-N loading regime, due to wind and wave lateral loading and the self-weight of the structure. The most convenient way to represent the behavior of foundations under combined loading is to define a three-dimensional failure surface in the M-Q-N loading space. Any combination of loads within the failure surface is considered safe, while any load combination outside the surface will violate the failure criterion. This approach is becoming more and more popular in the offshore geotechnical engineering field, and many researchers have attempted to define the failure envelopes utilizing experimental (e.g. Martin 1994, Gottardi et al. 1999), analytical (e.g. Bransby and Randolph 1998, Randolph and Puzrin 2003) and numerical methods (Bransby and Randolph 1998, Gourvenec and Randolph 2003, Gourvenec 2007).

3.3.1 Vertical Force – Horizontal Force Interaction

Horizontal capacity of a surface foundation is highly influenced by the vertical force, as mentioned in chapter 1. The hybrid foundation examined in this study implements a connection that allows the footing to carry the total vertical load, while lateral loads are carried by both the footing and the pile. Taking into consideration that vertical loads are rather low for an offshore wind turbine, it is important to examine the failure envelope in the N – Q loading plane (M = 0), mainly to investigate the performance of the footing.

To extract the failure envelopes, various constant ratios of u/w are imposed at the load reference point, and the reaction forces Q and N are given by ABAQUS. **Figure 3.14.a** illustrates the effect of the footing diameter on the shape and size of the N – Q failure envelopes, for a hybrid foundation with a 15 m monopile. A series of quite interesting observations can be made. To begin with, all the failure envelopes start at the same point, which represents the horizontal capacity of the 15 m monopile, as the footing is actually not working for a zero vertical load. This is attributed to the fact that horizontal capacity of the footing is directly proportional to the dead weight N, as dictated by the coulomb frictional law governing the interface. Each failure curve has an increasing part and after reaching a

peak value begins to decrease. The increasing part of each curve represents the area where footing uplift is dominant and the self – weight of the footing can be taken advantage of to improve the overall horizontal capacity of the system. On the decreasing part, the soil underneath the footing experiences significant yielding and larger vertical loads affect the total response negatively. The peak point corresponds to a vertical factor of safety almost equal to 2, traditionally for shallow foundations. Finally, each curve ends to a different point, representing the ultimate bearing capacity of each footing under vertical loading. Effect of soil inhomogeneity is also clear, as both the peak points and the ending points of the curves are smaller, implying that the weaker surface soil layers dominate the behavior of the footing, especially under vertical loading. The starting point of each curve remains the same because the 15 m pile penetrates the soil stratum to a depth where the mean undrained shear strength is almost equal to the strength of the homogeneous profile.

Effect of the pile embedment length is illustrated in **figure 3.14.b**; each curve now starts from a different point, that stands for the pure capacity of each monopile and all the curves end almost at the same point because they correspond to hybrid foundations with the same footing diameter. Once again, the inhomogeneous soil profile causes the vertical bearing capacity of the footing to decrease, while the horizontal capacity of each pile is practically unaffected. The weight of a 3.5 MW wind turbine (footing weight considered) is also depicted on the charts, to provide an estimate of the actual loading circumstances. All the failure curves end quite rapidly when the N_{ULT} is reached, because once the footing has failed, no more vertical load can be sustained.

The displacement probes used to construct the failure envelope of a D15 – L15 hybrid foundation, laying on homogeneous soil are shown in **figure 3.15.a**. and **figure 3.15.b** shows the failure mechanisms at four characteristic points of the envelope; the vertical factor of safety is also presented for each point. For the first point, where a relatively large FS_v is present, the typical scoop – wedge mechanism is developed, as previously discussed, with footing uplift and pile detachment being clearly visible. As the vertical load increases, footing uplift is no longer visible, and the wedge is translated deeper, as seen for the mechanism at point B, which is slightly after the peak value of the envelope. For even larger vertical load, the wedge tends to diminish and severe yielding of the soil starts to develop on both sides of the footing. Even pile detachment is no longer visible. Finally, as the vertical load is reaching the vertical bearing capacity of the footing, all the plasticity is concentrated at the top layers, and the mechanism tends to coincide with the vertical mode of failure.

To conclude, the same failure envelopes are depicted in **figure 3.16** in a normalized manner. Specifically, both the vertical load N and the horizontal load Q are divided by N_{ULT} and Q_{ULT} respectively. The benefit from the footing can be clearly seen, as the horizontal capacity can be doubled for a 15 m footing and even tripled for the larger one. This effect is slightly mitigated for the inhomogeneous profile. The increase of L, increases the monopile capacity, so the effect of the footing is presented to be smaller. This happens because the extra capacity provided by the 15 m footing has a constant value and while it doubles the 15 m monopile capacity, it increases the 25 m monopile capacity only by 1.2 because the latter is already larger.

3.3.2 Vertical Force – Overturning Moment Interaction

Capacity of shallow foundations under moment loading is also highly influenced by the acting vertical force. Maximum moment capacity of a shallow foundation is achieved for simultaneous act of a vertical force equal to half the vertical bearing capacity, while a vertically uncharged surface foundation has zero moment capacity. Vertical loads substitute interface tension when it comes to overturning, for tensionless foundation – soil interfaces.

The basic conclusions for the N – Q failure envelopes also apply here, as seen in **figure 3.17**, which depicts the N – M failure envelopes. The weight seems to have a beneficial effect on the moment capacity of the system, for factors of safety larger than 2. For smaller factors of safety, vertical load causes significant soil non-linearities and the total moment capacity is reduced. The weight of a 3.5 MW wind turbine along with the D15 footing, depicted as a dotted line, seems to be on the increasing part of the as the vertical factor of safety for all the D15 foundations is 6.8 for the homogeneous soil stratum and 4.2 for the inhomogeneous. This means that there is still a safe margin to design the footing heavier and take advantage of the extra weight to accomplish an increased moment capacity. This theoretical finding is just the first step, as many more parameters (mainly concerning economic feasibility and in-situ soil conditions) must be examined to conclude to a design practice for taking advantage of the extra weight.

An example of the displacement probes used to construct the D15 – L20 interaction diagram for the inhomogeneous soil profile is depicted in **figure 3.18**, as well as failure mechanisms at characteristic points of the curve. The failure mechanism at point A, where no vertical load is acting is in fact the failure mechanism of the L = 20 m monopile, with a wedge forming on the top side and a scoop on the bottom. As the factor of safety decreases, the footing sinks and vertical bearing capacity mechanism is becoming more dominant over the moment bearing capacity mechanism.

Finally, normalized failure envelopes in the M – N loading plane are presented in **figure 3.19**, both for D and L increasing. The footing contributes in a positive way to the overall moment capacity by taking advantage of the vertical loads, while the pile length increase overshadows the contribution of the footing, because the initial pile capacity becomes larger.

It must be stressed that during the Q – N and N – M failure envelope analysis, self – weight of the footing is neglected and there is no superstructure. The reason is that if the self – weights were imposed at the first step of the analysis, the resulting vertical reaction force would have a smaller value and to calculate the real value the weights must be added.

3.3.2 Horizontal Force – Overturning Moment Interaction

For an offshore wind turbine, the M – Q loading plane is by far the most critical, as wind and wave loads both act on a certain height, transferring a very large moment at the tower base,

along with the same-direction horizontal force. For all the analyses in the current sub-section the weight of a 3.5 MW wind turbine and of each footing is considered.

Interaction diagrams for a hybrid foundation with a 15 m monopile and various footings are shown in **figures 3.20.a** & **b**, for homogeneous and inhomogeneous soil respectively. The shape of the failure envelope is symmetrical, and a large peak can be observed, where both the moment and horizontal capacity are largely increased, compared to the pure moment and horizontal capacity, under uniaxial loading. This is the effect of embedment that causes a coupling between the horizontal and rotation degree of freedom at the pile head, and consequently at the load reference point which is at the center of the foundation lid. The maximum moment and horizontal capacities are developed in the second quadrant of the diagram, which means that moment and horizontal force are acting on opposite directions. In other words, the maximum moment capacity is developed when the horizontal degree of freedom is fixed and the maximum horizontal capacity when the rotational degree of freedom is fixed. This is an important theoretical finding that concerns all embedded foundations, but for the offshore wind turbine problem, this loading combination is highly unlikely to exist. On the other hand, the most common loading combination is that on the first quadrant of the interaction diagrams, where moment and horizontal force act on the same direction. In that case, an almost linear decrease of the moment capacity is observed when the horizontal load is increasing, and vice versa. The rate of decrease seems to be the same for all three footing diameters examined. The effect of the increasing footing diameter on the size of the failure envelope is an expansion, slight for the 15 m footing and more obvious for the 20 m. The shape of the failure envelopes seems to be independent of the footing diameter. For the inhomogeneous soil, significant differences are not observed. Only for the 20 m footing, there seems to be a slight narrowing of the failure envelope. Other than that, the capacity loss because of the footing laying on softer soil seems to be compensated from monopile reaching deeper and stronger soil layers.

Interaction diagrams for a hybrid foundation with a 15 m footing and various monopile lengths are shown in **figures 3.21.a** & **b**, for homogeneous and inhomogeneous soil respectively. Two basic differences are observed, compared to the diagrams discussed above; at first the rate of decrease of moment capacity with increasing horizontal force is different for each embedment length and second the shape of the interaction diagram is changing as monopile length increases. Regarding the first difference, as shown in a previous section of this chapter, as the monopile length increases, moment capacity is increasing more rapidly than horizontal capacity; this is the reason for the failure curve in the first quadrant declining more rapidly. For the second difference, it seems that the shape of the failure envelope (and not only the size) is changing, when the monopile length increases. In fact Gourvenec (2007) has proven that as the embedment ratio of an embedded foundation increases, the shape of the failure envelope becomes more asymmetric. The effect of the soil inhomogeneity is not that evident for the 15 m and 20 m monopiles, but for the hybrid foundation with 25 m monopile, the failure envelope is stretched, leading to increased moment and horizontal capacities.

The displacement probes (u/*ϑd)* used to construct the M – Q interaction diagram are shown in **figure 3.22.a** for a D15 – L15 hybrid foundation, laying on homogeneous soil. The displacement vectors, perpendicular to five characteristic points of the failure envelope are also depicted. Attention is drawn to points D and E, which correspond to the maximum moment and horizontal capacity respectively; the displacement vectors at those points are parallel to the M and Q axes, suggesting that plastic deformations are evolving on only one degree of freedom, the horizontal translation *u* for point D, or rotation *ϑ* for point E. This is a validation of the associated plastic flow rule interpreted in the soil constitutive model, which dictates that the incremental plastic strain vectors must be perpendicular to the failure curve.

Failure mechanisms under combined M – Q loading for the characteristic points of the diagram can be seen in **figure 3.22.b**. Point A corresponds to failure under pure horizontal loading (H_{ULT}) and point C corresponds to failure under pure moment loading (M_{ULT}), without restraining the other coupled degree of freedom. These failure mechanisms are discussed in previous sub-section of the current chapter. Point B corresponds to an intermediate loading state, which is more likely to occur to an offshore wind turbine, as it is a combined same-directional moment and horizontal force loading. The ratio M/Q that corresponds to point B is 23.5 m, and is in fact the height of action of the horizontal force above the foundation lid. The three above mechanisms do not have major differences, except that the rotation point for the pile is translating upwards and the scoop around it is becoming more evident, as moment loading dominates over horizontal. The mechanism at point D, where the Hmax is developed while the rotational degree of freedom is restrained, is a pure sliding mechanism that mobilizes a quite large part of soil. Finally, the mechanism under moment loading with no horizontal translation allowed, is a pendulum mechanism, where the full moment bearing capacity is developed (point E).

Normalized failure envelopes can be seen in **figure 3.23**, for the uniform soil, as well as for the linearly increasing S_U profile. The effect of normalization is reversed, compared to the other two loading planes. Increasing of the footing diameter results in smaller maximum capacities, while increasing of the pile length directly affects the maximum capacities by stretching the normalized curves. At the first quadrant of the diagrams, all the normalized curves seem to coincide. Finally, the effect of linearly increasing S_U with depth seems to be evident only for the hybrid foundations with the same 15 m pile; the curves seem to expand, because since the pile length is constant, the ultimate capacities of the foundations depend on the footing, the behavior of which is slightly deteriorated.

3.4 Conclusions

In this chapter bearing capacity of hybrid foundations was examined thoroughly, first under uniaxial loading conditions and then under combined loading. Two soil profiles were considered, a uniform clay with S_U = 60 kPa and a clay with linearly increasing S_U with depth, with $S_{U,0}$ = 30 kPa at the surface. A non-linear frictional contact interface is applied throughout the whole study. Vertical loads are exclusively undertaken by the footing, while both the

footing and the pile are mobilized to undertake lateral loads. The basic conclusions derived from the bearing capacity study are listed below.

- Vertical loading capacity is related to the square of the footing diameter. Mobilization of the soil's bearing capacity is realized via a failure mechanism resembling the one of a traditional shallow footing.
- Lateral capacity of a monopile can be improved by adding a footing in three ways; 1) the capacity of the footing alone contributes to the overall hybrid capacity 2) The footing provides a degree of rotational restraint on the pile head, improving the response of the pile. 3) The presence of the footing alters the monopile lateral failure mechanisms, mobilizing a larger soil mass and passive soil resistance at the footing edge is present to some extent.
- Overall horizontal capacity of the hybrid foundation is influenced both by the pile length and by the footing diameter, and the contribution of each element is almost equivalent, with the pile length slightly leading.
- Overall moment capacity of the hybrid foundation is dominated by the pile length, and the footing diameter plays a secondary role.
- Due to the connection implemented, the weight of the footing and the superstructure can be taken advantage of to increase the lateral capacity, as seen in the M – N and Q – N interaction diagrams.
- As far as the moment – horizontal force interaction is concerned, the hybrid system behaves as an embedded foundation. Coupling of the rotational and horizontal degree of freedom at the foundation lid is evident.
- The effect of inhomogeneous soil on the performance of the hybrid foundations depends on the loading state and the foundation geometry, mainly the ratio of the footing diameter to pile length D/L. The softer surface layers deteriorate the performance of the footing mainly against vertical loading, while the stronger soil located deeper may even improve the lateral performance of longer piles. It can be stated that foundations with larger D/L ratio tend to be more affected by the linearly increasing soil strength. To ballast the deterioration of the footing performance, it is recommended to use longer piles in such types of soil.

CHAPTER 3: FIGURES

Bearing Capacity of Hybrid Foundations

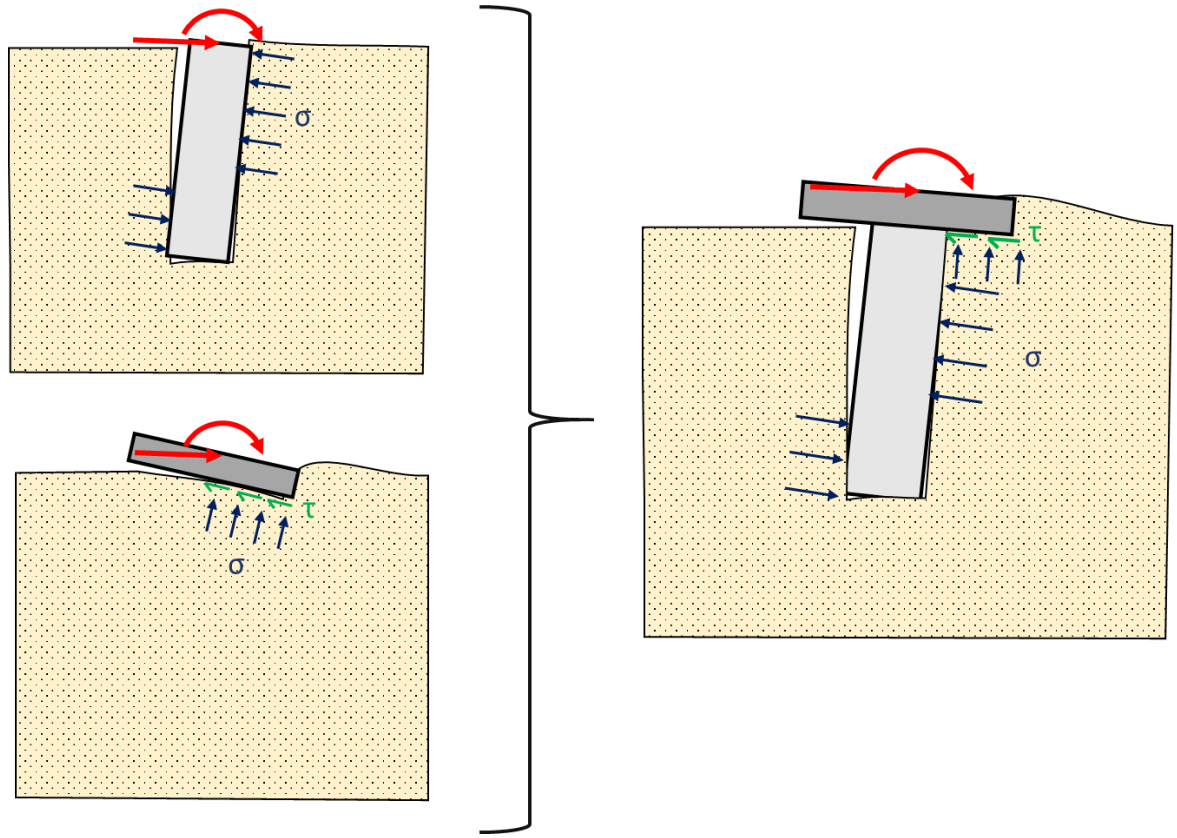

Figure 3.1. Sketch illustrating the basic load transfer mechanisms **a)** for a monopile and a footing and **b)** for a hybrid system, composing of a monopile and a footing.

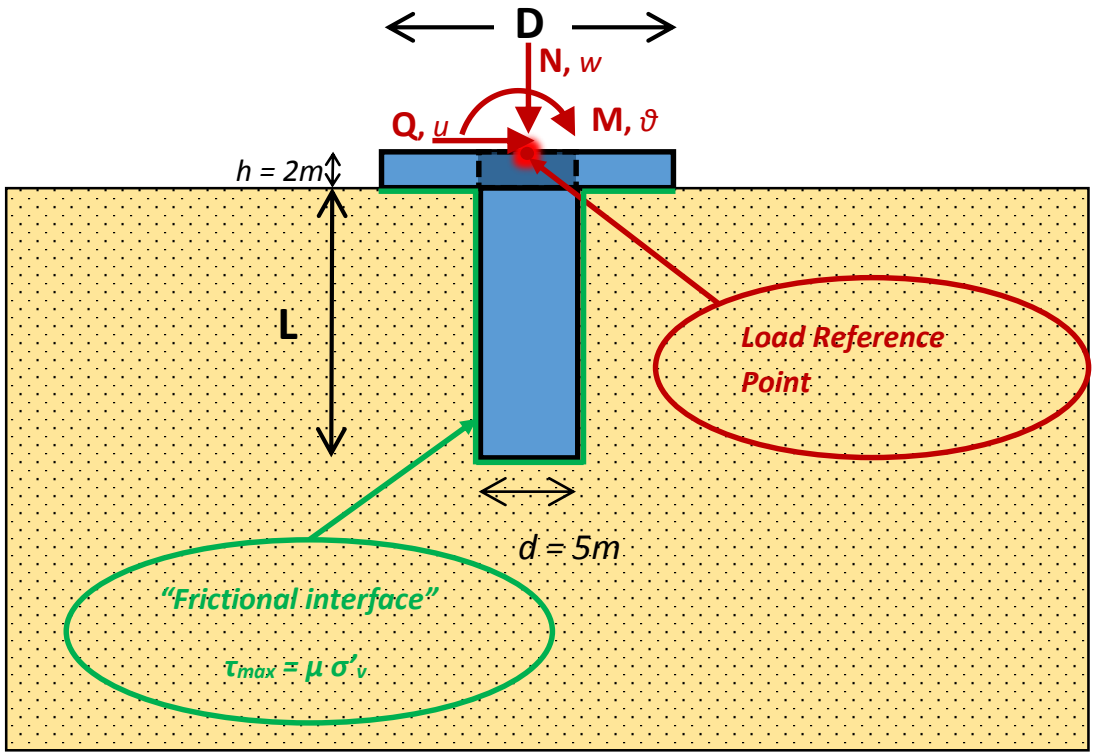

Figure 3.2. Sketch illustrating the definition of the bearing capacity problem and the main parameters involved.

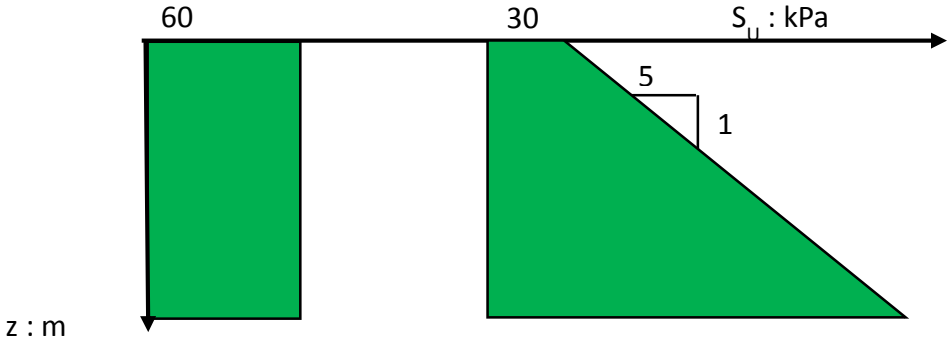

Figure 3.3. Clay soil profiles examined in the current thesis. Left: Homogeneous soil. Right: Inhomogeneous soil.

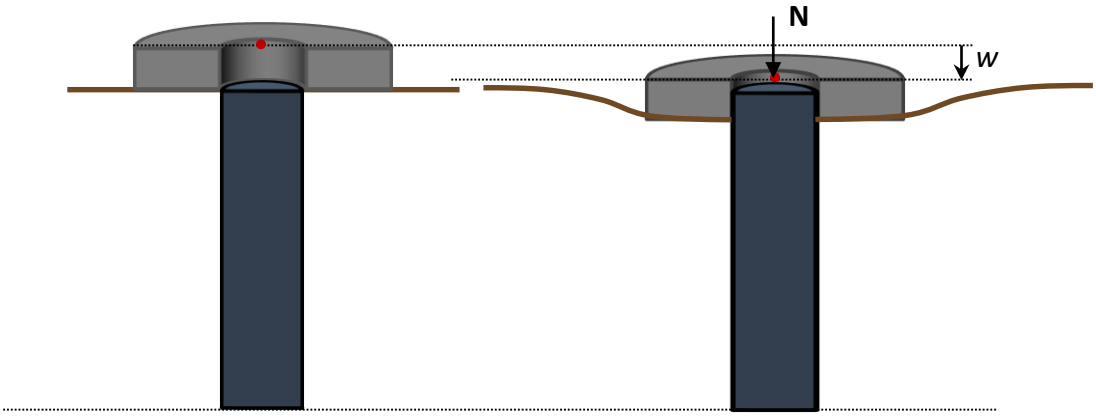

Figure 3.4. Illustration of the vertical translation release implemented in the current thesis.

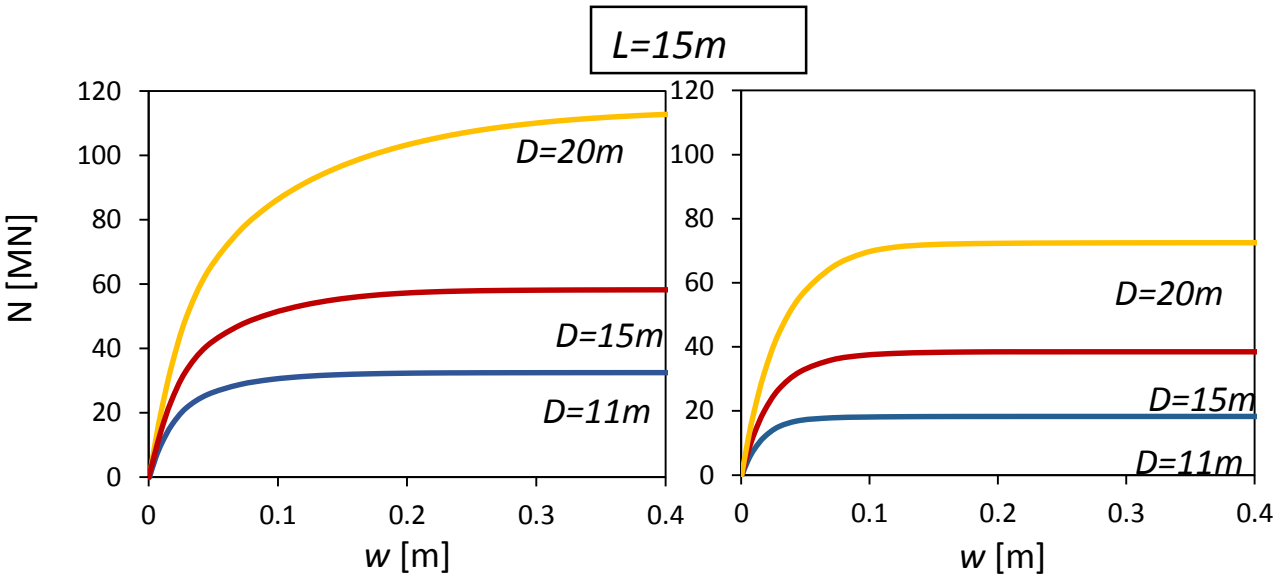

Figure 3.5. Vertical load – settlement curves for a hybrid foundation with monopile length L = 15m. Left: Homogeneous soil. Right: Inhomogeneous soil.

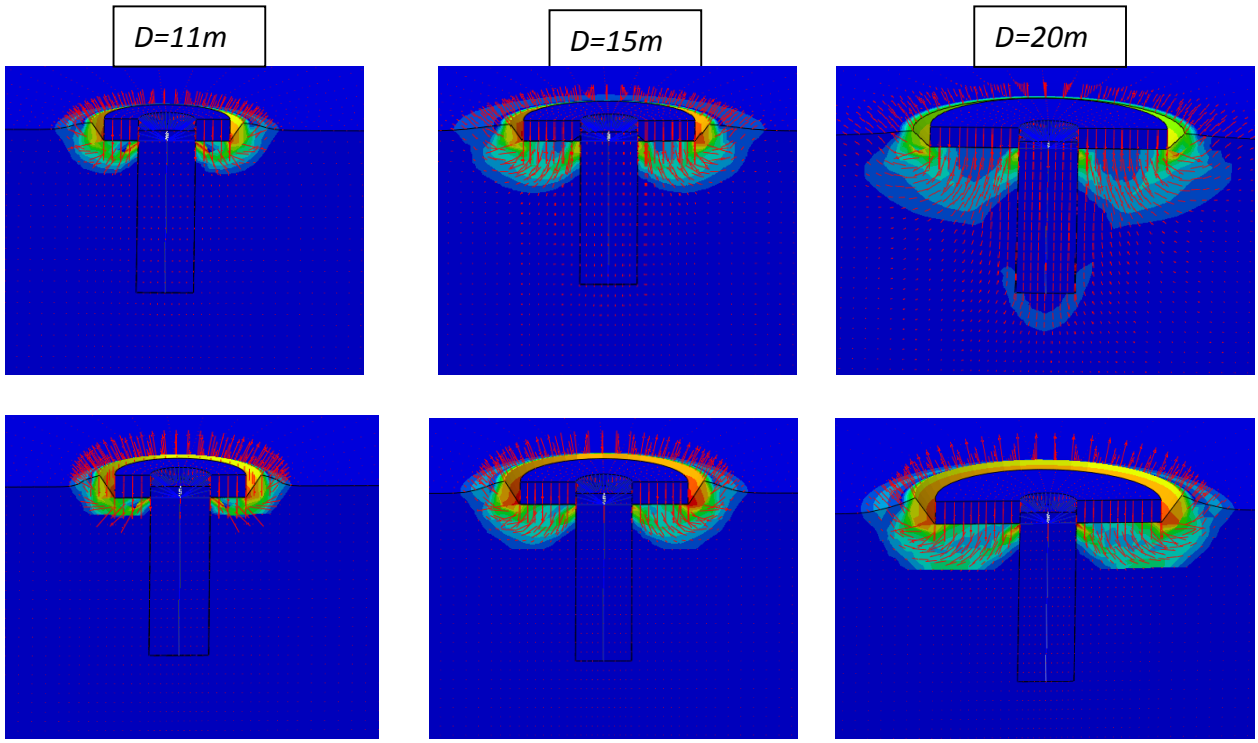

Figure 3.6. Failure mechanisms under vertical loading, in terms of plastic strain contours and displacement vectors, for a hybrid foundation with L = 15m monopile. Top row: Homogeneous soil. Bottom row: Inhomogeneous soil.

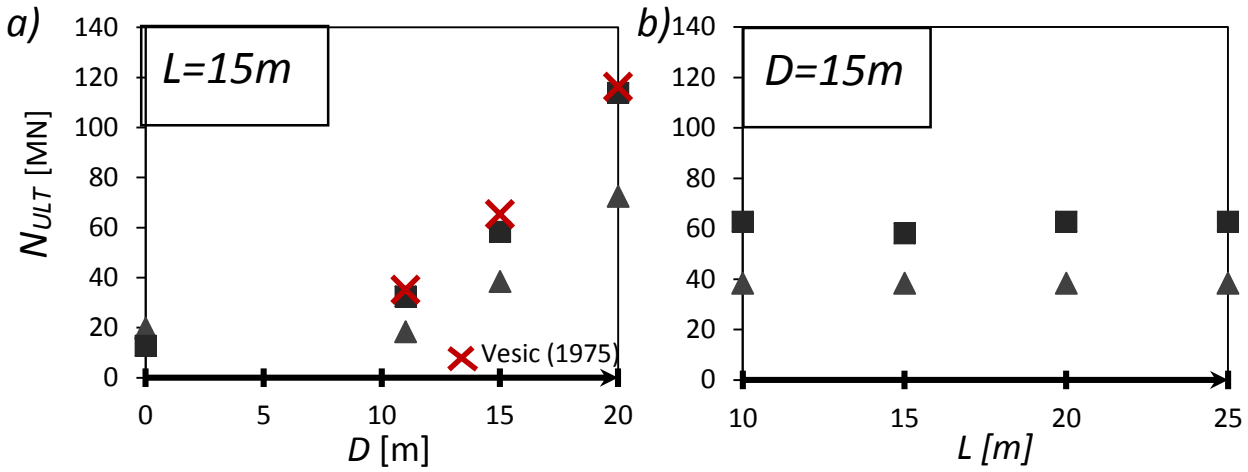

Figure 3.6. **a)** Vertical bearing capacity for a hybrid foundation with monopile length L = 15m against various footing diameters. **b)** Vertical bearing capacity for a hybrid foundation with footing diameter D = 15m against various monopile lengths. Results for homogeneous (rectangles) and inhomogeneous soil (triangles).

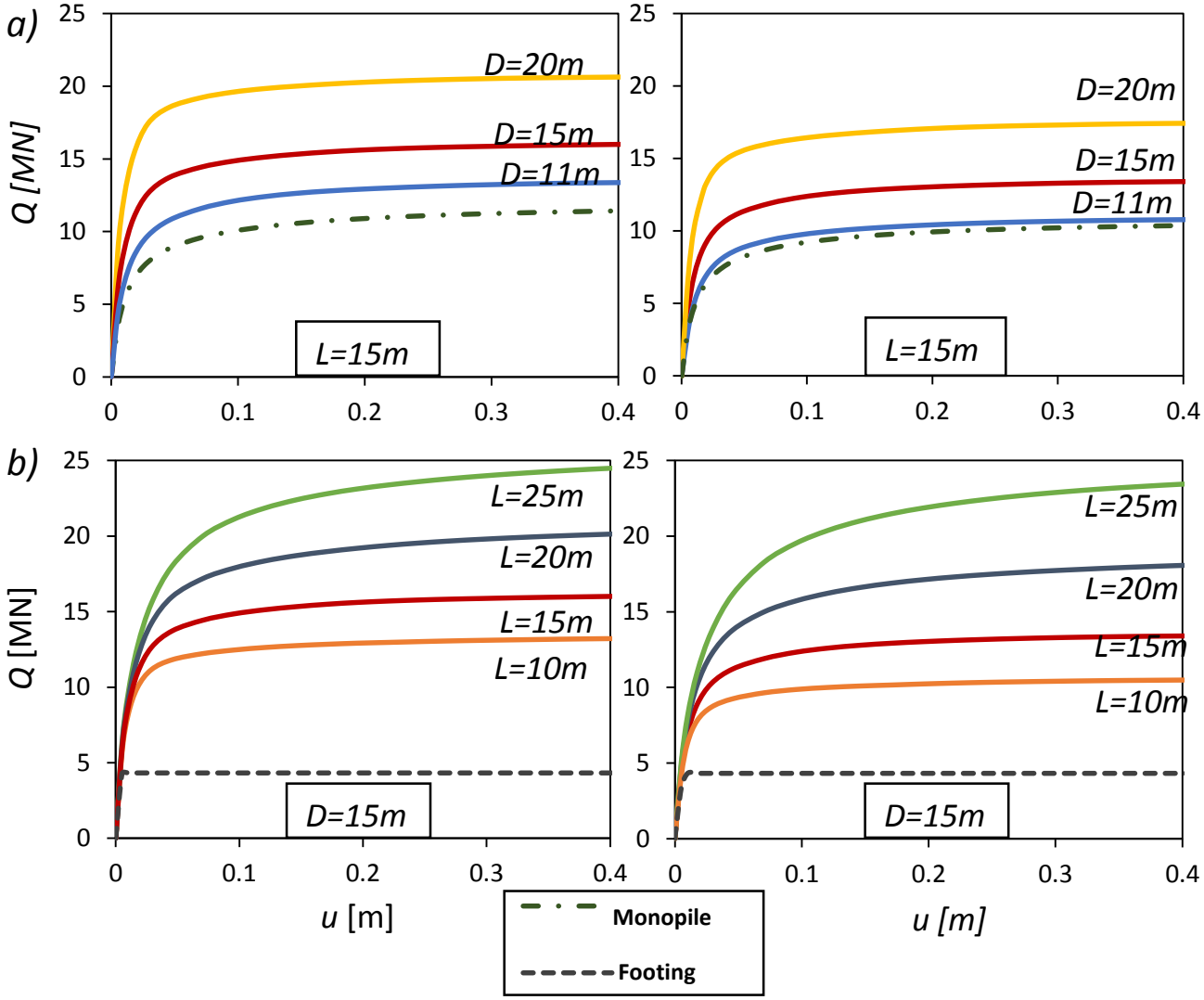

Figure 3.8. Horizontal load – displacement curves. **a)** Various footing diameters with monopile length L = 15m. **b)** Various monopile lengths with footing diameter D = 15m. Left column: Homogeneous soil. Right column: Inhomogeneous soil.

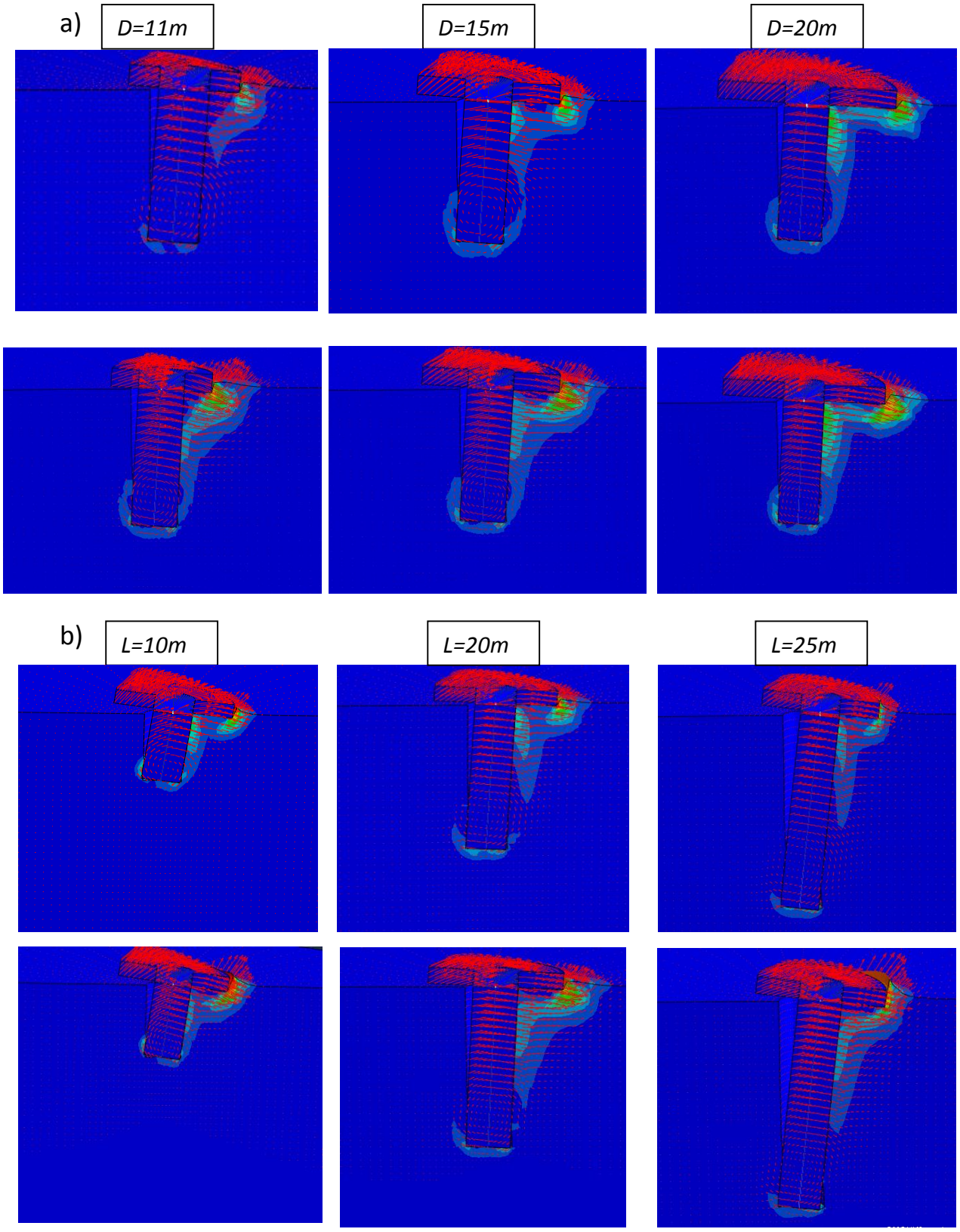

Figure 3.9. Failure mechanisms under vertical loading in terms of plastic strain contours and displacement vectors. **a)** Various footing diameters with constant L = 15m. (Top row: Homogeneous soil. Bottom row: Inhomogeneous soil.) **b)** Various monopile lengths with constant D = 15m. (Top row: Homogeneous soil. Bottom row: Inhomogeneous soil.)

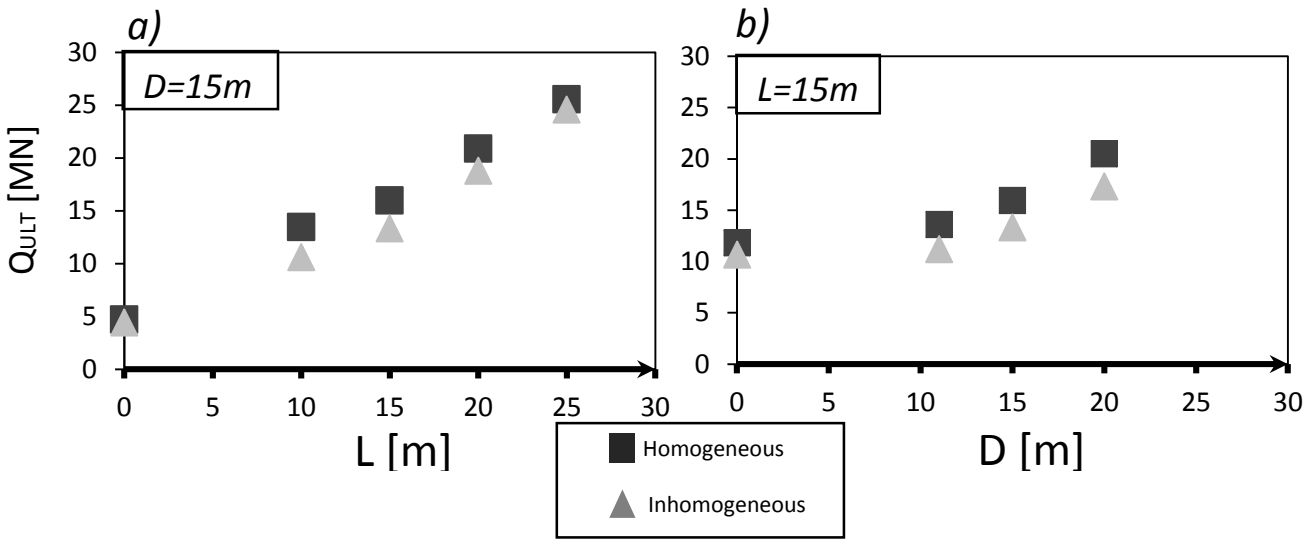

Figure 3.10. **a)** Monopile contribution to the total horizontal bearing capacity of a hybrid foundation with D = 15m. **b)** Footing contribution to the total horizontal bearing capacity of a hybrid foundation with L = 15m.

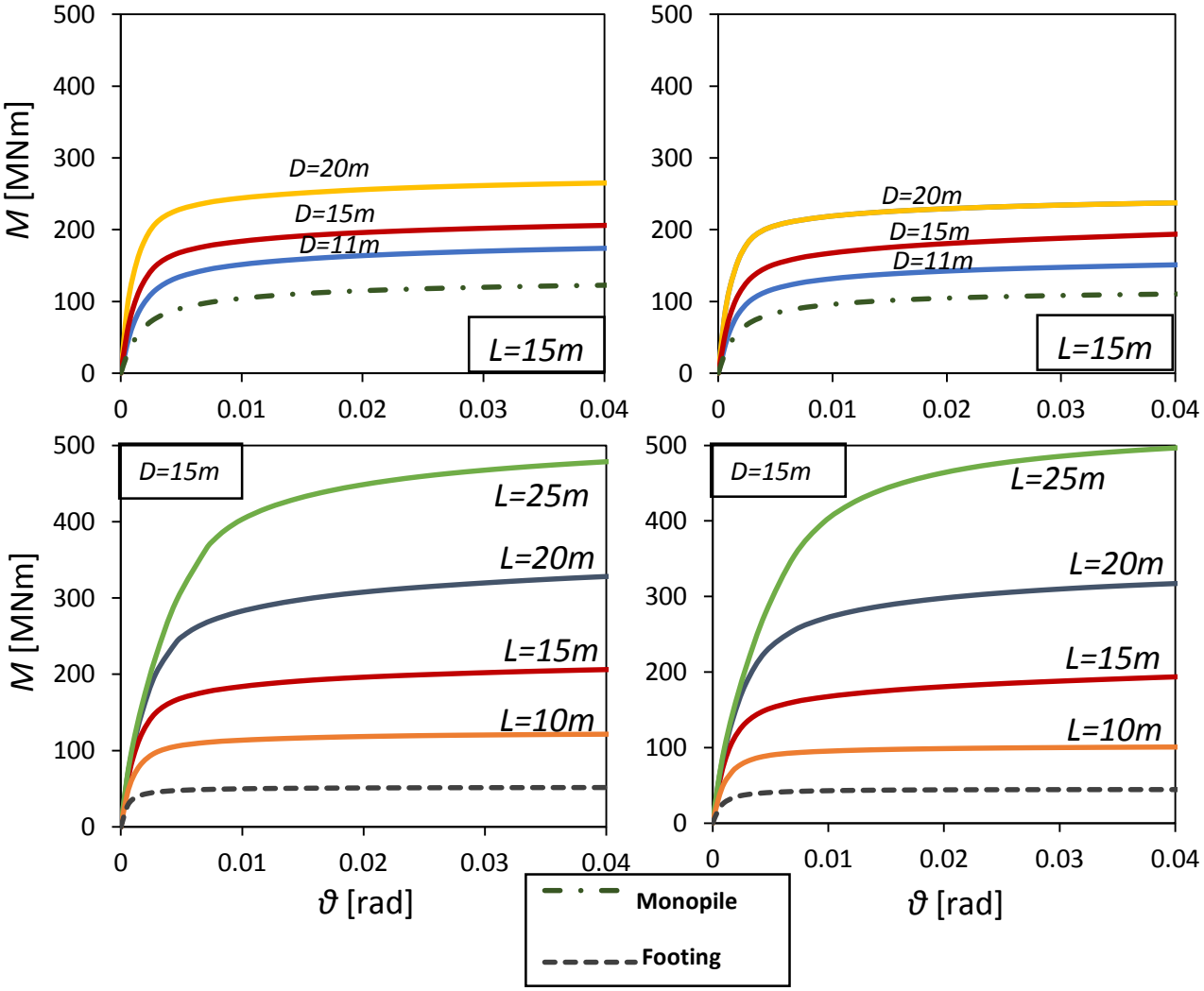

Figure 3.11. Moment – rotation curves. **a)** Various footing diameters with monopile length L = 15m. **b)** Various monopile lengths with footing diameter D = 15m. Left: Homogeneous soil. Right: Inhomogeneous soil.

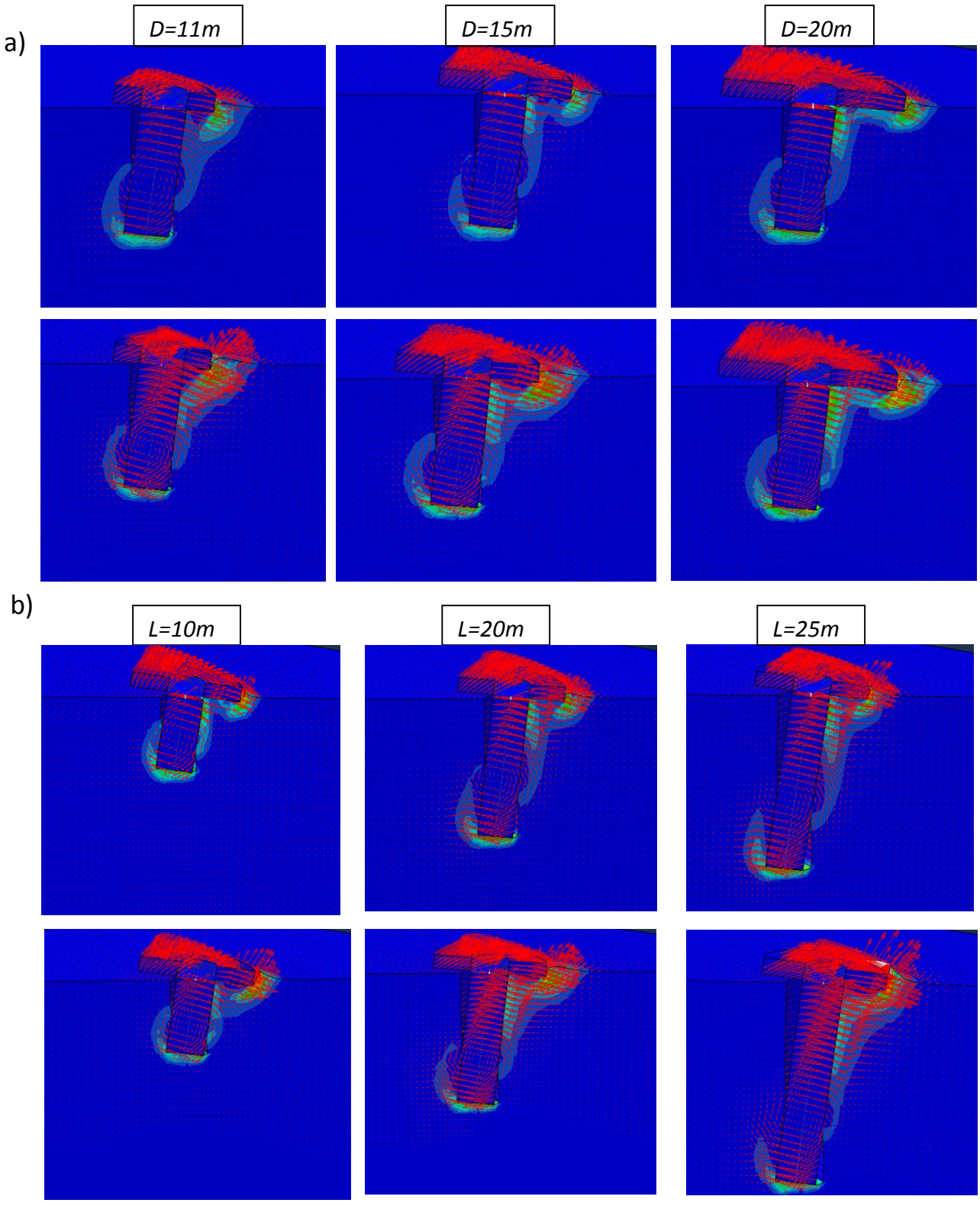

Figure 3.12. Failure mechanisms under moment loading in terms of plastic strain contours and displacement vectors. **a)** Various footing diameters with constant L = 15m. (Top row: Homogeneous soil. Bottom row: Inhomogeneous soil.) **b)** Various monopile lengths with constant D = 15m. (Top row: Homogeneous soil. Bottom row: Inhomogeneous soil.)

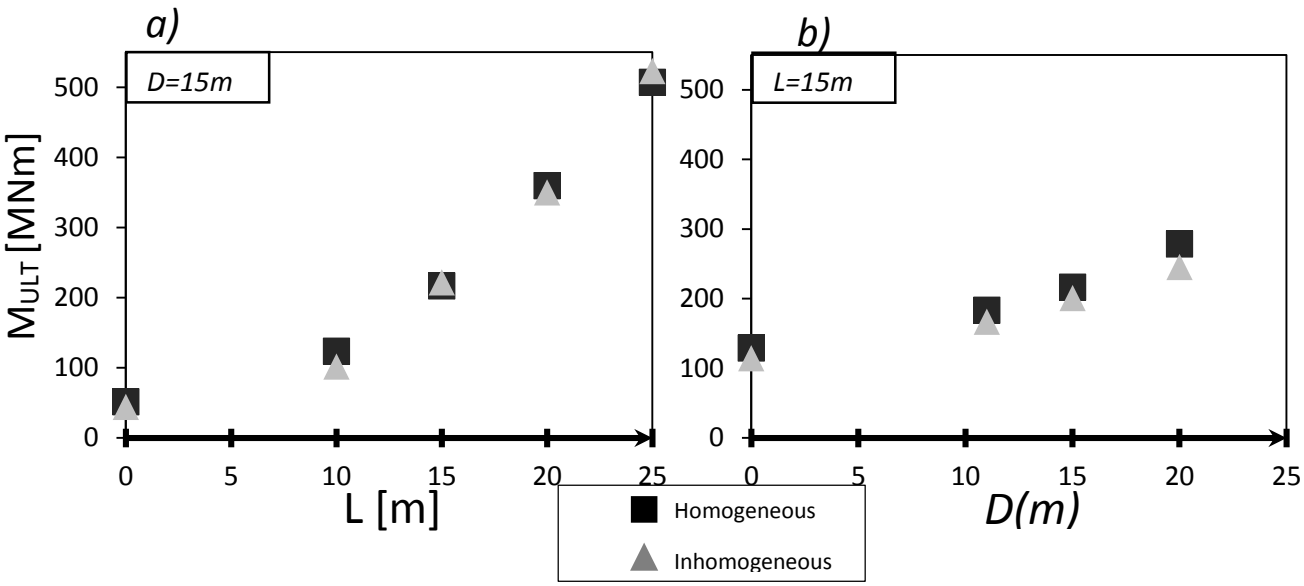

Figure 3.13. Left: Monopile contribution to the total moment bearing capacity of a hybrid foundation with D = 15m. Right: Footing contribution to the total moment bearing capacity of a hybrid foundation with L = 15m.

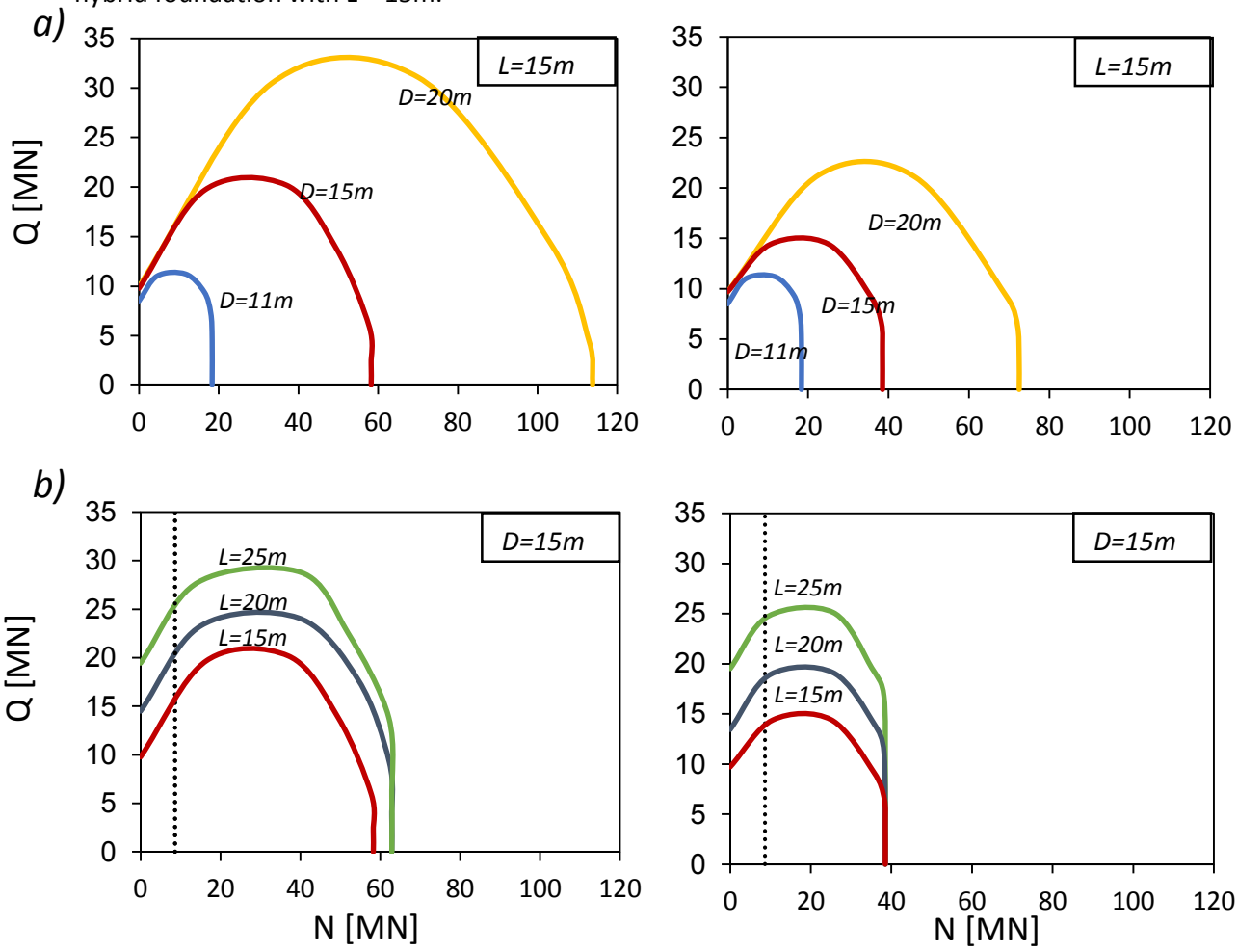

Figure 3.14. Failure envelopes under combined vertical – horizontal loading (M=0). **a)** Various footing diameters for a hybrid foundation with L = 15m. **b)** Various monopile lengths for a hybrid foundation with D = 15m. Left: Homogeneous soil. Right: Inhomogeneous soil.

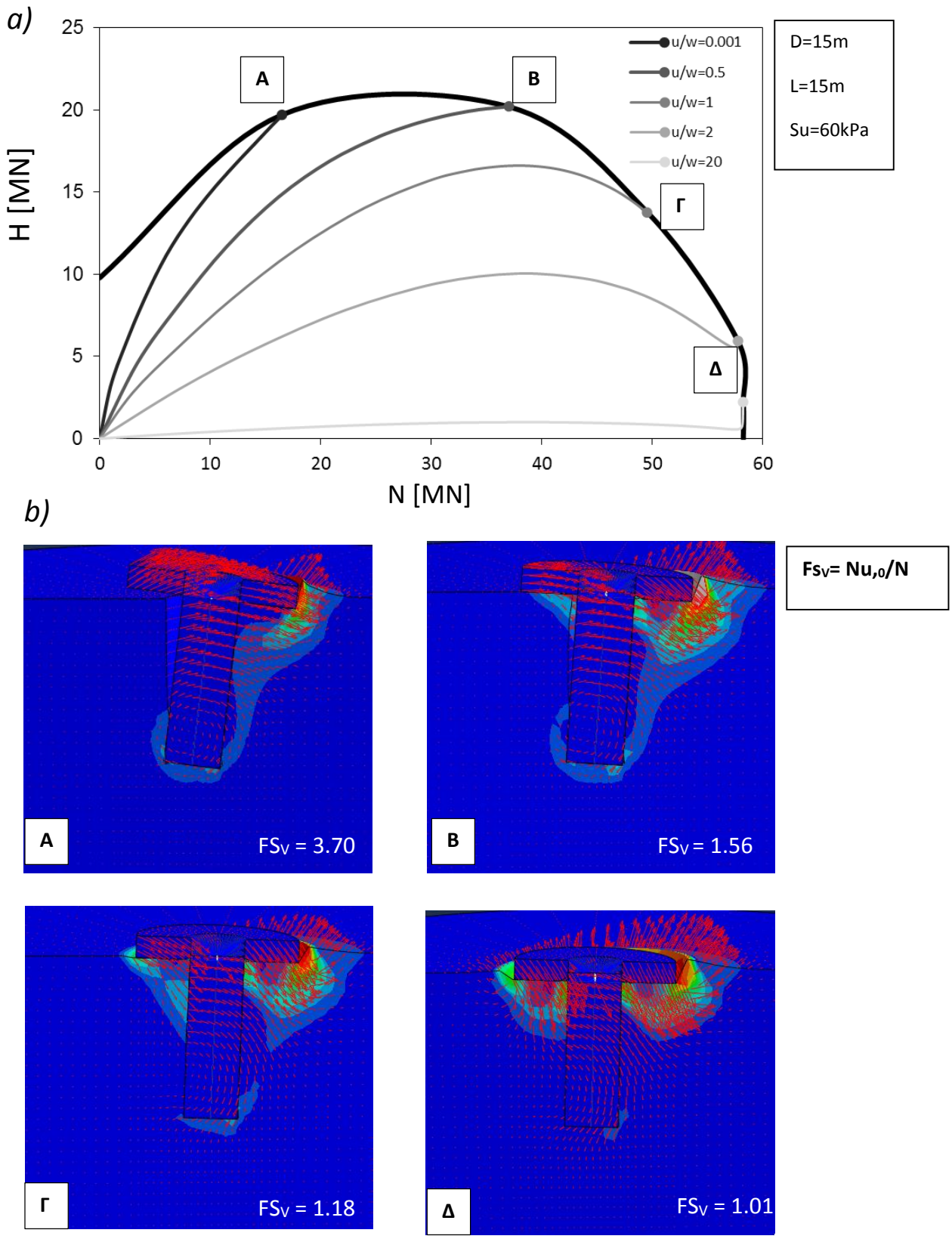

Figure 3.15. **a)** Displacement probes used to produce the Q-N interaction diagram for a hybrid foundation with D = 15m and L = 15m, lying on homogeneous soil. **b)** Failure mechanisms in terms of plastic strain contours and displacement vectors at characteristic points of the envelope. The vertical factor of safety is also noted.

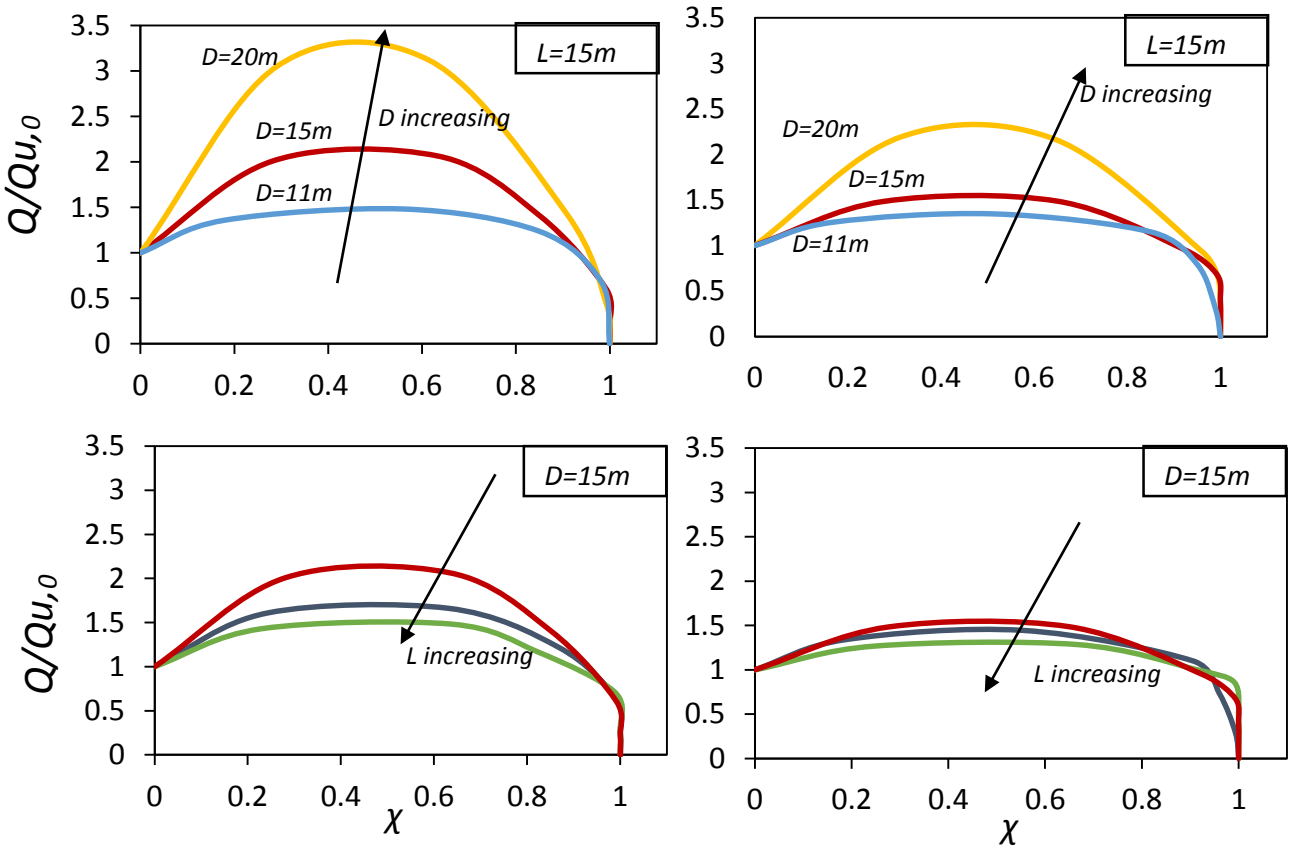

Figure 3.16. Normalized failure envelopes in the Q-N (M=0) loading plane. Top row: Various footing diameters for a hybrid foundation with L = 15m. Bottom row: Various monopile lengths for a hybrid foundation with D = 15m. Left: Homogeneous soil. Right: Inhomogeneous soil.

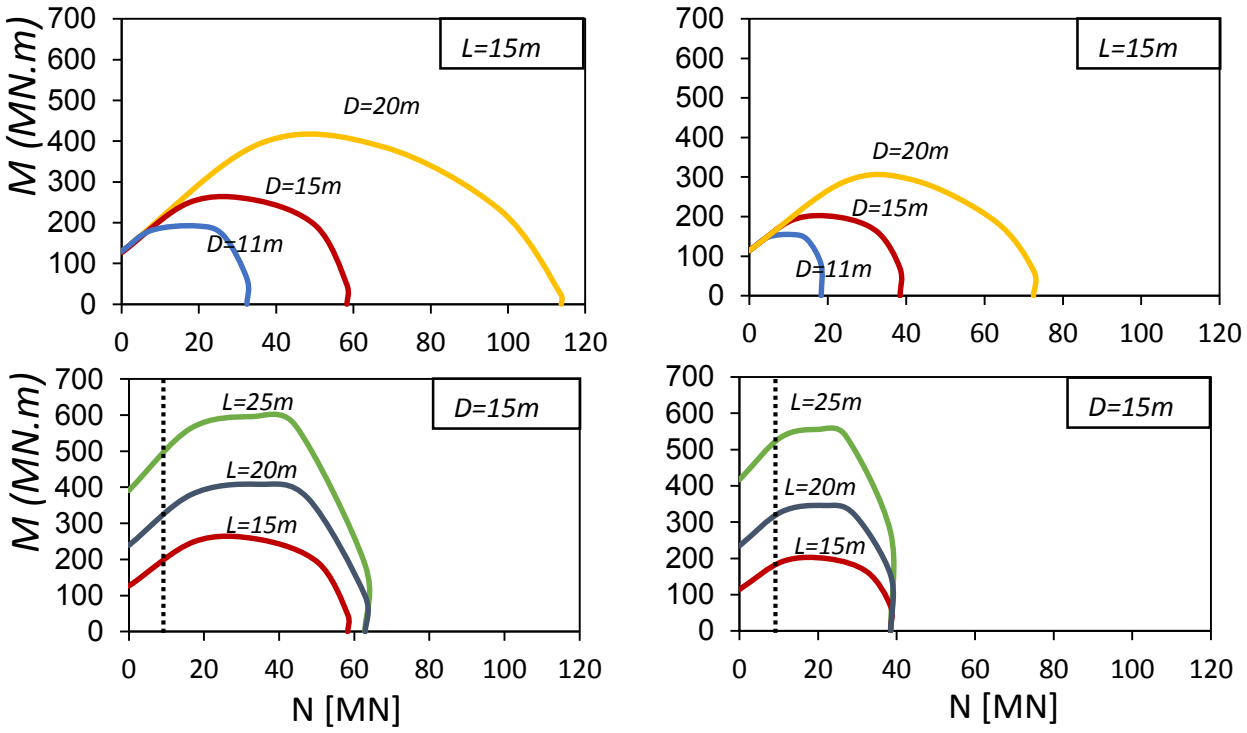

Figure 3.17. Failure envelopes under combined vertical – moment loading (Q=0). Top row: Various footing diameters for a hybrid foundation with L = 15m. Bottom row: Various monopile lengths for a hybrid foundation with D = 15m. Left: Homogeneous soil. Right: Inhomogeneous soil.

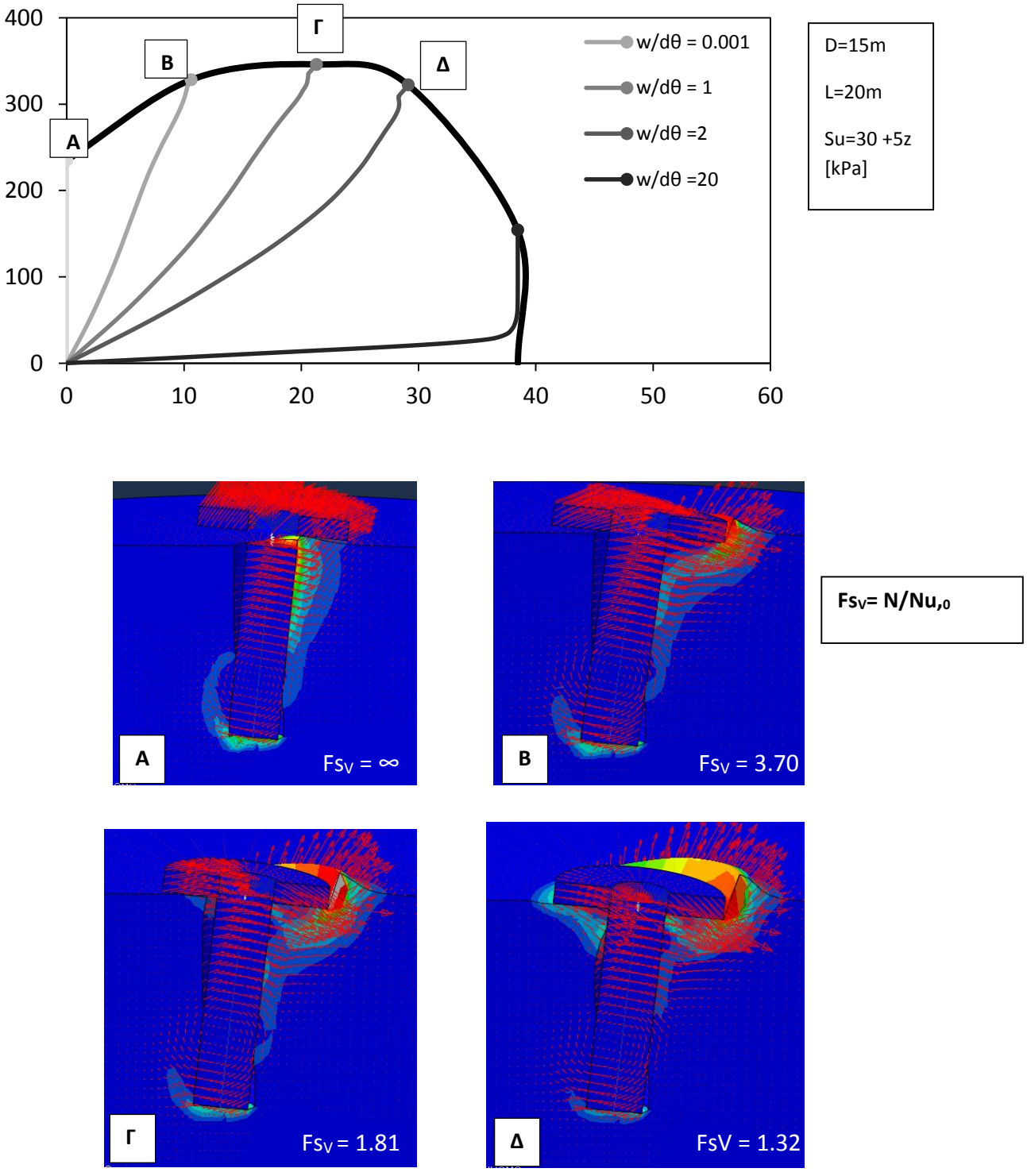

Figure 3.18. Top: Displacement probes used to produce the M-N interaction diagram for a hybrid foundation with D = 15m and L = 20m, lying on inhomogeneous soil. Bottom: Failure mechanisms in terms of plastic strain contours and displacement vectors at characteristic points of the envelope. The vertical factor of safety is also noted.

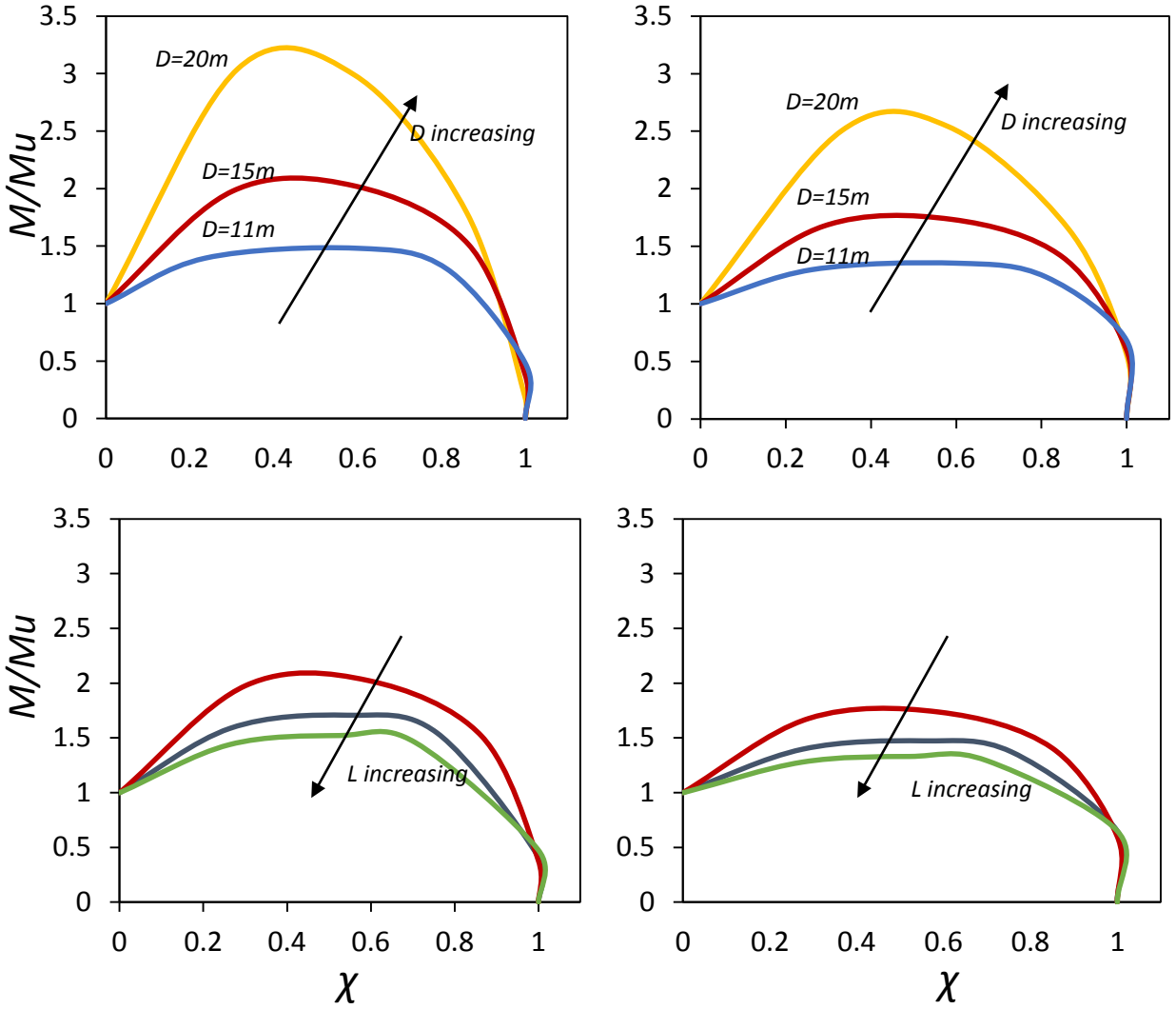

Figure 3.19. Normalized failure envelopes in the M-N (Q=0) loading plane. Top row: Various footing diameters for a hybrid foundation with L = 15m. Bottom row: Various monopile lengths for a hybrid foundation with D = 15m. Left: Homogeneous soil. Right: Inhomogeneous soil.

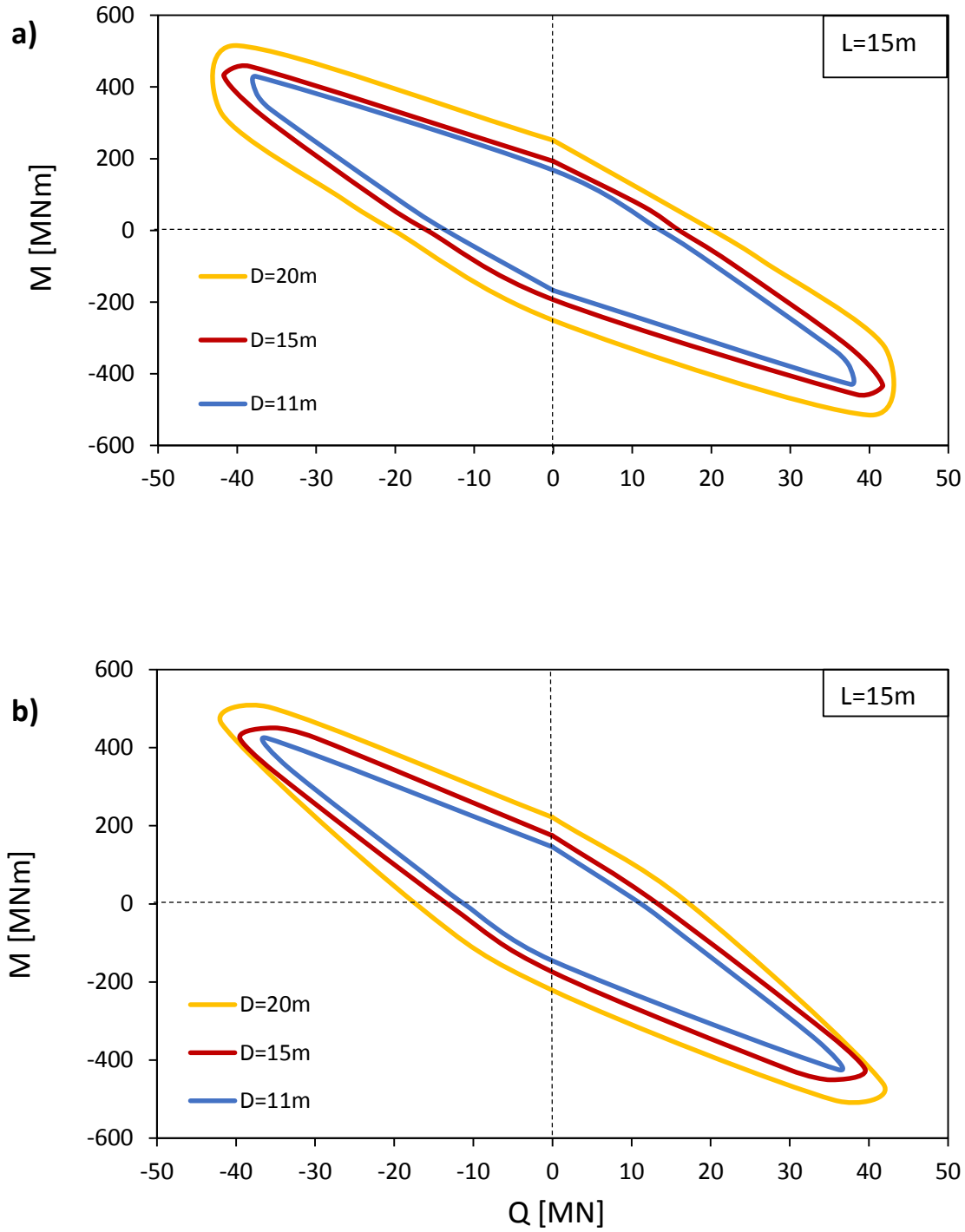

Figure 3.20. Moment – Shear force interaction diagrams for a hybrid foundation with L = 15m and various footing diameters. The weight of a typical 3.5 MW superstructure and of each footing is considered. **a)** Homogeneous soil. **b)** Inhomogeneous soil.

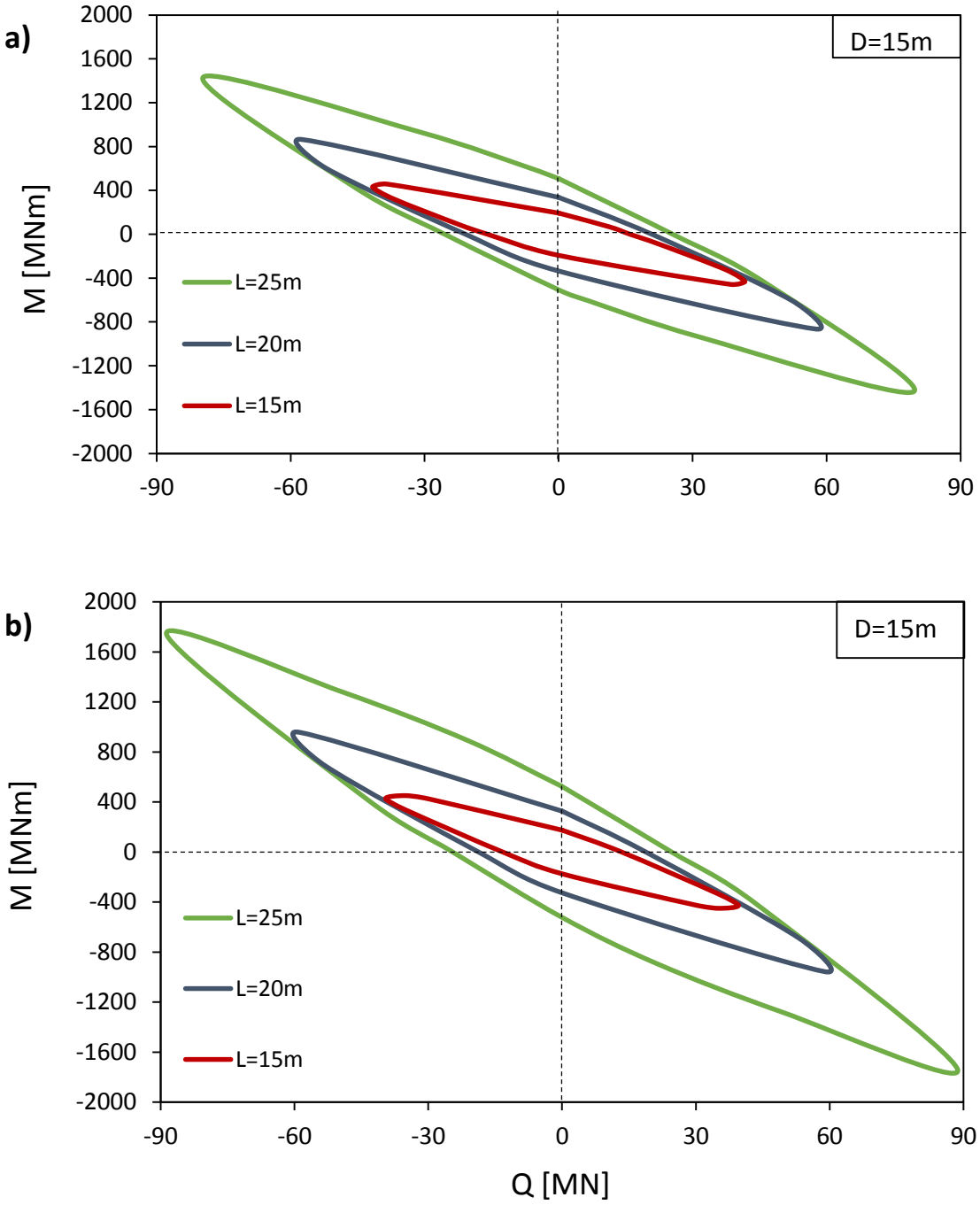

Figure 3.21. Moment – Shear force interaction diagrams for a hybrid foundation with D = 15m and various monopile lengths. The weight of a typical 3.5 MW superstructure and of the footing is considered. **a)** Homogeneous soil. **b)** Inhomogeneous soil.

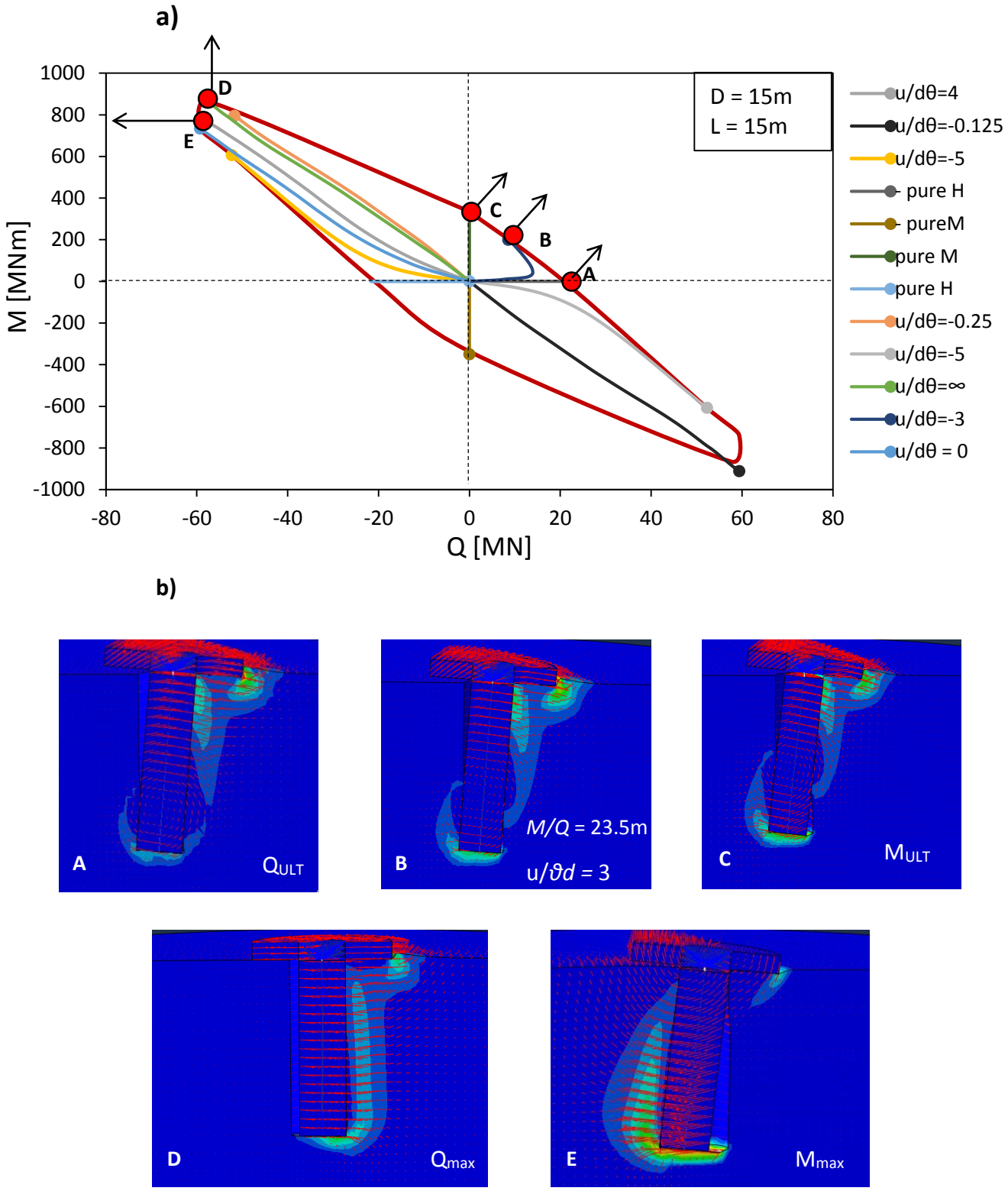

Figure 3.22. **a)** Displacement probes used to produce the M-Q interaction diagram for a hybrid foundation with D = 15m and L = 15m, lying on homogeneous soil. **b)** Failure mechanisms at characteristic points of the envelope. A) Pure horizontal loading (Qult). B) Combined moment and same direction horizontal loading. Γ) Pure moment loading (Mult). Δ) Horizontal loading with simultaneous rotation constrain (Qmax). E) Moment loading with simultaneous horizontal displacement constrain. (Mmax)

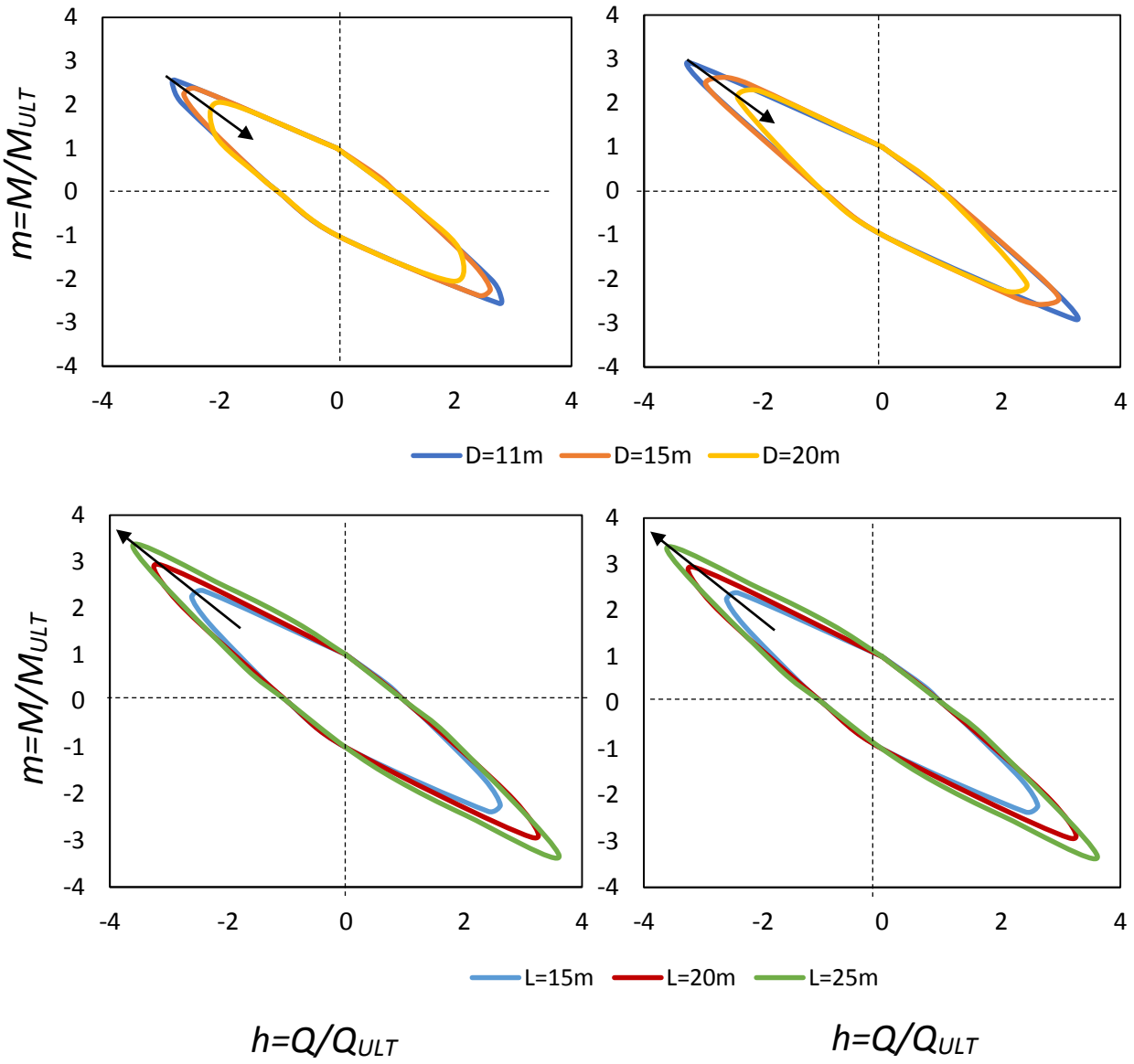

Figure 3.23. Normalized failure envelopes in the M-Q loading plane. Top row: Various footing diameters for a hybrid foundation with L = 15m. Bottom row: Various monopile lengths for a hybrid foundation with D = 15m. Left: Homogeneous soil. Right: Inhomogeneous soil.

CHAPTER 4

Stiffness of Hybrid Foundations

4.1 Prologue
4.2 Rocking Stiffness
4.3 Swaying Stiffness
4.4 Coupled Stiffness Components
4.5 Further Investigation
4.6 Conclusions

4.1 Prologue

Bearing capacity is an important design criterion and the study conducted in the previous chapter provides the necessary information to calculate the factors of safety, and to determine the response of each foundation near failure. In other words, bearing capacity concerns the behavior of the soil-foundation system in the large displacement area. However, there are several other crucial parameters for the problem of founding an offshore wind turbine, the most important being calculation of deformations. Considering that a quite large factor of safety will be implemented for each type of loading, the actual loads acting on the system will be a lot smaller than the capacity. In order to estimate the behavior of the system under real loading conditions, the stiffness of the system must be examined. A set of analyses is conducted in this chapter, in order to determine the initial stiffness components at very small deformations (elastic stiffness components), as well as the progressive stiffness degradation that occurs as deformations increase.

As far as the elastic stiffness is concerned, a variety of publications exist that investigate many aspects of the problem for various foundations [e.g. Poulos & Davis, 1974; Gazetas, 1983, 1987, 1991; Doherty et al., 2005]. A large part of the research already done concerns both the shallow footing and the pile, the components of the hybrid foundation. The elastic stiffness components can be used to form a stiffness matrix, that is equal to

$$[K] = \begin{bmatrix} KV & 0 & 0 \\ 0 & KHH & KHM \\ 0 & KMH & KMM \end{bmatrix}$$

for the three degree-of-freedom problem examined here.

Non-linearities have recently been introduced to the stiffness problem [Gazetas et al. 2012] for the case of shallow footings, as reported in chapter 1. In the current study, both geometrical (uplifting, sliding) and material (elastic-plastic soil constituve model) non-linearities are taken into consideration.

Attention is drawn to the lateral stiffness components; the rocking and swaying stiffness KMM and KHH respectively and the cross-coupled stiffness terms KHM and KMH, owing to embedment. Definition of each stiffness component, along with the load reference point are shown in **figure 4.1**. The vertical stiffness component is not examined in the current study because it is has minor importance on the offshore wind turbine problem.

Each analysis conducted follows the same steps: a) Imposition of dead load, b) imposition of rotation or horizontal displacement while the other degree of freedom is constrained and c) extraction of the reaction force or moment at the load reference point. It is important to note that all stiffness components are dependent on the magnitude of displacement, rotation and the factor of safety against vertical loads.

$K = f(u, \vartheta, FS_V)$

In the current study FS_V is not the same for all the hybrid foundations, as some have different footings. However, the weight of each foundation as well as of a 3.5 MW offshore wind turbine is considered in an effort to present more practical results, one step closer to the

foundation design. **Table 4.1** provides a full presentation of the vertical factors of safety for the three wind turbine towers that are examined in the next chapter.

Finally, as in chapter 3, the effect of each element of the hybrid foundation on the stiffness components is examined separately.

4.2 Rocking Stiffness

Rocking stiffness is extremely important for tall and slender structures such as wind turbines, because moment is the dominant load acting on the foundation base (M/N > 25, M/Q ≈ 24-25). To produce the rocking stiffness degradation curves, a rotation is imposed at the center of the foundation lid (L.R.P), while horizontal displacement is restricted. It was necessary to impose the rotation in increasing steps because if imposed all at once, the incremental step of ABAQUS was not small enough to capture the initial elastic stiffness for very small angles of rotation ϑ. Size of finite elements is found to play an important role on the initial stiffness; if the elements of the footing are not small enough, inaccuracies can occur in the initial stiffness. After the reaction moment is extracted, rocking stiffness is calculated by the following expression:

$$K_{MM} = M/\vartheta$$

Rocking stiffness degradation charts with increasing angle of rotation are depicted in **figure 4.2** for both soil profiles. A wider range of foundation geometries is examined in this chapter, including three footing diameters (D = 11 m, 15 m & 20 m) and five pile embedment lengths (L = 10 m, 15 m, 20 m, 25 m & 30 m).

First of all, the shape of all curves is similar and is characterized by a linear part that represents the initial (elastic) rocking stiffness for very small angles of rotation and a non-linear part that represents stiffness degradation with increasing rotation. Stiffness degradation is the result of both geometrical and material non-linearities.

Diameter of the footing D seems to have a direct impact on the initial rocking stiffness of the hybrid foundation. A 33 % increase in the diameter (from 15 m to 20 m) can lead to a 38 % increase in the rocking stiffness of the hybrid foundation, which is a significant gain. All of the foundations with the footing with D = 15 m have approximately the same initial stiffness except for the D15 – L10 system which presents an noticeable decrease. It is noteworthy that the hybrid foundation with the largest footing (D20 – L15) seems to be entering the stiffness degradation area earlier than the systems with a longer pile or smaller footing. This is probably the result of geometric non-linearities in the soil – footing interface and especially uplift, which is more significant for stiffer soils or larger footings. Consequently, uplift on the larger footing is developed earlier, reducing the contact surface and degrading the overall rocking stiffness.

Effect of the pile length L on the elastic stiffness is not that strong. In fact, all of the foundations with the same footing have approximately the same elastic stiffness except for the one with the shortest pile (10 m) which has a reduced stiffness. This may be attributed to

the fact that the elastic rocking stiffness of a pile depends mainly on its cross section and the soil properties and not on the embedment length, at least for L>15m. Since all the piles have the same diameter (d = 5 m), their elastic stiffness is the same. The difference between the curves is exposed as the angle of rotation gets larger. Foundations with longer piles tend to maintain larger values of stiffness even for quite large rotations, while the ones with shorter piles begin to degrade earlier; it seems that while the pile rotates, a larger part of its length is activated and stiffness degradation is less evident. Another interesting observation is that the curves of the three hybrid foundations with the same pile length and different footings (presented with the same color) tend to converge in the larger ϑ domain. Considering the above, it is made clear that the pile has a great influence at the large rotation area, close to failure. This is the reason why the pile length has a major influence on the overall moment bearing capacity of the hybrid foundation, as proven in chapter 3. It must be stressed out however, that the basic design criterion for offshore wind turbine foundations is the maximum accumulated rotation limit which is roughly 0.5° (0.087 rad), so it is beyond doubt that the ultimate bearing capacity will never be mobilized during the turbine's lifetime.

Effect of soil inhomogeneity on rocking stiffness degradation is considerable; it causes a reduction to the initial stiffness of all foundations, because of the direct influence it has on the footing; rocking response of a surface footing is pretty much defined by the superficial soil layers, which are softer for the inhomogeneous soil profile. On the other hand, the charts for the inhomogeneous soil appear a bit stretched horizontally, which implies that their stiffness degradation rate is smaller; this is caused by two reasons. First, the superficial soil layer is softer, allowing the footing to sink rather than uplift therefore maintain better contact with the underlying soil, which makes the resistance reduction more gradual. Second, for all of the piles except the one with L = 10 m, the pile tip has access to soil with larger values of S_U than in the uniform profile case. At larger angle of rotations, this stronger soil is mobilized, improving the rocking resistance.

4.3 Swaying Stiffness

Swaying stiffness is also crucial for offshore wind turbine foundations, which undergo significant horizontal forces and are prone to sliding. Swaying stiffness – horizontal displacement charts are depicted in **figure 4.3**, for uniform and inhomogeneous soil. The linear part of each curve represents the initial elastic swaying stiffness and the non-linear part depicts the progressive stiffness degradation until failure. To produce the charts, a similar procedure is followed as described above; a gradually increasing horizontal displacement u is imposed at the center of the footing lid with the rotation being simultaneously restricted. Swaying stiffness is defined as

$$K_{HH} = Q/u$$

where Q is the generated horizontal force and u the imposed horizontal displacement. The weight of a 3.5 MW wind turbine is taken into consideration.

It is evident that diameter of the footing has a direct influence on the initial swaying stiffness as well. Increasing the footing diameter contributes in two ways; by ensuring a larger contact area and by providing a larger overburden weight. The larger contact area develops a larger resisting horizontal force, while the effect of the footing weight also acts in a beneficial way. Embedment ratio of the pile, on the other hand, has a negligible effect on the overall swaying stiffness. It seems that the curves of all foundations with the same footing size almost converge, as swaying stiffness of a pile depends on the pile's cross-section and the soil properties. However, a slight increase in the overall resistance can be observed for the longer piles in the large displacement domain.

For the inhomogeneous soil, a significant reduction on all the initial stiffnesses is observed. Reduction on the contribution of the footing is also apparent, mainly because the surface soil is weaker and pre-yielding may have already taken place under the superstructure's self-weight.

4.4 Coupled Stiffness Components

The coupled stiffness components K_{MH} and K_{HM} are derived from the rocking and swaying stiffness analyses respectively. The first stands for the horizontal force required to restrain horizontal displacement during the K_{MM} analysis and the second stands for the resisting moment to restrain the rotation during the K_{HH} analysis, as described by the following expressions

$$KHM = M / u$$

$$KMH = H / \vartheta$$

Reduction charts for the coupled stiffness components are shown in **figure 4.4** & **figure 4.5**, for KMH and KHM respectively. General conclusions can be made regarding both of the charts. First of all, the coupled stiffnesses seem to be unaffected by the footing, as expected; these coupled stiffnesses are a result of the embedment length of the pile. The pile length however, starts to influence the curves only in the larger deformation area, while the elastic stiffnesses are approximately the same for all foundations. This is not true for the foundation with the shortest pile (L =10 m), which has a reduced value of both coupled initial stiffnesses. The two stiffness components do not show differences with each other, except for the D20 – L15 hybrid foundation, which appears to have a slightly stiffer response in terms of K_{HM}.

In case of the offshore wind turbine problem, rotation due to overturning moment is expected to dominate over horizontal displacement, due to the large height of such structures. For this reason, the K_{MH} coupled stiffness can be considered more representative.

4.5 Further Investigation

The results from the above discussion are summarized in **figures 4.6, 4.7, 4.8 & 4.9**, in which the initial elastic stiffness components are plotted against all the footing diameters and pile lengths examined. The gain in the initial rocking stiffness by increasing the footing diameter is clearly noticeable in **figure 4.6 (left)**; adding a 15 m footing to a 15 m monopile increases the total elastic rocking stiffness by 70 %, while adding a 20 m footing offers an increase of 158 %. Impact of inhomogeneity is magnified as the footing diameter get larger. The gain in the initial swaying stiffness is also significant but not as much as in the rocking stiffness case, as can be seen in **figure 4.7.b**; the maximum gain in the swaying stiffness is achieved by adding a 20 m footing to the 15 m monopile and it reaches 55 %.

Figure 4.10 gives the elastic stiffnesses for an arbitrarily-shaped shallow foundation and for a long pile, as proposed by Gazetas (1987, 1991). The above formulae are in quite good accordance with the results produced in this study (for the homogeneous soil stratum) and the maximum deviation does not exceed 18%, as seen in **table 4.2**. Gazetas (1987) has proposed a wide range of formulae for several footing shapes, including circular. However, formulae for an arbitrarily-shaped foundation are deemed more reasonable in order to take account for the hole in the center of the footing.

In an effort to further understand the impact of each component of the hybrid foundation on the overall response of the system, the same stiffness degradation charts are produced for a footing (D = 15 m) and a pile (L = 15 m) alone.

Figure 4.11 depicts rocking stiffness degradation of a hybrid foundation with D = 15 m and L = 15 m, as well as of each element comprising it. Some very interesting observations can be made; to begin with, the footing has smaller stiffness than the pile and tends to degrade earlier due to uplift. As aforementioned, detachment from the soil occurs as no tension can be held, leading to an immediate decrease of the rocking resistance. This is not occurring in the case of the monopile, which maintains a larger contact area with the surrounding soil, even when one side is detached. A common assumption is that in the elastic phase, it is valid to superimpose the result of two different actions. In order to investigate whether this assumption can be made for elastic stiffnesses of the hybrid foundation, the sum of the curves of the two components is also included along with the finite element results for the hybrid foundation. Interestingly, initial stiffness of the hybrid foundation is even larger than the sum of the initial stiffnesses of the two components, but not to a significant extent. This is caused by the beneficial presence of the footing; as the footing rotates it compresses the underlying soil, increasing the degree of confinement that the pile experiences. In this way, better contact conditions are achieved on the pile – soil interface and the behavior of the pile is also improved, compared to the monopile. However, this increase is rather small and can be neglected, leading to the conclusion that the formulae presented in **figure 4.11** can be used to approximately estimate the rocking stiffness of a hybrid foundation composed by a monopile and a footing, at least to a preliminary extent, by superimposing the results of the formulae for the two different rocking stiffnesses. Indeed, the results come to a good accordance, underestimating the total elastic rocking stiffness of the hybrid foundation by barely 5.2 %.

In a similar manner, swaying stiffness of a hybrid foundation with D = 15 m and L = 15 m, as well as of each element comprising it, is presented in **figure 4.12**. Swaying stiffness of a 15 m monopile alone is greater than the one of a 15 m footing alone. On the other hand, the sum of the stiffnesses of the two elements is quite larger than the actual stiffness of the hybrid foundation. This can be attributed to interaction of the two components; the lateral displacement fields caused by each element are superimposed in the area near the pile head, creating a "shadow effect" that deteriorates the overall lateral response.

Finally, the cross-coupled stiffness degradation charts are depicted in **figures 4.13 & 4.14** for a hybrid foundation with a 15 m footing and a 15 m monopile, as well as for each of its components. Limited information can be extracted from these charts, except that a parasitic coupling can be also observed for the footing alone which contributes to some extent in the overall coupled stiffness of the hybrid foundation.

4.6 Conclusions

In this chapter, an investigation of the stiffness of several hybrid foundations was performed and the basic geometrical parameters were associated to the stiffness components. In addition, the effect of each component was further examined and analyses to produce the stiffness degradation charts of each element were also performed. The results for these analyses were compared to the analytical expressions proposed by Gazetas (1987, 1991), and they were found to agree to a satisfying extent. Throughout the whole chapter two cohesive soil profiles were examined, a homogeneous and an inhomogeneous with linearly increasing S_U with depth. The basic conclusions are listed below.

- Larger footing diameters can offer a significant increase to the overall initial response of hybrid foundations in the small deformation domain. This effect is magnified for the rocking stiffness component, where gains of up to 100 % can be easily achieved, compared to the conventional monopile. On the other hand, the footing enters the stiffness degradation area quite earlier than the pile, due to uplift.
- The pile embedment length is dominant in the larger displacement domain, as shown in chapter 3. It seems that for very small displacements, only the top 15 m of the pile are mobilized.
- The effect of inhomogeneity is a decrease in all the initial stiffness components but the stiffness degradation rates also tend to be smaller, due to softer superficial soil layers which make footing sink rather than uplift.
- Especially for the elastic rocking stiffness, the analytical expressions proposed by Gazetas for a shallow arbitrarily shaped foundation (footing with hole in the middle) and a conventional monopile, can be simply superimposed to provide a conservative estimate of the hybrid elastic rocking stiffness.
- Stiffness degradation charts are produced for various hybrid foundations supporting a 3.5 MW offshore wind turbine and can be used to predict the response of the system via a simple iterative procedure, using the widely-known expression of matrix statics

  $[F] = [K(u)][\delta]$

CHAPTER 4: FIGURES

Stiffness of Hybrid Foundations

FSV	D20-L15	D15-L20	D15-L15	D11-L15
5MW	4.8	3.4	-	-
3.5MW	5.5	4.2	4.2	2.7
2MW	-	4.6	4.6	3.1

FSV	D20-L15	D15-L20	D15-L15	D11-L15
5MW	4.8	3.4	-	-
3.5MW	5.5	4.2	4.2	2.7
2MW	-	4.6	4.6	3.1

Table 4.1. Vertical factors of safety for wind turbine towers and foundations examined in the current thesis.

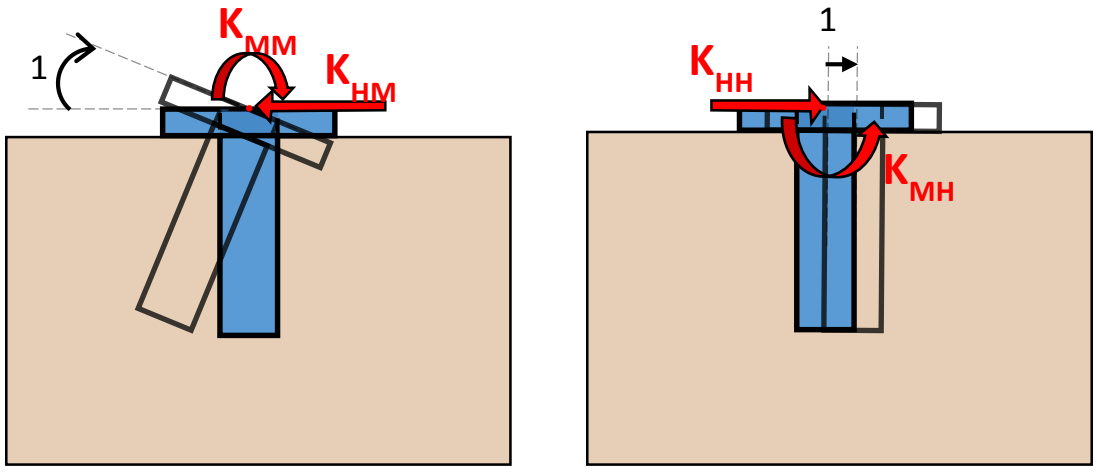

Figure *4.1.* Definition of the stiffness components calculated in the current chapter.

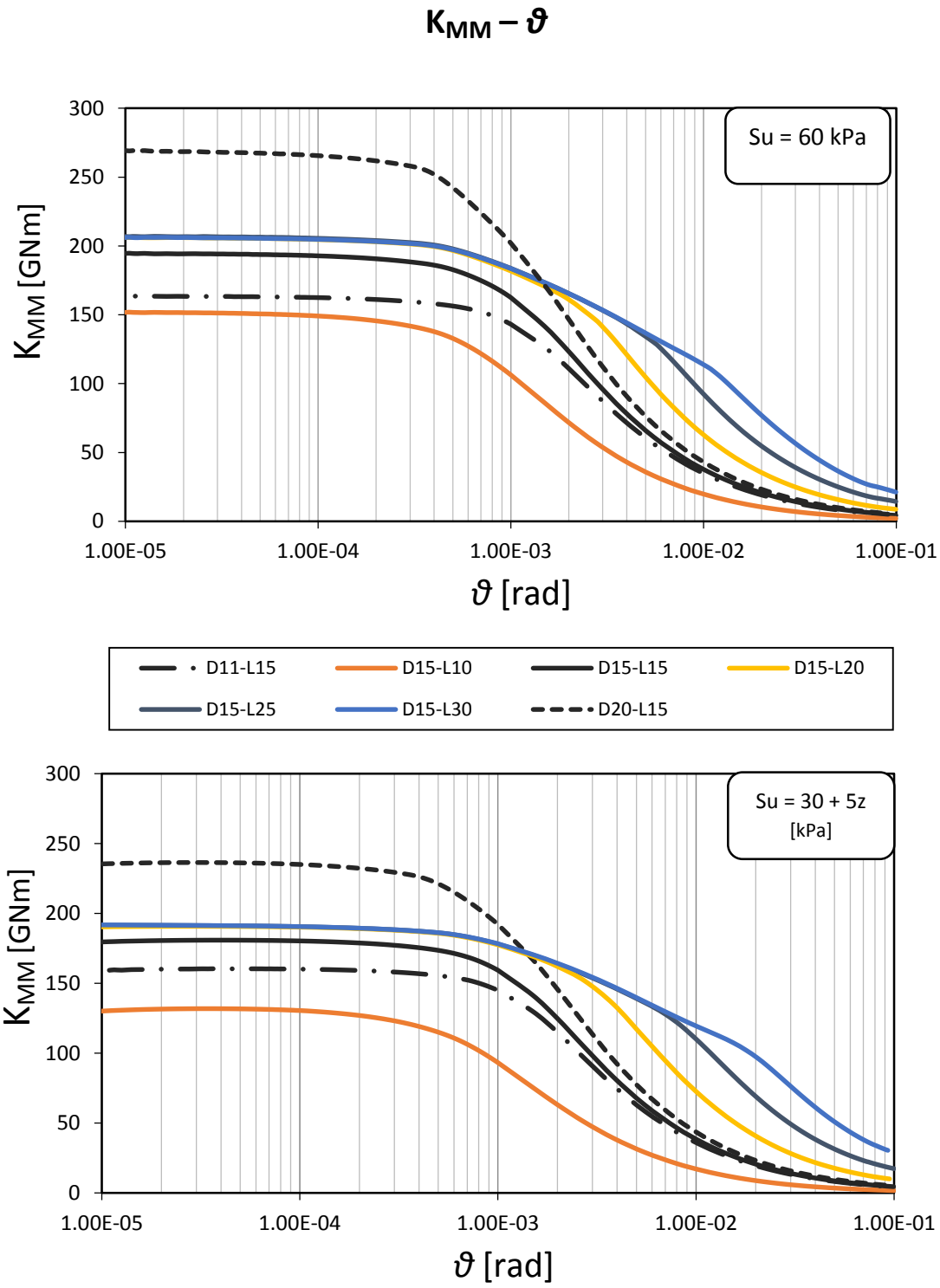

Figure *4.2.* Charts of the reduction in the rocking stiffness with increasing rotation, of various foundations supporting a 3.5 MW wind turbine. Top: Homogeneous soil. Bottom: Inhomogeneous soil

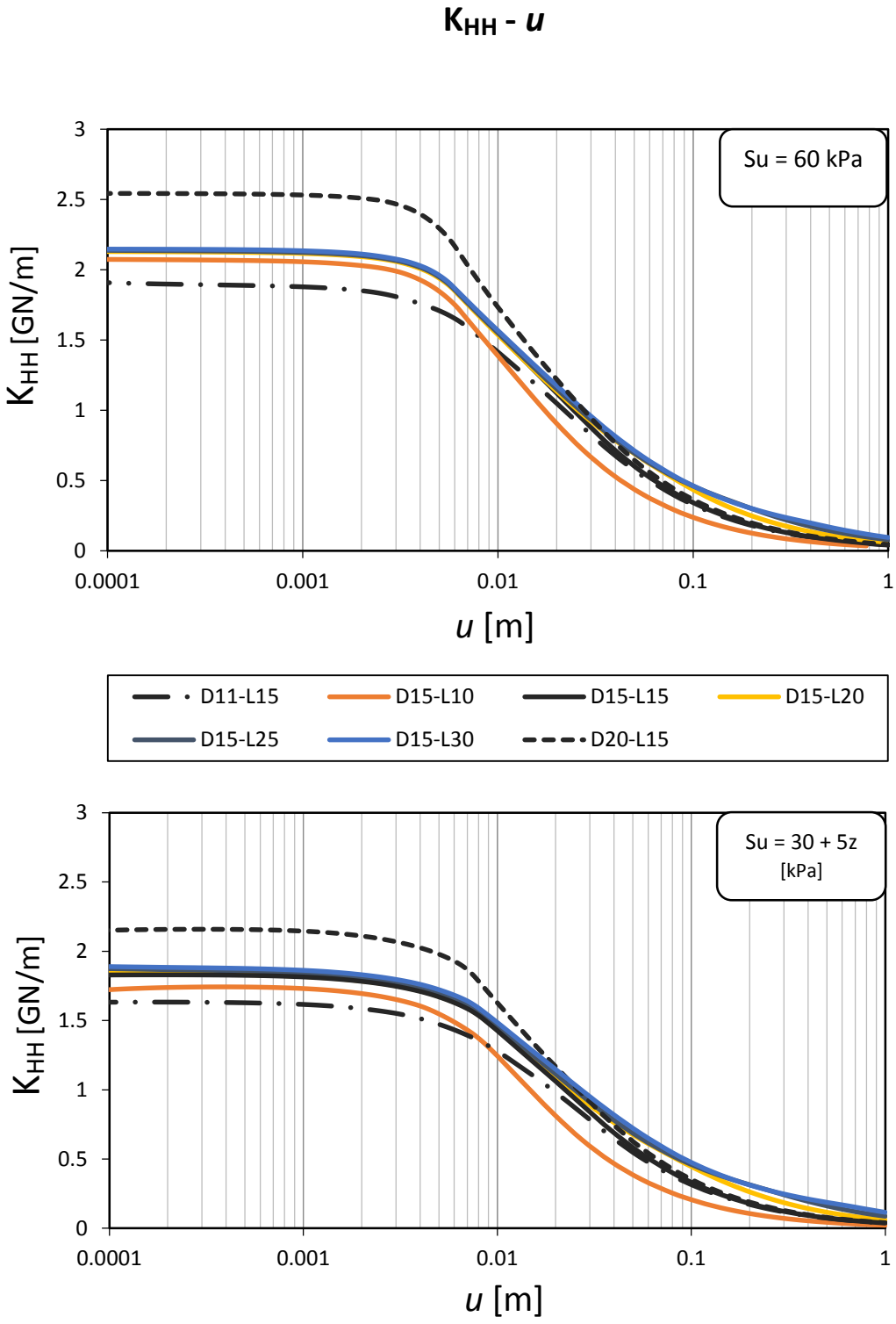

Figure *4.3.* Chart of the reduction in the swaying stiffness with increasing horizontal displacement of various foundations supporting a 3.5 MW wind turbine. Top: Homogeneous soil. Bottom: Inhomogeneous soil

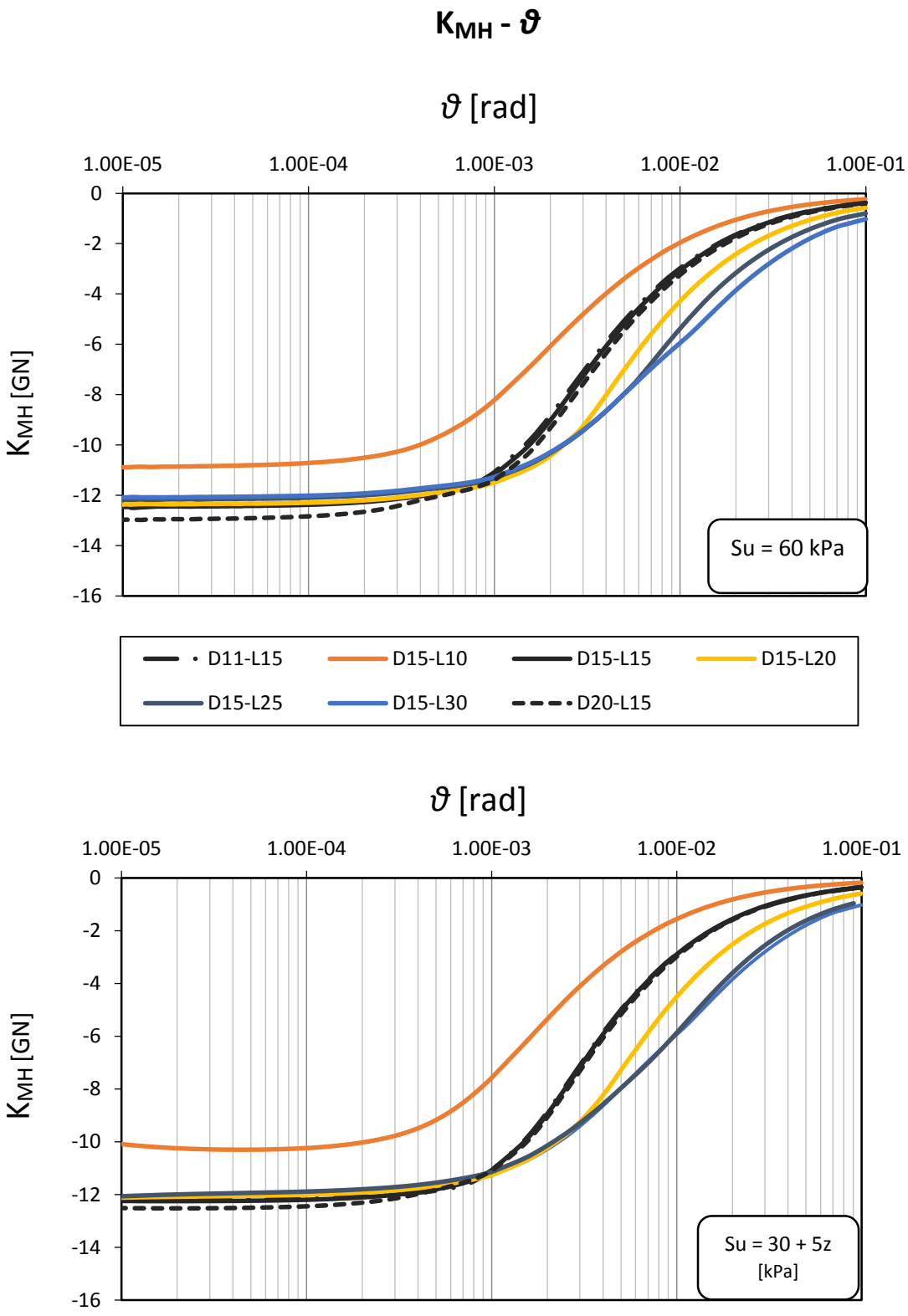

Figure *4.4.* Chart of the reduction in the coupled rocking – swaying stiffness with increasing rotation, of various foundations supporting a 3.5 MW wind turbine. Top: Homogeneous soil. Bottom: Inhomogeneous soil

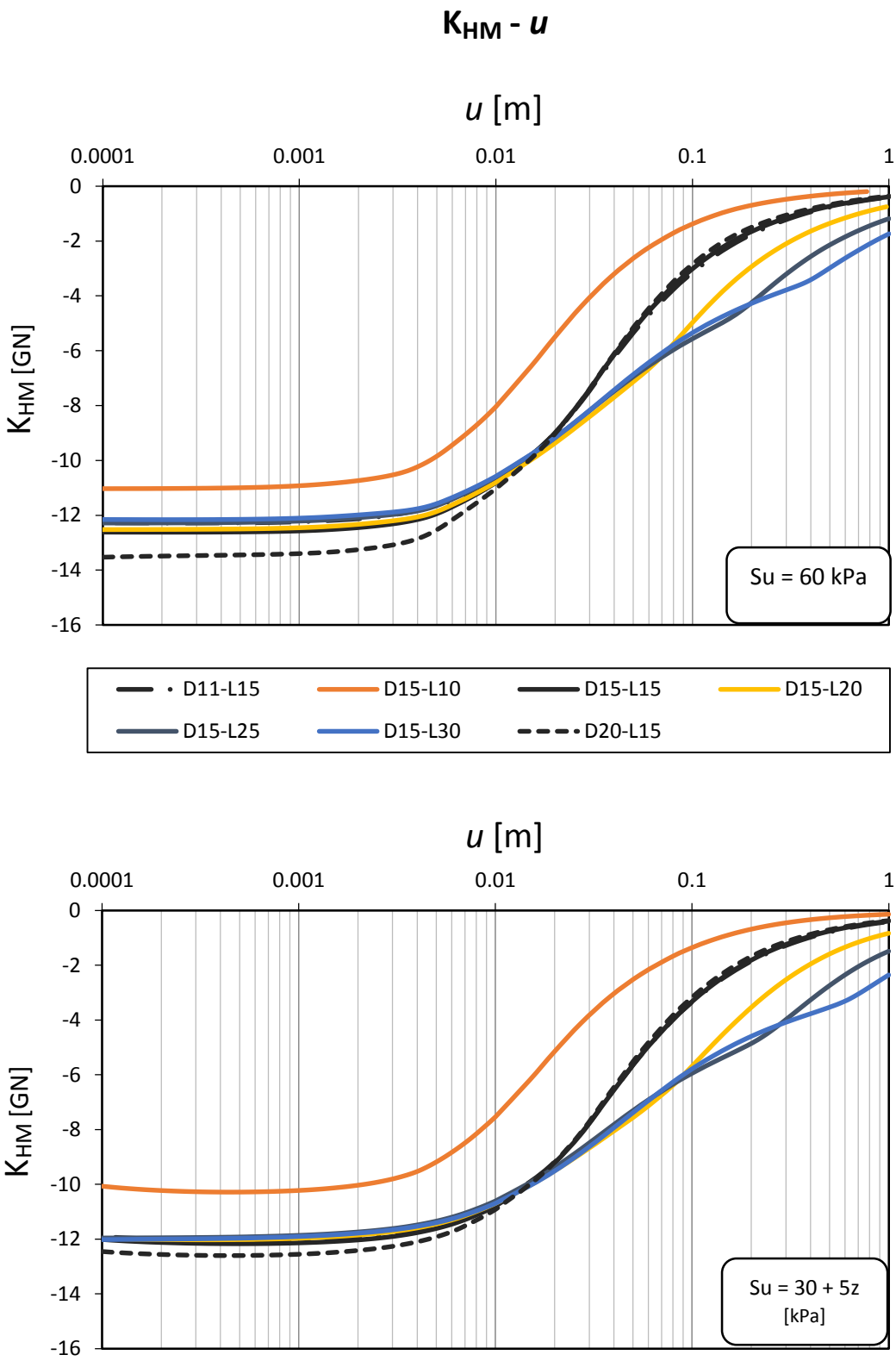

Figure *4.5.* Chart of the reduction in the coupled swaying - rocking stiffness with increasing horizontal displacement, of various foundations supporting a 3.5 MW wind turbine. Top: Homogeneous soil. Bottom: Inhomogeneous soil

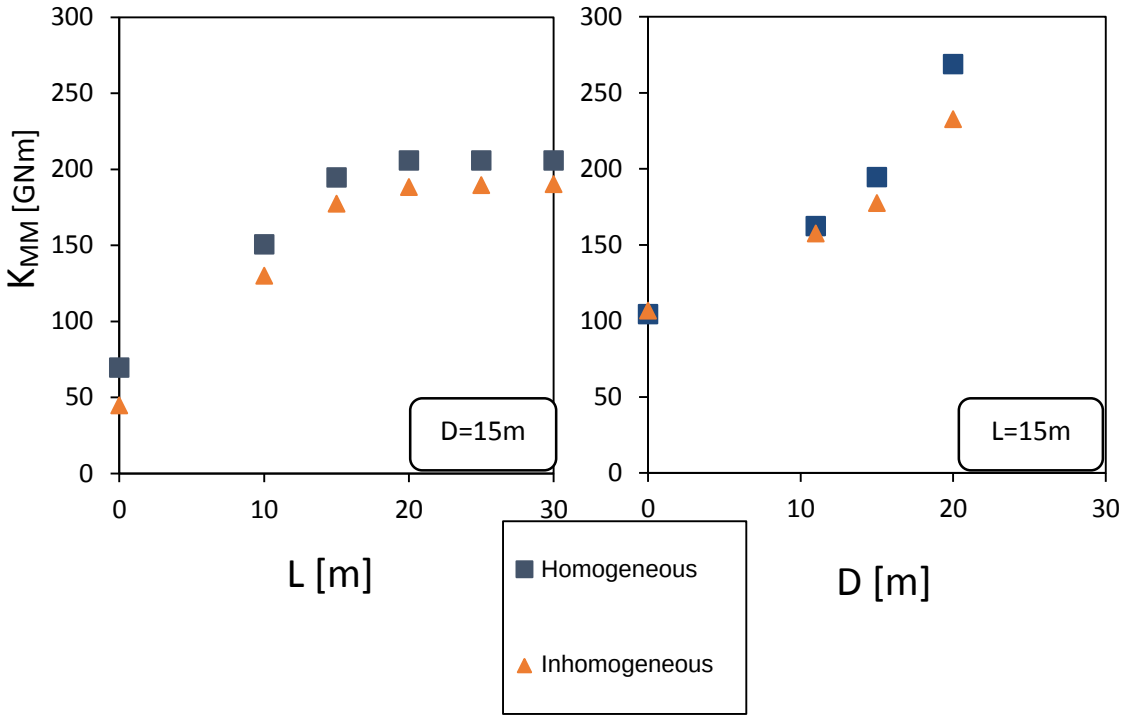

Figure 4.6. Left: Influence of the pile length on the initial rocking stiffness of a hybrid foundation with D = 15m. Right: Influence of the footing diameter on the initial rocking stiffness of a hybrid foundation with L = 15m.

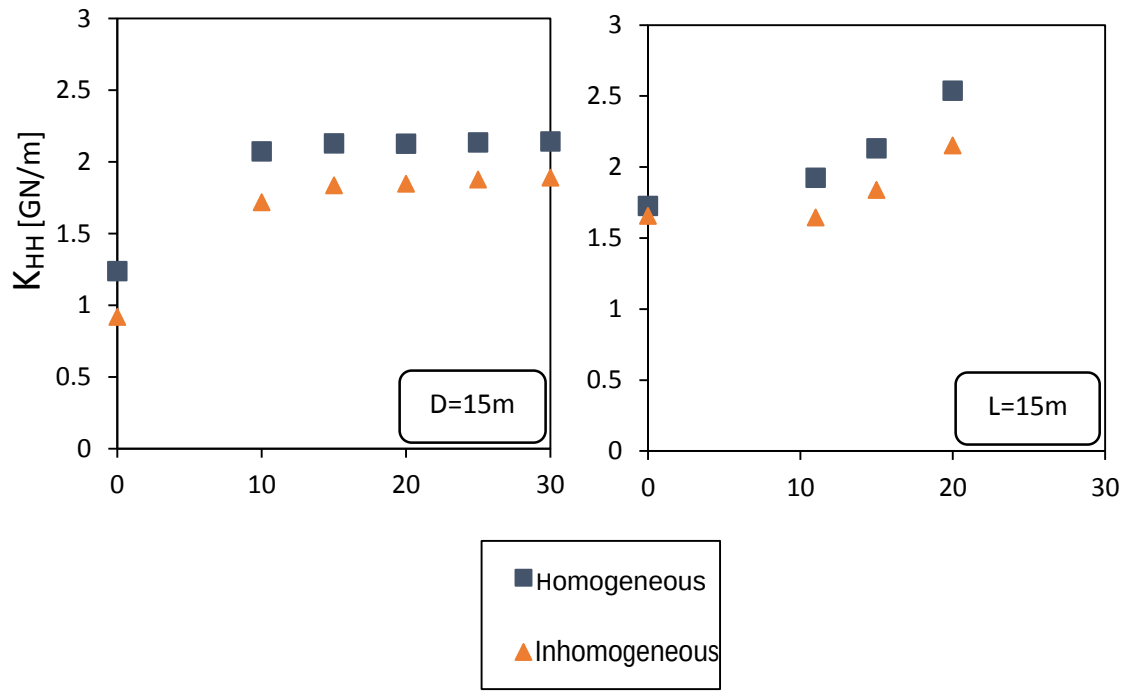

Figure *4.7.* Left: Influence of the pile length on the initial swaying stiffness of a hybrid foundation with D = 15m. Right: Influence of the footing diameter on the initial swaying stiffness of a hybrid foundation with L = 15m.

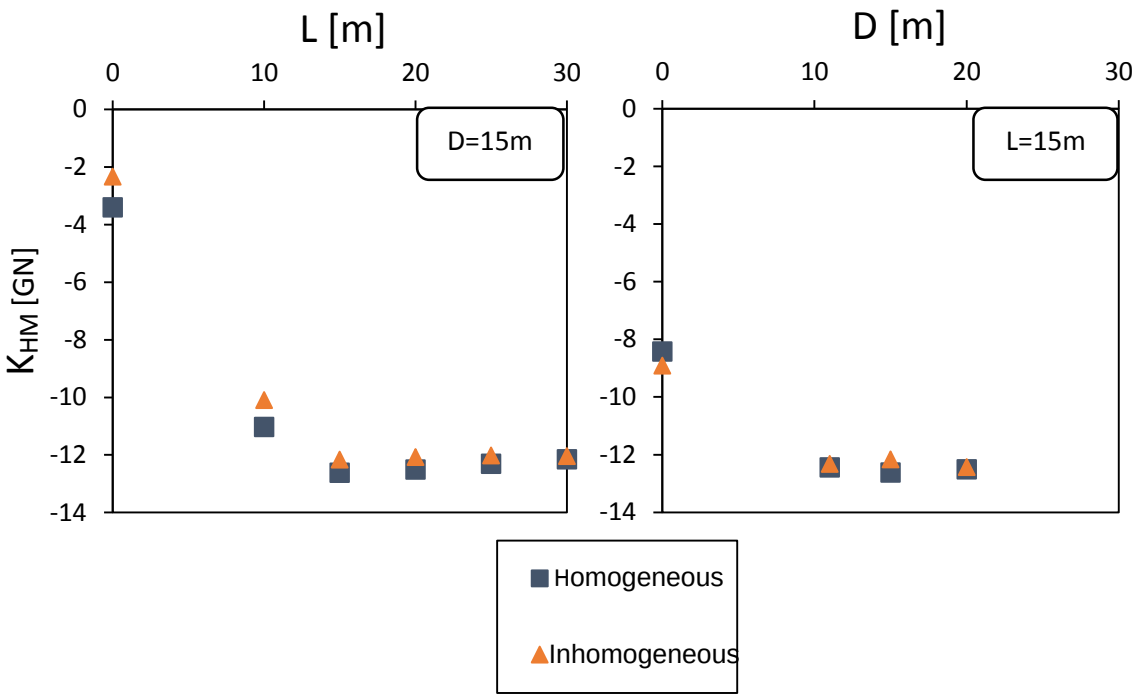

Figure *4.8.* Left: Influence of the pile length on the initial coupled swaying – rocking stiffness of a hybrid foundation with D = 15m. Right: Influence of the footing diameter on the initial coupled swaying - rocking stiffness of a hybrid foundation with L = 15m.

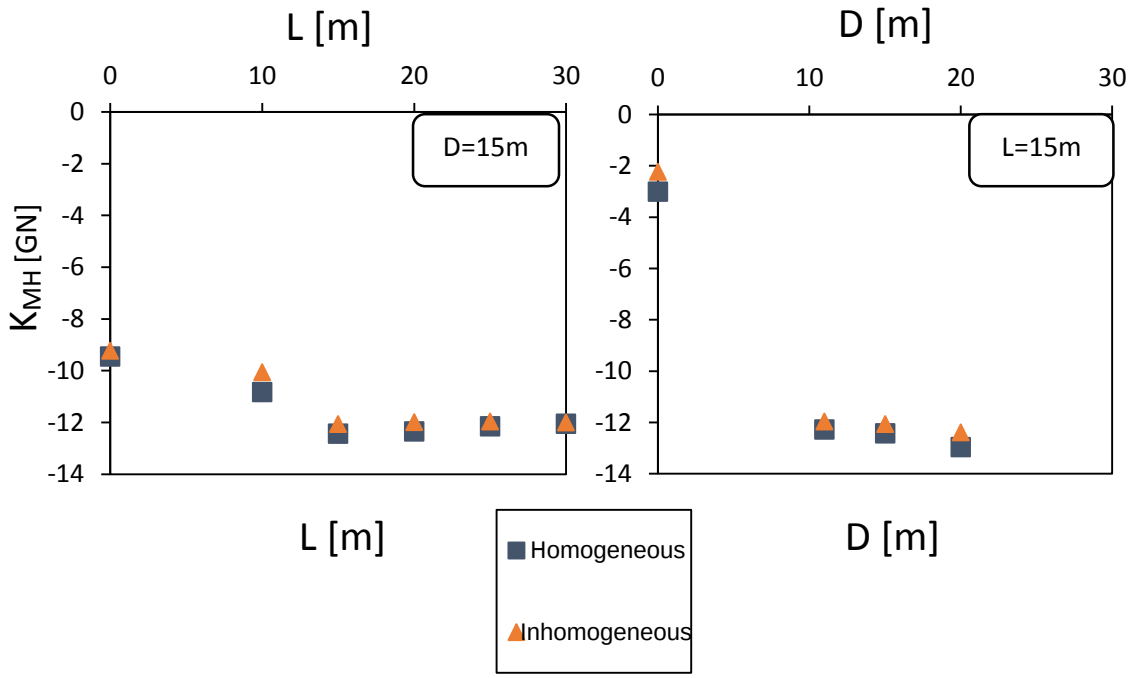

Figure 4.9. Left: Influence of the pile length on the initial coupled rocking - swaying stiffness of a hybrid foundation with D = 15m. Right: Influence of the footing diameter on the initial coupled rocking – swaying stiffness of a hybrid foundation with L = 15m.

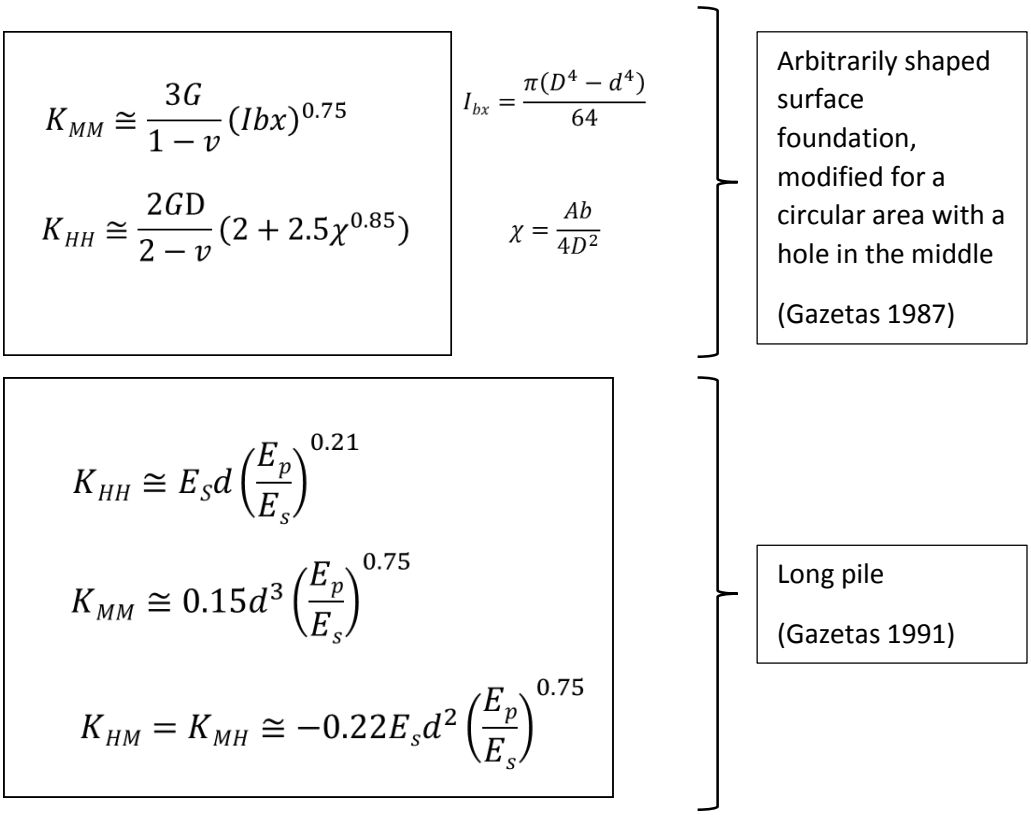

Figure *4.10.* Analytical expressions for the elastic lateral stiffness components of arbitrarily shaped surface foundations and long piles, for homogeneous soil.

L = 15 m	This study	Gazetas (1991)	Deviation
KMM : kNm	104424753	122392339	17.2 %
KHH : kN/m	1726348	1702809	1.4 %
KHM : kN	-8417299	-9148275	8.7 %
KMH : kN	-9454122	-9148275	3.2 %

D = 15 m	This study	Gazetas (1987)	Deviation
KMM : kNm	69523957	62076689	10.7 %
KHH : kN/m	1238975	1408149	12.0 %

Table 4.2. Comparison of the above expressions with the results produced in this study.

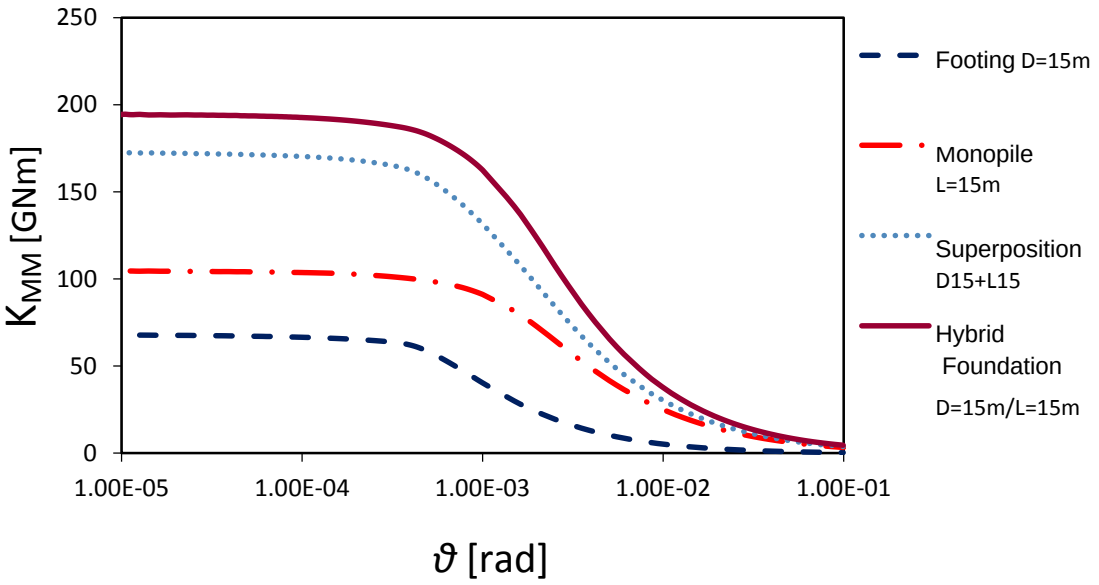

Figure *4.11.* Rocking stiffness of a D15-L15 hybrid foundation supporting a 3.5 MW wind turbine on homogeneous soil as well as of each component of the hybrid foundation calculated separately.

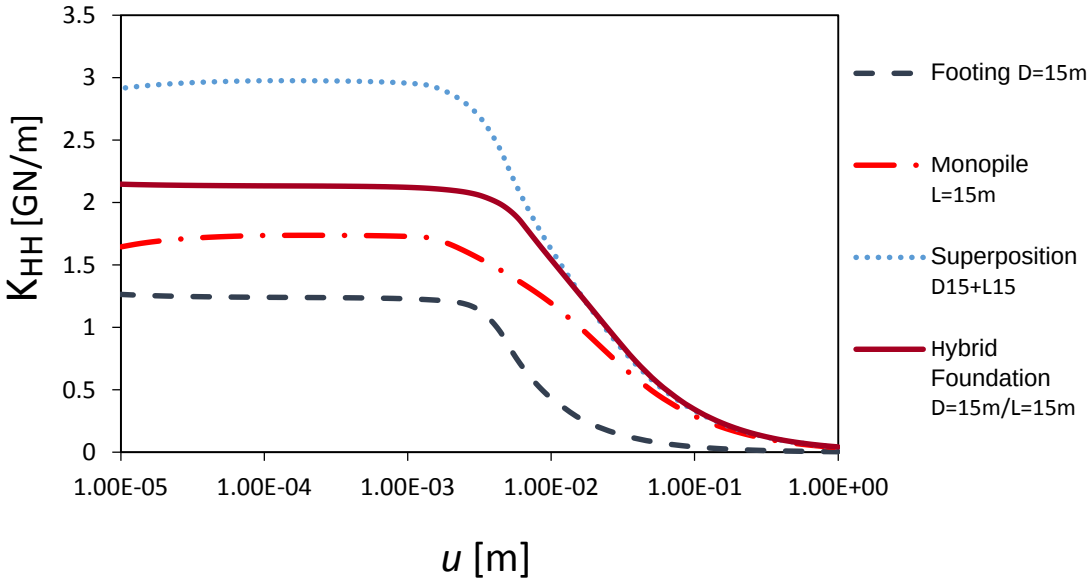

Figure 4.12. Swaying stiffness of a D15-L15 hybrid foundation supporting a 3.5 MW wind turbine on homogeneous soil as well as of each component of the hybrid foundation calculated separately.

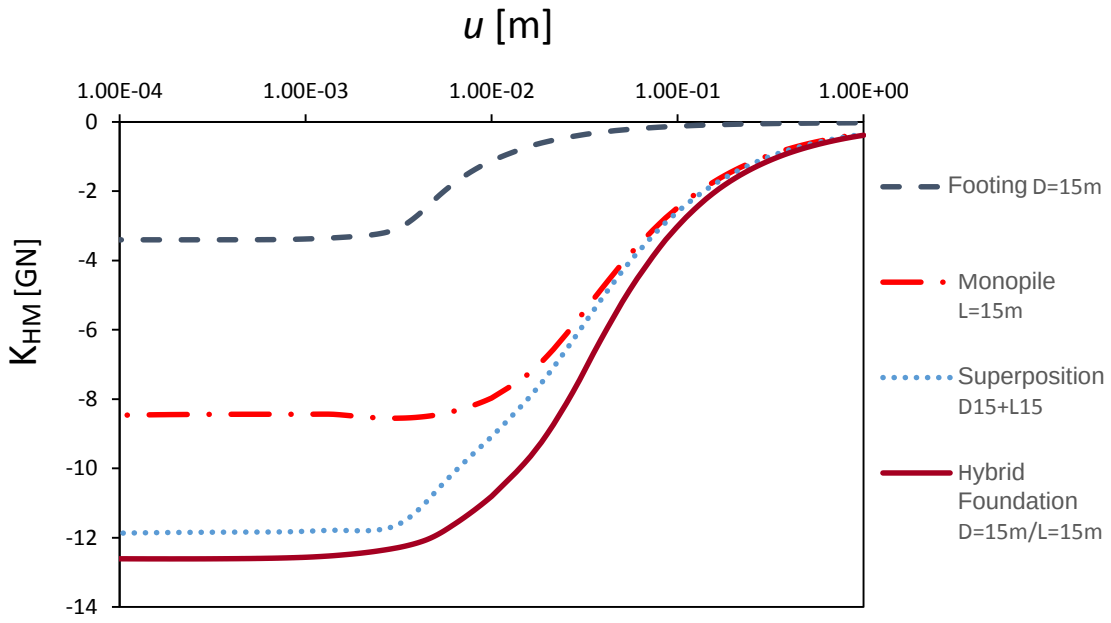

Figure 4.13. *Coupled* swaying - rocking stiffness of a D15-L15 hybrid foundation supporting a 3.5 MW wind turbine on homogeneous soil as well as of each component of the hybrid foundation calculated separately.

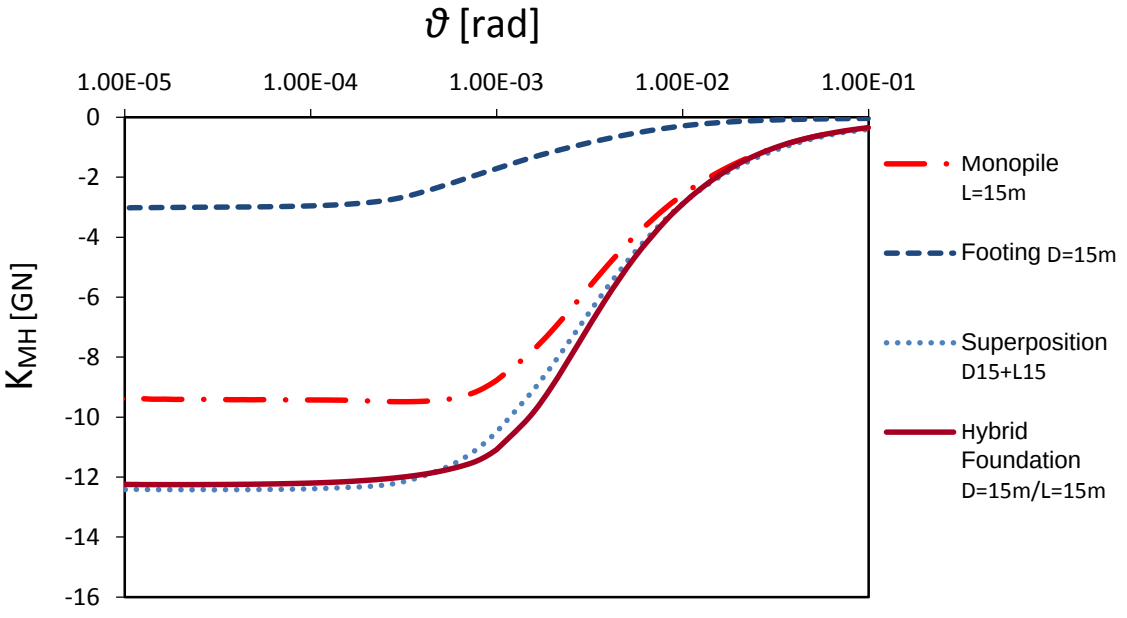

Figure *4.14.* *Coupled* rocking – swaying stiffness of a D15-L15 hybrid foundation supporting a 3.5 MW wind turbine on homogeneous soil as well as of each component of the hybrid foundation calculated separately.

CHAPTER 5

Lateral Loading of Hybrid Foundations Supporting Offshore Wind Turbines

5.1 Prologue
5.2 Monotonic Loading
5.3 Cyclic Loading
5.4 Further Investigation of Wave Cyclic Loading
5.5 Conclusions

5.1 Prologue

After investigating the response of hybrid foundations in the small-strain area and near failure, the next step is to examine the behavior of the soil-foundation-superstructure system under loading conditions that approach the problem in a more practical manner. To this end, the response of the whole system is examined for various hybrid foundations and wind turbine towers under two main types of lateral loading; Displacement-controlled monotonic loading and force-controlled cyclic loading.

Three superstructures are examined that correspond to wind turbines with nominal power capacity of 2 MW, 3.5 MW and 5 MW. A variety of hybrid foundations is chosen, with respect to the increasing size of the wind turbines as their capacity gets larger. In addition, two monopile foundations are used as benchmarks; for the 2 MW and 3.5 MW wind turbines a 30 m monopile is deemed as a reasonable foundation solution while for the 5 MW a 35 m monopile seems more proper. In this chapter the load reference point is taken at the mud line (z = 0), in order to directly compare the hybrid foundations to the monopiles. Taking the load reference point at the top of the foundation lid as in the previous chapters would result in a 2 m difference on the lever arm because the top of the monopile is located at the mud line (z = 0), while the top of the hybrid foundations in the lid (z = 2 m).

For the monotonic analyses, the wind turbines are modelled as stiff towers so that all displacements and rotations are concentrated at the foundation level. On the other hand, for the cyclic analyses, the wind turbine towers are modelled flexible by interpreting the corresponding cross-sectional bending stiffness. P-δ effects are taken into account in all the analyses presented in the current chapter. More details are provided in each subsection.

5.2 Monotonic Loading

In this subsection, an increasing horizontal displacement is imposed at the top of each turbine tower until failure. The general parameters of the monotonic problem are illustrated in **figure 5.1**, while the method of analysis as well as more specific parameters are presented in **figure 5.2**. As can be seen, the two soil bodies introduced in the previous chapters are examined here as well. The wind turbines are modelled as rigid beams, in order to concentrate the rotations and displacements at the foundation level and to evaluate the efficiency of each foundation without interference of the tower bending. Linear 2 – node beam elements are used. Each wind turbine is examined separately, in order to evaluate the performance of each hybrid foundation and compare it to the corresponding monopile. The influence of different superstructures on the monotonic curves of a given hybrid foundation is discussed in the end of the current subsection. It is worth noting that the variety of hybrid foundations examined here is different for each superstructure mainly because larger turbines have significantly larger acting forces and moments, thus demanding larger foundations. An effort is made to conclude to a hybrid foundation solution with satisfying performance for each wind turbine, always in comparison to the corresponding monopile.

To begin with, monotonic moment – rotation curves are presented in **figure 5.3** for the 2 MW wind turbine, both for the homogeneous and the inhomogeneous soil profiles. Three hybrid foundations are examined (D11-L15, D15-L15 & D15-L20) along with the 30 m monopile, which is considered a logical (perhaps conservative) monopile foundation for a 2 MW turbine. A first observation is that, for the homogeneous soil body, the hybrid foundation with the longest pile (D15-L20) has the largest capacity of 240 MNm while the other two (D15-L15 & D11-L15) do not exceed 150 MNm. The gain in terms of moment capacity is significant as the pile length increases, as discussed in chapter 3. Besides that, the 30 m monopile has a considerably larger moment capacity of 410 MNm but seems to demonstrate a softer initial response. For the inhomogeneous soil body, performance of the hybrid foundations is slightly decreased, while the monopile presents a gain in the ultimate moment capacity, owing to the pile tip mobilizing deeper and stronger soil layers. The monotonic settlement-rotation curves are displayed in **figure 5.4** for the two soil profiles examined. It is reminded that positive values of w stand for sinking while negative values represent uplift. For all hybrid foundations a small settlement is observed for smaller values of rotation, but as the angle of rotation ϑ gets larger uplift is evident. The monopile, on the other hand, is increasingly sinking as no uplift is possible, due to the pile being embedded into the soil. For the soil body with linearly increasing S_U with depth, sinking becomes more dominant over uplift.

Moving on, the same results are presented for a 3.5 MW wind turbine. As this wind turbine is larger, it was deemed reasonable to examine the 20 m footing – 15 m pile hybrid foundation (D20 – L15) along with the rest of the foundations that were examined in the previous case. The pushover curves are presented in **figure 5.5**. All the previous observations can also be made for the case of the 3.5 MW turbine. It is interesting that, while the D20 - L15 foundation has slightly smaller ultimate moment capacity than the D15 – L20, it appears to be quite stiffer in the elastic part of the curve; this contribution of the extra 5 m of footing diameter to the initial rocking stiffness is quite beneficial, as discussed in chapter 4. For the inhomogeneous profile the difference between the capacities of the two aforementioned hybrid foundations is larger, due to the large footing laying on weaker soil, while the 20 m pile remains unaffected. The settlement-rotation curves are shown in **figure 5.6**, in which we can observe significant sinking of the D11 – L15 foundation, while the others present uplifting. Sinking is considerably enhanced in the inhomogeneous soil body case.

Finally, for the 5 MW the D11-L15 and D15-L15 hybrid foundations are substituted by larger ones, D15-L25 and D20-L20, to take account for the significant increase of the superstructure's size. To this end, a larger 35 m monopile is also implemented and used as benchmark. The moment – rotation curves are presented for both soil profiles in **figure 5.7**; once again, the largest moment capacity is observed for the hybrid foundation with the longest pile (D15-L25), while the stiffer initial response is observed for the foundation with the largest footing diameter (D20-L20). The 35 m monopile is superior in terms of moment capacity but its initial response is significantly softer compared to all the hybrid foundations. In the case of inhomogeneous soil, initial stiffness of all hybrid foundations is slightly decreased, along with the ultimate moment capacity. This is not the case for the monopile, which seems to gain in terms of moment capacity due to linearly increasing S_U with depth.

Finally, the settlement – rotation curves are presented in **figure 5.8**. It is clear that the response in terms of settlement is dominated by the footing diameter, as expected. The foundations with the 20 m footing demonstrate significant uplift even for small angles of rotation, while the ones with the 15 m footing tend to sink into the soil. Sinking is more intense for the case of inhomogeneous soil, where the surface soil layers are weaker. Regarding the monopile, it seems that the inhomogeneous soil improves the performance in terms of settlement, as the pile tip reaches very strong soil layers that prevent settlement of the pile.

All the above monotonic analyses are conducted by imposing the displacement at the top of the tower, which corresponds to the wind load application point. Before moving on to cyclic loading, it is important to examine the influence of the load application point to the monotonic response. To do this, a monotonic analysis is performed for the 3.5 MW wind turbine founded on the D15 – L15 foundation, with the displacement being imposed at the wave load application point which is located at 8 m above the mud line. The results are compared to wind monotonic loading in **figure 5.9**, both in terms of moment – rotation and horizontal force – displacement. If we focus on the moment – rotation curves, a very important observation can be made; both the ultimate moment capacity and initial rocking stiffness are larger for the case of wind loading. On the other hand, horizontal bearing capacity and stiffness are larger for the case of wave loading. The latter results demonstrate the significant role of the load application point (which can be expressed by the normalized M/Qd ratio) on the lateral response of the system. To better understand this impact on the ultimate bearing capacity, the load paths until failure in the M – Q plane are depicted in **figure 5.10**, along with the corresponding M – Q failure envelope, extracted in chapter 3. As previously discussed, the ultimate moment capacity drops almost in a linear manner, with increasing shear force acting on the same direction. The tangent of each load path represents the lever arm of each load application point. It is very interesting that the same observation seems to apply on the initial rocking stiffness of the system, possibly due to non – linearities becoming more intense when a moment – horizontal force combination is applied, than when each load is imposed independently.

5.3 Cyclic Loading

5.3.1 Preface

Offshore wind turbines are subjected to a complex loading regime throughout their lifetime, due to wind and wave loads. The true nature of these loads is dynamic, however in the current study it is assumed that no resonance will occur, therefore the loads are applied in a static (slow – cyclic) manner. The basic parameters of the cyclic problem are depicted in **Figure 5.11**. Two cyclic load cases are examined; the first involves cyclic wind loading, while the second concerns monotonic wind loading and cyclic wave loading, as seen in **figure 5.12**. The towers

are modelled as flexible, using the real values of bending stiffness EI that correspond to each superstructure. The tower characteristics of each superstructure are displayed in **table 5.1**, while the nomenclature is depicted in **figure 5.13.** P – δ effects are taken into account and the second order moments are found to be quite large, due to flexibility of the tower. Wind and wave loads are calculated using expressions from the literature (1.5 and 1.3 respectively) and the values are presented in **table 5.2** & **table 5.3** respectively. The deformation limits adopted in this study are the following:

- Maximum allowable rotation $\vartheta_{lim} = 0.5^o = 0.0087$ rad
- Maximum allowable settlement $w_{lim} = 0.05D_{min} = 5.5$ cm

5.3.2 Wind Cyclic Loading

The first cyclic loading scenario concerns cyclic wind loading. Wind loads only act when the turbine is operative, as when the turbine is not working the wind passes through the blades and does not act as a force on the superstructure. Most wind turbine models allow rotation of the nacelle about a vertical axis so as to optimally direct the turbine to face the prevailing wind [Malhotra, 2007]. In the current load case wind loading is fully alternating, to take account for the worst case scenario of the nacelle rotating 180°. Wind loading is simulated as a concentrated force acting on the rotor – nacelle level and is imposed in static force – controlled loading steps, each with opposite sign than the previous. 9 loading cycles are examined, therefore 18 alternating wind loading steps. Before applying the wind load the dead weights are imposed during the first step of each analysis.

Shear force on the base of each wind turbine due to wind loading is plotted in **figure 5.14** against loading steps. As the turbine size increases, the wind load is augmented by approximately 0.5 MN. **Figure 5.15** depicts the overturning moment acting on the base of each tower against loading steps. The difference between base moments of each turbine is significant, as for larger turbines both the tower height (and thus the lever arm) and the acting wind force increases. The latter is indicative of the geotechnical challenges that arise, when it comes to founding a larger wind turbine. The load paths in the M – Q plane for each wind turbine are presented in **figure 5.16**; the gradient of each line represents the lever arm of the wind load on each wind turbine.

2 MW wind turbine

To begin with, results for the 2 MW wind turbine are presented. This is the smallest superstructure examined and the performance of three hybrid foundations is compared to a 30 m monopile; the hybrid foundations examined are D11 – L 15, D15 – L15 & D20 – L15. Cyclic moment – rotation curves are presented in **figure 5.17**, both for homogeneous and inhomogeneous soil profiles. The generated moment is relatively small and does not exceed 30 MNm. The shape of the curve of the monopile is almost linear, but the angle of rotation

reaches larger values than in case of all hybrid foundations. The shape of the curves in case of hybrid foundations is different; a first peak is reached during the first cycle of loading, but after unloading back to zero a small residual rotation can be observed, due to inevitable yielding of the soil mainly underneath the footing, along with generation of non-linearities on the soil – foundation interfaces. The value of this residual rotation is smaller as the length of the pile increases, but it never reaches zero due to presence of the footing. The best performance is observed for the D15 – L20 hybrid foundation, followed by the D15 – L15. All the hybrid foundations seem to perform better than the monopile in terms of maximum rotation, however even the monopile does not exceed a rotation of 0.6 mrad, which is very small and far from the 87 mrad limit. For the inhomogeneous soil stratum, a slight decrease on the stiffness can be observed for all the hybrid foundations, while the benchmark monopile remains intact. However, rotations remain very small and the relative performance of all hybrid foundations is still better than the one of the monopile.

The cyclic settlement – rotation diagrams for the 2 MW wind turbine can be seen in **figure 5.18** for both soil profiles. In case of the uniform soil, the maximum settlement is observed for the D11 – L15 hybrid foundation. It is worth noting that the monopile presents smaller settlements than all the hybrid foundations; this is attributed to the fact that the vertical loads are carried exclusively by the footings of each hybrid foundation, all of which have smaller vertical stiffness than a 30 m monopile. Another observation is that for most foundations, the largest part of the total settlement is caused by the dead loads imposed in the first step. The remaining settlement is caused by rotation of the foundation and is almost negligible for larger foundations that rotate less. The effect of soil inhomogeneity is an increase of settlements of all hybrid foundations, while settlement of the monopile is decreased. It can be said at this point that the monopile is less sensitive to settlements and soil inhomogeneity, due to its embedment. The hybrid foundation on the other hand tends to develop larger settlements and is affected in a more straightforward manner by soil inhomogeneity.

An important aspect of wind turbine foundations is the investigation of rotation and settlement accumulation due to many cycles of loading. To this end, the maximum values of angle of rotation and settlement (w_{max} & ϑ_{max}) are plotted against the loading cycles. It is stressed at this point that the analyses are conducted for the first 9 cycles of loading, to reduce computational effort. Logarithmic trendlines are adapted to each curve and an extrapolation is made to provide a rough estimation of the accumulations at the end of the project's lifetime. These predictions may not be very accurate, but the results are deemed acceptable mainly for qualitative comparison of the performance of the foundations. In the end of the current chapter the same method is used on a 40-cycle analysis and a comparison is made to validate the accuracy of the predictions derived from the 9-cycle analyses. There are many indications however, that the response can be very well predicted be interpreting the results from a certain number (about 20) of initial cycles (Lekkakis, 2012).

The maximum angle of rotation at the end of each cycle is plotted against the 9 first cycles of loading in **figure 5.19**, for both soil profiles. At first, it can be seen that the monopile experiences larger rotations than all of the hybrid foundations. The D11 – L15 system is the worst among the hybrid foundations while the other two present similar maximum rotation

values, with the D15 – L20 being slightly stiffer. For the inhomogeneous soil rotations are increased, but the relative performance of all foundations is almost the same. The predictions concerning the maximum angle of rotation at the end of the project's lifetime are presented in **figure 5.20**; there is no significant evidence of rotation accumulation due to wind cyclic loading, and the maximum accumulated rotations do not exceed 0.6 mrad for all the foundations examined.

In the same manner, the maximum settlement at the end of each cycle is presented in **figure 5.21** for the two soil profiles. As aforementioned, the monopile experiences the smallest settlement, due to its increased initial vertical stiffness. The hybrid foundations tend to settle more, however even the settlement of the D11 – L15 foundation is quite small, as it does not exceed 70 mm in the case of uniform soil. Concerning the inhomogeneous soil, settlements are increased for the hybrid foundations, while the monopile settles even less. The maximum settlement in this case reaches 1cm and is realized for the D11 – L15 foundation. In addition, there seems to be an accumulation of settlement for the latter. This accumulation is better depicted in **figure 5.22**, which contains the logarithmic predictions of the maximum settlement for large number of loading cycles. Settlement accumulation is noticeable for the D11 – L15 foundation, especially when it lays on the inhomogeneous soil. The rest of the foundations examined present a quite satisfactory behavior, as settlement accumulation at the end of the project's lifetime is predicted to be negligible. It is reminded at this point that the 2 MW wind turbine is the smallest of the turbines examined and there is serious evidence that cyclic wind loading can cause significant settlement accumulation, as will be seen later on.

In order to obtain a perception of the safety factor against moment loading due to wind forces, the cyclic moment – rotation curves are depicted in **figure 5.23** along with the monotonic moment – rotation curves that were produced in the previous subsection. It can be seen that the overturning moment factor of safety FS_M is larger than 2 for all the foundations examined, which is deemed adequate. The largest value of FS_M is observed for the 30 m monopile, which has the highest moment capacity.

To sum up, when it comes to wind loading of a 2 MW wind turbine, all the hybrid foundations respond quite well, even the smallest with the 11 m footing diameter and 15 m pile. Compared to a 30 m monopile, the hybrid foundations present quite smaller rotations, but the settlements are larger. However, even the largest settlement is not significant as it does not exceed 1 cm for the first 9 cycles of wind loading. The hybrid foundation with the smallest footing seems to accumulate settlements, especially in case of the inhomogeneous soil profile, but even so the largest settlement does not exceed 2 cm at the end of the project's lifetime. Concerning the factor of safety against overturning moment, all foundations have a FS_M larger than 2, which is considered acceptable.

3.5 MW wind turbine

Moving on, the 3.5 MW wind turbine is examined. This is a medium – sized superstructure which has been widely used up to date. The wind industry is already moving on to the use of larger wind turbines, but the 3.5 MW wind turbines remain a quite good indicator of the foundation demands. Moment – rotation curves for the first 9 cycles of wind loading are presented in **figure 5.24** for the two soil profiles. Starting with the hybrid foundations laying on homogeneous soil, it can be seen that the footing diameter plays a significant role to the initial stiffness, as well as to the overall response during wind cyclic loading, in terms of maximum angle of rotation. The hybrid foundation that has a 20 m footing diameter displays the smallest angle of rotation, which does not exceed 5 mrad. An initial soil yielding and residual rotation are visible at the end of the first cycle of loading, but as the rest of the cycles take place the residual rotation is minimized, exposing a quasi – elastic behavior. As the footing diameter gets smaller, the residual rotation is not totally diminished and the cyclic behavior becomes more hysteretic, as the cyclic loop area increases. Among the two hybrid foundations with the same footing diameter, the one with the longer pile has a slightly better response. The hybrid foundation with the smallest footing diameter (11 m) has the worst response, as it experiences the largest angle of rotation. As far as the 30 m monopile is concerned, the same observations as for the smaller wind turbine can be made; The angle of rotation is larger than the one of all hybrid foundations, but a "tightening" of the curves when moment reaches near – zero values is apparent, which indicates less soil yielding around the pile. All the hybrid foundations compare very well to the monopile in terms of maximum rotation reached. Considering the inhomogeneous soil, all the hybrid foundations expose a stiffness degradation therefore larger rotations are reached. The difference between the two hybrid foundations with the same footing diameter of 15 m is more obvious now, as the one with the 20 m pile is almost unaffected by the degree of soil inhomogeneity. The D11 – L15 hybrid foundation displays a worse response than the 30 m monopile, which is also practically unaffected by the soil inhomogeneity.

Cyclic settlement – rotation curves for the 3.5 MW wind turbine are presented in **figure 5.25** for both soil profiles. Starting with the homogeneous soil profile, a first observation is that the monopile settles less than the hybrid foundations, similarly to the previous subsection. The curves are divided into two sections; a straight line which represents the settlement caused by dead loads with no rotation ($\vartheta = 0$), and the settlements caused by cyclic rotation. Among the hybrid foundations, the D11 – L15 demonstrates the worst behavior, as the settlement increases with each cycle of loading, indicating severe settlement accumulation. The rest of the hybrid foundations respond quite well, with the D20 – L15 being the best both in terms of settlement and rotation. Concerning the inhomogeneous soil, the D15 – L15 hybrid foundation seems to accumulate settlements as well, while the D11 – L15 is totally inappropriate. The settlements are generally increased for all foundations except the monopile, which stays intact.

The maximum angle of rotation at the end of each cycle, for the first 9 cycles of loading and the two soil profiles is presented in **figure 5.26**. The smallest angle of rotation is demonstrated

by the D20 – L15 hybrid foundation. Among the hybrid foundations with the same footing diameter of 15 m, the one with the longer pile exhibits smaller rotations. The hybrid foundation with the 11 m footing diameter experiences quite larger rotation, but the 30 m monopile still has the softer response. For the inhomogeneous soil, all the rotations are generally increased.

The logarithmic predictions for the maximum angle of rotation at the end of the project's lifetime are presented in **figure 5.27**. Starting with the homogeneous soil, we can observe that the three larger hybrid foundations (D20 – L15, D15 – L20 & D15 – L15) do not show signs of serious accumulation of rotations due to wind loading. This is not the case for the monopile, which seems to experience some rotation accumulation, of the order of 0.5 mrad. Finally, the hybrid foundation with the small 11 m footing seems to demonstrate a decrease in the maximum rotation as the cycles of loading increase. This is attributed to the fact that, as the footing is quite small, severe soil yielding is caused by vertical loads and the soil surface is reconstructed as the footing sinks deeper into the soil, hence rotation of the footing is eradicated. The latter is an indication that the 11 m footing may not be able to support a 3.5 MW wind turbine, due to its small vertical factor of safety. This effect is more obvious when it comes to inhomogeneous soil. In that case, the D11 – L15 hybrid foundation demonstrates a significant drop in the maximum rotation, which reaches almost zero at the end of the project's lifetime. Other than that, the inhomogeneous soil causes the rest of the foundations to rotate slightly more.

The maximum settlement is plotted in **figure 5.28** against the first 9 cycles, for the two soil profiles. For the homogeneous profile on the left, the main observation is that all the settlements do not exceed 1 cm, except for the D11 – L15 hybrid foundation. The latter has quite larger settlements as the 11 m footing is not adequate to sustain the weight of a 3.5 MW wind turbine. There is also evidence of settlement accumulation even during the initial cycles of loading, leading to the conclusion that the D11 – L15 hybrid foundation is not sufficient. The monopile settles less, but the other hybrid foundations do not respond much worse. When it comes to the inhomogeneous soil profile where the surface soil layers are weaker, the D11 – L15 is certainly insufficient; the initial settlement is of the order of 2 cm due to dead weights, but the settlement reaches 6 cm at the end of the 9^{th} cycle, indicating severe settlement accumulation. Settlements are increased for the rest of the hybrid foundations as well, but the response seems to be sufficient at least for the initial cycles. As expected, the 30 m monopile is not affected by the soil inhomogeneity and maintains the best response in terms of vertical displacement.

Settlement accumulation is better depicted in **figure 5.29** that presents logarithmic predictions for maximum settlement at the end of the project's lifetime. As expected, settlement accumulation is dominant in the case of the D11 – L15 foundation, which exceeds the settlement limit of 5.5 cm before the end of the project's lifetime. The rest of the foundations demonstrate a satisfying response both in terms of settlement magnitude and accumulation rate. The effect of soil inhomogeneity is quite profound; the magnitude of all settlements is increased and severe settlement accumulation is also realized in the case of the D15 – L15 hybrid foundation. The two remaining hybrid foundations however display a

satisfactory response. It is interesting that the two foundations with the same footing diameter of 15 m and different pile lengths do not settle in the same way; the D15 – L20 hybrid system accumulates smaller rotations than the D15 – L15, although vertical loads are exclusively sustained by the footing. This is attributed to the fact that the total settlement is divided into two components; the static load component due to self – weights and the cyclic load component, which is caused by rotation due to lateral cyclic loading. Even though the static load component is the same for the two foundations, as it depends solely on the footing diameter, the cyclic load component is smaller for the foundation with the longer 20 m pile, as it experiences smaller rotations under the same cyclic load. The 30 m monopile displays once again the best performance in terms of settlement but as will be seen later on, vertical displacement is not considered a critical aspect of the design of offshore wind turbines.

Cyclic moment – rotation curves are depicted in **figure 5.30**, along with monotonic moment – rotation curves of each foundation, in order to estimate the factor of safety against moment loading. As can be seen, only the two larger hybrid foundations achieve a satisfying value of FS_M, larger than 2. As noticed before, the monopile has the largest moment capacity, while the two smaller hybrid foundations do not have enough moment capacity. The above observations are valid for the inhomogeneous soil profile as well, which does not expose significant differences.

In order to better understand the effects of cyclic wind loading on an offshore wind turbine foundation, the same curves as above are presented only for the D15 – L15 hybrid foundation laying on homogeneous soil in **figure 5.31**, along with the plastic strain contours at characteristic load stages. The first picture on the top – left corresponds to the initial wind loading of the wind turbine, i.e. first operation of the turbine. As can be seen, soil yielding is occurring mainly at the side of the footing which is in the direction of the load. The second picture on the top – right represents the first time the turbine is turned off; of course, yielding of the soil does not diminish. If the rotor – nacelle assembly rotates 180 degrees and the procedure is repeated, the same soil yielding will occur on the other side of the footing, as seen in the pictures in the middle row. Finally, more cycles of wind loading will lead to expansion of plastic strains in the surface of the soil that is in contact with the footing, leading to settlement accumulation, as can be seen in the two pictures in the bottom. Regarding the shape of the cyclic curve, we notice that the first cycle lays on the monotonic curve, while a small residual rotation is occurring during discharge. The rest of the cycling occurs in a quasi – elastic manner, and there is no evidence of rotation accumulation or stiffness degradation.

5 MW wind turbine

This is the largest wind turbine examined and, as the wind load is acting on a height of 90 m above mud – line, the generated cyclic moment is of the order of 150 MNm. To deal with the increased challenges of founding such large superstructures, larger foundations have been implemented. Specifically, the 20 m footing is now combined with a 20 m pile to form the D20 – L20 hybrid foundation, and the 15 m footing is combined with a 25 m pile to form the D15 – L25 hybrid foundation. The D20 – L15 and D15 – L20 hybrid foundations are also examined

in this subsection. Finally, the 30 m monopile benchmark is substituted by a 35 m monopile which is considered sufficient based on the study of Christou (2012).

Cyclic moment – rotation curves are presented in **figure 5.32** for both soil profiles. Basic remarks made above are still valid, concerning the shape of the curves and differences between the curves of hybrid foundations and the curve of the monopile. For the homogeneous soil profile, it seems that performance of the hybrid foundations in terms of angle of rotation is mainly controlled by the diameter of the footing. Indeed, the response of the D15 – L20 and D15 – L25 hybrid foundations is almost the same. The extra 5 m of pile embedment length does not have a significant contribution to the response. On the other hand, increasing the footing diameter offers a remarkable benefit, as the two hybrid foundations with the 20 m footing respond in a stiffer manner and achieve the smallest rotations. Among the two systems, the one with the longer 20 m pile behaves better than the one with the 15 m pile in a more obvious manner. This leads to the conclusion that the pile length that contributes to the performance is limited in the top 20 m of the pile, as further increase does not offer any improvement. The 35 m monopile exhibits the softest response, with the angle of rotation reaching a maximum value that is at least 100% increased, compared to all hybrid foundations. The effect of soil inhomogeneity is a degradation of initial stiffness, accompanied by an increase in the magnitude of rotations. Stiffness degradation is more intense for the hybrid foundations with the larger 20 m footing.

Figure 5.33 depicts the corresponding cyclic settlement – rotation curves. Starting with the homogeneous soil profile, the same observations are made as for the other wind turbines. Settlements are mainly influenced by the diameter of the footing in hybrid systems, while the monopile still exhibits the smallest vertical deformation. When it comes to the inhomogeneous soil body, the 15 m footing is probably insufficient, as the two hybrid foundations composed of that footing tend to accumulate significant settlements. Response of hybrid foundations composed of the 20 m footing remains satisfactory.

The maximum angle of rotation is plotted against the first 9 cycles of loading in **figure 5.34**. As pointed out before, there is no significant difference between the D15 – L20 and the D15 – L25 hybrid foundations, for both soil profiles. A difference between the D20 – L15 and the D20 – L20 hybrid foundations is more obvious, especially for the inhomogeneous soil profile. The 35 m monopile exhibits the largest rotations in both cases.

Logarithmic predictions for the maximum angle of rotation after millions of load cycles are presented in **figure 5.35**. Concerning the homogeneous soil profile, there is no evidence of rotation accumulation due to wind loading among the hybrid foundations. There are some signs of reduction in the magnitude of ϑ_{max} for the 15 m footing diameter, indicating settlement accumulation as explained in the previous subsection. For the inhomogeneous soil profile, reduction of rotation is more evident for the 15 m footing diameter, while a small accumulation can be observed for the 20 m footing diameter. In both cases, the monopile benchmark experiences larger values of ϑ_{max} and rotation accumulation.

As aforementioned, settlement accumulation is critical over rotation accumulation when it comes to wind loading. Maximum settlement at the end of each loading cycle is plotted in **figure 5.36** for the two soil bodies examined. For the homogeneous soil, the initial settlement is of the order of 1 cm for all hybrid foundations and slightly smaller for the monopile, about 0.6 cm. A settlement accumulation seems to occur, mainly for the hybrid foundations with the smaller 15 m footing. For the inhomogeneous soil, settlement of the monopile is even smaller, as it does not exceed 0.5 cm. This is not the case for the hybrid foundations, which accumulate severe settlements. The accumulation rate is larger and more severe for the 15 m footings, but it is not negligible for the 20 m footings as well.

Accumulation of settlements is better observed in **figure 5.37**, where the maximum settlement at the end of the turbine's lifetime is predicted via a logarithmic relationship. For the homogeneous soil, severe accumulation seems to occur for the two hybrid foundations with a footing diameter of 15 m, while the larger ones respond in a satisfying manner. For the inhomogeneous profile, where the superficial soil layers are weaker, severe settlement accumulation is realized for all hybrid foundations. Consequently, the hybrid foundations with a 15 m footing are not suitable for the foundation of a 5 MW wind turbine on the inhomogeneous soil. Severe settlement accumulation is also observed for the D20 – L15 hybrid foundation, while the most satisfying response is observed for the D20 – L20 hybrid foundation. Settlement accumulation due to cyclic wind loading is proved to be a crucial aspect of the foundation design and the monopile responds better in that case. This is caused by the special connection that is implemented in the current study that forces the footing to sustain the total vertical load, while the pile remains intact.

Cyclic moment – rotation curves are plotted along with monotonic pushover curves in **figure 5.38**, in order to obtain an estimation of the factor of safety against moment loading. As explained before, a drawback of hybrid foundations is that the moment capacity is not greatly increased, as it depends on the pile embedment length.

5.3.3 Wave Cyclic Loading

This loading scenario consists of a constant wind force acting on the rotor – nacelle level and an alternating wave force acting on the wave application point, located at 8 m above mud line. Both of the environmental forces acting on the wind turbines are cyclic in nature, however wind periods are quite larger (can be of the order of minutes) than wave periods, which are commonly 2 – 10 seconds; consequently, the assumption of monotonic wind loading and cyclic wave loading is considered reasonable in order to approach the complex loading regime imposed by the naval environment. Another important assumption that is made in the current thesis is that the excitation periods are not close to the natural period of the system, therefore no resonance should occur and the loads can be imposed in a static manner. This assumption is deemed reasonable, as the wind excitation frequencies are indeed far from the eigenfrequencies of any wind turbine. However, wave frequencies can be close to the system's eigenfrequencies, but there is evidence leading to a favorable response due to aerodynamic damping, when the wind turbine is operative (Van Der Tempel, 2005).

Anyhow, the scope of the current study is to investigate the viability of hybrid foundations in a preliminary level, hence many aspects of the problem including dynamic response due to wind and wave loading and fatigue investigation are not considered. P – δ effects are taken into account for all analyses conducted in the current section and, unlike wind cyclic loading, are proven to be quite unfavorable in the case of wave cyclic loading combined with a constant wind load. In fact, the large mass of the rotor – nacelle assembly is deviated from the point of equilibrium by the wind force, leading to the production of a large second – order base moment. Wave cyclic loading causes an eccentric oscillation which can lead to severe accumulation of rotations at the foundation level. This is the reason why the current loading scenario is considered the most unfavorable and is therefore critical to the design of the foundations. It is reminded that the rotation limit is taken

$$\vartheta_{lim} = 0.5^{o} = 0.0087 \text{ rad.}$$

The wind turbines examined here are the same as in the previous load scenario; a smaller 2 MW wind turbine, a medium – sized turbine of the 3.5 MW class and a larger 5 MW wind turbine. Base shear force for all wind turbines is plotted in **figure 5.39** against loading steps. 9 cycles of loading are imposed. Shear force is significantly larger in this case, as the force of waves is of the order of 2 MN. The base shear has an alternating sign but the positive values are quite larger than the negatives, as the wind force is constant towards the positive direction of the x axis. Base moment for the three wind turbines due to wave cyclic loading is depicted in **figure 5.40**. Contribution of the constant wind force to the magnitude of base moment is significant and defines the sign of moment loading, which does not change during cycling, making the eccentric nature of this type of loading obvious. As the turbine size increases, maximum base moment due to wave cyclic loading is almost 100 % larger than the previous value. Load paths in the M – Q plane are presented in **figure 5.41**. The tangent of each line corresponds to the lever arm of each force; the lever arm of wave loading remains constant at 8 m above mud – line as it solely depends on the sea depth, which is the same for the three wind turbines.

2 MW wind turbine

The same foundations are examined as for the wind loading scenario. To begin with, moment – rotation curves are presented in **figure 5.42**. The shape of the curves is the same in all cases. Moment due to wind loading is approximately $l_{wind}F_{wind}$ = (65 m)(0.5 MN) = 32.5 MNm, and this value is reached via a linear – elastic response. At this point the tangent of the curve changes, indicating a softer response to wave loading. This stiffness degradation is caused by the change of the load application point, as explained in the monotonic loading subsection; the rotational stiffness decreases as the M/H ratio decreases. This effect is more intense for the monopile and the smaller D11 – L15 hybrid foundation, while the other two seem to be less affected by the M/H ratio. For the homogenous soil, the 30 m monopile exhibits the softest response, followed by the D11 – L15 hybrid foundation. The other two hybrid foundations respond in a very satisfying manner both in terms of maximum rotation and initial stiffness. This is a very interesting finding, as if a 30 m monopile is substituted by a pile half

its size combined with a 15 m footing, a significantly improved response can be achieved. Concerning the D15 – L15 and D15 – L20 hybrid foundations, it seems that increasing the embedment length of the pile of a hybrid foundation can lead to an improvement in the response, however not that significant. If the soil is weaker on the surface and exhibits a linearly increasing S_U, the hybrid foundations exhibit a drop in the initial stiffness, as can be seen in the charts for the inhomogeneous profile; larger rotations are reached while the monopile remains intact. The difference between the D15 – L15 and the D15 – L20 hybrid systems is now more obvious, as the 20 m pile can reach deeper and stronger soil layers. Consequently, increasing the pile length of a hybrid foundation can be quite beneficial for this type of soil profiles despite the fact that it has little effect on uniform clays.

Wave cyclic settlement – rotation diagrams are presented in **figure 5.43** for the two soil profiles examined. Starting with the homogeneous profile, the first observations is that the monopile experiences once again the smallest settlement, only reaching 3.5 mm. Settlement of the hybrid foundations is not quite larger, as it reaches 6.5 mm for the D11 – L15. The monopile prevails both in terms of settlement due to dead loads and due to cyclic rotation, however response of hybrid foundations is also satisfactory. For the inhomogeneous soil profile prevalence of the monopile is more intense, as it settles even less while the hybrid foundations settle more. Maximum settlement now reaches 11.5 mm for the D11 – L15 foundation, which also seems to accumulate settlements even during the first 9 cycles of loading. The remaining two hybrid foundations respond quite well, with a slight prevalence of the D15 – L20.

Moving on, maximum angle of rotation at the end of each cycle (ϑ_{max}) is plotted against the 9 first cycles of loading in **figure 5.44**. Concerning the homogeneous soil, results are very satisfying. The maximum angle of rotation does not exceed 1 mrad for any of the foundations. The worse response is observed for the monopile, followed by the D11 – L15 hybrid foundation. Rotation is significantly reduced for the two remaining hybrid foundations (D15 – L15 & D15 – L20). The two hybrid foundations with the 15 m footing diameter demonstrate a similar response, suggesting that increasing the pile length from 15 m to 20 m does not have a contribution on the maximum rotation when the soil is uniform. On the other hand, increasing the footing diameter from 11 m to 15 m, while keeping the pile length constant at 15 m has a beneficial effect in terms of maximum rotation. When it comes to the inhomogeneous soil, rotations are slightly augmented mainly for the hybrid foundations. The D15 – L20 hybrid foundation is now marginally superior to the D15 – L15, owing to the increase of undrained shear strength of the clay with depth. On the contrary, performance of the D11 – L15 hybrid foundation is deteriorated, making it the most inadequate foundation.

To predict the maximum rotation at the end of the turbines lifetime a logarithmic extrapolation is performed, based on the data from the first 9 cycles; the results are depicted in **figure 5.45**. In case of uniform clay, rotation accumulation is not evident for any of the foundations. A small accumulation tendency can be observed for the monopile and the D11 – L15 hybrid foundation, however the accumulation rate is negligible. The remaining hybrid foundations perform in an adequate manner, as the angle of rotation does not increase at all. The effect of inhomogeneity is evident for the D11 – L15 hybrid foundation which tends to

accumulate rotations in a more intense rate. A minor deterioration is also observed for the remaining hybrid foundations and the monopile but it is not deemed considerable. This type of wave cyclic loading suggests the danger of rotation accumulation even for the smallest 2 MW wind turbine.

Maximum settlement – cycles of loading diagrams are presented in **figure 5.46**. The results are similar to the wind – induced settlements and all the basic observations made in the corresponding subsection apply here as well. In general, the monopile settles less than the hybrid foundations and all settlements do not exceed 7 mm which is a rather adequate value. A slight increase in the settlements of hybrid foundations is noted for the inhomogeneous profile, making the D11 – L15 foundation an insufficient solution.

Logarithmic predictions for the accumulation of settlements are presented in **figure 5.47**. As expected, the results are also very similar to the ones of wind cyclic loading. Settlement accumulation is severe only for the D11 – L15 hybrid foundation laying on the inhomogeneous soil.

An important aspect that has not been addressed so far is stiffness degradation due to cyclic loading. To assess this possibility, the secant rocking stiffness at the end of each cycle is divided by the initial rocking stiffness at the end of the first cycle and plotted against the 9 first cycles of loading in **figure 5.48**. The secant rocking stiffness is simply extracted from the cyclic moment – rotation diagrams presented in **figure 5.42**, by dividing the maximum moment at the end of each cycle by the corresponding angle of rotation. Starting with the homogeneous soil profile, there is no significant evidence of stiffness degradation during the first 9 cycles, as it does not drop below 90% of the initial value for any of the foundations. For the inhomogeneous soil, the D11 – L15 hybrid foundation exhibits a deterioration as the rate of stiffness decrease with each cycle of loading is more intense.

Finally, pushover curves are plotted along with cyclic moment – rotation curves in **figure 5.49**. For the homogeneous soil profile factor of safety against overturning moment is satisfactory for all hybrid foundations, while for the heterogeneous soil profile the D11 – L15 hybrid foundation seems to have a value of FS_M smaller than 2. Concerning the shape of the cyclic curves, the initial response due to wind loading lays exactly on the pushover line but when the waves begin to act, the tangent of the line decreases; this reflects the decrease of stiffness due to the simultaneous act of moment and larger horizontal force.

3.5 MW wind turbine

These are currently medium – sized offshore wind turbines, which have been used widely so far, but are already being substituted by even larger models. However, the top 3 operational offshore wind farms (London Array, Greater Gabbard & Anholt) consist exclusively of such wind turbines (source: Wikipedia.com). Tower size and magnitude of acting forces are both quite larger than the 2 MW wind; therefore, founding these superstructures is more challenging and the D20 – L15 hybrid foundation is also implemented among the ones

previously examined. The monopile that is used as a benchmark has once again an embedment length of 30 m, which is also deemed as a rational solution by Christou (2012).

Cyclic moment – rotation curves are presented in **figure 5.50**. For both soil profiles, the best performance is observed for the D20 – L15 hybrid foundation which presents a very stiff response with no signs of rotation accumulation or stiffness degradation. The second best response is the one of the D15 – L20 hybrid foundation, followed by the D15 – L15. As found in chapter 4, these two hybrid foundations have almost the same initial rocking stiffness, which is also obvious here as the two curves start from the same line. However, the diversification between the two curves with increasing angle of rotation is starting to be obvious quite early; consequently, it is apparent that the initial rocking stiffness is a very important factor, but it is not enough to fully prescribe the response due to wind and wave loads; it can be applied only in the domain of very small angles of rotation. As the turbine size increases, the role of the pile on the response of the hybrid foundation is getting more important. The D11 – L15 hybrid foundation does not exhibit a satisfying response, as the angle of rotation is very large and severe rotation accumulation is obvious even during the first cycles of loading. Except the latter, performance of the remaining hybrid foundations is superior, compared to the monopile. The effect of soil heterogeneity is a decrease on the rocking stiffness, accompanied by an increase on the angle of rotation for all the hybrid foundations. In that case, the response of the D15 – L15 hybrid foundation is inferior to the monopile, while the remaining two hybrid foundations are still apparently better. Finally, the D11 – L15 hybrid foundation is found to be totally inappropriate.

Cyclic settlement – rotation curves are presented in **figure 5.51**. All of the hybrid foundations respond quite well in the uniform soil profile case except for the D11 – L15. The latter is once again found to be incapable to sustain the working loads of a 3.5 MW wind turbine, both in terms of rotation and settlement. The remainining hybrid foundations present a satisfying maximum settlement, that does not exceed 8 mm. The monopile is stiffer in the vertical direction and demonstrates a maximum settlement that does not exceed 4.5 mm. In case of the heterogeneous soil, the results are quite diversified. The 11 m footing is out of the question, as even the initial settlement component due to dead loads is more than 1 cm. Performance of the D15 – L15 and D15 – L20 hybrid foundations is very deteriorated as well. Only the settlement of the hybrid foundation with the largest footing (20 m diameter) stays practically unaffected by the heterogeneity of the soil.

The maximum angle of rotation is plotted against the initial cycles of loading in **figure 5.52**. Starting with the homogeneous profile, the maximum angle of rotation for the monopile is about 2 mrad. Only the D11 – L15 hybrid foundation demonstrates an inferior response, as ϑ_{max} starts from a value of 4 mrad and presents signs of rotation accumulation. The remaining hybrid foundations respond better than the 30 m monopile and the prevailing performance is noted for the system with the largest footing diameter. Among the hybrid foundations with the 15 m footing diameter, the one with the longer 20 m pile experiences smaller rotation. In case of non – homogeneous soil, response of the D11 – L15 hybrid foundation is considerably deteriorated, as the rotation limit of 0.0087 rad is already being surpassed during the initial cycles of loading. Response of the monopile is not affected, but a slight deterioration is

noticeable for the D15 – L15, which is now outperformed by the monopile. The remaining two hybrid foundations also present a slight deterioration, which is almost negligible, as the maximum rotation remains below 2 mrad.

Logarithmic predictions of rotation accumulation are presented in **figure 5.53** for the number of cycles that corresponds to the lifetime of a wind turbine. In case of uniform soil, severe rotation accumulation is apparent for the D11 – L15 hybrid foundation and the rotation limit is surpassed. The rest of the foundations examined, including the monopile, seem to respond quite well as there is no evidence of severe accumulation tendency. It is noteworthy that the remaining three hybrid foundations outperform the monopile. For the heterogeneous soil body, the monopile is outperformed by the two larger hybrid foundations, as the response of the D15 – L15 is deteriorated. The D11 – L15 is already beyond the rotation limit, even after the first cycle of loading.

Maximum settlement due to wave cyclic loading is presented in **figure 5.54**. As discussed before, the wind cyclic loading is more critical in terms of vertical displacement. The results presented here are slightly more favorable; the largest settlement for the uniform soil is observed for the D11 – L15 hybrid foundation, while the smallest settlement is observed for the monopile. The three remaining hybrid foundations respond in a similar manner, presenting a settlement on the order of 7 mm, which is very satisfying. For the heterogeneous soil, all settlements are increased. The hybrid foundation with the 11 m footing is sinking excessively, while the D15 – L15 also presents a deterioration. The remaining hybrid foundations, along with the monopile, demonstrate a satisfying response.

Settlement accumulation is not critical for this type of loading, as seen in **figure 5.55**, which presents the logarithmic trendlines concerning the maximum settlement. Only the D11 – L15 hybrid foundation is deemed inappropriate in case of uniform soil, while the D15 – L15 also seems to present a poor response in case of the inhomogeneous soil profile. The settlement accumulation rates for the same turbine due to wind loading, as presented in **figure 5.29** are quite larger.

Secant rocking stiffness degradation is depicted in **figure 5.56** for both soil profiles. Concerning the homogeneous soil, severe stiffness degradation is observed for the D11 – L15 hybrid foundation, leading to the conclusion that this foundation is not capable of supporting a 3.5 MW wind turbine. Interestingly, the 30 m monopile benchmark presents the same amount of stiffness degradation as the D15 – L15 hybrid foundation, while the performance of the larger hybrid foundations is quite superior. If the soil has a linearly increasing shear strength with depth, performance of the D15 – L15 hybrid foundation is deteriorated, as a 10 % loss in the initial stiffness is observed. The larger hybrid foundations respond very well and the performance of the monopile is slightly enhanced.

Finally, pushover curves are plotted among cyclic moment – rotation curves in **figure 5.57**, in order to estimate the factor of safety against moment loading. For the homogeneous soil stratum, a value of FS_M in the order of 2 is noted for the two larger hybrid foundations, while the D15 – L15 demonstrates a FS_M value on the order of 1.5. A smaller value is observed for the D11 – L15, which carries a load near to the moment capacity, demonstrating a FS_M that

does not exceed 1.2. The magnitude of FS_M is slightly decreased in case of the heterogeneous soil, for all hybrid foundations except the D15 – L20; the longer pile ensures a steady performance that is less affected by soil heterogeneity. Finally, the 30 m monopile exhibits the largest moment capacity, accompanied by the softest initial response, as previously noted.

5 MW wind turbine

This is the largest wind turbine examined in the current thesis, with the rotor – nacelle level being at + 90 m above mud line (z = -90 m). Offshore wind farms consisting of such wind turbines are currently both operational (BARD offshore 1, source: Wikipedia.com) and under construction (Trianel Borkum West II, Global Tech I, source: Wikipedia.com). However, the trend of the offshore wind turbine industry towards the construction of even larger wind turbine models is so excessive, that 5 MW wind turbines are already being outsized by models of larger nominal capacity that can reach up to 7 MW. Investigating the performance of hybrid foundations sustaining larger turbines is thus, of high importance. The two larger hybrid foundations from the previous cases are also examined here (D15 – L20 & D20 – L15), along with two even larger (D20 – L20 & D15 - L25). A 35 m monopile is deemed as a reasonable foundation solution for the 5 MW wind turbine, as proposed by Christou (2012).

Cyclic moment – rotation curves are depicted in **figure 5.58**. Monotonic moment due to constant wind force is (1.5 MN) (90 m) = 135 MNm, while cyclic moment due to wave loading is (± 2.2 MN) (8 m) = ± 17.6 MNm, leading to a maximum base moment of 152.6 MNm. However, the actual maximum base moment generated at the tower base is larger, reaching 160 MNm due to second – order effects. For the uniform soil stratum, performance of hybrid foundations is dominated by the diameter of the footing; the foundations with the 20 m footing present the stiffer response, while a softer response is observed for the ones with the 15 m footing. Among the foundations with the same footing, the ones with the longer pile respond in a stiffer manner. It is interesting that the diversification begins to show in the upper – half of the diagram, as the initial response depends solely on the footing diameter and not on the pile length. In addition, increasing the pile length from 15 m to 20 m seems to be more effective than increasing it from 20 m to 25 m; this indicates that the effective length of the pile is limited into the top 4 – 4.5 pile diameters. The 35 m monopile presents the softest response, compared to all the hybrid foundations. For the heterogeneous soil profile, the results are different; the D20 – L15 hybrid foundation is severely degraded and is outperformed by the D15 – L25 system. The D20 – L20 remains the best and the D15- L20 the worst among the hybrid foundations. Performance of the monopile is also slightly degraded.

Settlement – rotation diagrams are presented in **figure 5.59**. For the uniform soil, all hybrid foundations do not exceed a maximum settlement of 1 cm; the hybrid foundations with the larger footing undergo lightly smaller settlement. The monopile outperforms all the hybrid

foundations is terms of vertical displacement, even though it demonstrates the largest angle of rotation. For the inhomogeneous soil, sinking is enhanced for the foundations that have a 15 m footing diameter, while there is not a significant effect for the rest of the foundations.

The maximum rotation at the end of each cycle of loading is plotted against the 9 first cycles in **figure 5.60**. For the homogeneous soil, the small`lest angle of rotation is observed for the D20 – L20 hybrid foundation, followed by the D20 – L15. Among the remaining two hybrid foundations, the one with the longer (25 m) pile exhibits a better response than the one with the 20 m pile. It is once again suggested that increasing the footing diameter has a larger benefit over increasing the pile embedment length. When it comes to the inhomogeneous soil, the angle of rotation for the D20 – L15 foundation is increased. There also seems to be an accumulation of rotation during the first 9 cycles of loading for that foundation. It seems that the weaker superficial soil causes a severe degradation of the performance of the 20 m footing, which forces the 15 m pile to sustain the majority of the lateral load. Increasing the pile length to 20 m seems to solve that problem, as the D20 – L20 hybrid foundation still prevails over all the other foundations examined. Performance of the D15 hybrid foundations is also degraded, but in a smaller extent. Finally, the monopile remains practically unaffected by the soil heterogeneity.

The accumulation of rotation is better depicted in **figure 5.62**, where the logarithmic trendlines for the maximum rotation at the approximate lifetime of a wind turbine are provided. If the soil is homogeneous, all the hybrid foundations display a satisfying performance, as no significant accumulation is obvious and all the maximum rotations stay below the 0.0087 rad rotation limit. For the inhomogeneous soil, performance of the D20 – L15 hybrid foundation is deteriorated and it seems to accumulate rotations in a rapid rate. An accumulation of rotation is also detectable for the D15 – L20 hybrid foundation. Compared to the monopile benchmark, response of all hybrid foundations is superior. Nevertheless, the performance of all foundations including the monopile stays in the acceptable area, as there is no excess of the rotation limit in all cases.

Maximum settlements are plotted against the 9 first cycles of loading in **figure 5.63**. All settlements stay below 1 cm for the homogeneous soil profile, while the maximum settlement observed for the inhomogeneous profile is 1.5 cm for the D15 – L20 hybrid foundation. The monopile is proven once again to be superior in terms of vertical displacement. As discussed before, this type of loading is not as critical as wind – induced cyclic loading, when it comes to settlements.

The above statement also holds true when it comes to settlement accumulation, as can be seen in **figure 6.63**. The predicted maximum settlements and settlement rates are significantly smaller compared to the case of wind loading.

Degradation of the initial secant rocking stiffness is depicted in **figure 5.64**, for both soil profiles. For the homogeneous soil profile, the largest degradation is observed for the monopile; even this degradation is nevertheless not important, as the secant rocking stiffness at the end of the 9^{th} cycle stays above 90 % of the initial stiffness. Interestingly, for the inhomogeneous soil profile the largest stiffness degradation is observed for the D20 – L15

hybrid foundation. As discussed before, the 20 m footing laying on weaker superficial soil results to a deterioration of its contribution to the overall performance of the D20 – L15 hybrid foundation. In addition, in order to ensure satisfying performance in case of the heterogeneous soil, a pile embedment length larger than 15 m is required.

Finally, cyclic moment – rotation curves are plotted along with monotonic pushover curves in **figure 5.65** If a factor of safety of the order of 2 is demanded, only the D20 – L20 and D15 – L25 hybrid foundations can be accepted, for both soil profiles. However, a demand of such high factor of safety is questionable, as it can result in an overall impractical and uneconomical design. For example, the 35 m monopile may have the largest moment capacity compared to all hybrid foundations, but it demonstrates the most inadequate response it terms of maximum rotation.

5.4 Further Investigation of Cyclic Wave Loading

5.4.1 Effect of Many Cycles of Loading

So far, response of hybrid foundations due to cyclic wind and wave forces is calculated for the first 8 – 10 cycles of loading in order to reduce computational effort. In reality, the wind turbine – foundation – soil system undergoes millions of cycles of loading, as the approximate lifetime of such structures is 20 years. This corresponds to approximately 10^8 cycles of wave loading and 10^7 cycles of wind loading. As previously discussed, the accumulated rotations and settlements at the end of the project's lifetime are predicted via a simple logarithmic extrapolation. The accuracy of these predictions is arguable and the main question raised is whether the actual deformations will be larger, therefore leading towards non – conservative design. In order to validate the results, a 40 – cycle analysis is conducted for the D15 – L15 hybrid foundation laying on homogeneous soil. As observed by Lekkakis (2012), very accurate results can be deduced from the first 20 – 30 cycles of loading, so 40 cycles are considered enough to verify the results produced in the current thesis.

The cyclic moment – rotation curve is depicted on the left side of **figure 5.66**. An additional accumulation of rotation is evident, compared to the 9 – cycle analysis. The additional accumulation is also noticeable in case of settlement, as seen in the settlement – rotation diagram, also depicted in **figure 5.66**.

Angle of rotation (ϑ) is plotted against the 40 loading cycles in **figure 5.67 (left)**. The additional accumulation is more evident here; the angle of rotation is still increasing when the loading cycles go beyond the initial 10. Tower drift is also depicted in the same figure. The drift is quite large, but is mainly due to the flexibility of the tower.

The maximum rotation at the end of each cycle is depicted in **figure 5.68** – left. The red line stands for the 40 – cycle analysis, while the blue line stands for the 9 – cycle analysis. Accumulation of rotation seems to expand beyond the first 9 cycles, but in a quite smaller rate. The effect of many cycles of loading is better depicted in **figure 5.68** – right, where a logarithmic prediction, identical to the ones made before, is made for both the 40 – cycle and

the 9 – cycle analysis. The estimation for maximum rotation at the end of the project's lifetime derived from the interpretation of 40 cycles of loading, is slightly larger than the one derived from the first 9 cycles. The difference is of the order of 8%.

Maximum settlement at the end of each cycle and the corresponding logarithmic predictions for the 40 and 9 – cycle analyses are presented in **figure 5.69**. In this case, there are no signs of diversification, as the trendline extracted from the first 9 cycles seem to match the one extracted from the 40 – cycle analysis.

Ultimately, the effect of many cycles of loading in stiffness degradation is examined in **figure 5.70**. On the left, degradation of the initial secant rocking stiffness is depicted, as derived from the 9 and 40 cycle analyses. It seems that the stiffness degradation rate is larger during the first 10 cycles and tends to gradually flatten as the number of cycles increases. An attempt to predict the stiffness degradation is performed and the results are depicted in the right chart of the same figure. There seems to be severe loss of stiffness, as the final stiffness after 20 years seems to be reduced by 50 %. However, this prediction is quite questionable and further analysis is required.

5.4.2 Response of Each Individual Component

The response in terms of moment – rotation of each component of the hybrid foundation is depicted in **figure 5.71**. As can be seen, the pile carries about 60 % of the maximum moment, while the footing carries about 40 %. This is a particularly important finding, which indicates that the presence of the footing can change the distribution of bending moment along the pile.

5.5 Conclusions

In this chapter, response of hybrid foundations sustaining wind turbine towers under lateral loading was thoroughly investigated. Two cohesive soil profiles where taken into account: a homogeneous and an inhomogeneous soil stratum. Three typical offshore wind turbine towers were examined; the towers had nominal capacities of 2 MW, 3.5 MW and 5 MW. At first, monotonic displacement – controlled pushover analyses were carried out in order to obtain a first estimation of the lateral capacity of the whole superstructure – foundation – soil system. Moving on, two force – controlled cyclic load cases were examined: cyclic wind loading, which consists of an alternating wind force applied to the top of the tower, and cyclic wave loading combined with a constant wind force. A variety of hybrid foundations was examined, along with logical monopile solutions for each turbine. Comparison between the hybrid foundations and the monopile was performed in each case. The geometrical parameters of hybrid foundations were correlated to their performance, which was evaluated mainly in terms of maximum rotation and settlement. Factor of safety against moment loading was also considered. Logarithmic extrapolations were made to predict the

accumulated rotations and settlements at the end of a typical wind farm's lifetime, which is considered 20 years. To check the validity of these predictions, a 40 cycle analysis was performed and the results were compared to the 8 – 10 cycle analyses. The basic conclusions are summarized below:

- Lateral capacity of hybrid foundations is governed by the length of the pile, while lateral stiffness and initial response is governed by the diameter of the footing.
- Lever arm of an applied force plays a significant role on both lateral capacity and lateral stiffness. This can be expressed by the ratio of moment to shear force that is transmitted to the foundation (M/Q). If this ratio is small, thus large shear forces act simultaneously to moments of the same direction, moment capacity and rocking stiffness can be significantly decreased.
- Monopile foundations have an increased moment capacity compared to hybrid foundations, due to their large embedment length. However, hybrid foundations demonstrate a superior response in terms of stiffness and maximum rotation, which are the key design criterions for offshore wind turbines.
- For all examined wind turbines, the corresponding "traditional" monopile foundation, which is deemed as a reasonable solution, can be substituted by a hybrid foundation with a reduced pile embedment length. This reduction ranges from 40 to 50 % in all cases. In this way, lateral response of the system in terms of rotation can be significantly improved.
- Increasing the diameter of the footing is found to be highly effective in improving the overall response of the system under operational environmental loads. In this way, larger wind turbines can be supported by hybrid foundations very efficiently.
- The role of P – δ effects is different for the two cyclic load scenarios. For cyclic wind loading, where the oscillation is symmetrical, P – δ effects can have a beneficial "re – centering" role, which helps reduce the accumulated rotations. On the other hand, for the case of cyclic wave loading combined with a monotonic wind load, the system is subjected to eccentric oscillations and P – δ effects can be devastating; the additional second – order moment can further increase the accumulated rotation.
- Logarithmic predictions made using the results from the first 8 – 10 cycles of wave loading can slightly under-predict the maximum accumulated rotation, however the quantitative comparisons are still considered valid.
- Soil inhomogeneity can deteriorate the contribution of the footing and cause significant stiffness deterioration after a number of loading cycles. Therefore, longer piles should be used.
- Hybrid foundations with different combinations of L and D can have similar responses. This makes the design of such foundations more flexible, as it can adapt to the in – situ soil conditions.
- Based on the above, satisfying hybrid foundation solutions for the three wind turbines examined are the following:

	Homogeneous soil	Inhomogeneous soil
2 MW	D11 – L15	D15 – L15
3.5 MW	D15 – L20	D15 – L20
5 MW	D20 – L20	D15 – L25

The above foundations were found to satisfy all the criteria that were considered in study, which are the following:

- Maximum allowable rotation $\vartheta_{lim} = 0.5^o = 0.0087$ rad
- Maximum allowable settlement $w_{lim} = 0.05D_{min} = 5.5$ cm
- Minimum allowable factor of safety against moment loading $FS_M = 2$

All of the above foundations significantly outperform the corresponding monopiles.

CHAPTER 5: FIGURES

Lateral Loading of Hybrid Foundations Supporting Offshore Wind Turbines

Ανωδομή	2 MW / 3.5 MW / 5 MW
D	11 m / 15 m / 20 m
L	15 m / 20 m / 25 m

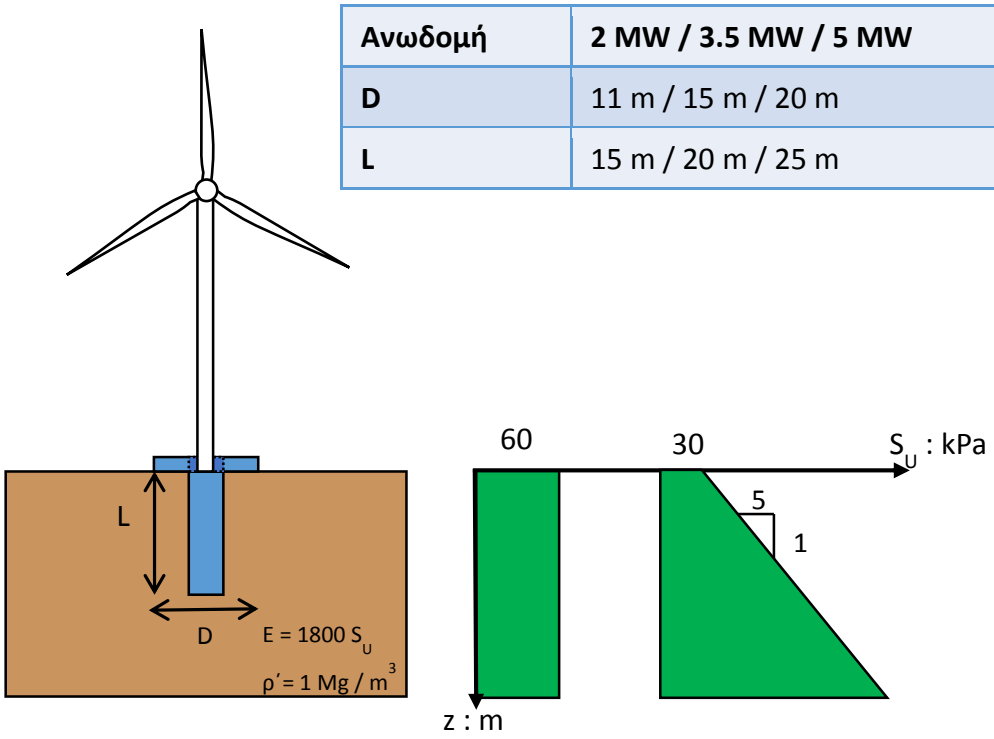

Figure 5.1. Monotonic loading: Sketch illustrating the problem and the examined parameters.

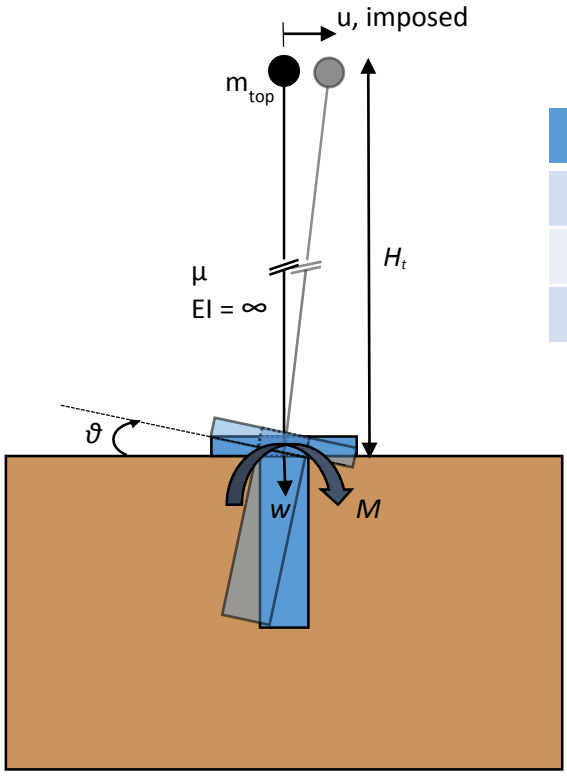

Ανωδομή	m_{top} : Mgr	μ : Mgr / m	Ht : m
2 MW	200	2.13	60
3.5 MW	220	2.44	80
5 MW	350	3.01	90

Figure 5.2. Model characteristics and basic parameters of the monotonic loading analyses.

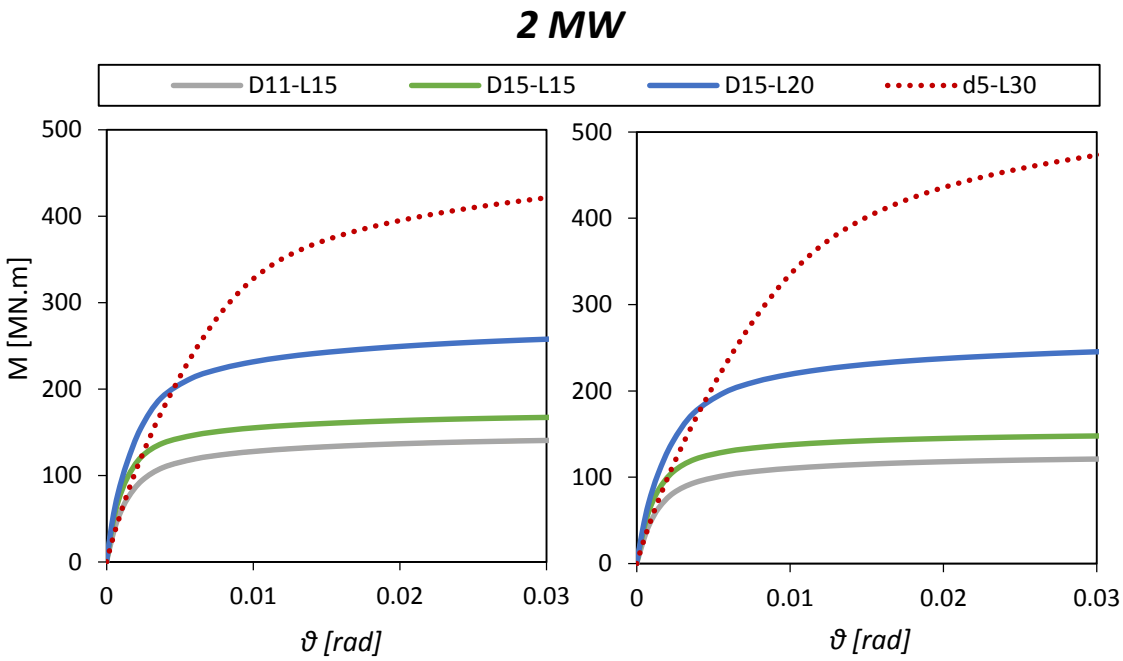

Figure 5.3. Monotonic moment – rotation curves for the 2MW wind turbine. Left: Homogeneous soil. Right: Inhomogeneous soil.

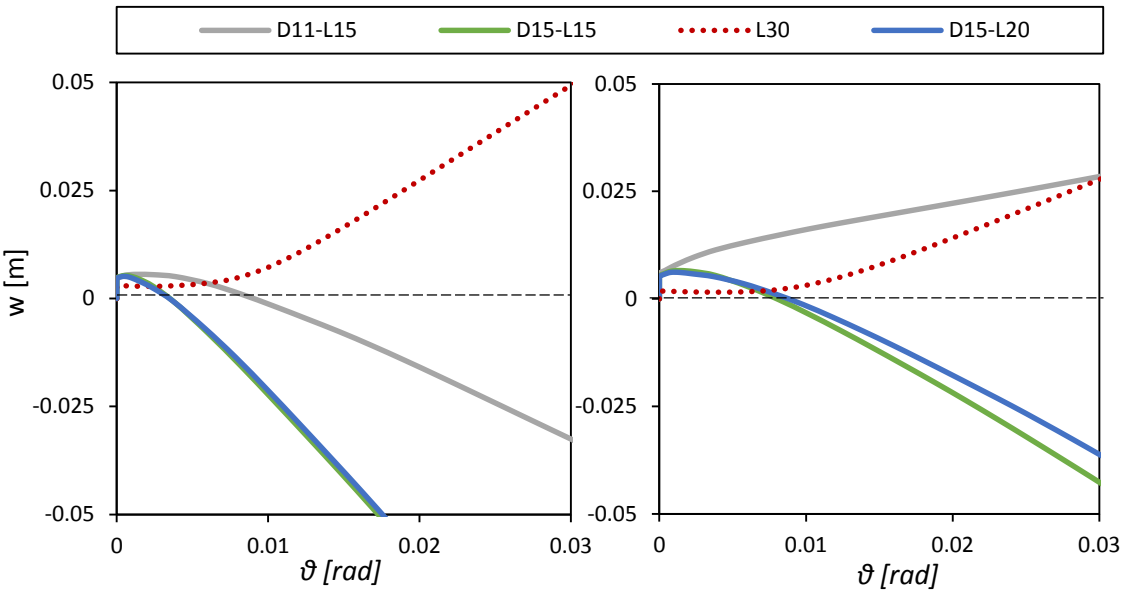

Figure 5.4. Monotonic settlement – rotation curves for the 2MW wind turbine. Left: Homogeneous soil. Right: Inhomogeneous soil.

3.5 MW

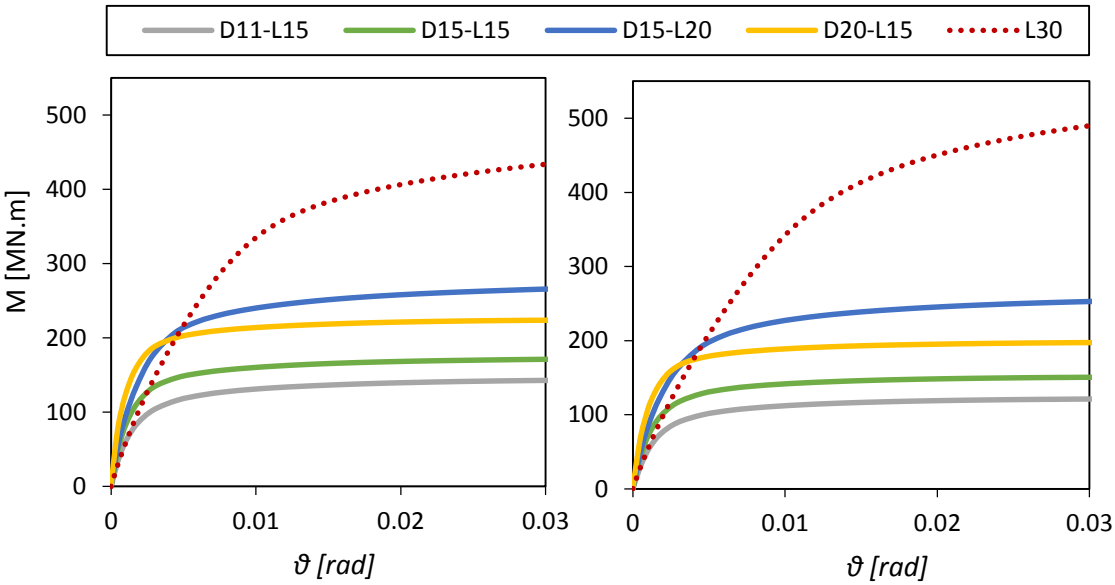

Figure 5.5. Monotonic moment – rotation curves for the 3.5MW wind turbine. Left: Homogeneous soil. Right: Inhomogeneous soil.

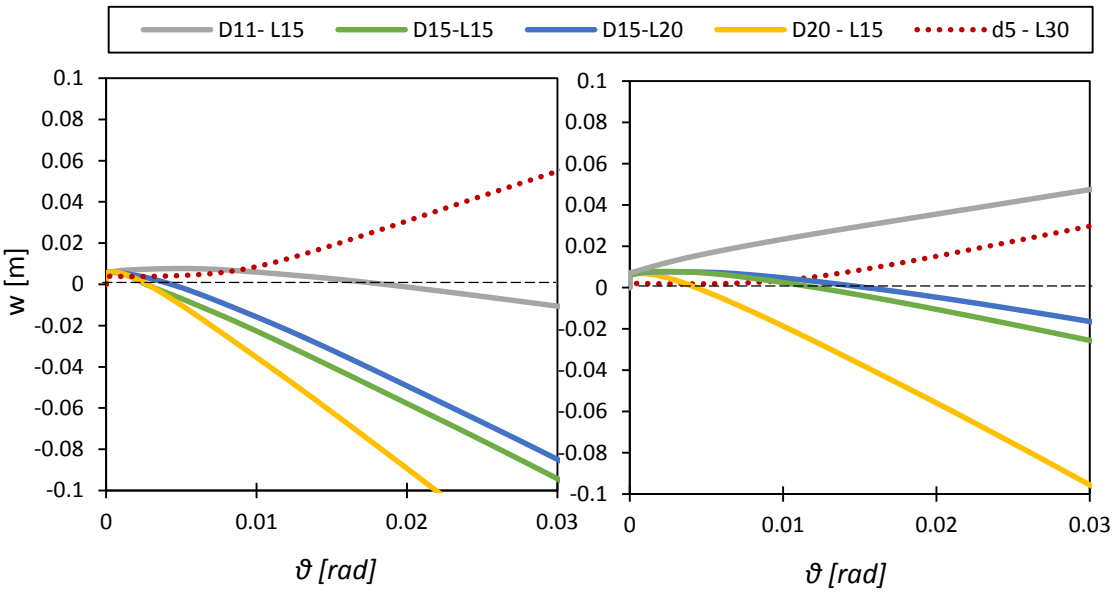

Figure 5.6. Monotonic settlement – rotation curves for the 3.5MW wind turbine. Left: Homogeneous soil. Right: Inhomogeneous soil.

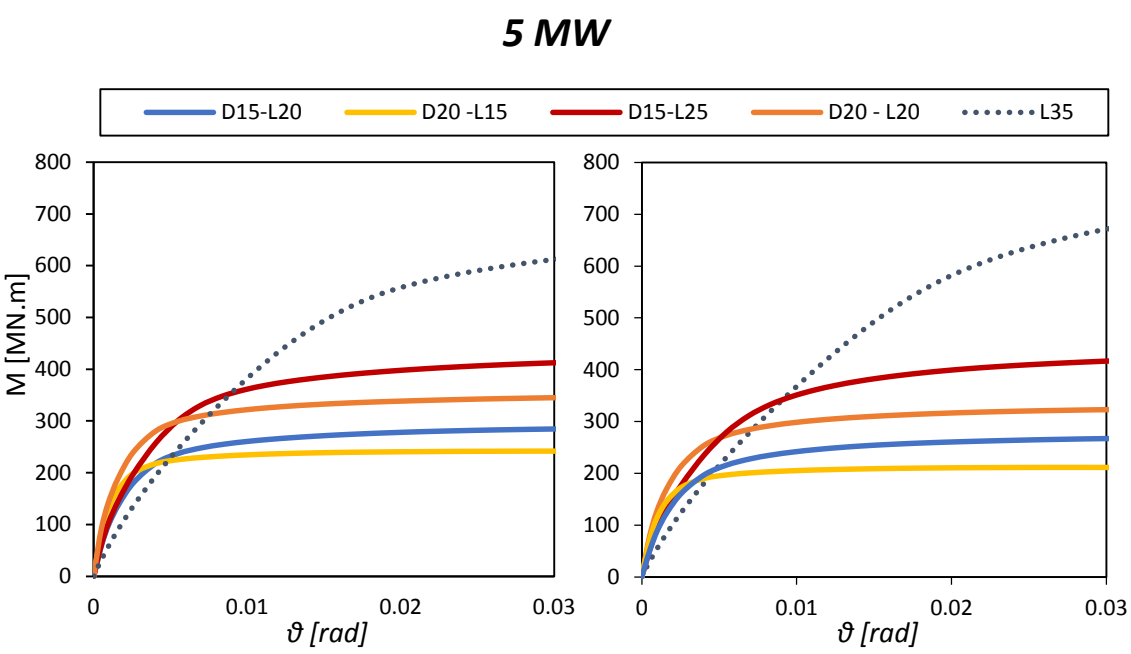

Figure 5.7. Monotonic moment – rotation curves for the 5MW wind turbine. Left: Homogeneous soil. Right: Inhomogeneous soil.

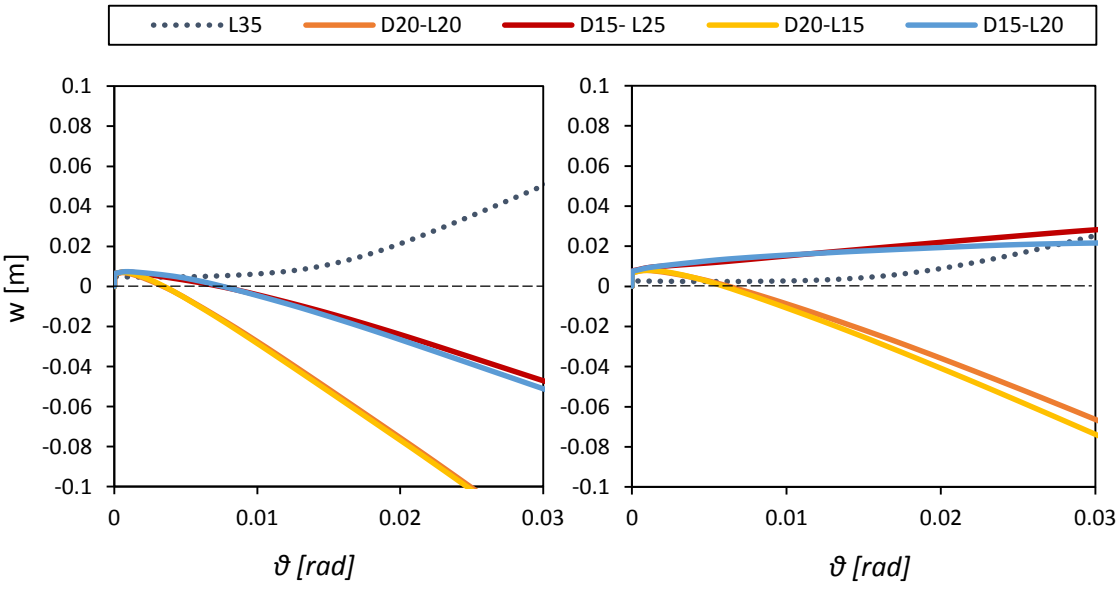

Figure 5.8. Monotonic settlement – rotation curves for the 5MW wind turbine. Left: Homogeneous soil. Right: Inhomogeneous soil.

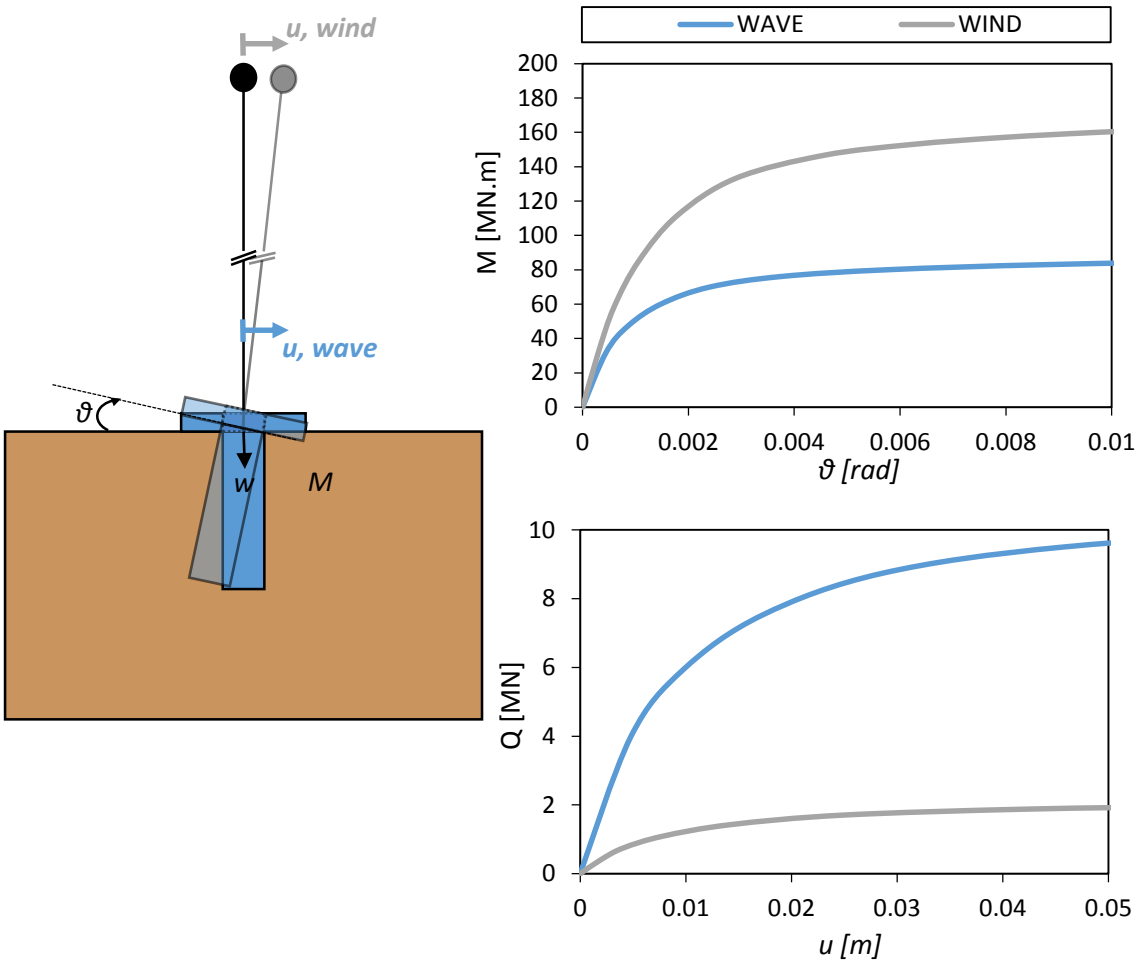

Figure 5.9. Impact of the lever arm of the monotonic loading on a) the moment – rotation curve and b) the shear force – horizontal displacement curve of a 3.5 MW wind turbine and D = 15m, L = 15m.

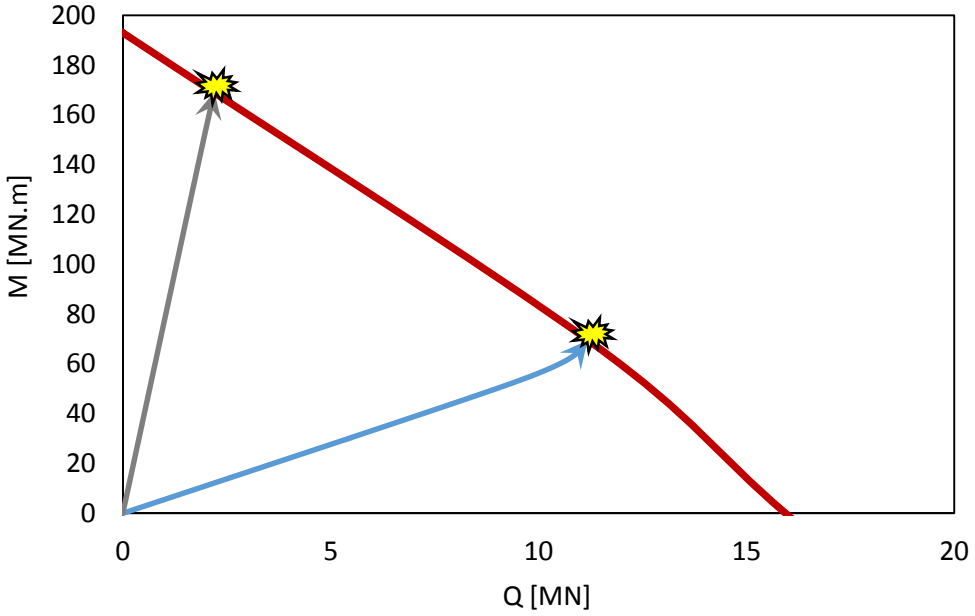

Figure 5.10. Load paths until failure in the M – Q plane corresponding to imposed displacement and the wind and wave lever arms (80m and 8m respectively) on a 3.5 MW wind turbine with D = 15m and L = 15m.

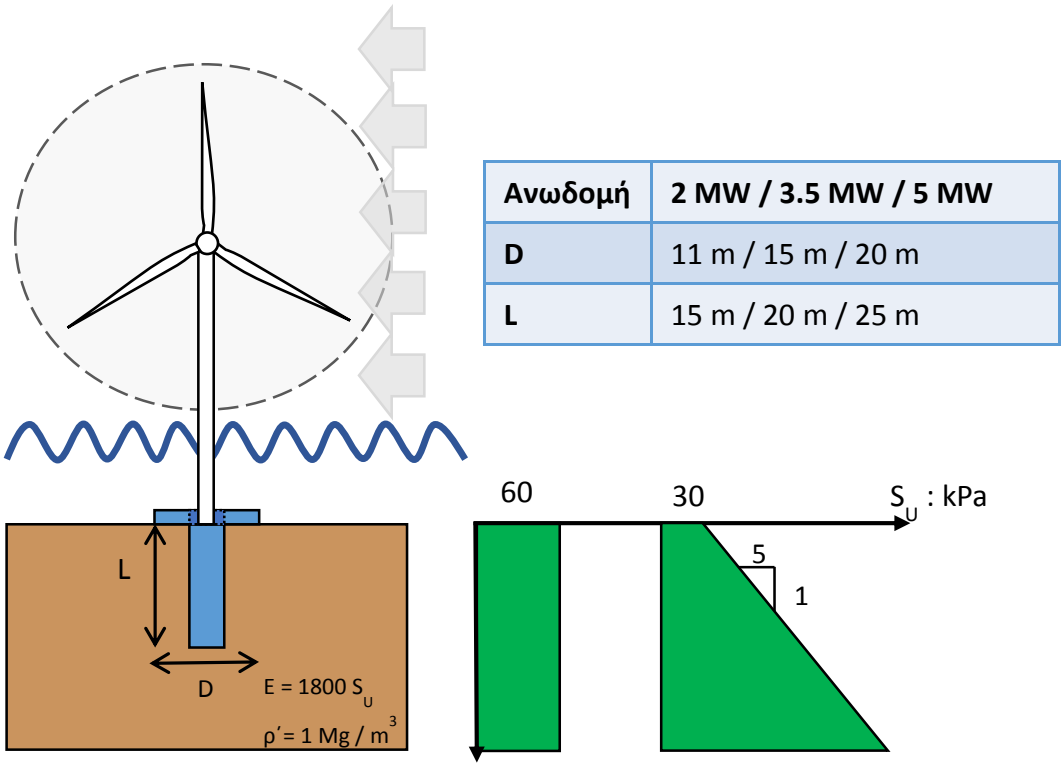

Ανωδομή	2 MW / 3.5 MW / 5 MW
D	11 m / 15 m / 20 m
L	15 m / 20 m / 25 m

Figure 5.11. Cyclic loading: Sketch illustrating the problem and the examined parameters.

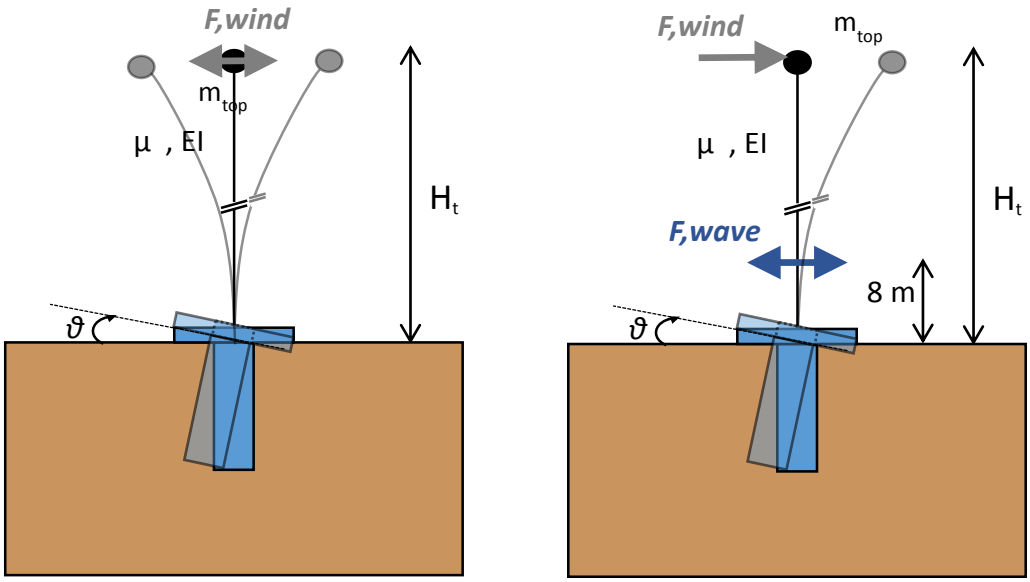

Figure 5.12. Sketch illustrating the model and the two cyclic loading scenarios: (a) Cyclic wind loading and (b) Monotonic wind and cyclic wave loading.

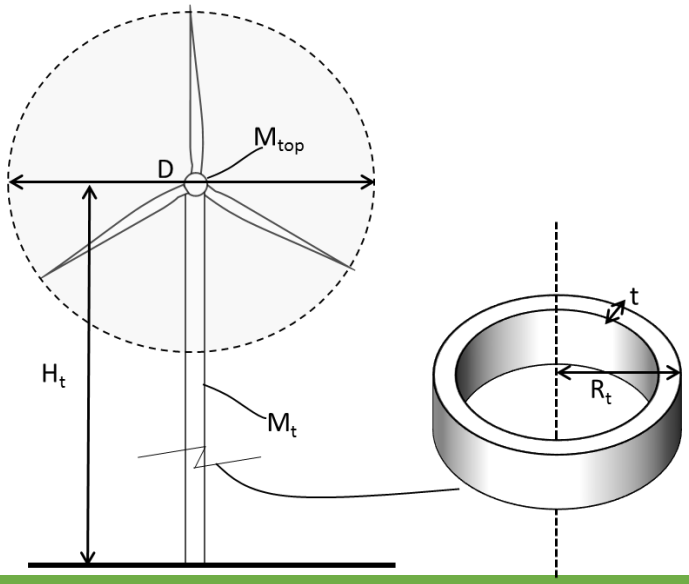

Figure 5.13. The basic geometrical parameters of a wind turbine tower.

	D : m	Ht : m	Rt : m	t : m	m_{top} : Mg	Mt : Mg	I : m^4	E : GPa
2 MW	65	60	2	0.02	200	128	0.495	210
3.5 MW	90	80	2	0.023	220	195	0.568	210
5 MW	110	90	2.46	0.023	350	271	1.071	210

Table 5.1. Tower characteristics of the wind turbines examined.

	P = w/g	V : m/sec	Cg	D : m	Fwind : kN
2 MW	1.25	25	0.3	70	**500**
3.5 MW	1.25	25	0.3	100	**1000**
5 MW	1.25	25	0.3	120	**1500**

$$F = \frac{w}{2g} V^2 C_g A$$

(API 1993)

Table 5.2. Wind loads of the wind turbines examined.

	F, wave : kN
2 MW	1800
3.5 MW	2000
5 MW	2200

$$p = p_D + p_M = C_D \frac{1}{2} \gamma_w D\, u\, |u| + C_M \frac{\gamma_w}{g} \frac{\pi D^2}{4} \dot{u}$$

(Morison 1950)

Table 5.3. Wave loads of the wind turbines examined.

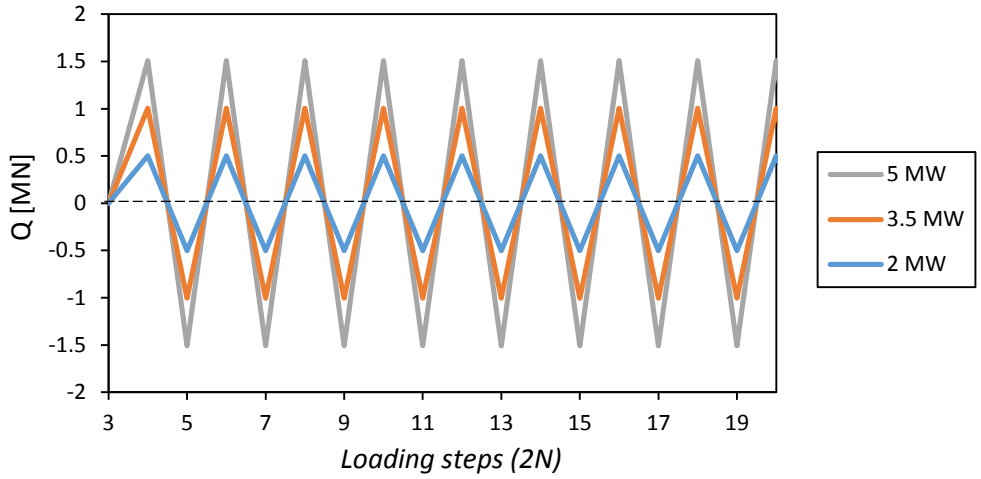

Figure 5.14. Shear force on the base of each wind turbine tower for the wind cyclic loading scenario.

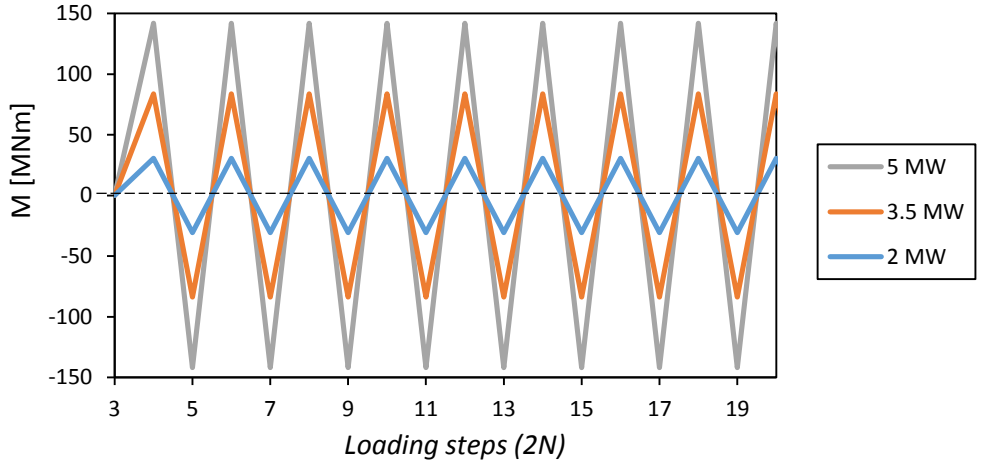

Figure 5.15. Overturning moment on the base of each wind turbine tower for the wind cyclic loading scenario.

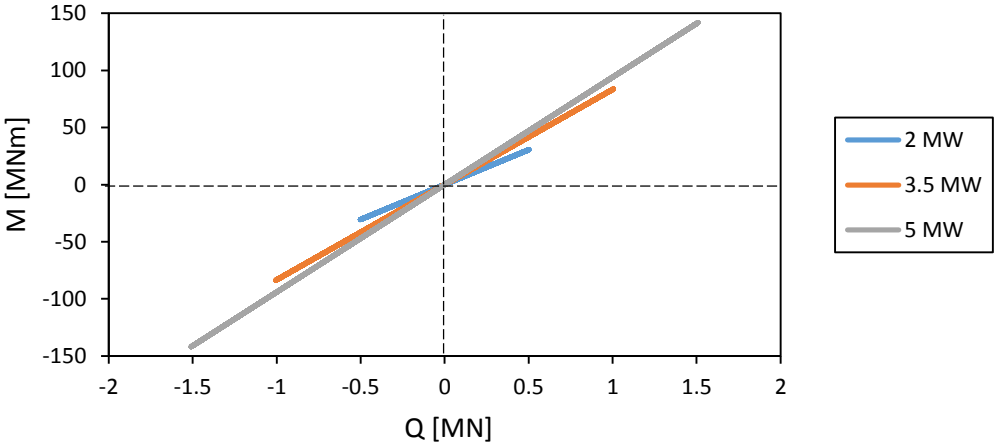

Figure 5.16. Load paths in the M – Q plane for the wind cyclic loading scenario.

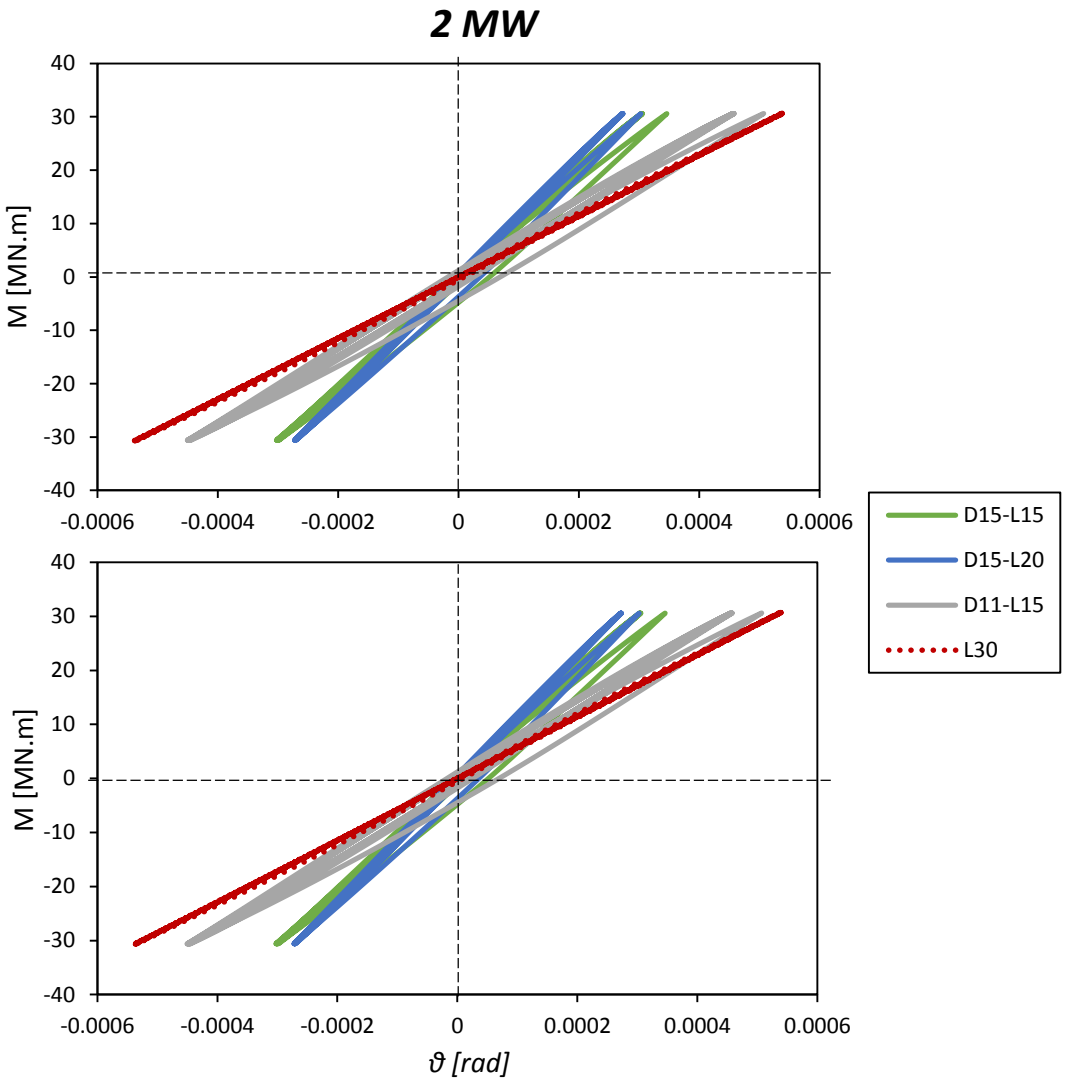

Figure 5.17. Cyclic moment – rotation diagrams for the 2 MW wind turbine. Up: Homogeneous soil. Down: Inhomogeneous soil.

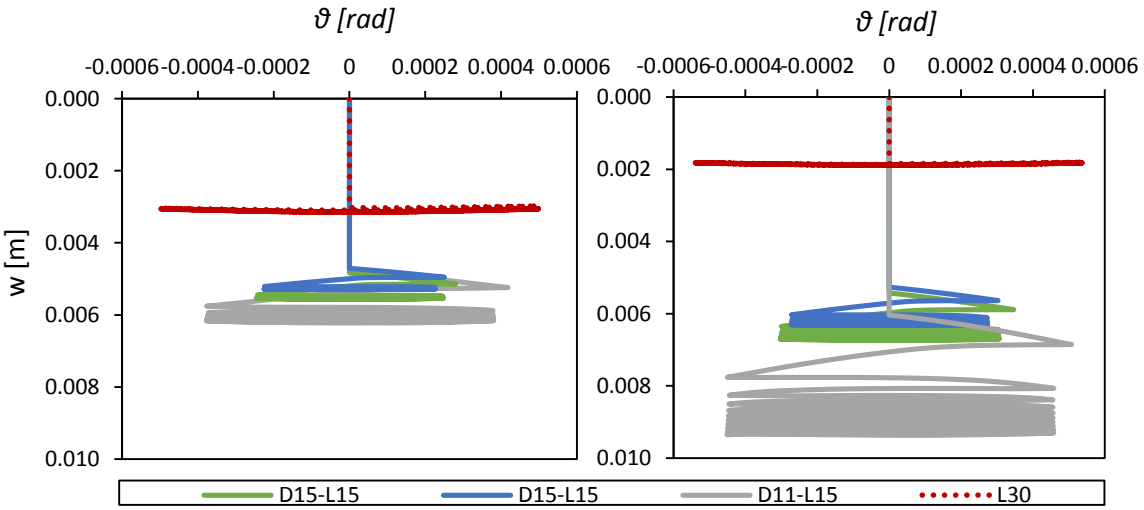

Figure 5.18. Cyclic settlement – rotation diagrams for the 2 MW wind turbine. Left: Homogeneous soil. Right: Inhomogeneous soil.

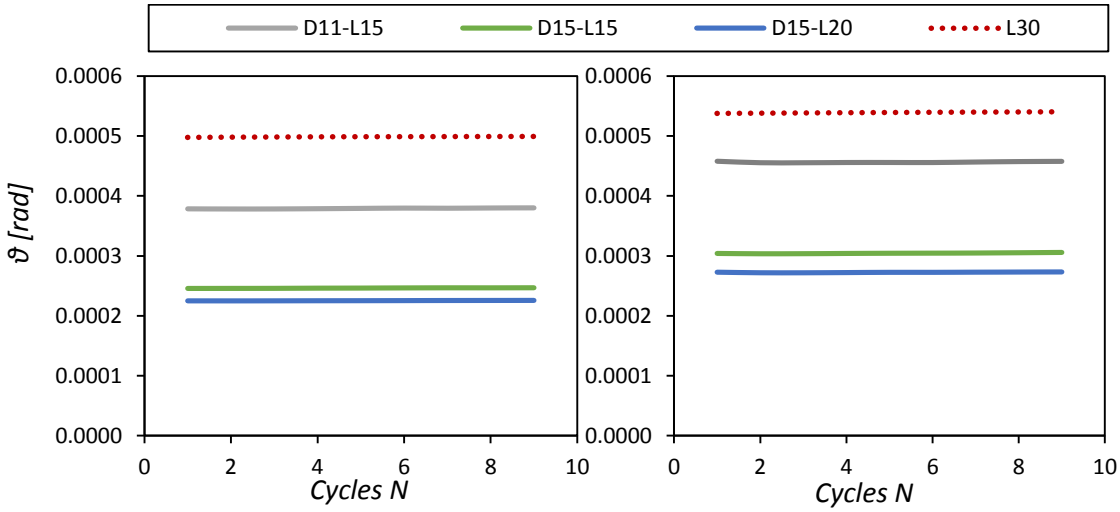

Figure 5.19. Accumulated rotations for the first 9 cycles of wind cyclic loading for the 2 MW wind turbine. Left: Homogeneous soil. Right: Inhomogeneous soil.

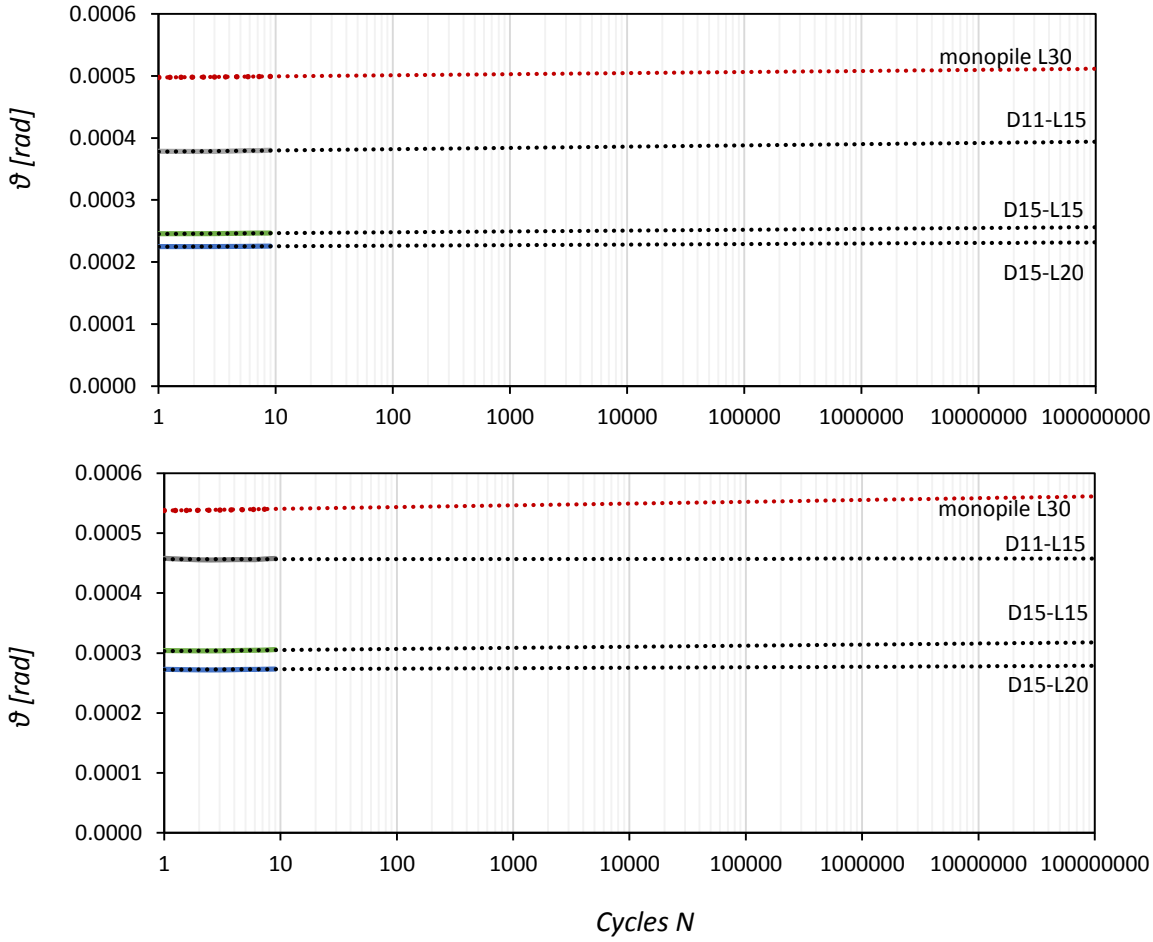

Figure 5.20. Accumulated rotations for the first 9 cycles of wind cyclic loading for the 2 MW wind turbine: Extrapolation with a logarithmic relationship to the lifetime of a wind turbine. Up: Homogeneous soil. Down: Inhomogeneous soil.

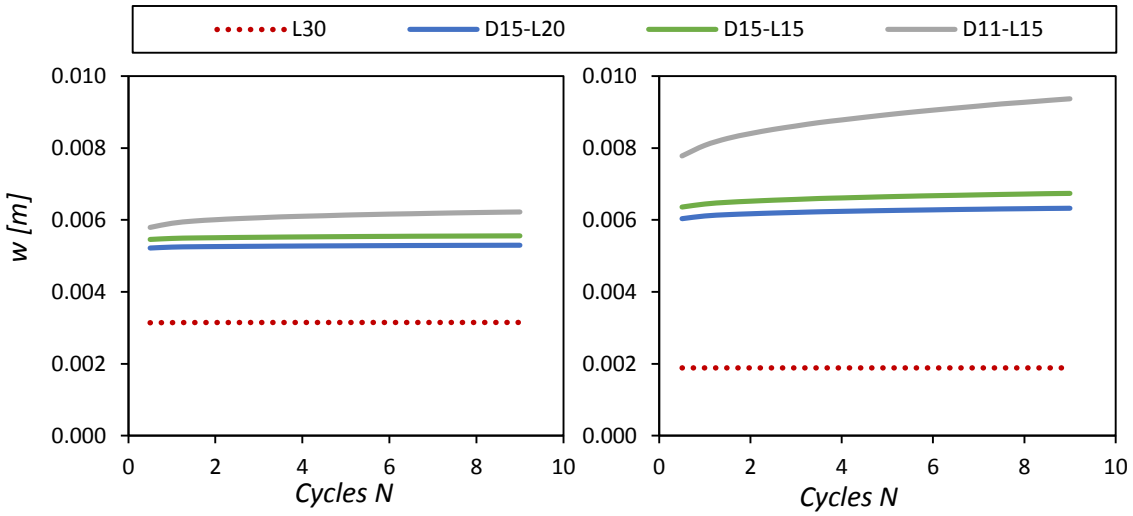

Figure 5.21. Accumulated settlements for the first 9 cycles of wind cyclic loading for the 2 MW wind turbine. Left: Homogeneous soil. Right: Inhomogeneous soil.

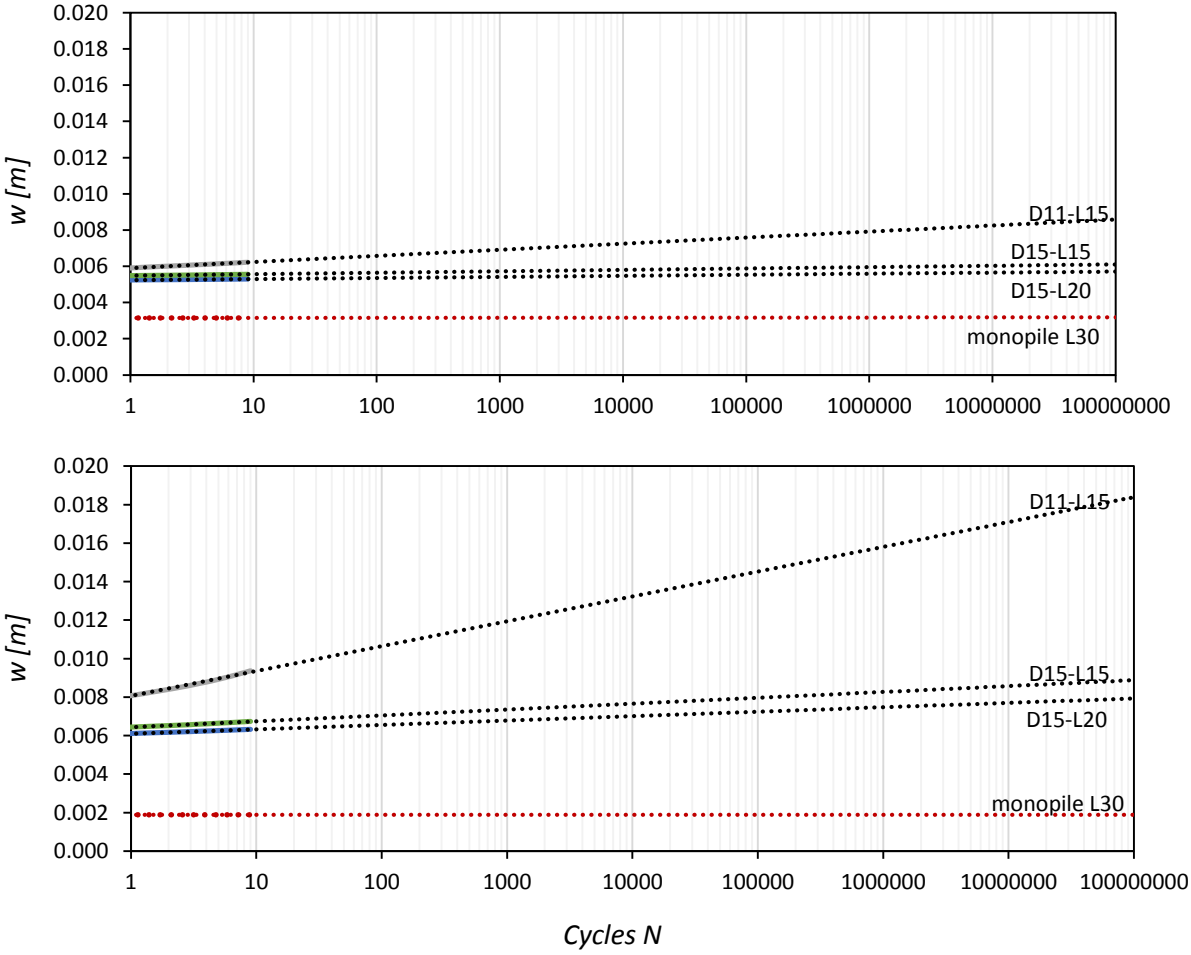

Figure 5.22. Accumulated settlements for the first 9 cycles of wind cyclic loading (2 MW wind turbine): Extrapolation with a logarithmic relationship to the lifetime of a wind turbine. Up: Homogeneous soil. Down: Inhomogeneous soil.

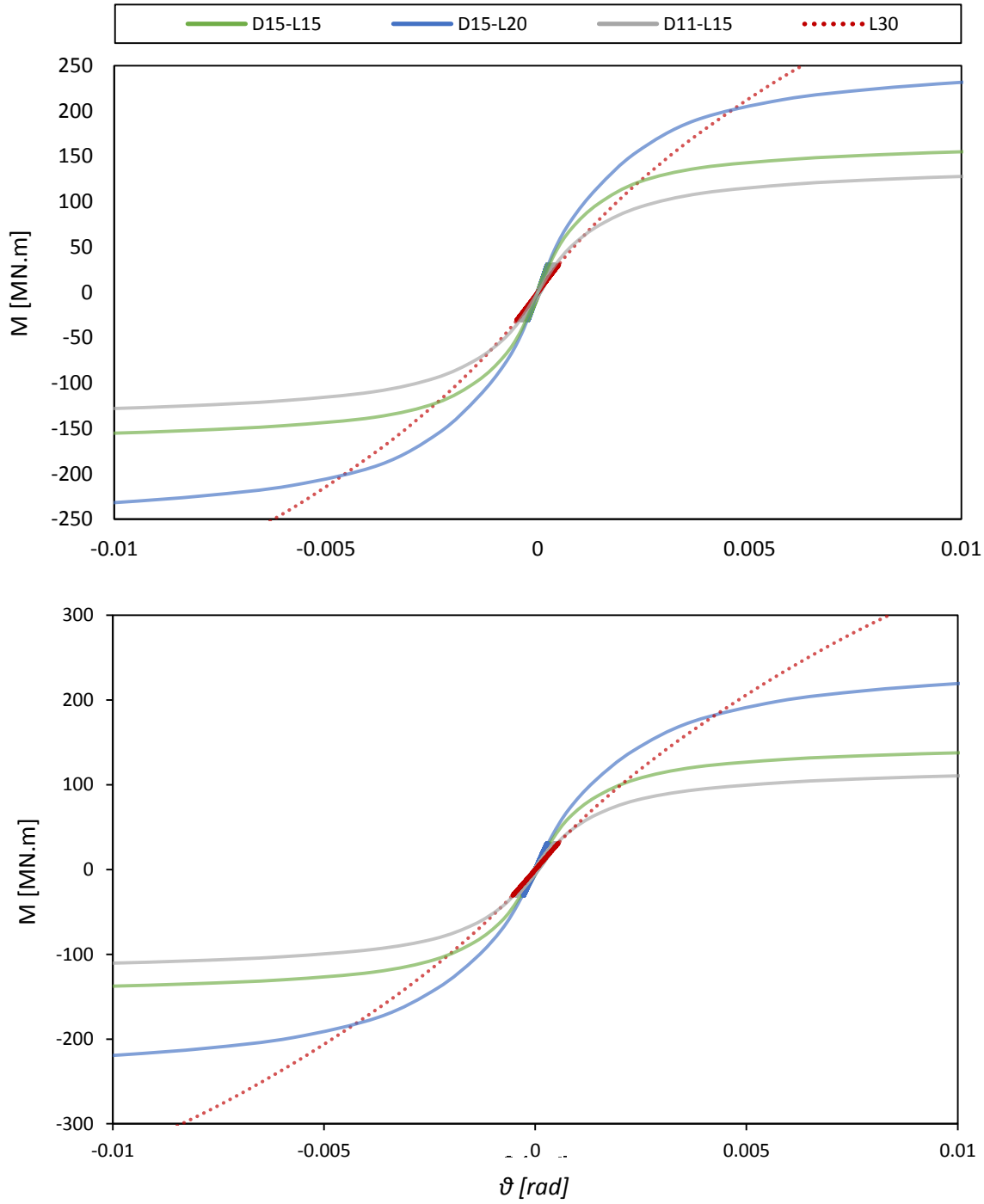

Figure 5.23. Cyclic and monotonic moment – rotation diagrams for the 2 MW wind turbine. Up: Homogeneous soil. Down: Inhomogeneous soil.

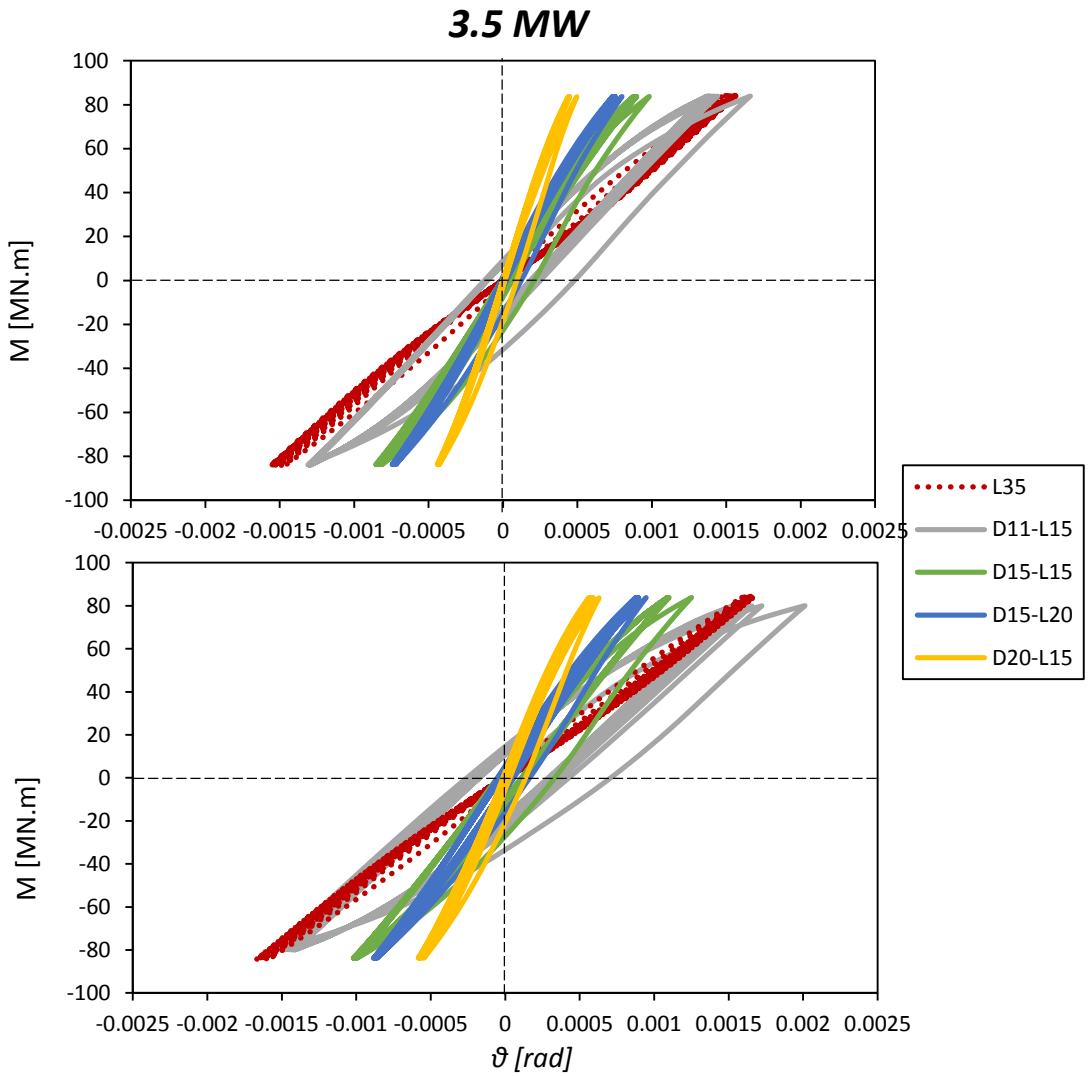

Figure 5.24. Wind - cyclic moment – rotation diagrams for the 3.5 MW wind turbine. Up: Homogeneous soil. Down: Inhomogeneous soil.

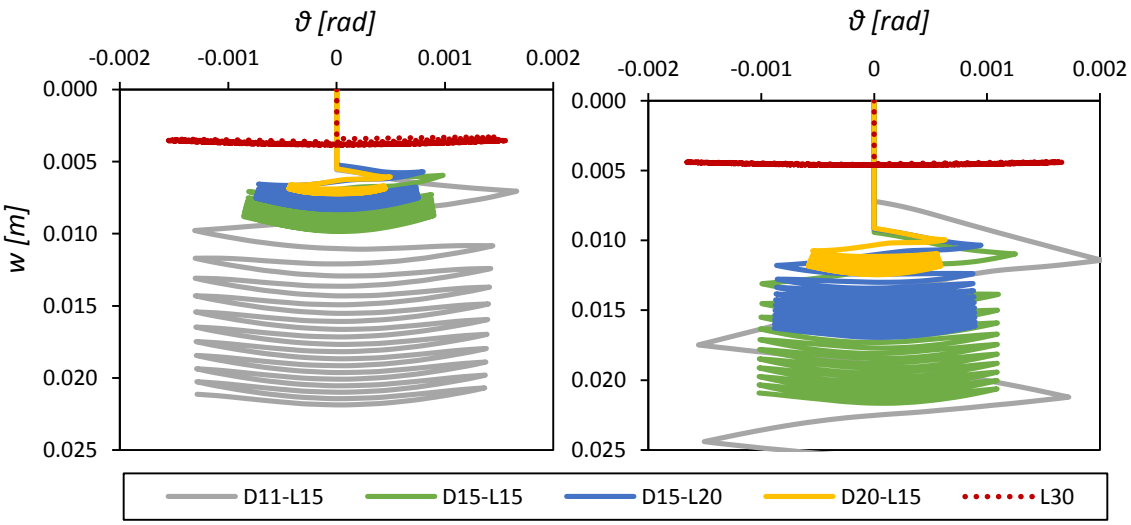

Figure 5.25. Cyclic settlement – rotation diagrams for the 3.5 MW wind turbine. Left: Homogeneous soil. Right: Inhomogeneous soil.

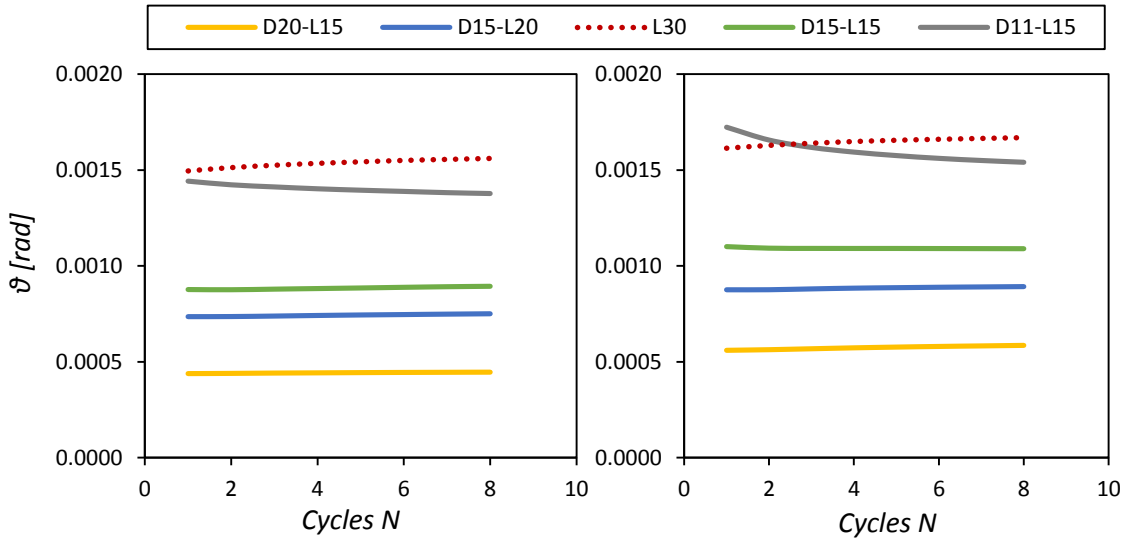

Figure 5.26. Accumulated rotations for the first 9 cycles of wind cyclic loading for the 3.5 MW wind turbine. Left: Homogeneous soil. Right: Inhomogeneous soil.

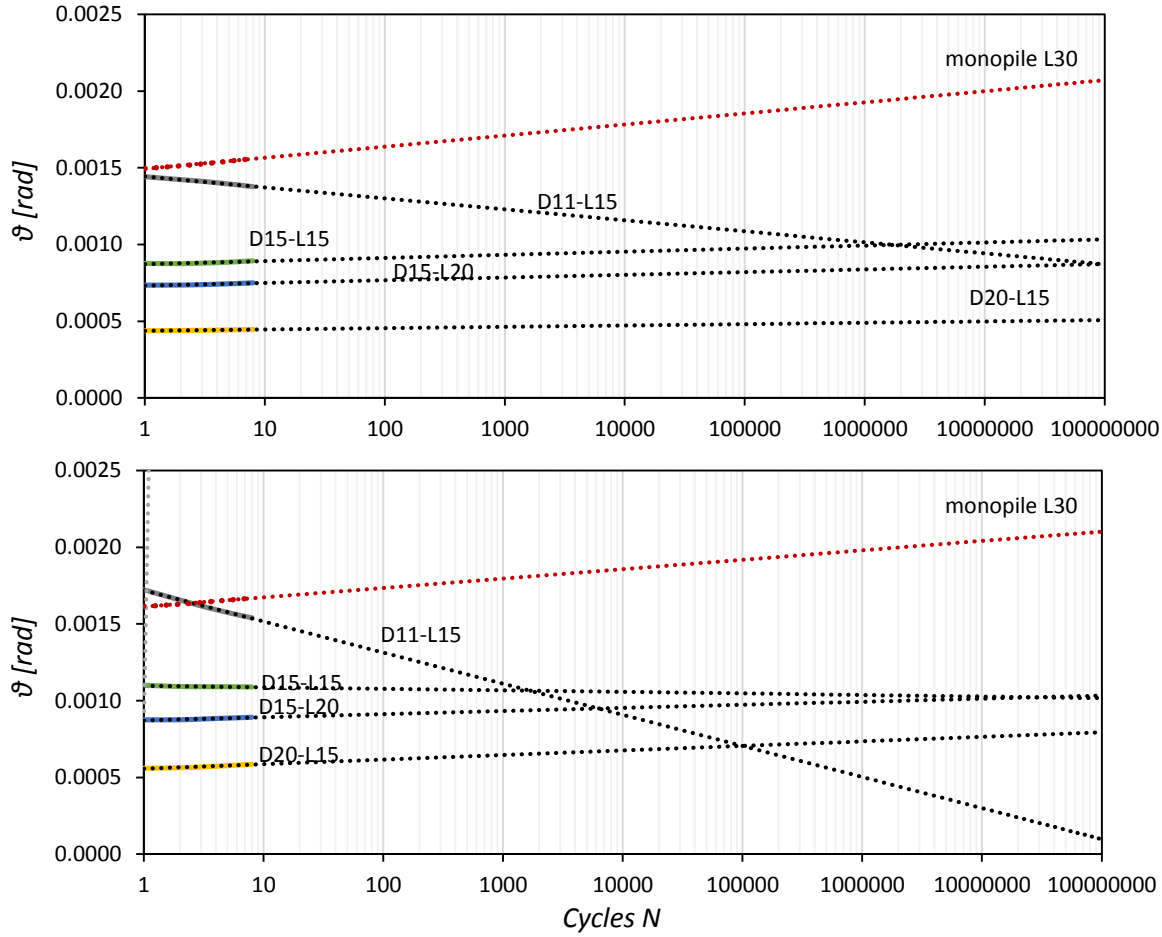

Figure 5.27. Accumulated rotations for the first 9 cycles of wind cyclic loading for the 3.5 MW wind turbine: Extrapolation with a logarithmic relationship to the lifetime of a wind turbine. Up: Homogeneous soil. Down: Inhomogeneous soil.

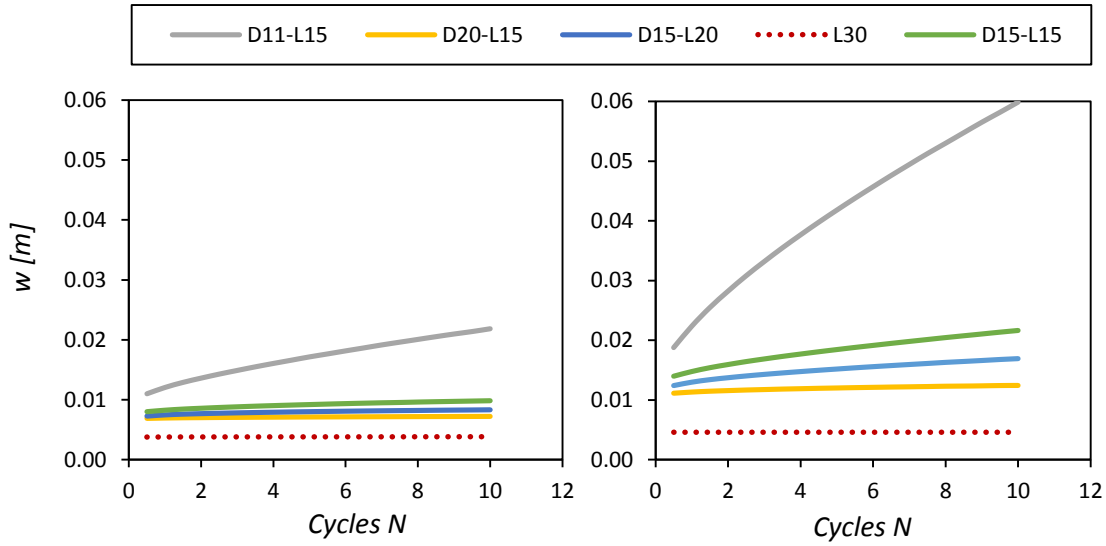

Figure 5.28. Accumulated settlements for the first 9 cycles of wind cyclic loading for the 3.5 MW wind turbine. Left: Homogeneous soil. Right: Inhomogeneous soil.

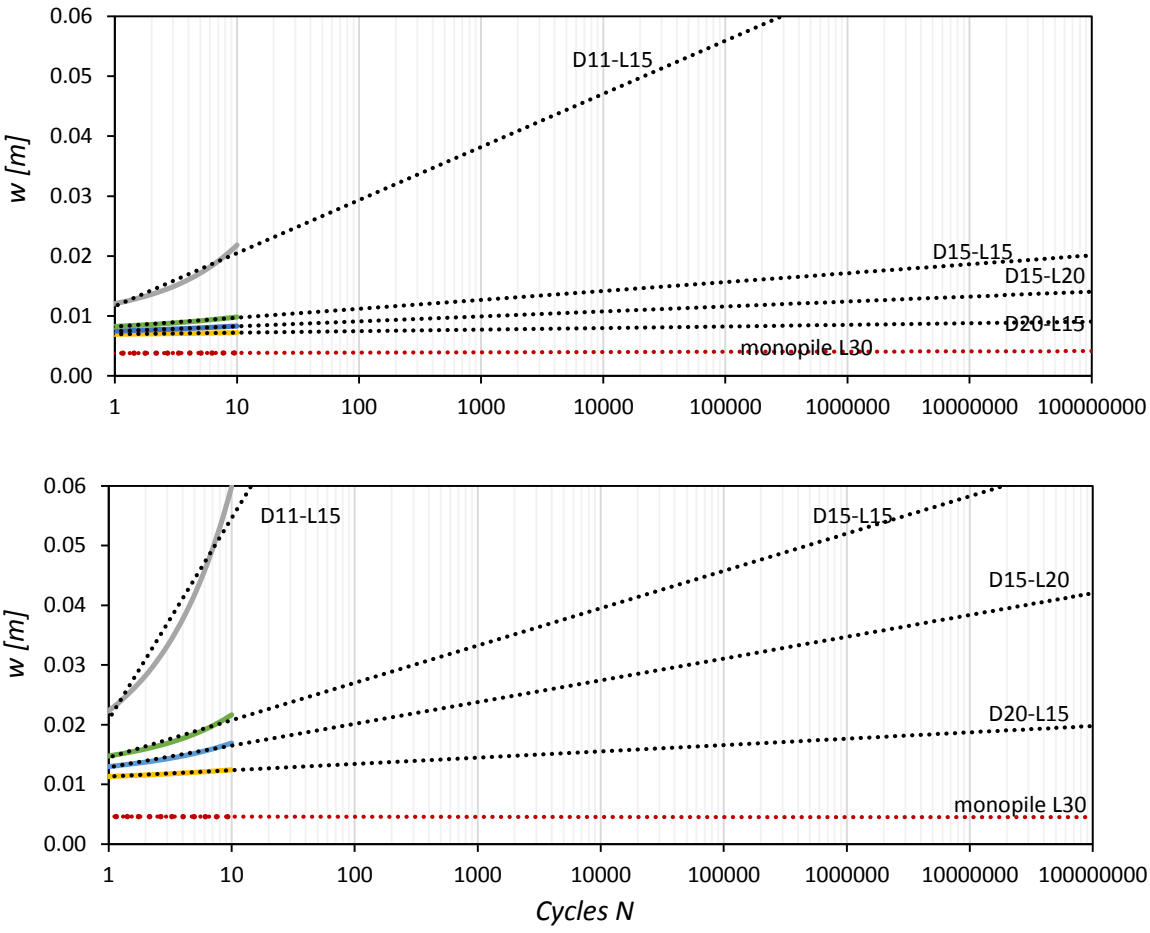

Figure 5.29. Accumulated settlements for the first 9 cycles of wind cyclic loading (3.5 MW wind turbine): Extrapolation with a logarithmic relationship to the lifetime of a wind turbine. Up: Homogeneous soil. Down: Inhomogeneous soil.

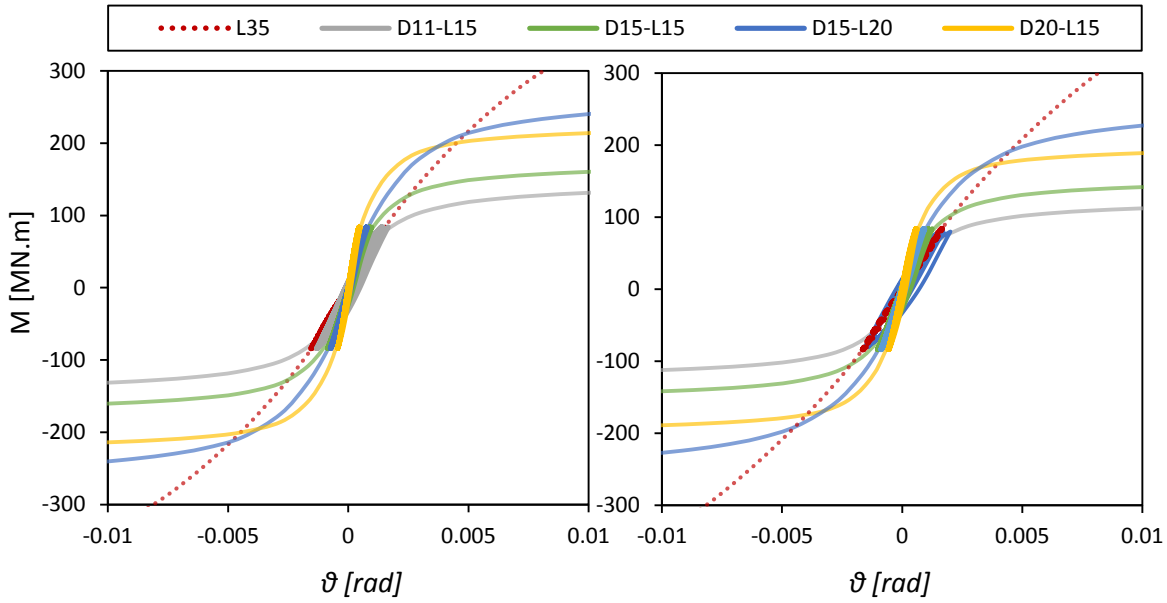

Figure 5.30. Cyclic and monotonic moment – rotation diagrams for the 3.5 MW wind turbine. Left: Homogeneous soil. Right: Inhomogeneous soil.

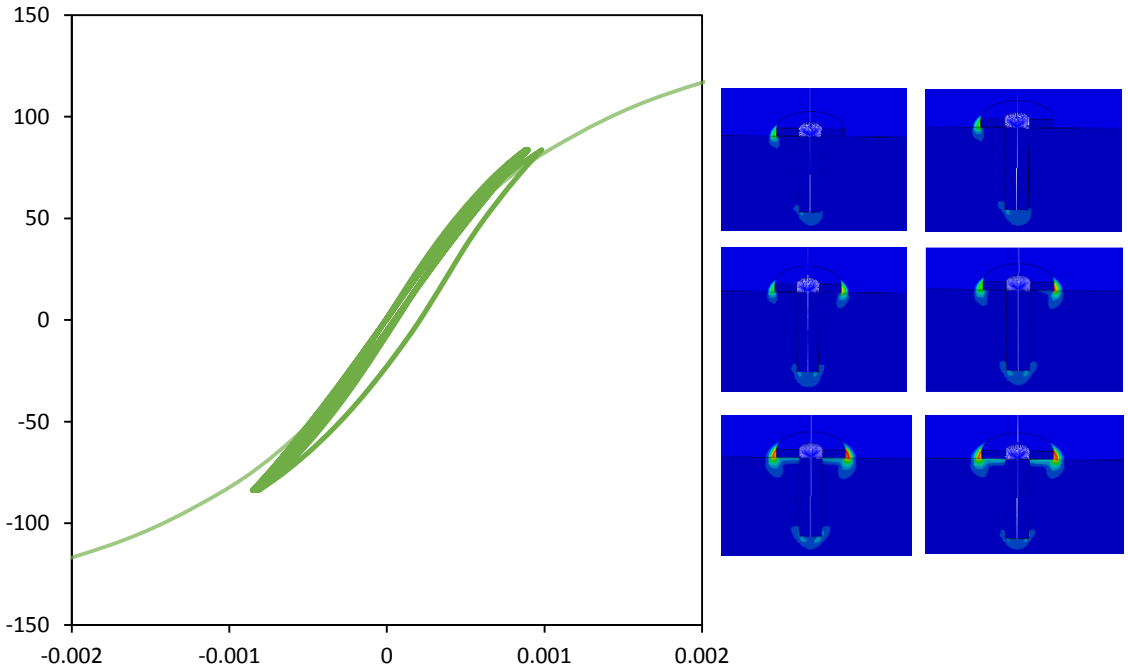

Figure 5.31. Cyclic and monotonic moment – rotation diagrams for the 3.5 MW wind turbine founded on a hybrid foundation with D = 15m and L = 15m (homogeneous soil). Right: Plastic strain contours during the wind cyclic loading.

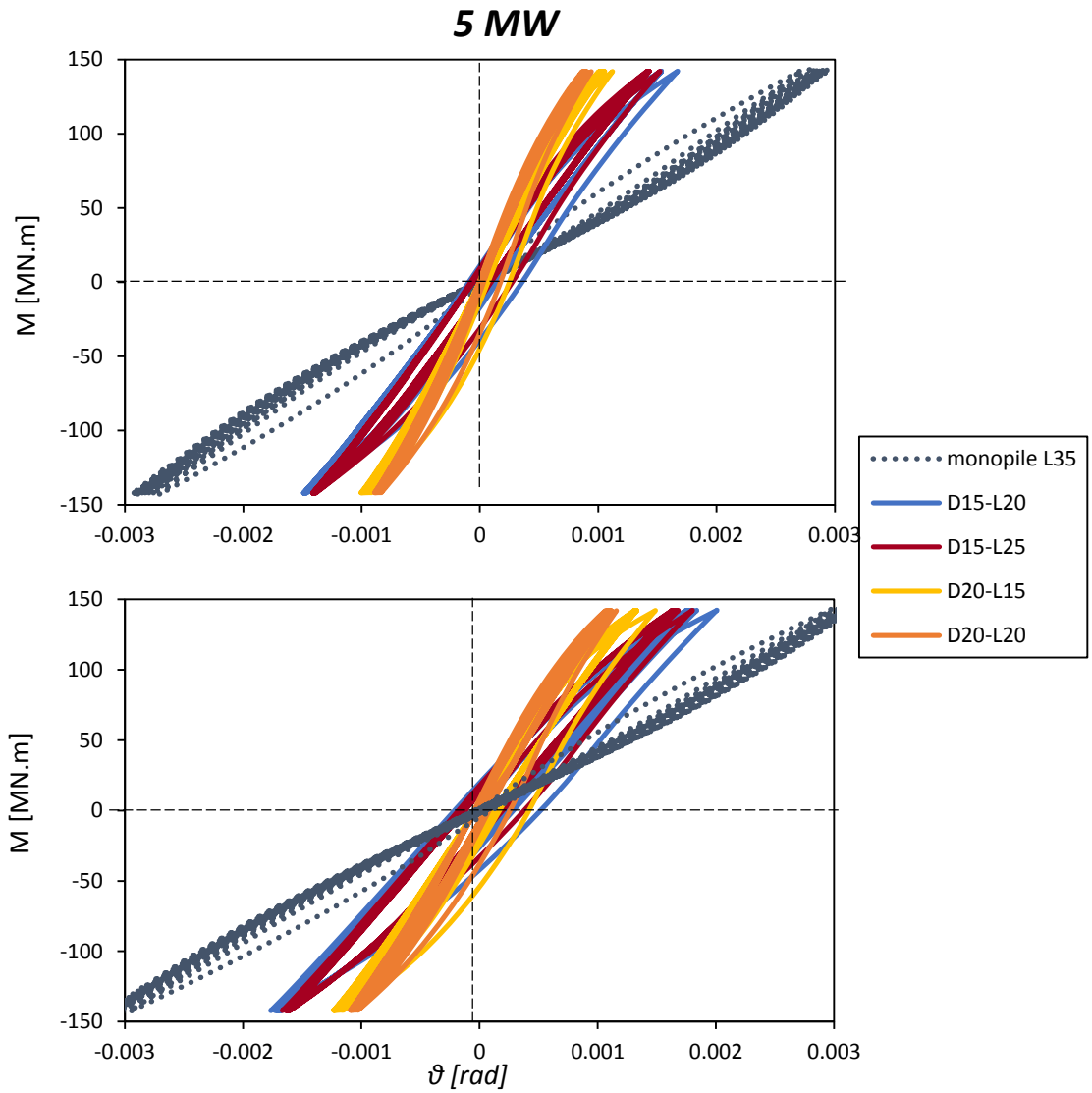

Figure 5.32. Cyclic moment – rotation diagrams for the 5 MW wind turbine. Up: Homogeneous soil. Down: Inhomogeneous soil.

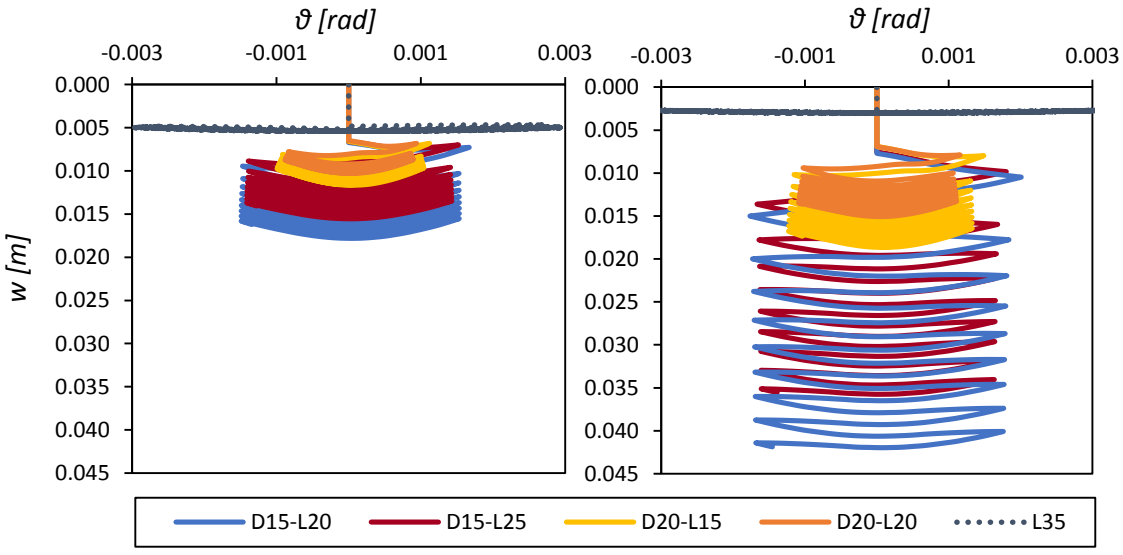

Figure 5.33. Cyclic settlement – rotation diagrams for the 5 MW wind turbine. Left: Homogeneous soil. Right: Inhomogeneous soil.

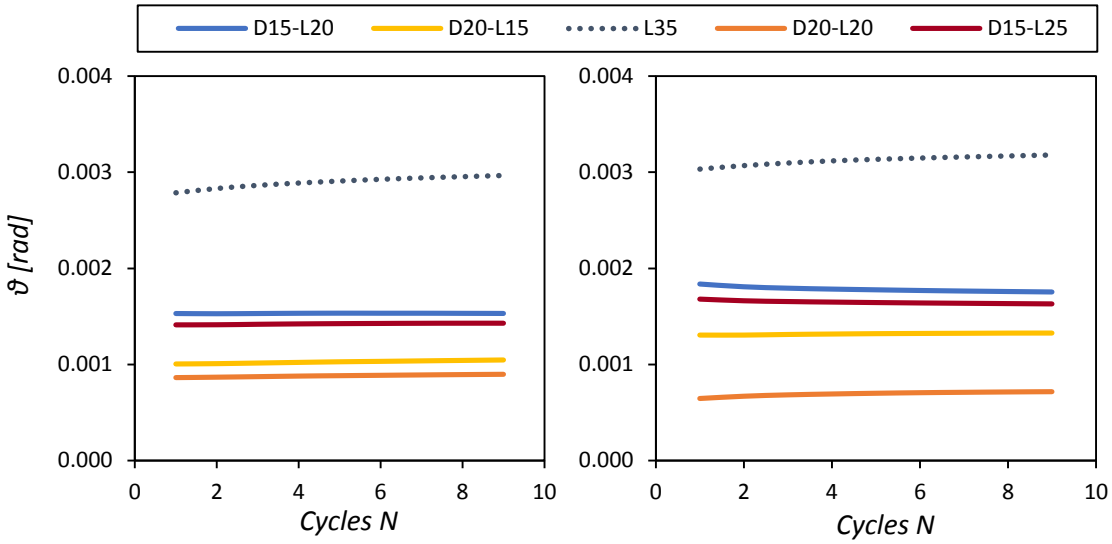

Figure 5.34. Accumulated rotations for the first 9 cycles of wind cyclic loading for the 5 MW wind turbine. Left: Homogeneous soil. Right: Inhomogeneous soil.

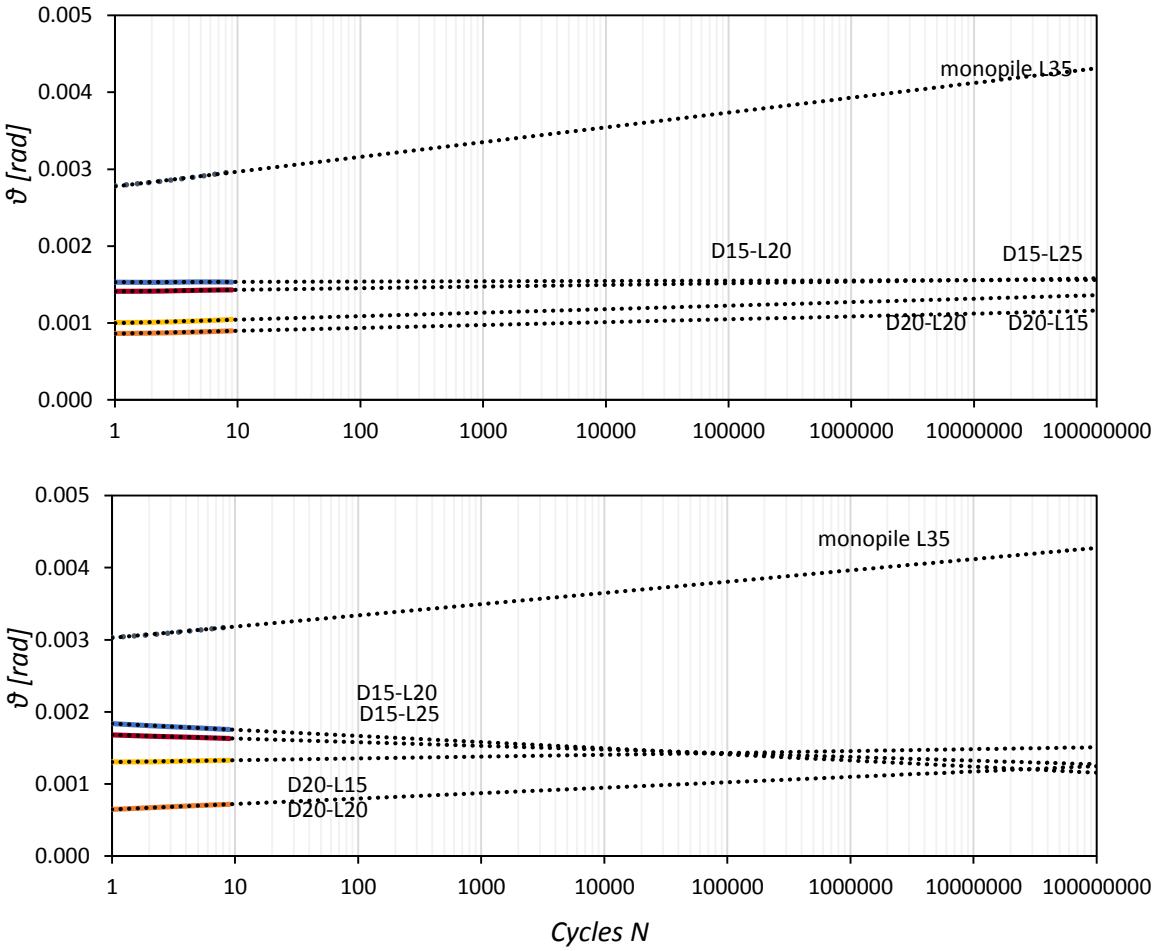

Figure 5.35. Accumulated rotations for the first 9 cycles of wind cyclic loading for the 5 MW wind turbine: Extrapolation with a logarithmic relationship to the lifetime of a wind turbine. Up: Homogeneous soil. Down: Inhomogeneous soil.

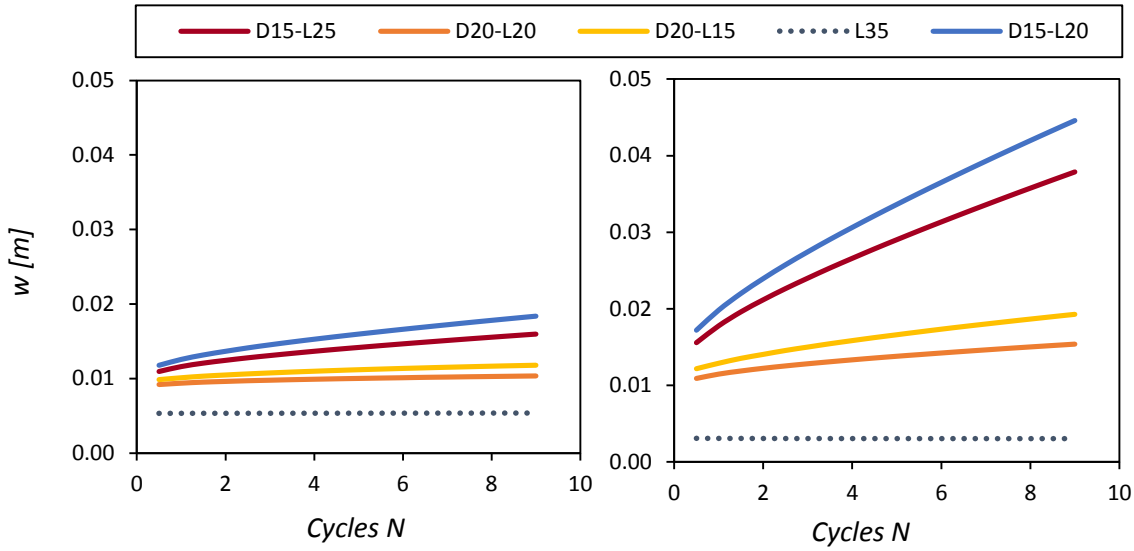

Figure 5.36. Accumulated settlements for the first 9 cycles of wind cyclic loading for the 5 MW wind turbine. Left: Homogeneous soil. Right: Inhomogeneous soil.

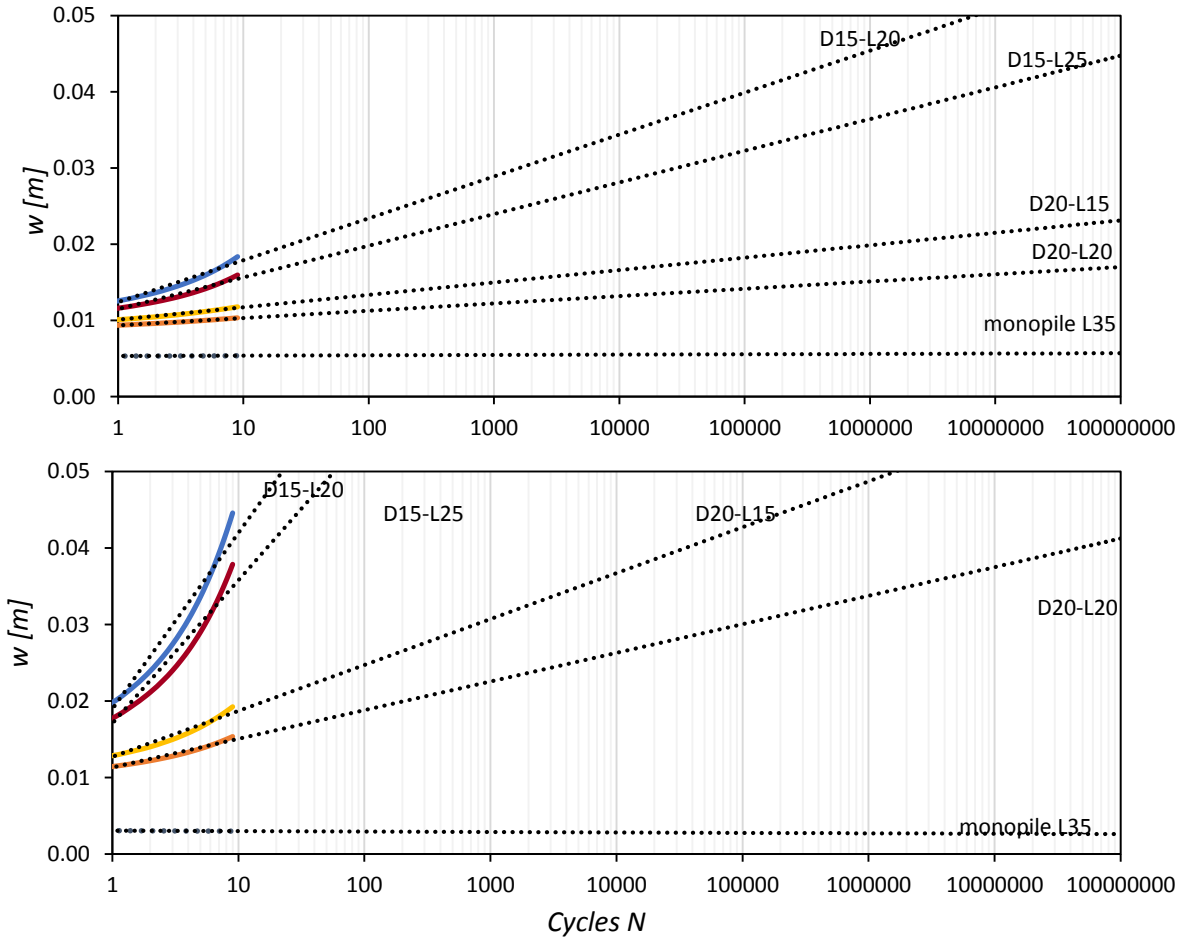

Figure 5.37. Accumulated settlements for the first 9 cycles of wind cyclic loading (5 MW wind turbine): Extrapolation with a logarithmic relationship to the lifetime of a wind turbine. Up: Homogeneous soil. Down: Inhomogeneous soil.

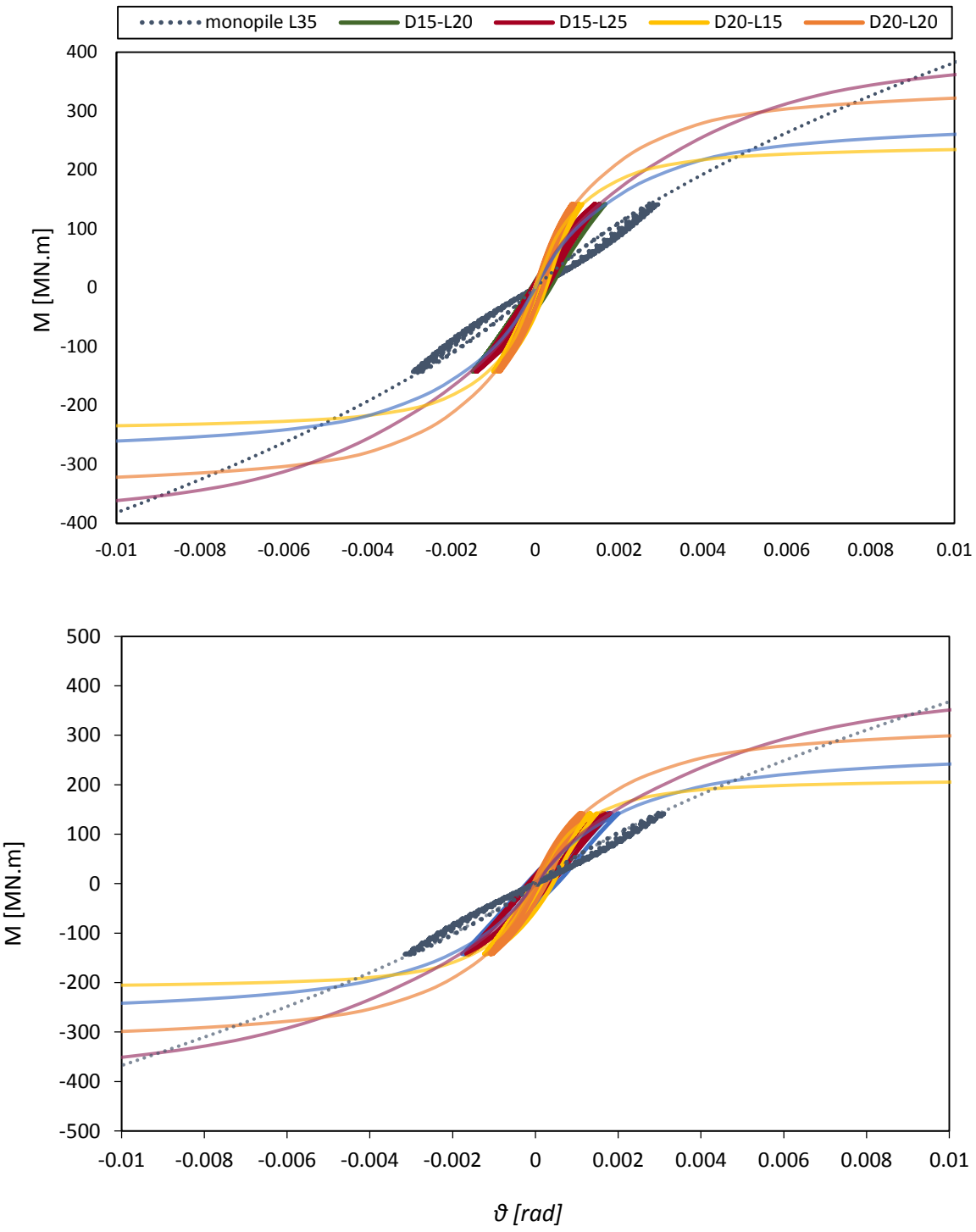

Figure 5.38. Cyclic and monotonic moment – rotation diagrams for the 5 MW wind turbine. Up: Homogeneous soil. Down: Inhomogeneous soil.

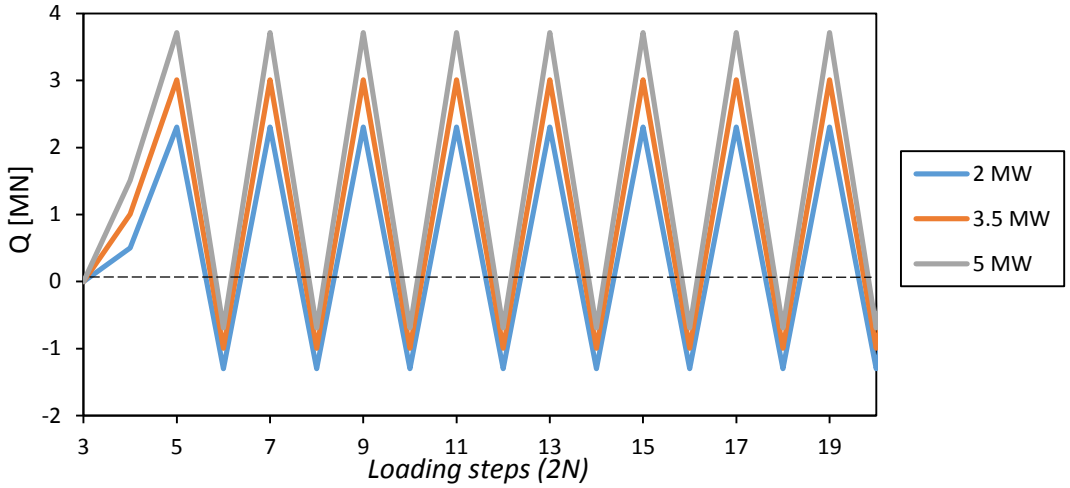

Figure 5.39. Shear force on the base of each wind turbine tower for the wave cyclic loading scenario.

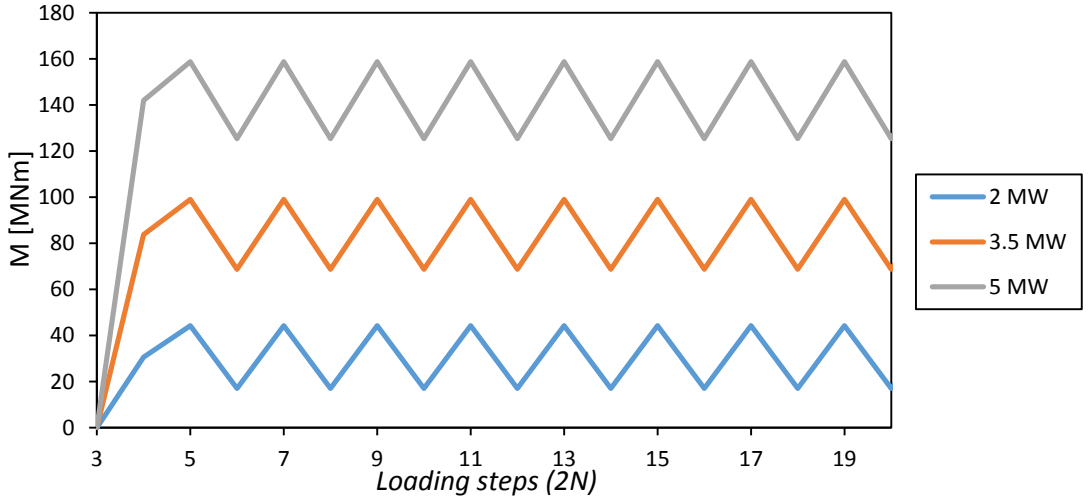

Figure 5.40. Overturning moment on the base of each wind turbine tower for the wave cyclic loading scenario.

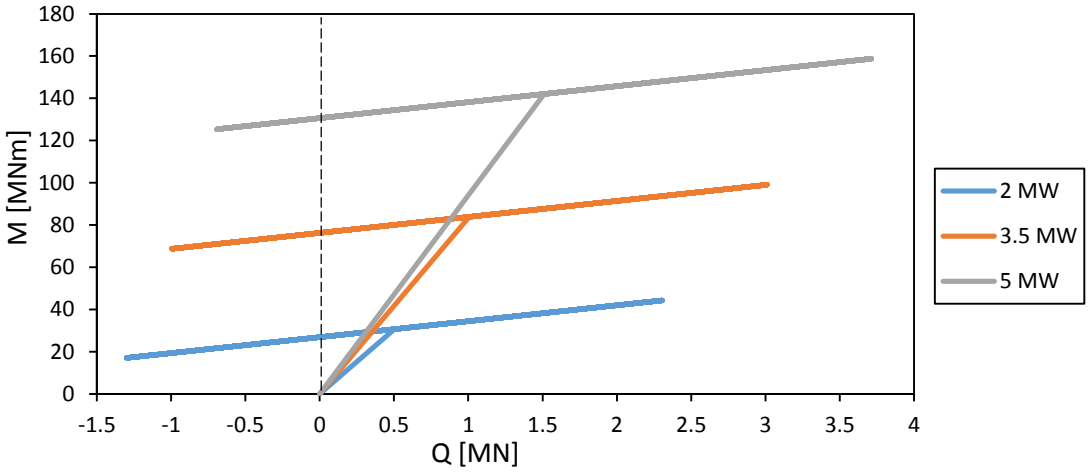

Figure 5.41. Load paths in the M – Q plane for the wave cyclic loading scenario.

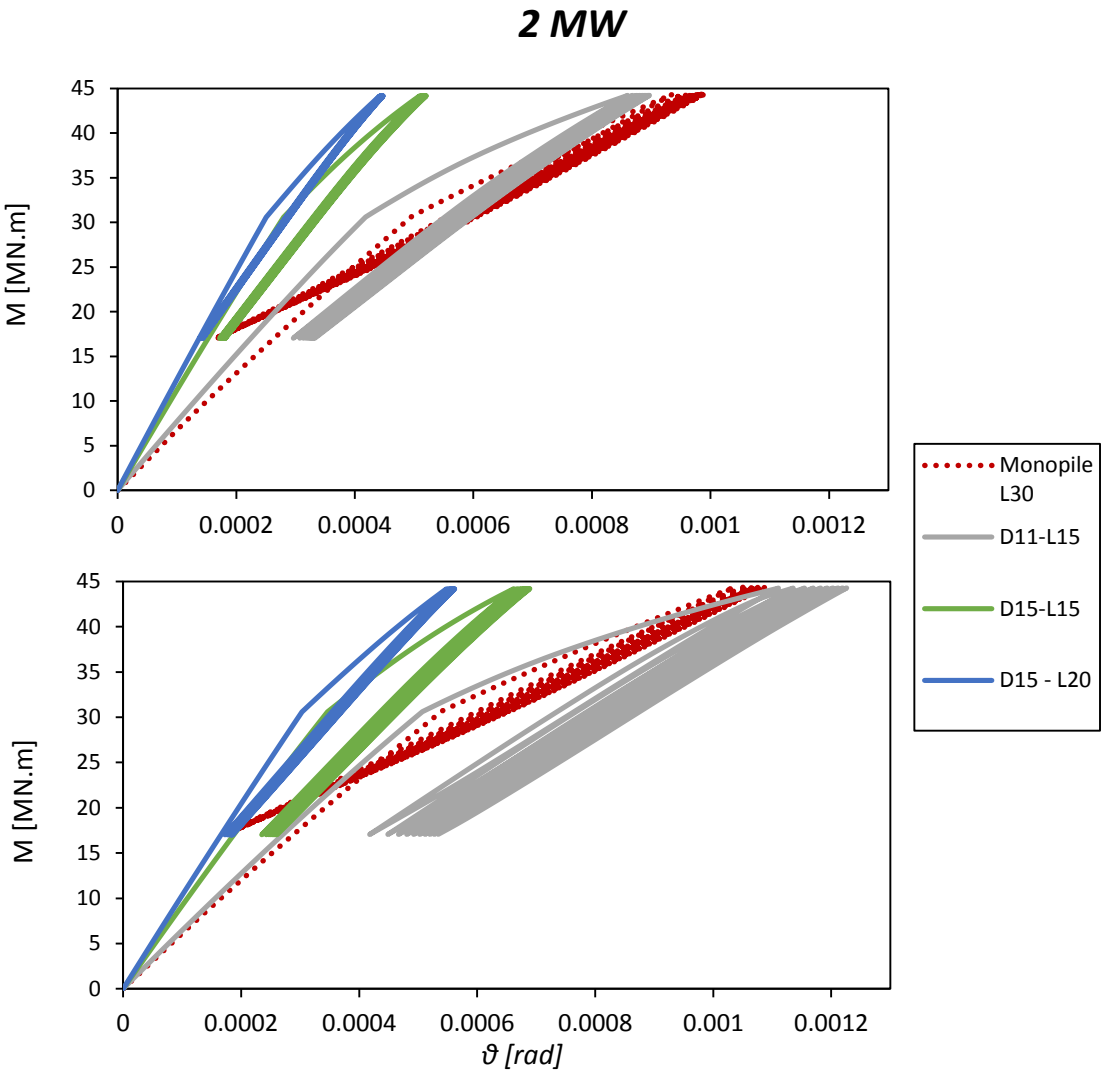

Figure 5.42. Wave cyclic moment – rotation diagrams for the 2 MW wind turbine. Up: Homogeneous soil. Down: Inhomogeneous soil.

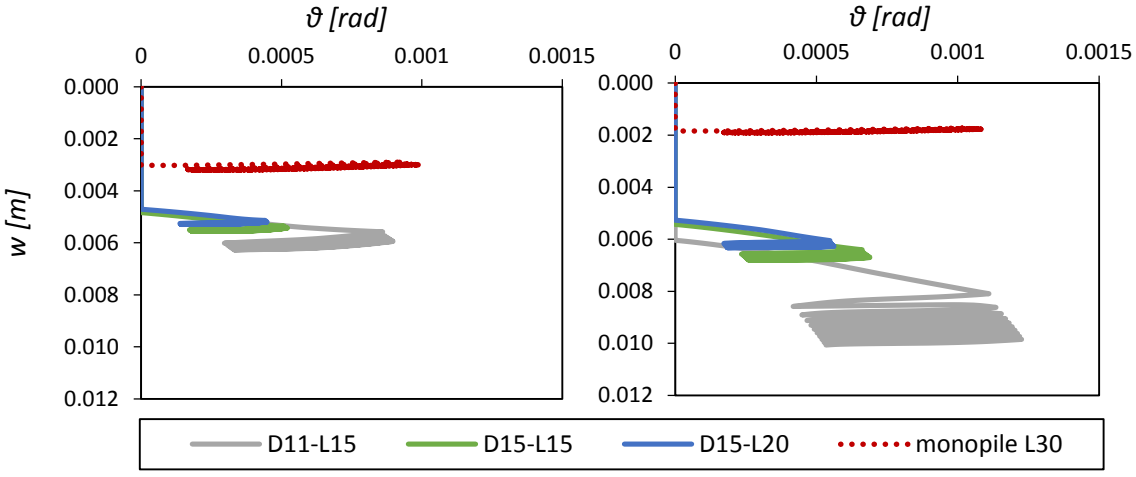

Figure 5.43. Wave cyclic settlement – rotation diagrams for the 2 MW wind turbine. Left: Homogeneous soil. Right: Inhomogeneous soil.

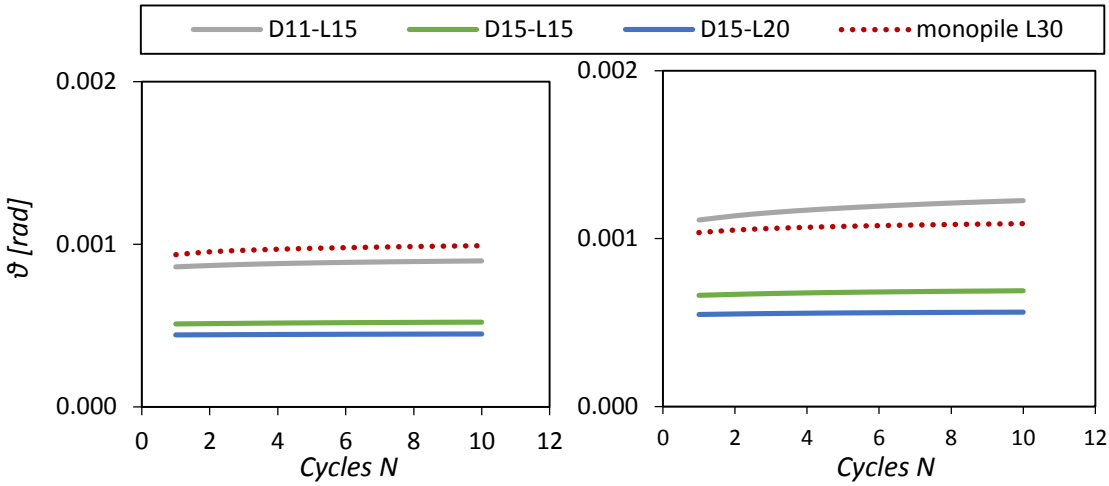

Figure 5.44. Accumulated rotations for the first 9 cycles of wave cyclic loading for the 2 MW wind turbine. Left: Homogeneous soil. Right: Inhomogeneous soil.

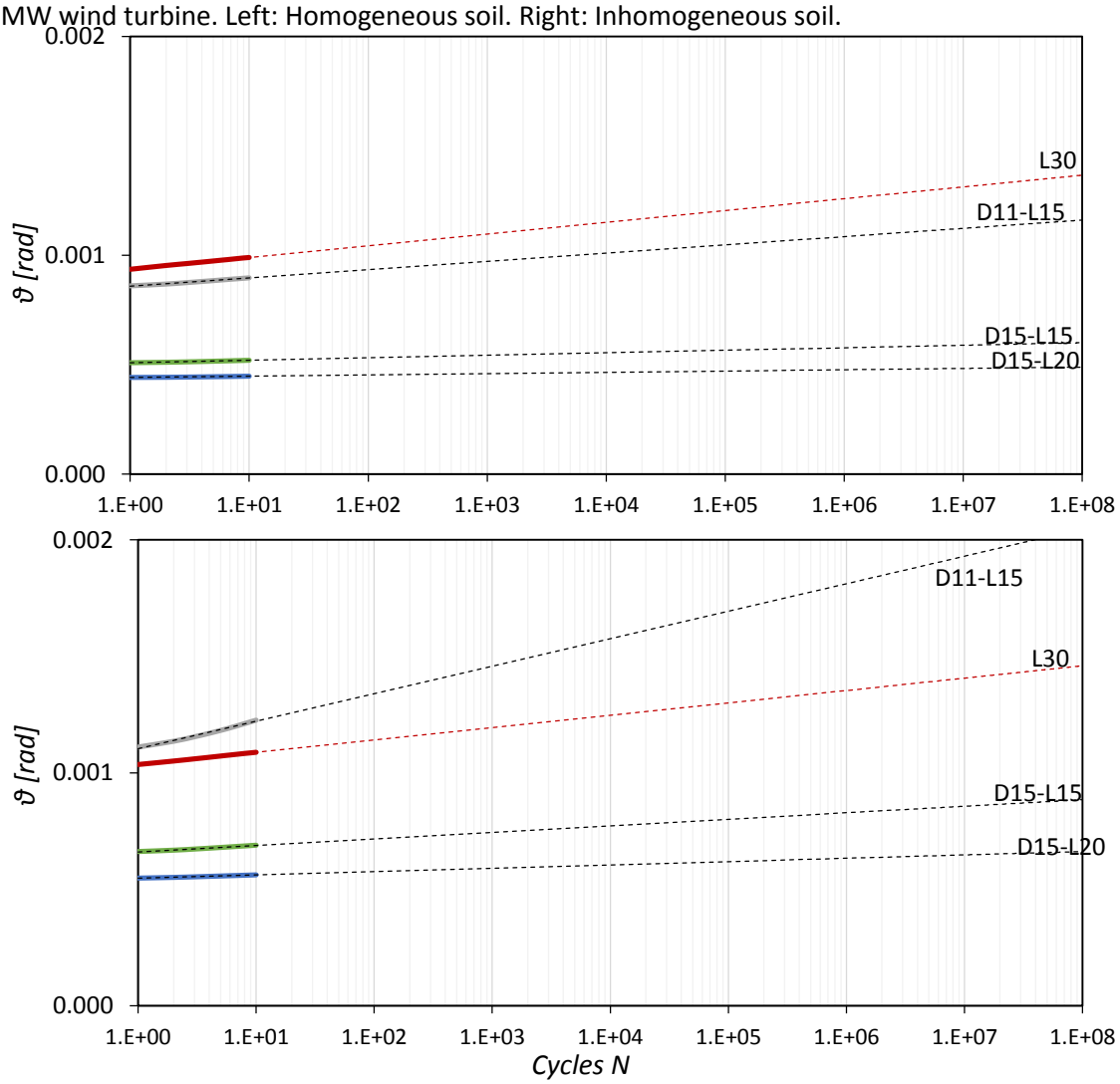

Figure 5.45. Accumulated rotations for the first 9 cycles of wave cyclic loading for the 2 MW wind turbine: Extrapolation with a logarithmic relationship to the lifetime of a wind turbine. Up: Homogeneous soil. Down: Inhomogeneous soil.

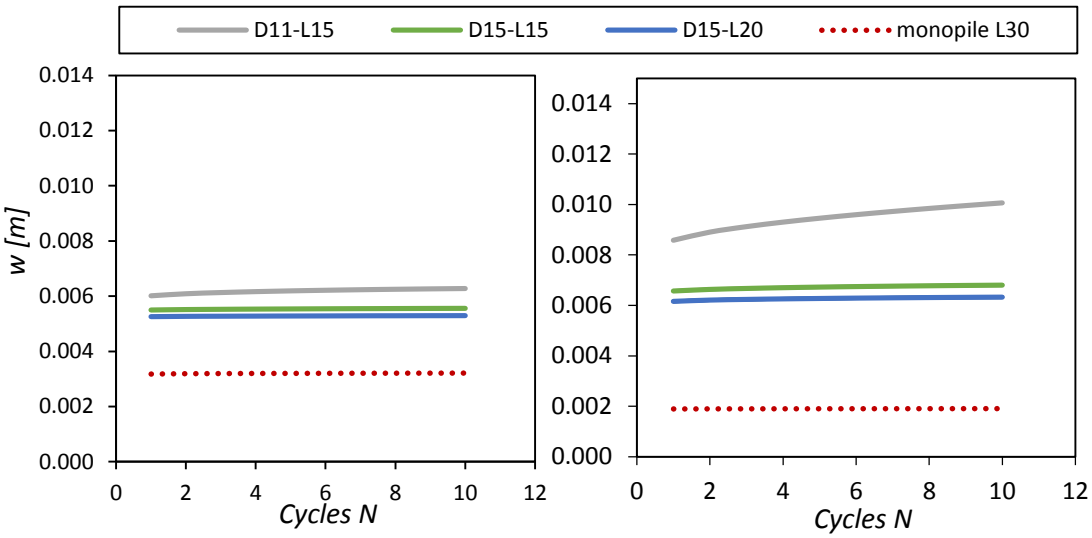

Figure 5.46. Accumulated settlements for the first 9 cycles of wave cyclic loading for the 2 MW wind turbine. Left: Homogeneous soil. Right: Inhomogeneous soil.

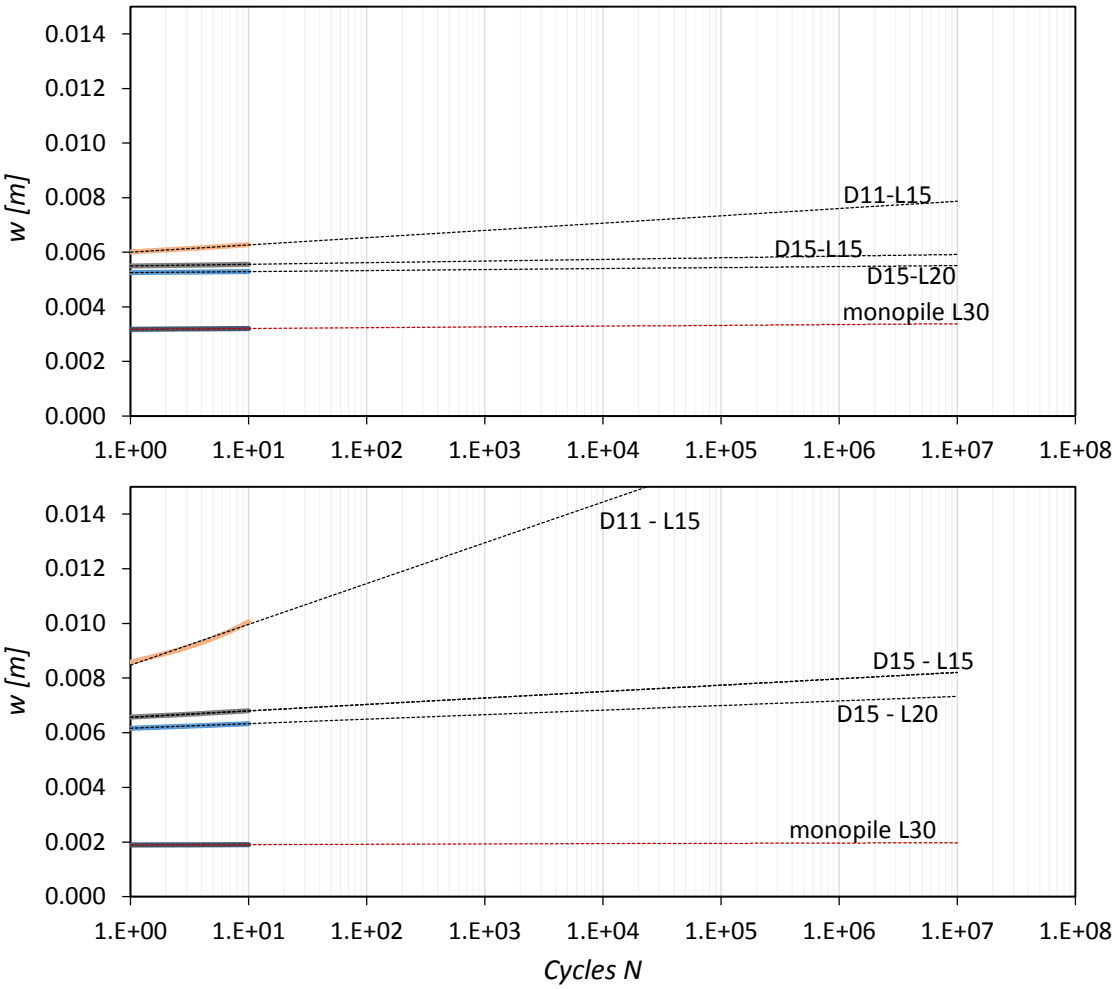

Figure 5.47. Accumulated settlements for the first 9 cycles of wave cyclic loading (2 MW wind turbine): Extrapolation with a logarithmic relationship to the lifetime of a wind turbine. Up: Homogeneous soil. Down: Inhomogeneous soil.

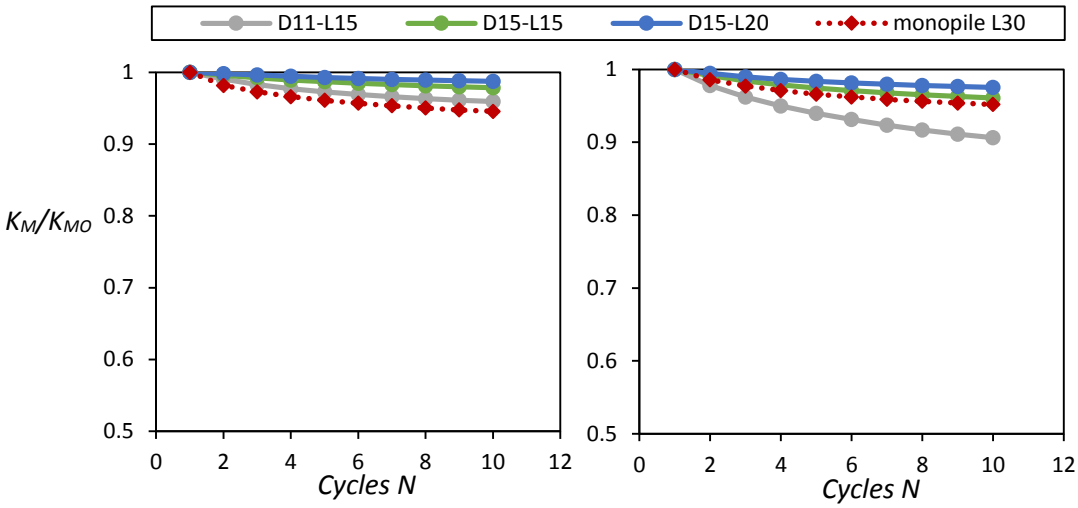

Figure 5.48. Stiffness degradation for the first 9 cycles of wave cyclic loading for a 2 MW wind turbine. Left: Homogeneous soil. Right: Inhomogeneous soil.

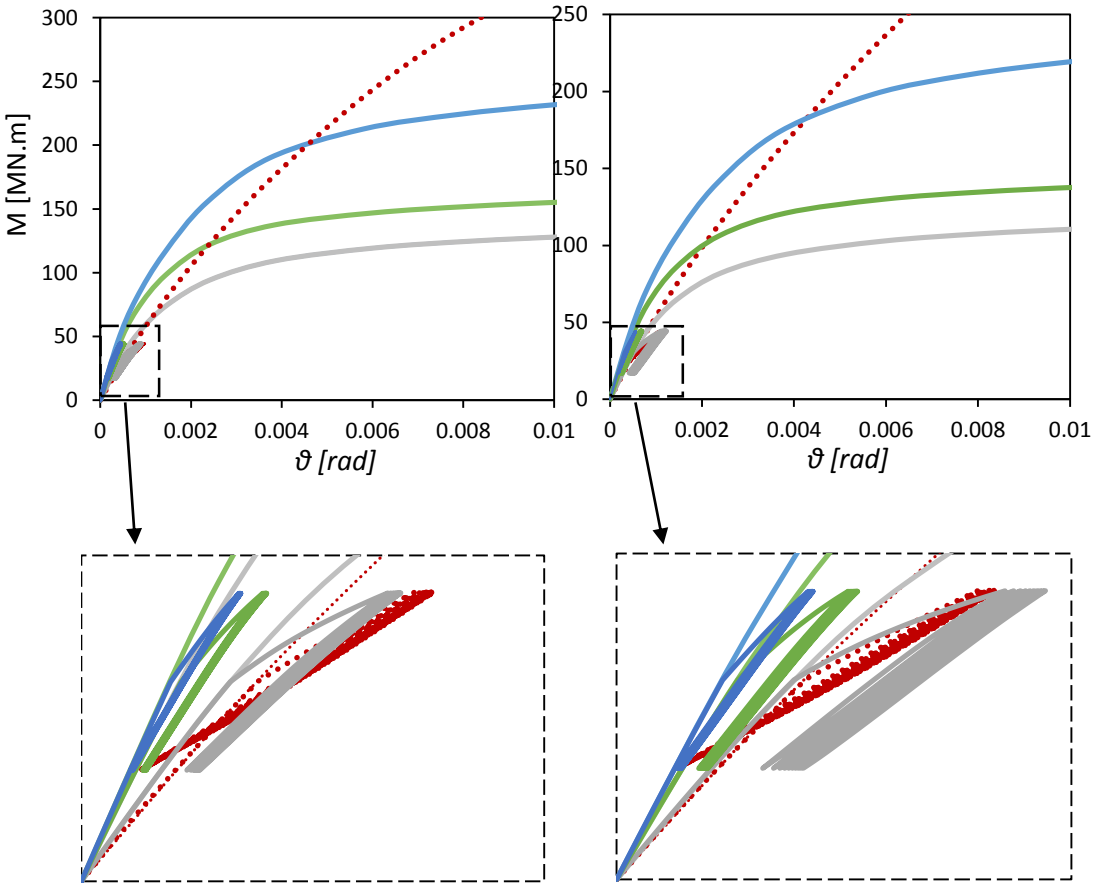

Figure 5.49. Wave cyclic and monotonic moment – rotation diagrams for the 2MW wind turbine. Left: Homogeneous soil. Right: Inhomogeneous soil.

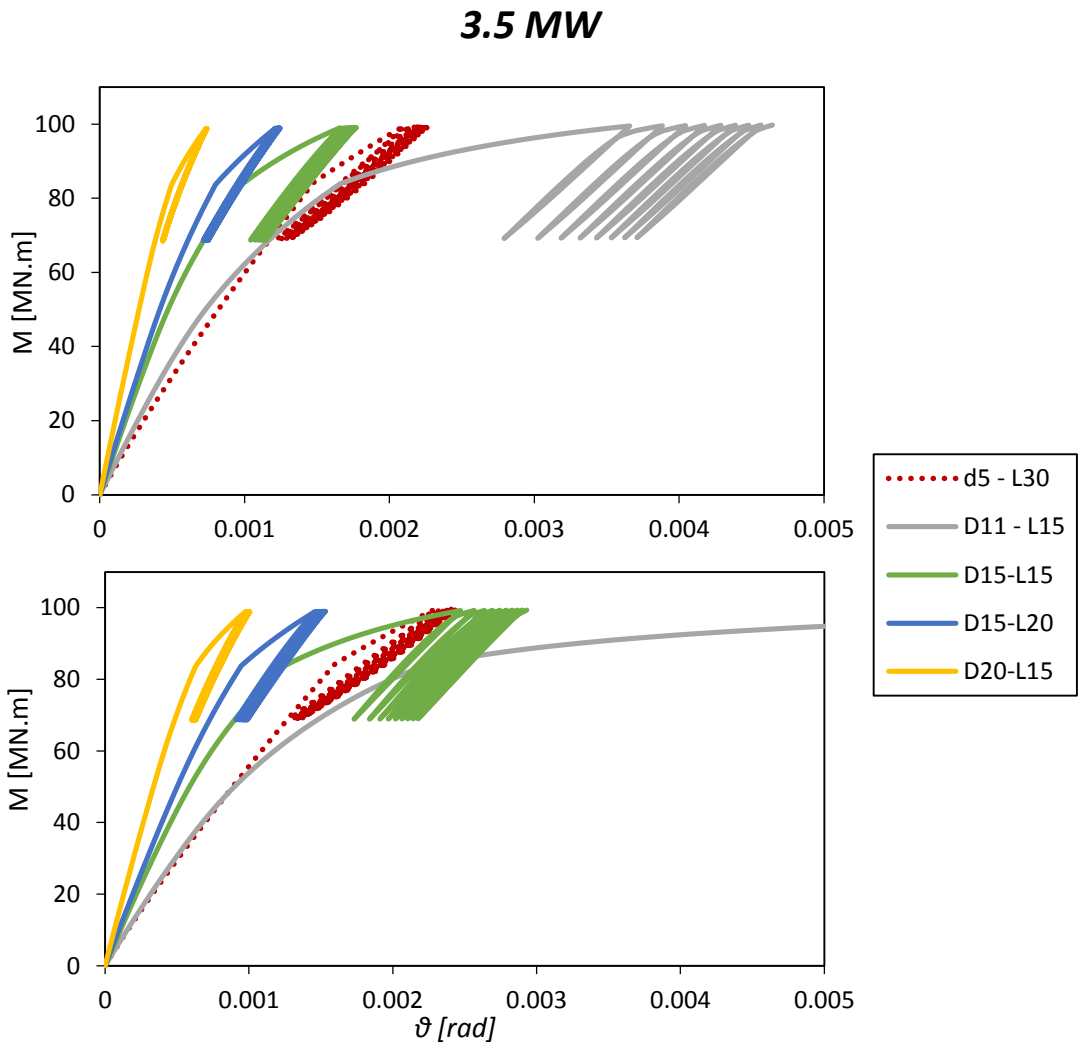

Figure 5.50. Wave cyclic moment – rotation diagrams for the 3.5 MW wind turbine. Up: Homogeneous soil. Down: Inhomogeneous soil.

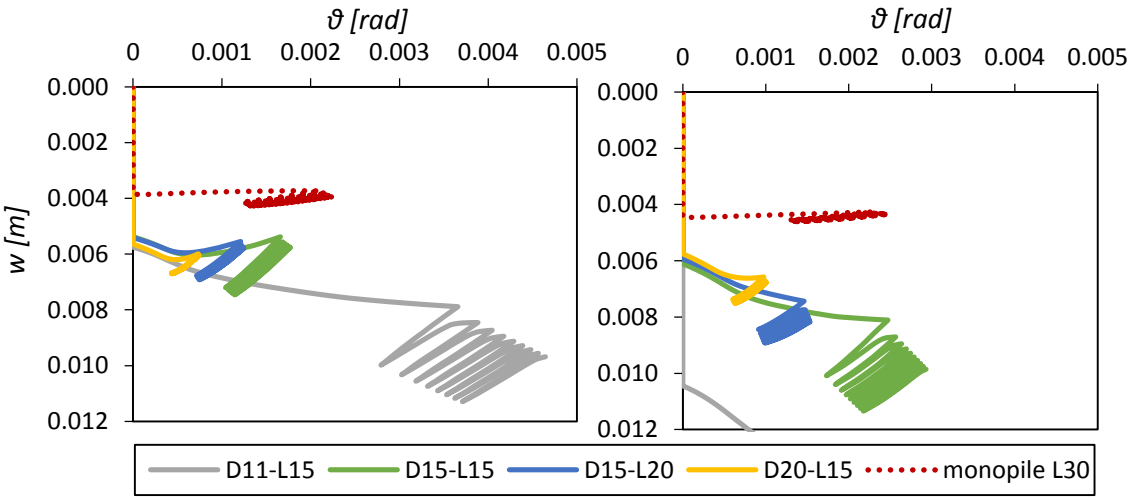

Figure 5.51. Wave cyclic settlement – rotation diagrams for the 3.5 MW wind turbine. Left: Homogeneous soil. Right: Inhomogeneous soil.

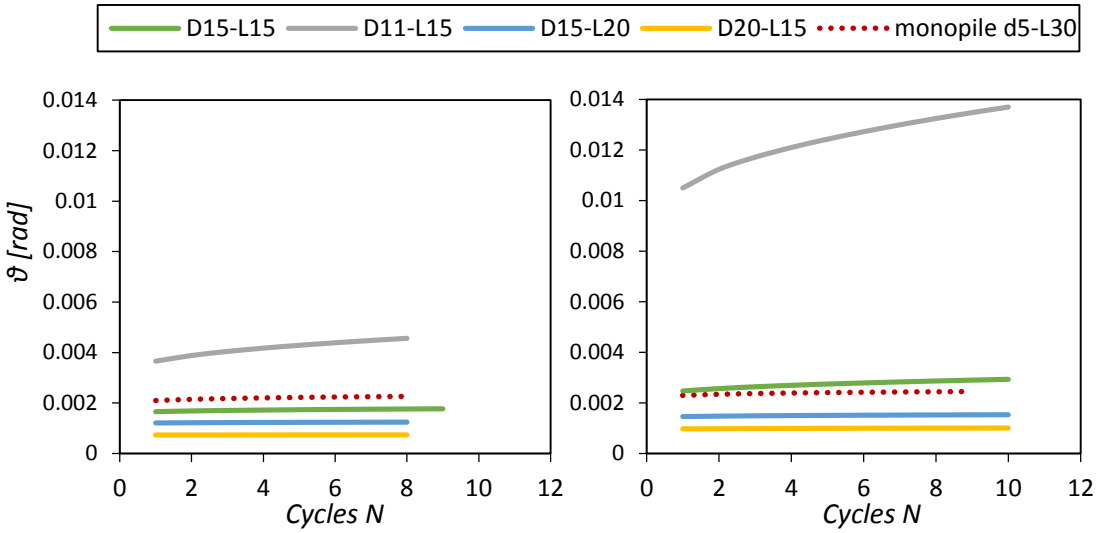

Figure 5.52. Accumulated rotations for the first 9 cycles of wave cyclic loading for the 3.5 MW wind turbine. Left: Homogeneous soil. Right: Inhomogeneous soil.

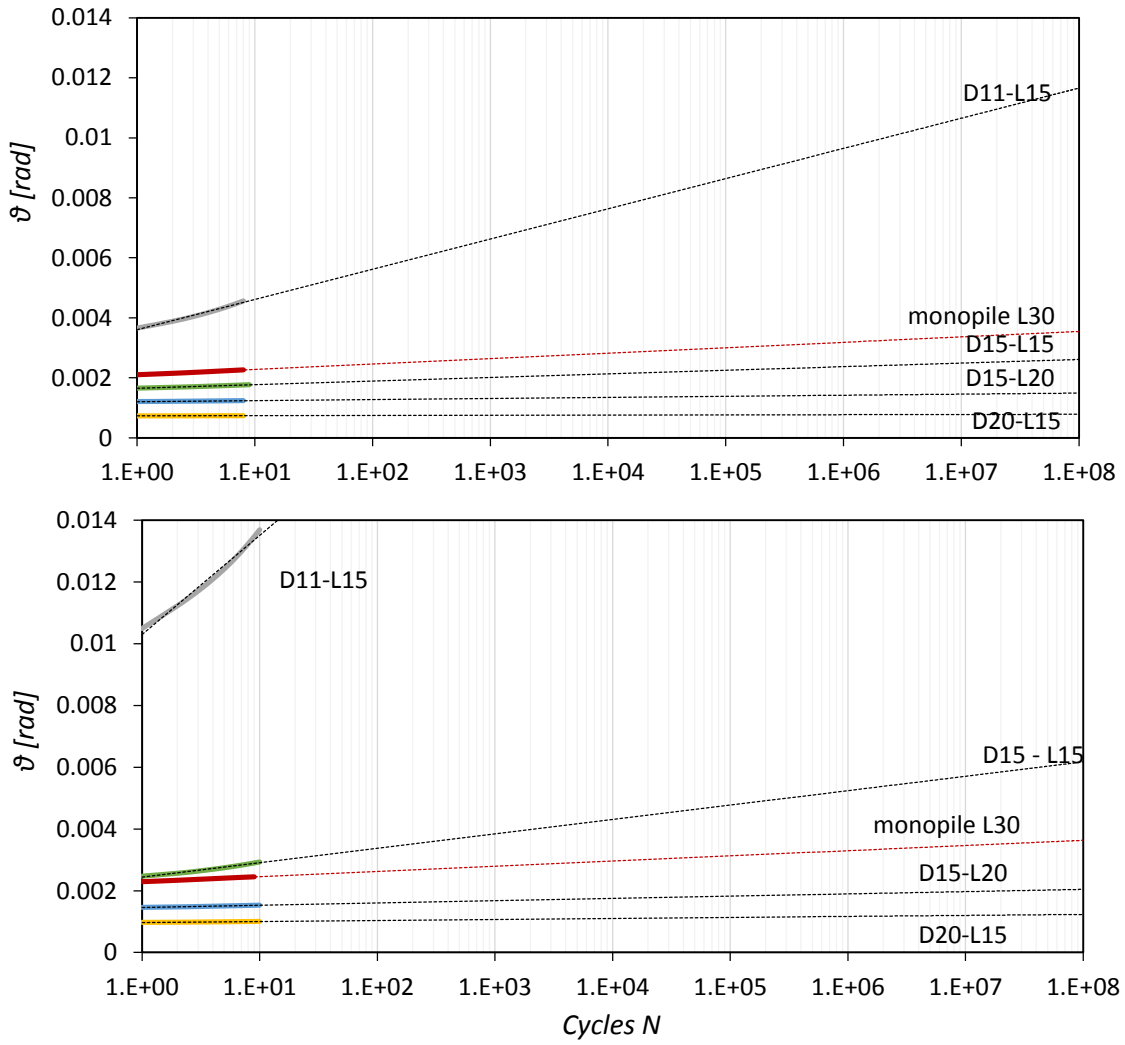

Figure 5.53. Accumulated rotations for the first 9 cycles of wave cyclic loading for the 3.5 MW wind turbine: Extrapolation with a logarithmic relationship to the lifetime of a wind turbine. Up: Homogeneous soil. Down: Inhomogeneous soil.

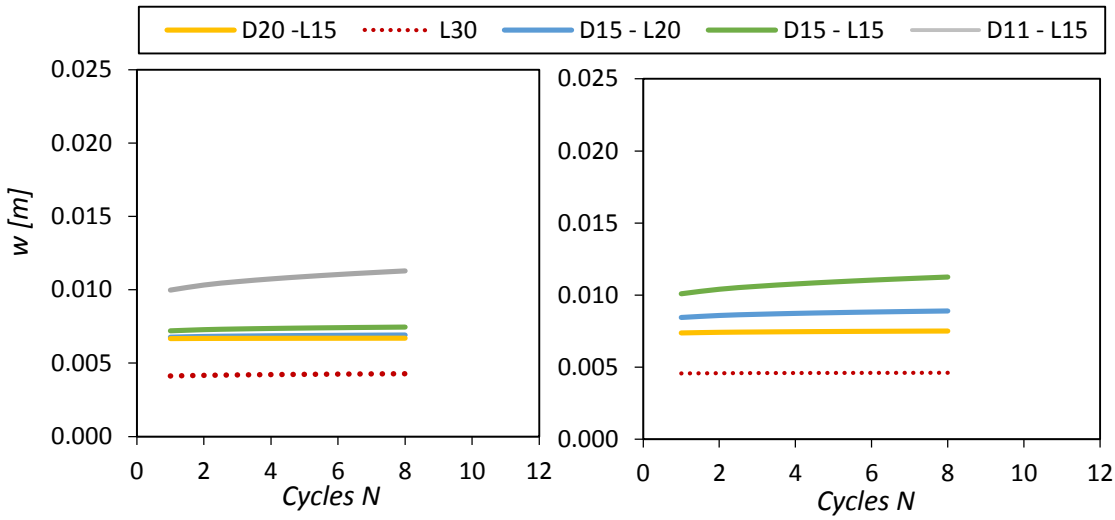

Figure 5.54. Accumulated settlements for the first 9 cycles of wave cyclic loading for the 3.5 MW wind turbine. Left: Homogeneous soil. Right: Inhomogeneous soil.

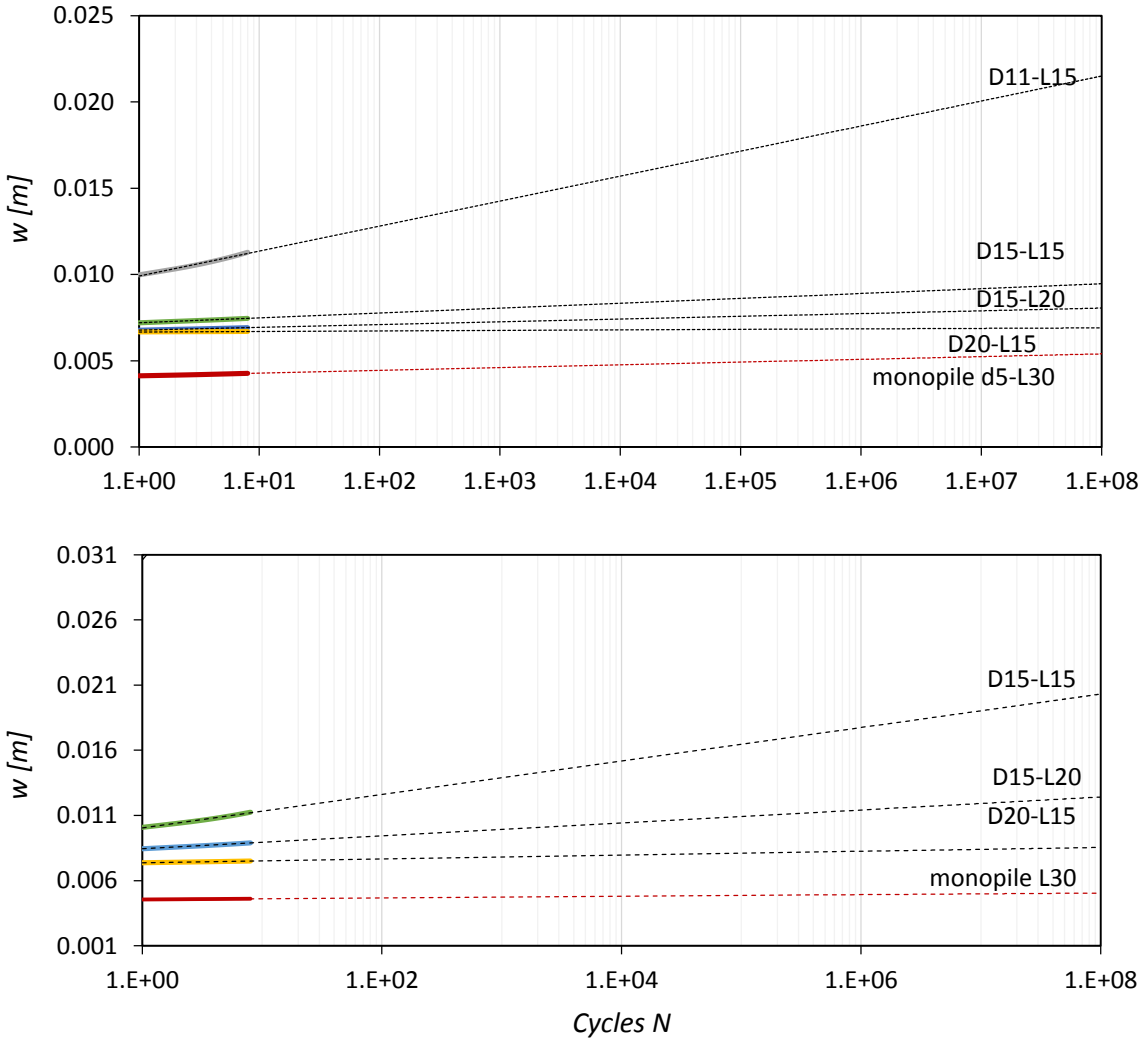

Figure 5.55. Accumulated settlements for the first 9 cycles of wave cyclic loading (3.5 MW wind turbine): Extrapolation with a logarithmic relationship to the lifetime of a wind turbine. Up: Homogeneous soil. Down: Inhomogeneous soil.

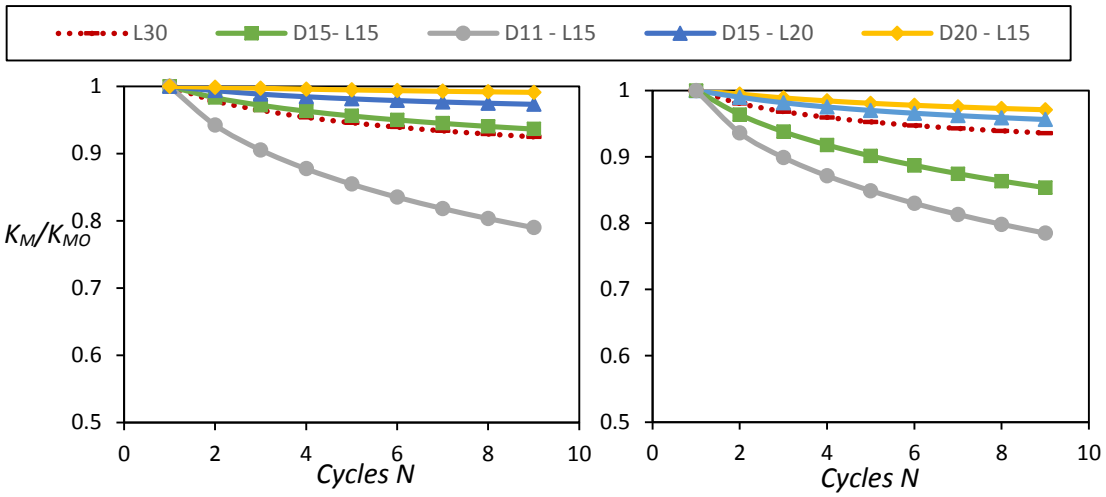

Figure 5.56. Stiffness degradation for the first 9 cycles of wave cyclic loading for a 3.5 MW wind turbine. Left: Homogeneous soil. Right: Inhomogeneous soil.

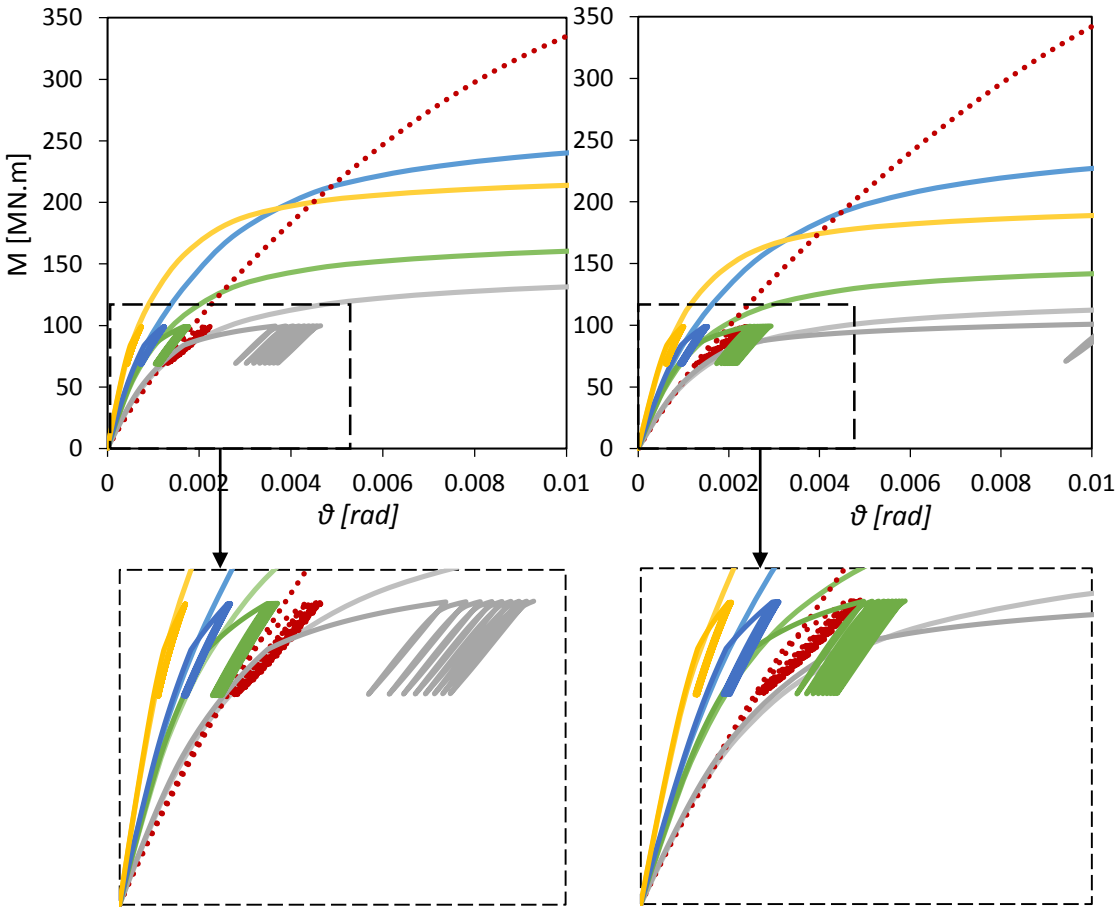

Figure 5.57. Wave cyclic and monotonic moment – rotation diagrams for the 3.5MW wind turbine. Left: Homogeneous soil. Right: Inhomogeneous soil.

5 MW

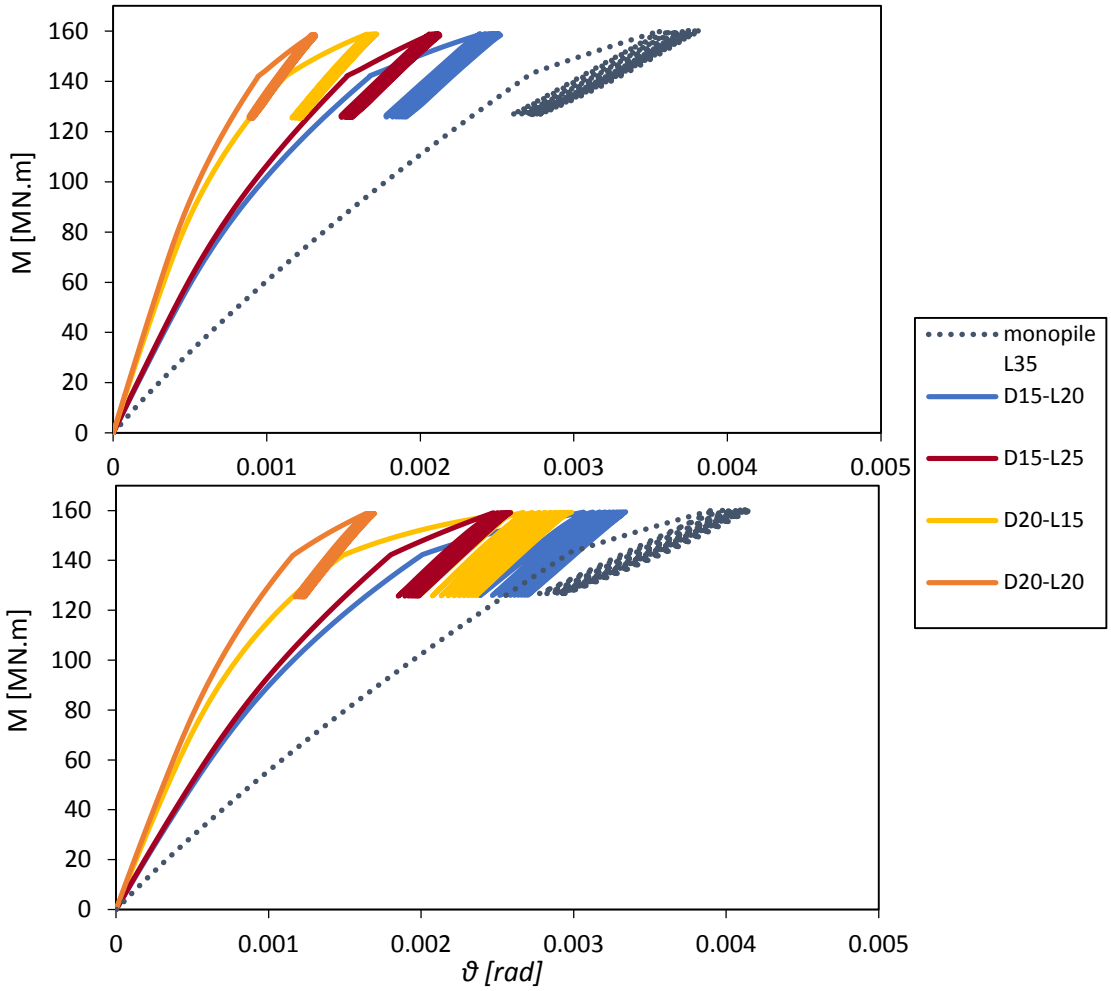

Figure 5.58. Wave cyclic moment – rotation diagrams for the 5 MW wind turbine. Up: Homogeneous soil. Down: Inhomogeneous soil.

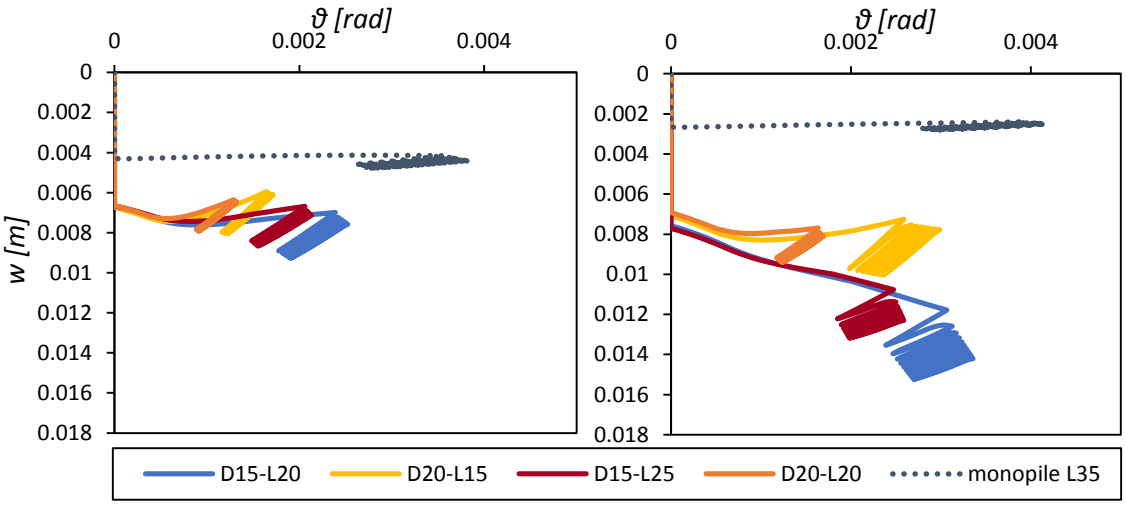

Figure 5.59. Wave cyclic settlement – rotation diagrams for the 5 MW wind turbine. Left: Homogeneous soil. Right: Inhomogeneous soil.

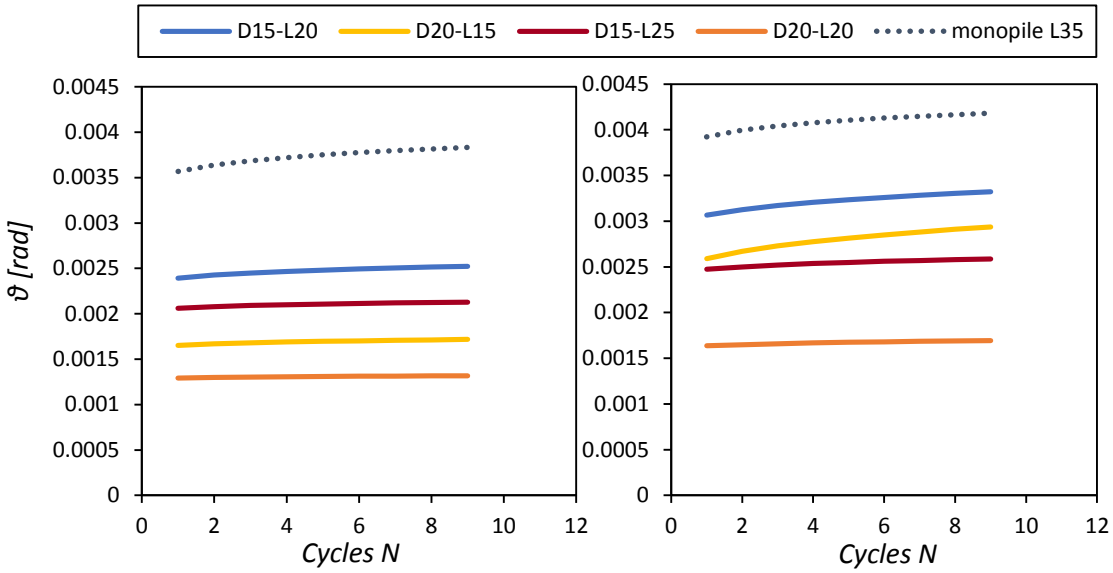

Figure 5.60. Accumulated rotations for the first 9 cycles of wave cyclic loading for the 5 MW wind turbine. Left: Homogeneous soil. Right: Inhomogeneous soil.

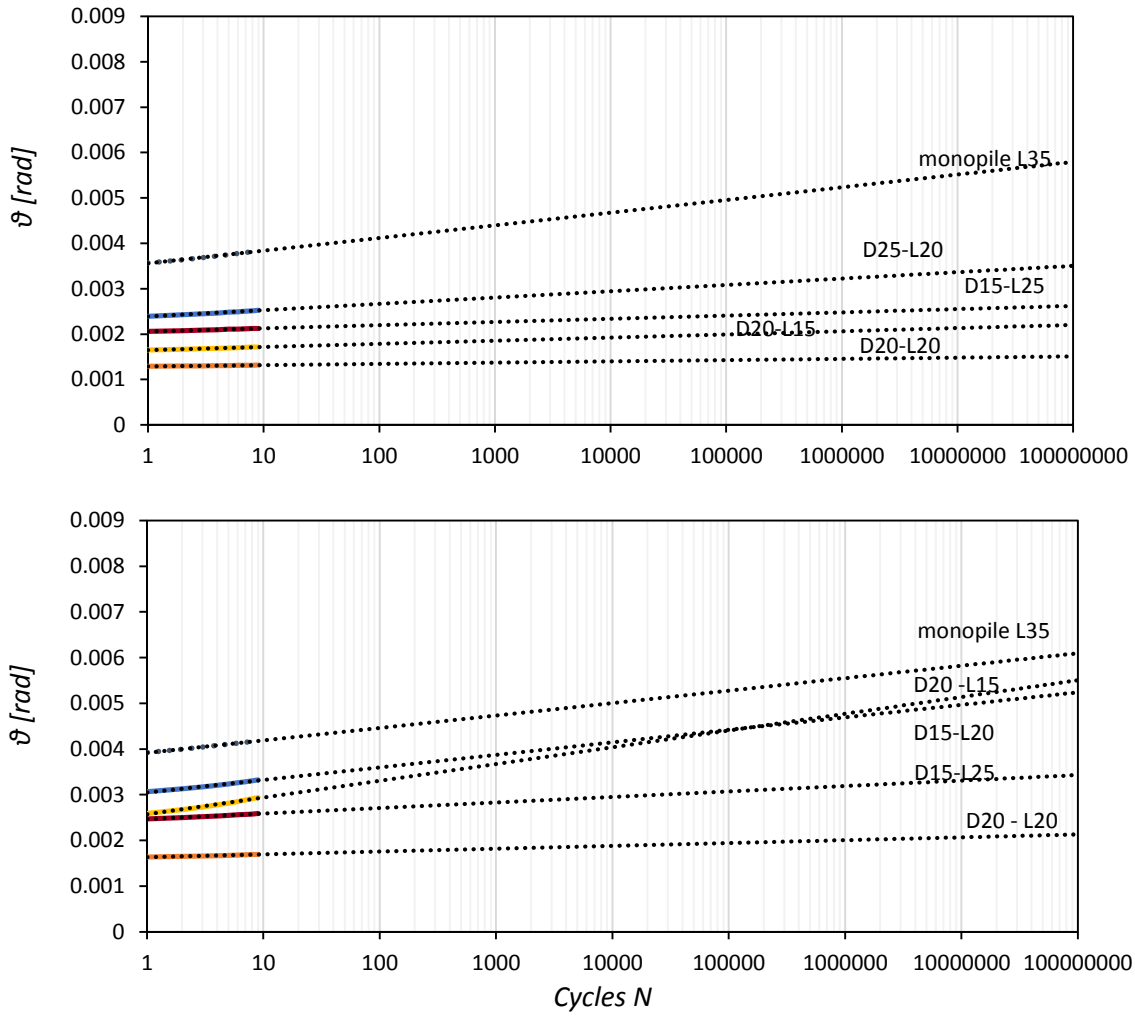

Figure 5.61. Accumulated rotations for the first 9 cycles of wave cyclic loading for the 5 MW wind turbine: Extrapolation with a logarithmic relationship to the lifetime of a wind turbine. Up: Homogeneous soil. Down: Inhomogeneous soil.

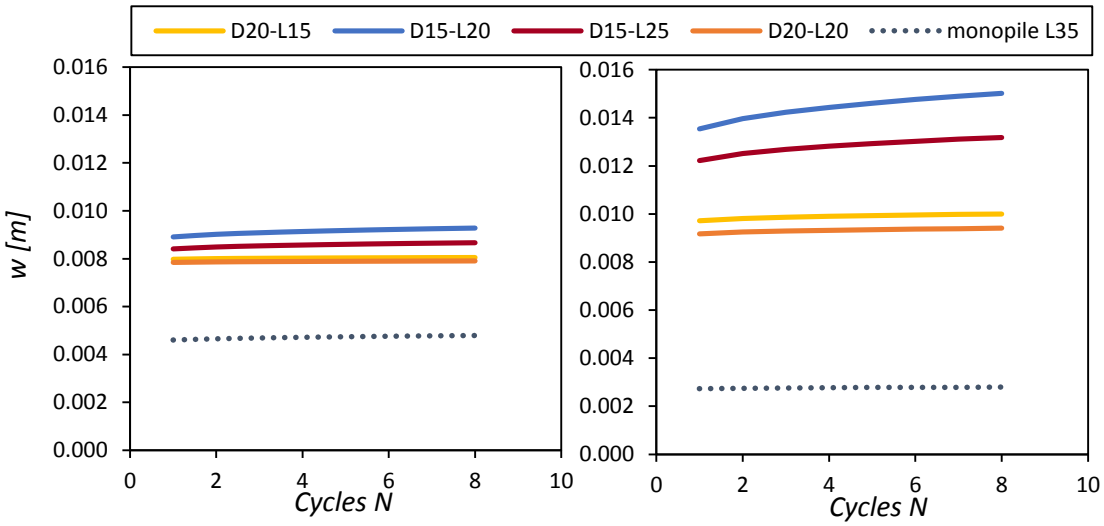

Figure 5.62. Accumulated settlements for the first 9 cycles of wave cyclic loading for the 5 MW wind turbine. Left: Homogeneous soil. Right: Inhomogeneous soil.

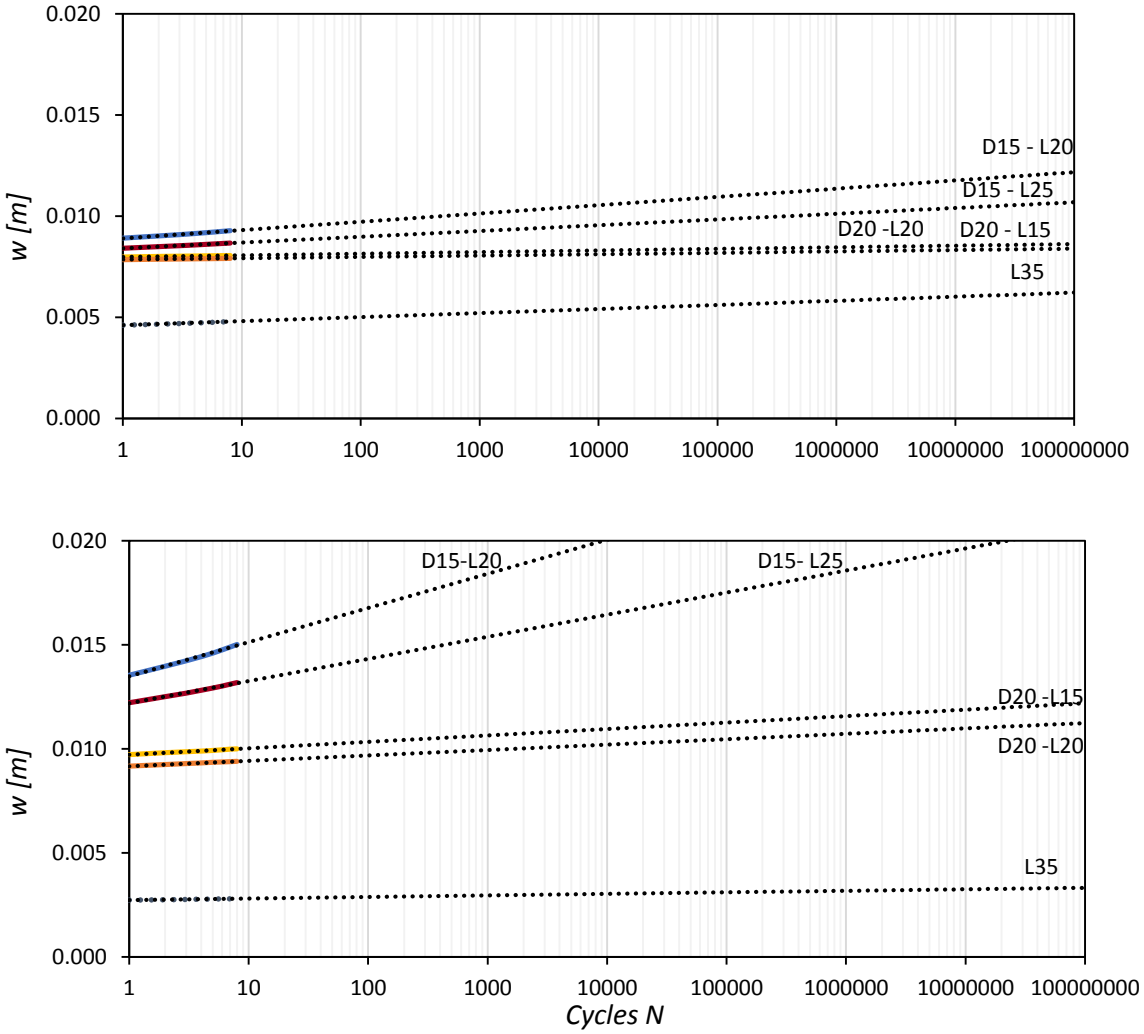

Figure 5.63. Accumulated settlements for the first 9 cycles of wave cyclic loading (5 MW wind turbine): Extrapolation with a logarithmic relationship to the lifetime of a wind turbine. Up: Homogeneous soil. Down: Inhomogeneous soil.

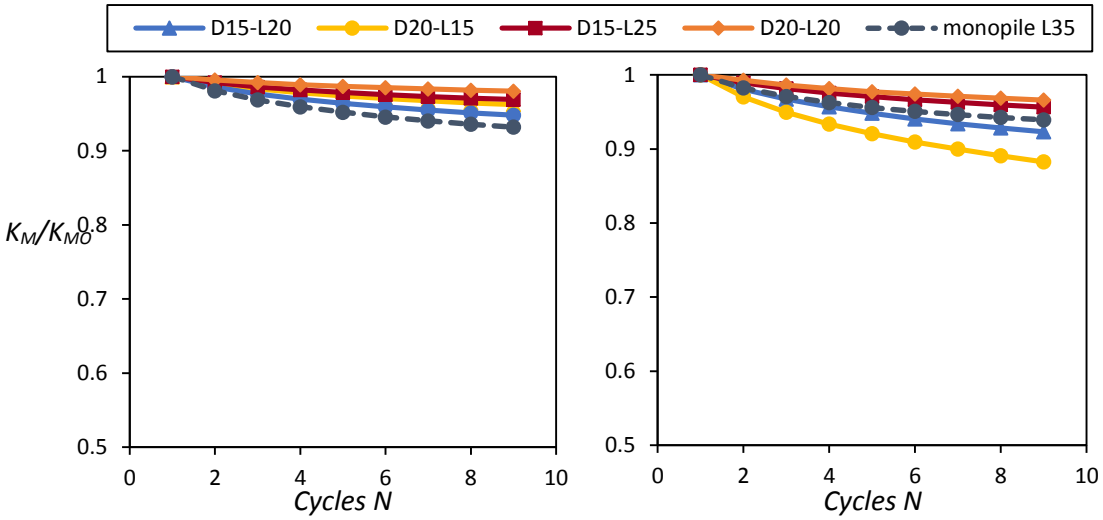

Figure 5.64. Stiffness degradation for the first 9 cycles of wave cyclic loading for a 5 MW wind turbine. Left: Homogeneous soil. Right: Inhomogeneous soil.

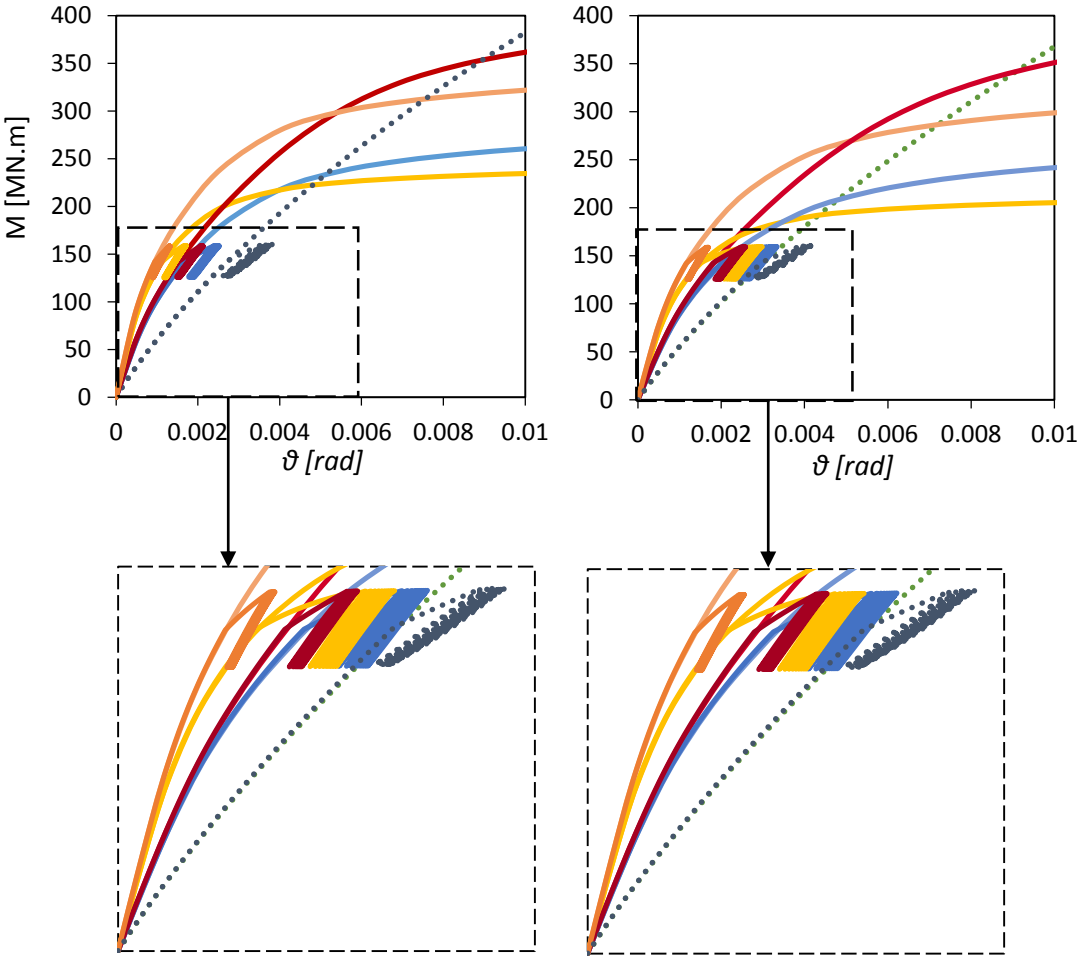

Figure 5.65. Wave cyclic and monotonic moment – rotation diagrams for the 5MW wind turbine. Left: Homogeneous soil. Right: Inhomogeneous soil.

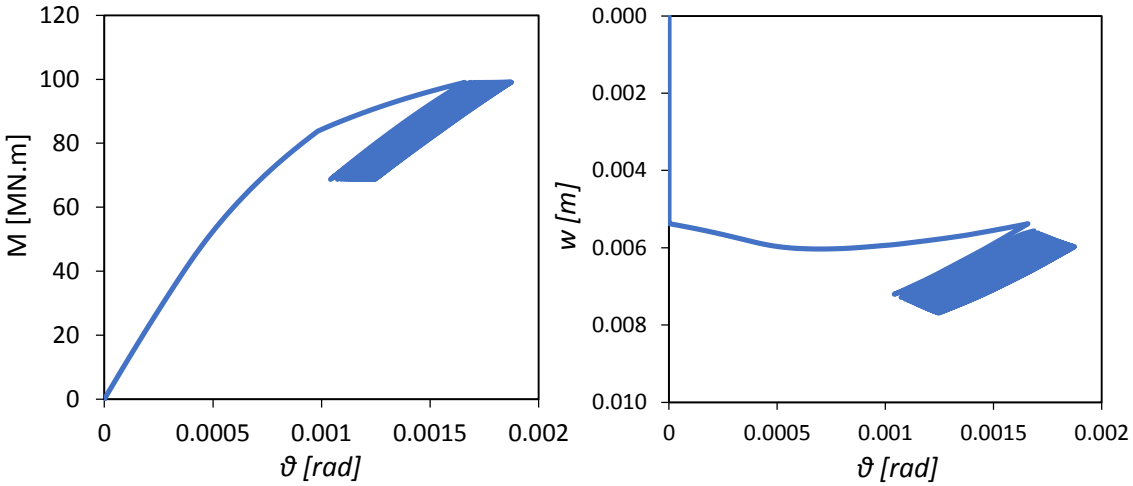

Figure 5.66. Effect of many cycles on the D 15 - L 15 foundation of a 3.5 MW wind turbine on homogeneous soil. Left: Moment – rotation curve. Right: Settlement -rotation curve.

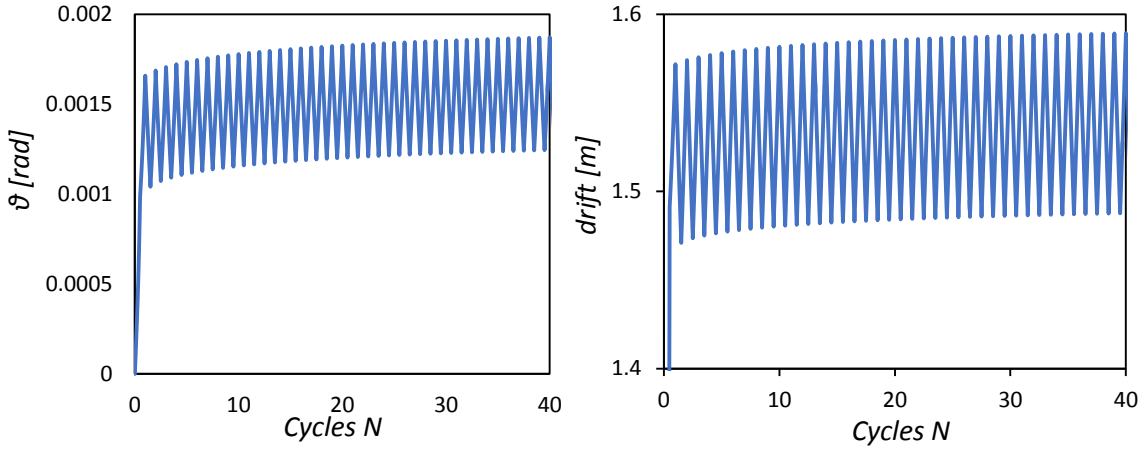

Figure 5.67. Effect of many cycles on the D 15 - L 15 foundation of a 3.5 MW wind turbine on homogeneous soil. Left: Rotation against cycles of loading. Right Tower head drift against cycles of loading.

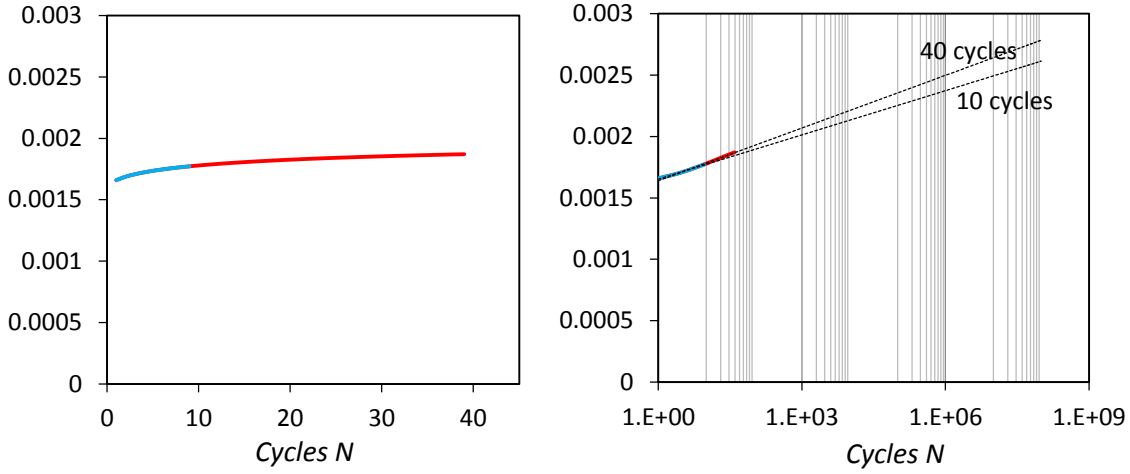

Figure 5.68. Effect of many cycles on the D 15 - L 15 foundation of a 3.5 MW wind turbine on homogeneous soil. Left: Accumulated rotation against cycles of loading. Right: Effect of many cycles in the logarithmic prediction of the accumulated rotation to the end of the turbine's life cycle.

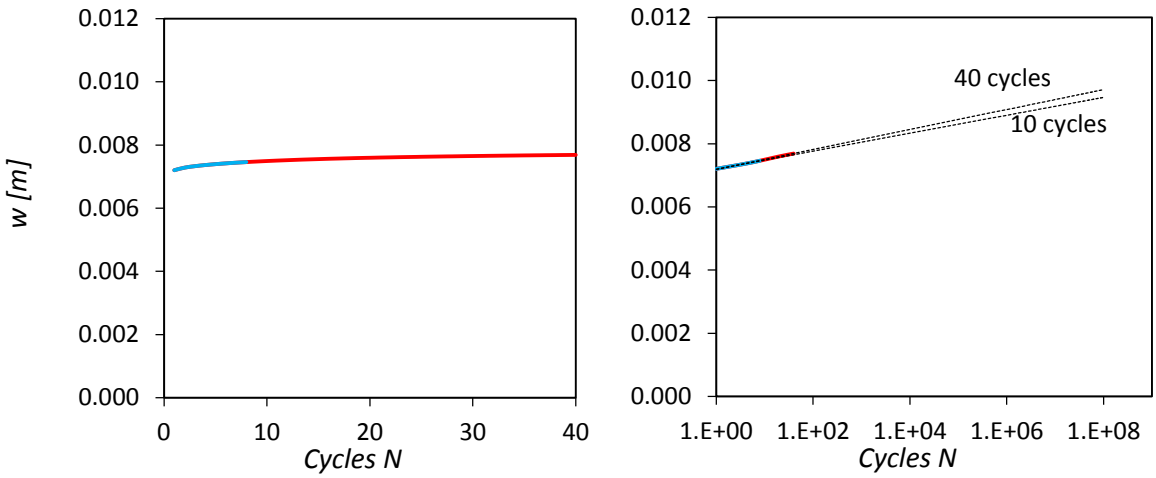

Figure 5.69. Effect of many cycles on the D 15 - L 15 foundation of a 3.5 MW wind turbine on homogeneous soil. Left: Accumulated settlement against cycles of loading. Right: Effect of many cycles in the logarithmic prediction of the accumulated settlement to the end of the turbine's life cycle.

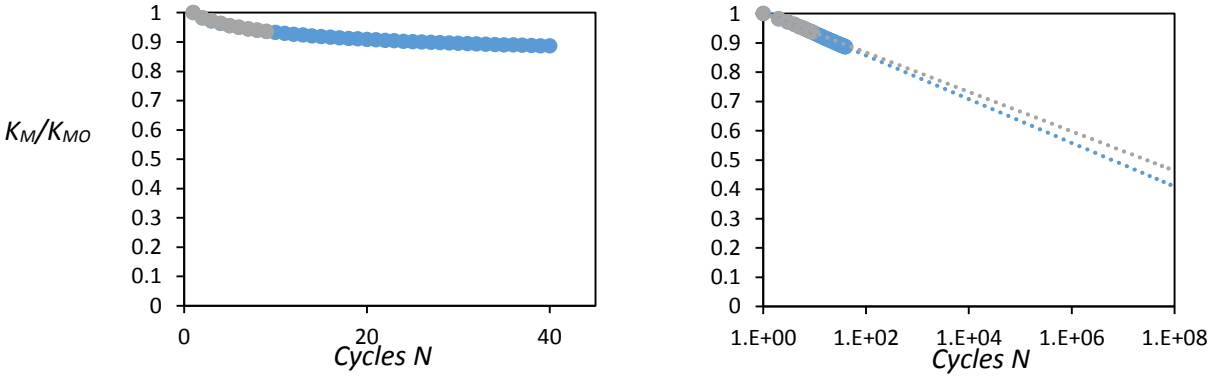

Figure 5.70. Effect of many cycles on the D 15 - L 15 foundation of a 3.5 MW wind turbine on homogeneous soil. Left: Accumulated settlement against cycles of loading. Right: Effect of many cycles in the logarithmic prediction of the accumulated settlement to the end of the turbine's life cycle.

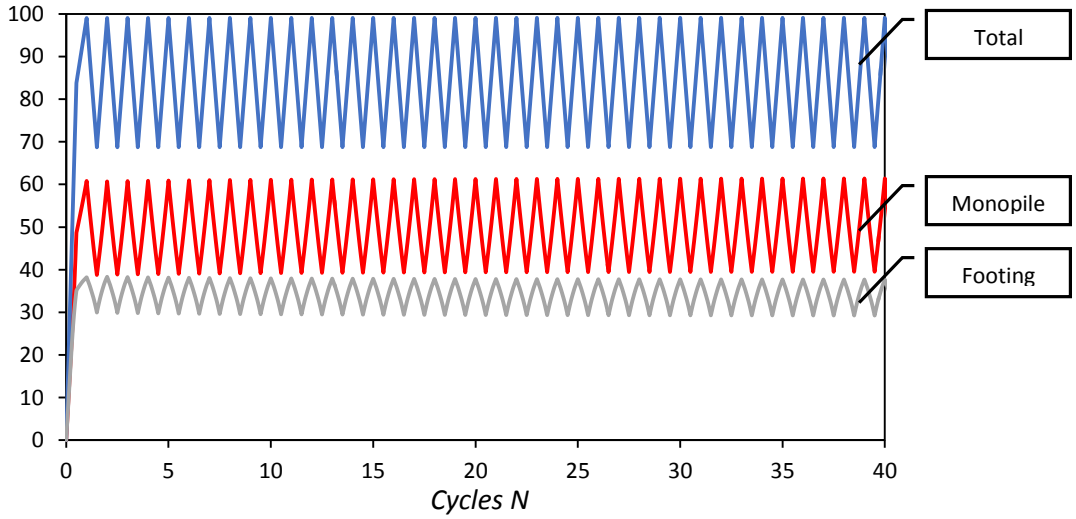

Figure 5.71. Response of the components of the D15 – L15 hybrid foundation in terms of moment against cycles of loading. (3.5 MW wind turbine on homogeneous soil).

CHAPTER 6

Seismic Response of Hybrid Foundations

6.1 Prologue
6.2 Modal Analysis
6.3 Seismic Evaluation Against the Takatori_090 Motion
6.4 Conclusions

6.1 Prologue

So far, the performance of hybrid foundations has been evaluated against static loading. Even cyclic loads such as wind and waves have been imposed in a static manner, assuming that their excitation frequencies are not capable of causing resonant response. This does not hold true for seismic events which have an intensively dynamic and kinematic nature, thus dynamic analysis of the problem is inevitable.

An important aspect of systems exposed to dynamic loads is the determination of their natural frequencies. Therefore, the first and second natural frequencies of three wind turbines of nominal capacity 2 MW, 3.5 MW and 5 MW are extracted in the first sub – section of this chapter, assuming a fixed base for the turbine towers. The effect of soil – structure interaction is also taken into consideration for a 3.5 MW turbine laying on several hybrid foundations and a monopile.

Moving on, the performance of two hybrid foundations is compared against a 30 m monopile for the case of a 3.5 MW offshore wind turbine. The earthquake record used as an input motion is the Takatori_090 seismic record, one of the most adverse motions ever recorded. The choice of this seismic record is made in order to compare the performance of hybrid foundations to the conventional 30 m monopile against an extreme seismic event, not the typical design earthquake. Note that the point of reference for this chapter is taken at the mud line (x,y,z) = (0,0,0).

6.2 Modal Analysis

The first two modes of oscillation for the wind turbines examined are presented in **figure 6.1**, along with their corresponding natural frequencies and periods. Fixed base conditions are considered, in order to get a first estimation and also validate the model through the use of expression 1.1 from the literature. As can be seen, the eigenfrequencies are quite larger for the 2 MW wind turbine than for the remaining two. This can be attributed to the fact that the 2 MW turbine is shorter and stiffer than the other two, which are taller and more flexible. The first natural frequency is also calculated using the expression Van Der Tempel (2005) proposed and the results are presented in **table 6.1**; the results from this study compare quite well with the expression from the literature, as the deviation does not exceed 4.5 % in any of the cases. Lekkakis (2012) has shown that using more accurate shell elements to model the tower does not lead to deviations larger than 0.2% compared to the simple beam model utilized here.

The effect of soil – structure interaction on the first natural frequency is examined for the 3.5 MW wind turbine. In order to calculate the eigenmodes, the soil is modelled as linear elastic. The first eigenmode has been extracted for various hybrid foundations and a monopile. As shown in **table 6.2**, the hybrid foundation with the largest footing (D20 – L15) has the largest first natural frequency (0.257 Hz); this is logical if we take into consideration the results from chapter 4, in which this system was found to have the largest rocking and swaying stiffness. The 30 m monopile demonstrates the softest response and in this case the natural frequency

is the smallest (0.241 Hz). Generally, it is evident that the effect of soil – structure interaction causes a slight decrease in the first natural frequency of the system, compared to fixed base conditions. As pointed out in chapter 1, this decrease can cause wave resonance problems if the system is designed in the "soft – soft" response area.

6.3 Seismic Evaluation Against the Takatori_090 Motion

6.3.1 Definition of the Seismic Problem and Model Properties

As aforementioned, this chapter deals with the evaluation of two hybrid foundations and a 30 m monopile against the Takatori earthquake. The seismic problem is schematically illustrated in **figure 6.3**. Concerning the hybrid foundations, the length of the pile is kept constant at 15 m and two different footings are examined with diameters of 15 and 20 m. As observed in the previous chapters, the D15 – L15 hybrid system is a rather un – conservative foundation solution for a 3.5 MW wind turbine, which barely satisfies the performance criteria, especially when it comes to moment bearing capacity. On the other hand, the D20 – L15 hybrid system is proven to be a very adequate choice, especially in terms of rocking stiffness and limitation of rotations. Finally, the 30 m monopile is considered a conventional foundation solution for such a wind turbine and is once again used as benchmark.

Due to the dynamic nature of the problem, the model used in the previous chapters needs to be slightly modified. Specifically, the peripheral boundary conditions have been removed, in order to avoid amplification due to waves reflecting off the boundaries. In an attempt to model the soil body as a shear beam, all the peripheral nodes at each height z are tied together to a central node at the same height, as illustrated in **figure 6.4**. Other than that, the homogeneous cohesive soil stratum has the same properties as in the previous chapters: an undrained shear strength equal to S_u = 60 kPa and an elastic modulus E = 1800S_u. The Von – Mises failure criterion is used to capture the plastic response of the soil, along with an associative plastic flow rule and combined hardening, as described in chapter 2. Damping of the soil is taken ξ = 2% and for the steel damping is taken ξ = 5%.

In reality, a seismic event will occur during the turbine's operational lifetime so becomes clear that wind and wave forces will also be acting on the turbine. The exact interaction between the two types of loading is hard to determine and a simplified approach is adopted in this study. Two seismic load cases are considered. In the first load case, the earthquake acceleration is imposed on the uncharged superstructure; thus, a preliminary estimation of the "net" effect of the earthquake on each foundation can be made. In the second load case an attempt is made to capture the effect of seismic excitation after some stiffness degradation has already occurred, due to cyclic wave and monotonic wind loading. Therefore, before applying the input seismic motion, a monotonic wind load and 10 cycles of wave loading are applied to the superstructure, in a similar manner to the cyclic wave loading scenario of chapter 5. To make things worse, the earthquake is imposed when the tower head still experiences a large deflection due to wind and wave forces and not when the tower is at its point of equilibrium (P – δ effects are taken into account for all the analyses of this chapter). It is made clear from the above that the examined load cases represent two extreme

circumstances; given that the Takatori motion is one of the most unfavorable records, it is pointed out once again that the seismic problem is approached in a quite exaggerated manner in this study.

6.3.2 The Takatori_090 Record

In order to evaluate the seismic performance of hybrid foundations and compare them to the monopile, the Takatori_090 record is used as an input seismic motion. The acceleration time series is presented in **figure 6.5**. A large number of high amplitude and high frequency cycles can be observed during the first 5 seconds of the motion. Just after the fifth second, a distinctive high amplitude sinusoid pulse with a larger period is also present. A few more high amplitude and high frequency pulses follow and then the amplitude is significantly decreased for the rest of the record. The dominant periods of this seismic excitation are estimated to be 0.3 – 0.5 sec for the high frequency pulses and 1.2 sec for the distinctive sinusoid pulse. As mentioned before, this is one of the most devastating seismic events ever recorded.

The elastic acceleration spectra at the base of the model (rock) and the soil surface are presented in **figure 6.6**, for two damping ratios of $\xi = 2\%$ and $\xi = 5\%$. Concerning the spectrum at the base, three peaks with very high amplification can be observed; the first two are realized in the small period domain, where $T < 0.5$ sec, and correspond to the high frequency cycles described above. The third large peak of the spectrum has a period of 1.25 sec and corresponds to the distinctive sinusoid pulse (5 – 7.5 sec of the record). The effect of the soil stratum is damping for the largest part of periods, except for $T = 0.5$ sec, where an amplification can be observed. It seems like the second peak of the spectrum is forced to move to a slightly larger period (from 0.4 to 0.5 sec), due to wave propagation into the clay stratum.

Since the superstructure is modelled as linear – elastic, its response can be estimated through the elastic acceleration spectrum at the soil surface of **figure 6.6** ($\xi = 2\%$). As discussed in the previous subsection, the 3.5 MW wind turbine which is examined here has a first natural period of $T_1 = 3.84$ sec and second natural period of $T_2 = 0.35$ sec. The modal shapes are presented in **figure 6.1**. Based on the above, the second mode of the tower is expected to be excited by the Takatori_090 record. The tower is quite flexible with a large first natural period which is not expected to be excited by earthquakes. Yielding behavior of the soil and interface non – linearities which are taken into account in the analyses do not allow the use of elastic spectra and eigenfrequencies to estimate the response of the whole soil – foundation – superstructure system.

6.3.3 Seismic Excitation Without Action of Wind and Waves

The first seismic load case considered consists of the earthquake motion being applied to the uncharged system. This is a rather unrealistic case because the offshore wind turbine will always be subjected to wind and wave forces during its operational lifetime. However, this simplified approach can provide useful information on the “net” effect of the earthquake to

each foundation type; in this way, the complex interaction between the seismic motion and loading due to wind and waves can become more comprehensible.

To begin with, the acceleration time history at the foundation lid can be seen in **figure 6.6 (top)**. The green line corresponds to the D15 – L15 foundation lid (z = -2m) while the dotted red line corresponds to the monopile's head (z = 0). There seems to be no significant difference between the two lines. As a matter of fact, the time history is similar to the original input motion, only slightly modified due to the interference of the clay stratum. After the end of the input motion (t = 25 sec), the soil experiences free oscillation which does not appear to undergo significant damping for at least 3 more seconds.

The acceleration time history at the head of the tower is presented in **figure 6.6 (bottom)**. The resulting acceleration seems to be a combination of a high frequency component which is possibly caused by resonance of the tower's second mode of oscillation, and a lower frequency sinusoid response. The general response is the same for the two foundation types, however the footing seems to limit the magnitude of acceleration experienced by the superstructure, possibly due to its rocking response and its small size which allows bearing capacity mechanisms of the soil to be mobilized. The above information is summarized into **figure 6.7**, which depicts the elastic acceleration spectra at the foundation lid (left) and tower head (right). It is obvious from the spectrum at the tower head that the second mode of the tower is heavily excited, as expected. The peak of the spectrum is observed for a natural period of T = 0.35 sec which corresponds exactly to the second natural period of the tower. Another important observation is that the tower which is founded on the monopile experiences a 33% larger spectral acceleration than the tower founded on the hybrid foundation.

Bending moment at the base of the tower due to seismic excitation is presented in **figure 6.8 (top)** for the three foundations examined. The high frequency content of the time series derives from resonance of the second mode, as previously discussed. The magnitude of moment is approximately the same for all three foundations, however the hybrid systems seem to initiate damping earlier than the monopile. The maximum instantaneous moment demand of the Takatori_090 earthquake is approximately 40 – 50 MNm, about 1/3 of the lowest moment capacity which is exhibited by the D15 – L15 hybrid foundation.

As discussed in the previous chapter, the most important design criterion for offshore wind turbine foundations is limitation of rotations. Time history of rotation at the base of each tower is plotted in **figure 6.8 (bottom)** for the three foundations examined. Prevalence of the hybrid foundations against the monopile can be easily observed; the magnitude of rotation is significantly smaller, up to 150%. Another important advantage of the hybrid foundations is that residual rotation is minimized, compared to the monopile which experiences a permanent rotation of 1mrad after the seismic event. Concerning the hybrid foundations, the difference in their performance is negligible; the extra 5m in the diameter of the footing do not seem to provide any benefits. However, it has to be reminded that the results discussed here concern seismic excitation of an uncharged superstructure. Hence, in order to ensure the advantages of the hybrid system against earthquakes the results of the next subsection also need to be taken into consideration.

Settlement time histories are presented in **figure 6.9**. Interestingly, it seems that the hybrid foundations demonstrate a significant advantage in settlement accumulation as well. Despite the fact that the monopile tends to settle less for static loads as proven in the previous chapter, it seems to have a significant disadvantage when it comes to seismic excitation; residual settlement of the monopile after the seismic event reaches 10 cm, while the hybrid foundations both reach a maximum of 4.5 cm. This can be attributed to the nonlinear behavior of the foundation – soil interfaces and the different vertical load transfer mechanisms of the two systems. When the peripheral area of the monopile is detached from the soil due to the violent earthquake shake, shaft resistance of the pile is minimized and the vertical loads are only transmitted to the ground via the pile base; thus, a large part of the monopile's vertical resistance is diminished. On the other hand, vertical loads are carried exclusively by the footing of the hybrid system which transmits the vertical load mainly via the generation of normal stresses. In addition, the monopile experiences severe rotation during the earthquake which can definitely lead to detachment of the sidewalls. Settlement – rotation diagrams for the three foundations are presented in **figure 6.10**.

Finally, time histories of the drift at the tower head are depicted in **figure 6.11**. Solid lines correspond to total drift, while fainted lines correspond to rotational drift. Total drift of the tower laying on the monopile is slightly larger than the other two, but with no significant differences. However, rotational drift of the monopile is quite larger, as expected. On the other hand, rotational drift is negligible for the hybrid systems and the total drift in that case is a consequence of the tower bending. It has to be pointed out that the maximum drift in the case of the Takatori earthquake excitation does not exceed 80 cm, which is smaller than the maximum drift due to wind and waves, which is found to reach values of the order of 150 cm in chapter 5 of the current study.

6.3.4 Seismic Excitation After Monotonic Wind and 10 Cycles of Wave Loading

As discussed in the previous subsection, the simultaneous act of seismic, wind and wave forces on a wind turbine is a very complex phenomenon which is hard to simulate realistically. Consequently, a simplified approach is adopted in the current study, in which the seismic motion is applied after 10 cycles of wave loading. Monotonic wind loading is also applied in the first step of the analysis. This load case is identical to the second loading scenario of chapter 5, with the only difference that the seismic motion is applied afterwards. The earthquake starts to take place when the monotonic wind force and a same – direction wave force are also acting on the superstructure, thus the system is already deflecting. Based on the above, it is undisputable that this load case represents an extreme situation, not the average earthquake design conditions. The goal is to investigate the seismic performance of the foundations, when the superstructure is already quite vulnerable to P- δ effects and the soil has experienced a significant amount of yielding, thus stiffness degradation of the soil – foundation system.

Initially, time histories of acceleration at the foundation lid are presented in **figure 6.12 (top)**. As in the previous case, there is no significant difference between the accelerations that are

transmitted at the base of each tower because they basically depend on the characteristics of the soil medium. Moving on, acceleration time histories at the head of each tower are presented in **figure 6.12 (bottom)**. All the observations made in the previous subsection apply here as well. The information contained in the acceleration time histories is better depicted in **figure 6.13**, which contains the corresponding elastic spectra. An important observation can extracted from the spectra at the head of each tower; while the D15 – L15 hybrid foundation demonstrates a dampened peak of spectral acceleration, this damping is absent for the D20 – L15 system. This can be explained through the theory of rocking systems: in order to mobilize bearing capacity mechanisms into the underlying soil, thus achieve energy dissipation and damping through soil yielding, it is necessary that the vertical factor of safety is quite small. This is not the case for the hybrid system with the larger 20 m footing, which provides a larger value of FS_V. In addition, the spectra of **figure 6.13 (left)** exhibit a smaller value of SA compared to the ones of **figure 6.7 (left)**. This indicates that the soil has already experienced an amount of yielding and stiffness degradation due to the wind and wave loading, so the maximum acceleration that can be developed at the tower head is smaller, as the softer soil allows energy dissipation through rocking mechanisms.

Moreover, time histories of bending moment at the base of each tower are depicted in **figure 6.14 (top)** for the three foundations examined. Note that the moment due to wind and wave loading has already reached a value of 100 MNm by the time the earthquake begins to act. The maximum instantaneous moment demand is approximately 150 MNm; this value overpasses the moment capacity of the D15 – L15 hybrid foundation, however this does not necessarily lead to failure due to the kinematic nature of the earthquake.

Moving on, time histories of rotation at the base of each tower are depicted in **figure 6.14 (bottom)**. The results indicate that the effect of a violent shake while the wind turbine is sustaining its operational loads can be devastating. The monopile and the D15 – L15 hybrid foundation both surpass the rotation limit of 0.0087 rad, which refers to the end of the project's lifetime. It is interesting that, while the D15 – L15 hybrid foundation presents smaller angles of rotation caused by wind and wave loads, its response to the consecutive seismic event is the worst. This is probably a consequence of the reduced bearing capacity of the particular hybrid foundation system, which is surpassed several times during the earthquake event. As discussed before this might not lead directly to failure, however excessive accumulation of rotation occurs during the time intervals in which moment demand is larger than the existing capacity. Note that in the previous subsection the monopile did not perform better than the D15 – L15 foundation in terms of rotation. The effect of the earthquake to the monopile – founded tower is also devastating, as it develops a residual rotation larger than the rotation limit. Only the D20 – L15 foundation presents a relatively satisfying performance, considering that it does not exceed the rotation limit during the event. In that case, the residual rotation is about 0.005 rad. Hence, it becomes clear that an earthquake incident in unfavorable conditions can lead to surpassing of the rotation limit far earlier in the project's lifetime.

Furthermore, time histories of drift at the head of each tower are presented in **figure 6.15**. The solid lines correspond to total drift while dotted lines correspond to rotational drift. A

first observation is that the turbines experience an initial drift of the order of 1.5 – 1.7 m before initiation of the earthquake. This large initial deflection makes the system particularly vulnerable to P – δ effects that result to a further increase in the bending moment applied to the foundation. The maximum drift is exhibited by the tower founded on the D15 – L15 hybrid system and exceeds 3 m. Unlike the case of wind and wave loading, rotational drift is significantly increased here as well.

Finally, settlement time histories are depicted in **figure 6.16**. The largest residual settlement is observed for the monopile and reaches 10 cm. Despite the fact that the monopile exhibits the best response in terms of vertical displacement under static loads, the extensive interface non – linearities developed during the earthquake significantly reduce its vertical resistance, as previously explained. Vertical response of the monopile under this load case does not differ from previous load case, since the same magnitude of settlement is developed (10 cm). The settlement is also plotted against the angle of rotation in **figure 6.17**.

6.4 Conclusions

In this chapter, preliminary seismic analysis has been conducted in order to assess the seismic response of hybrid foundations and compare them to a conventional monopile solution. Initially, the first two modal shapes of three different wind turbines of nominal capacity 2 MW, 3.5 MW and 5 MW were extracted along with the corresponding natural frequencies and periods, for fixed base conditions. Moving on, the effect of soil – structure interaction on the first natural frequency has been examined for a 3.5 MW wind turbine laying on an elastic cohesive soil stratum. Furthermore, the performance of two hybrid foundations (D15 – L15 and D20 – L15) and a 30 m monopile with a diameter of 5 m has been assessed against two seismic load cases: 1) Imposition of the input motion on the system without any environmental loads acting. 2) Imposition of the input motion after the action of monotonic wind loading and 10 cycles of cyclic wind loading. The Takatori_090 record has been used as an input motion. The main conclusions are summarized below:

- Increasing the nominal capacity of wind turbines leads to larger and more slender structures with lower first natural frequencies. Especially for larger turbines, the second natural frequency is more likely to be excited by seismic motions, as the first can be quite small.
- The effect of soil – structure interaction on the first natural frequency is generally a small decrease compared to the fixed base conditions, which depends on the initial stiffness of the foundation applied. Increasing the elastic stiffness of foundations leads them to approach the fixed base conditions.
- Expression (1.1) can lead to quite accurate approximations of the first natural period of a wind turbine tower.
- When the motion is imposed to an uncharged system, both hybrid foundations outperform the monopile in terms of maximum and residual rotation. However, if the earthquake acts on a system which is already sustaining operational loads, maximum

rotation limits can be easily surpassed, mainly due to P – δ effects and large moments applied to the foundations.

- Increasing the diameter of the footing of a hybrid foundation can significantly improve its seismic performance.
- Moment bearing capacity plays an important role, as if the operational loads and seismic forces act simultaneously on the foundation, excessive rotation can be experienced.
- Performance of hybrid foundations in terms of settlement is superior, compared to the monopile. Detachment of the latter's sidewalls from the surrounding soil during a violent seismic event can easily lead to diminishment of the pile's shaft resistance. This effect is the same for both load cases examined.
- The cases considered in this study concern two extreme opposite conditions. In order to prove the superiority of hybrid foundations against monopiles under seismic loading, further research should be done.

CHAPTER 6: FIGURES

Seismic Response of Hybrid Foundations

		2MW	3.5MW	5MW
f1 : Hz	F.E.A	0.41203	0.26014	0.23725
	Literature*	0.424045	0.271044	0.24761
	Deviation	2.92 %	4.19 %	4.37 %
f2 : Hz	F.E.A	5.0551	2.8735	2.753

$$f1 \cong \frac{D_{av}}{L^2}\sqrt{\frac{E}{104(\alpha + 0.227)\rho_{steel}}}$$

*[Van Der Tempel 2005]

Table 6.1. First and second eigenfrequencies for the wind turbines considered. Results for a fixed base tower.

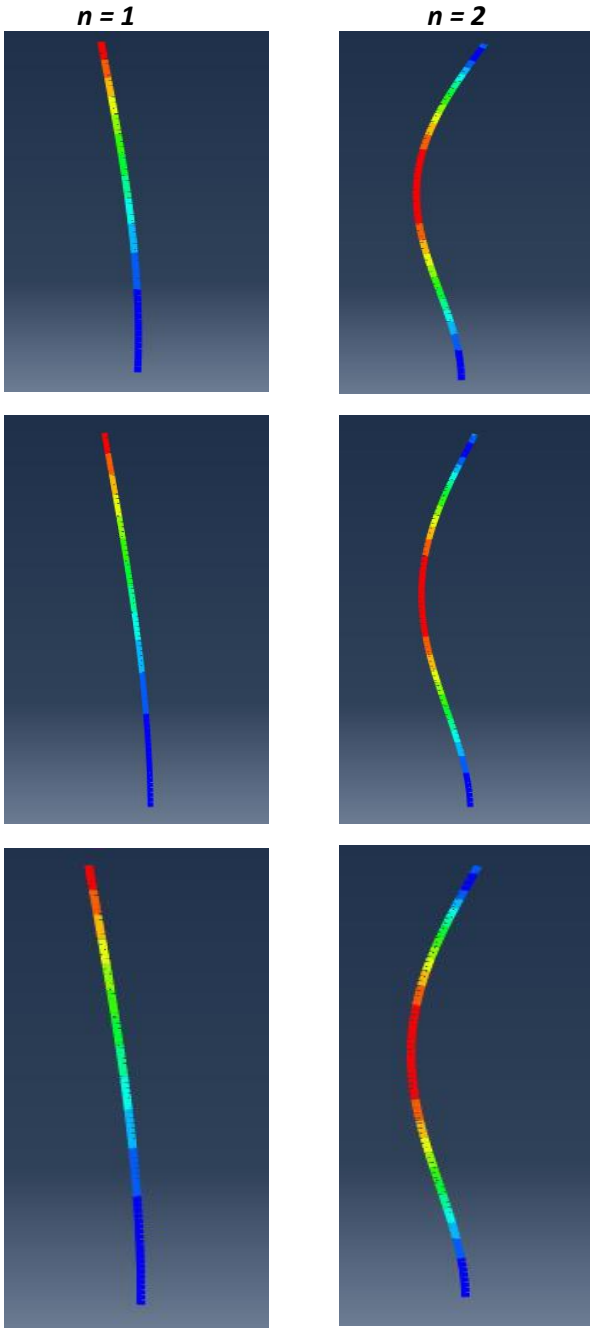

Figure *6.1.* First and second eigenmodes for the wind turbines considered. Results for a fixed base tower.

3.5 MW	D11-L15	D15-L15	D15-L20	D20-L15	Monopile L30
f1 : Hz	0.24889	0.25378	0.25423	0.25673	0.24113

Table 6.2. First eigenfrequency for the 3.5 MW wind turbine, for various foundations. Soil – foundation interaction is considered.

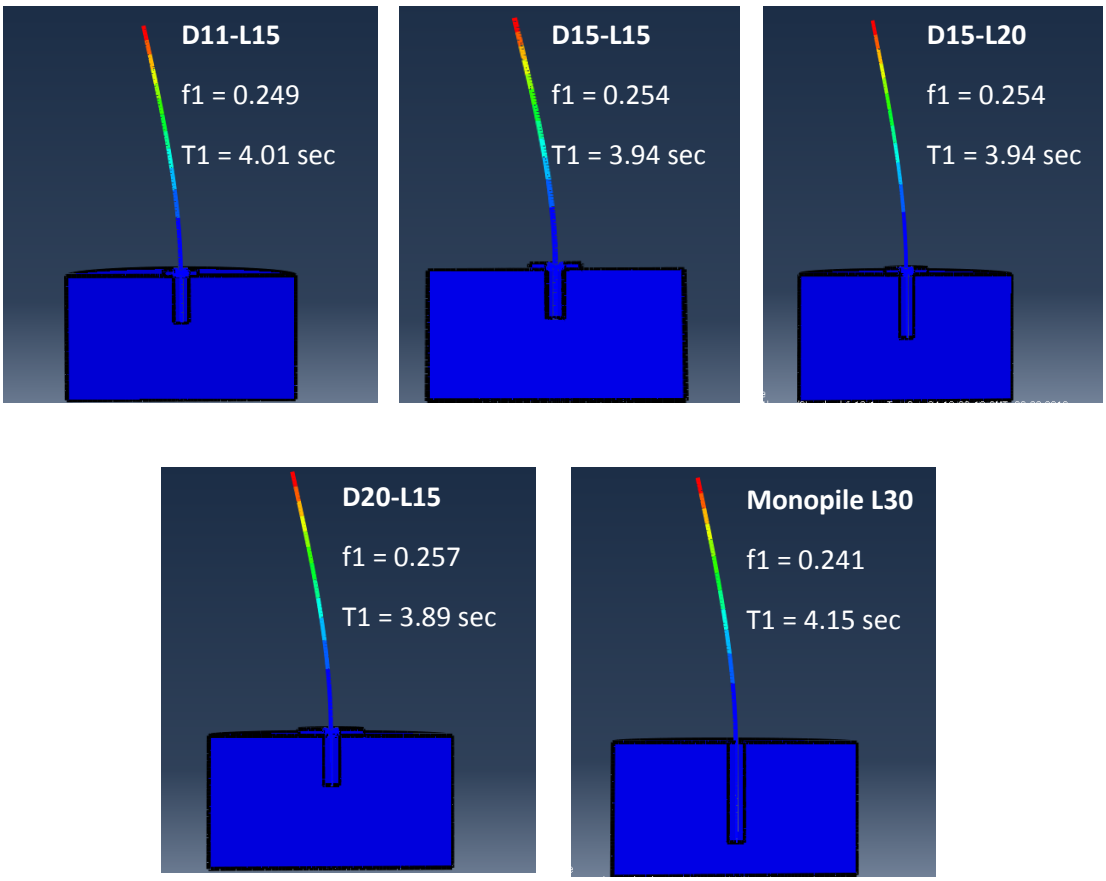

Figure 6.2. First eigenfrequency for the 3.5 MW wind turbine, for various foundations, considering soil – foundation interaction.

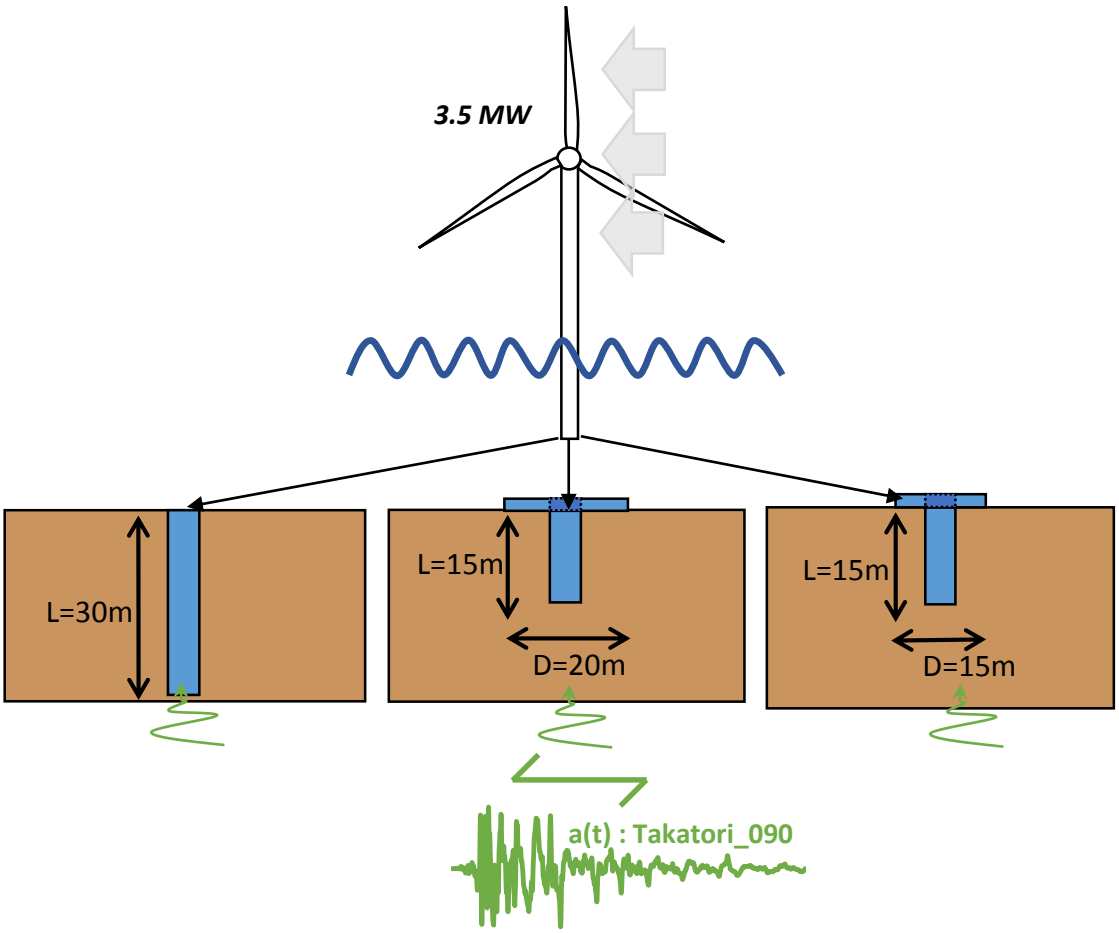

Figure 6.3. Sketch illustrating the foundations examined for the seismic problem.

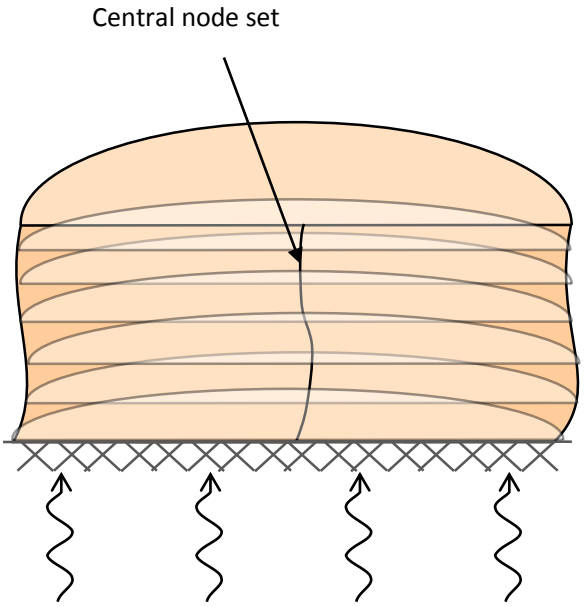

Figure 6.4. Illustration of the soil model examined for the seismic excitation.

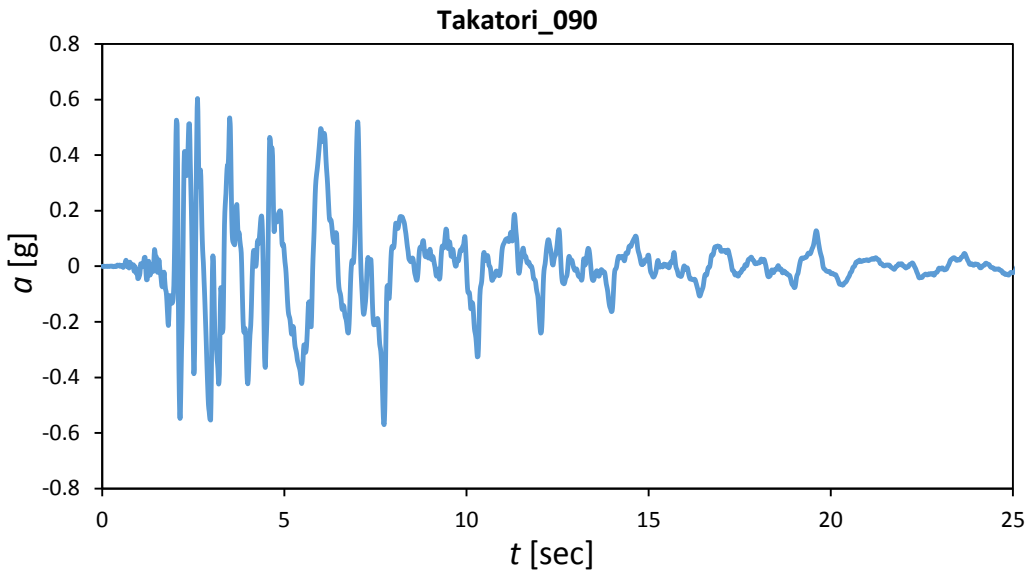

Figure 6.5. The Takatori_090 seismic record, used as input motion for the seismic problem.

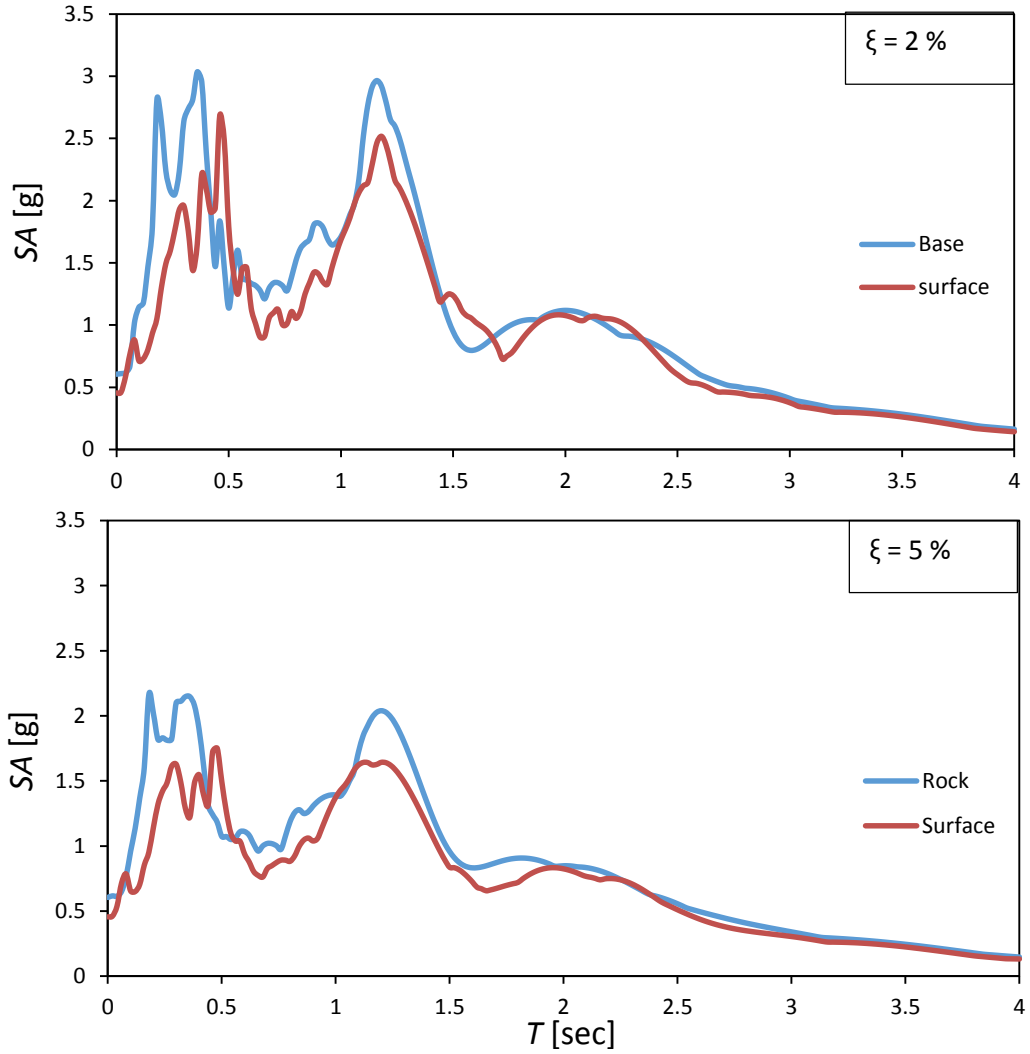

Figure 6.6. Acceleration spectra at the soil base and surface, for ξ = 2 % and 5 %.

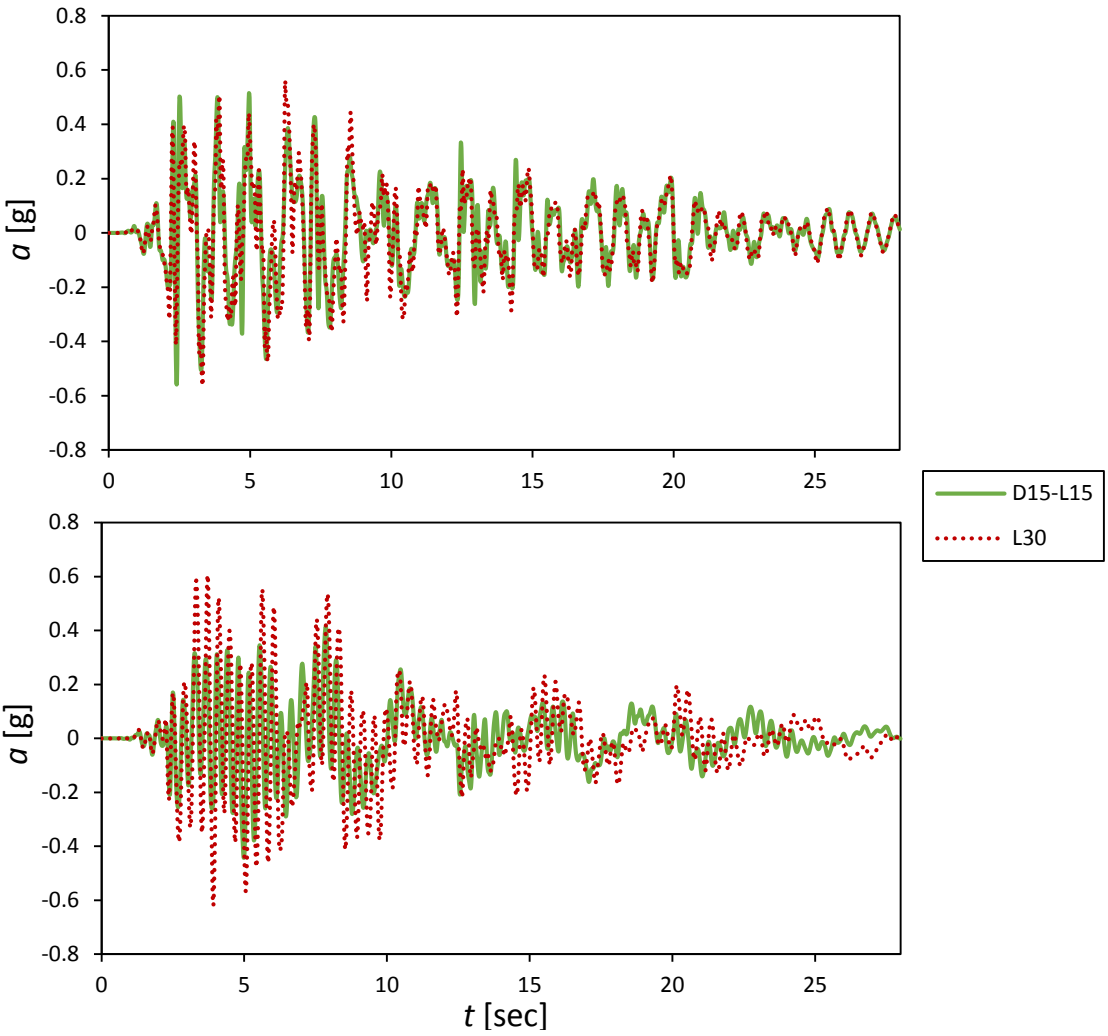

Figure *6.6.* Top: Acceleration time histories at the foundation lid. Bottom: Acceleration time histories at the tower head. Seismic excitation without waves and wind acting.

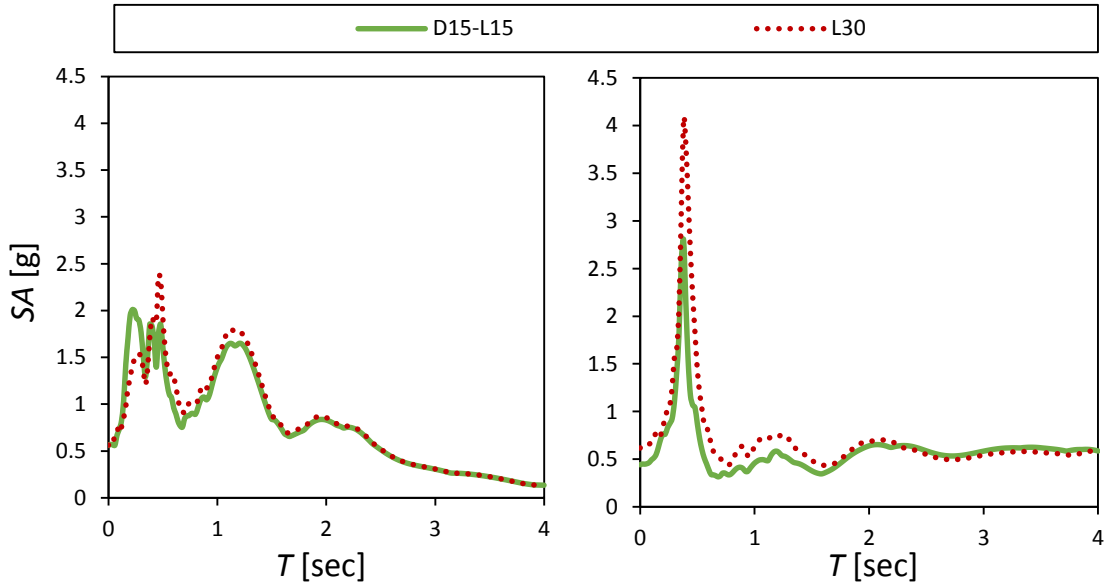

Figure 6.7. Left: Acceleration spectra at the foundation lid. Right: Acceleration spectra at the tower head. Seismic excitation without waves and wind acting.

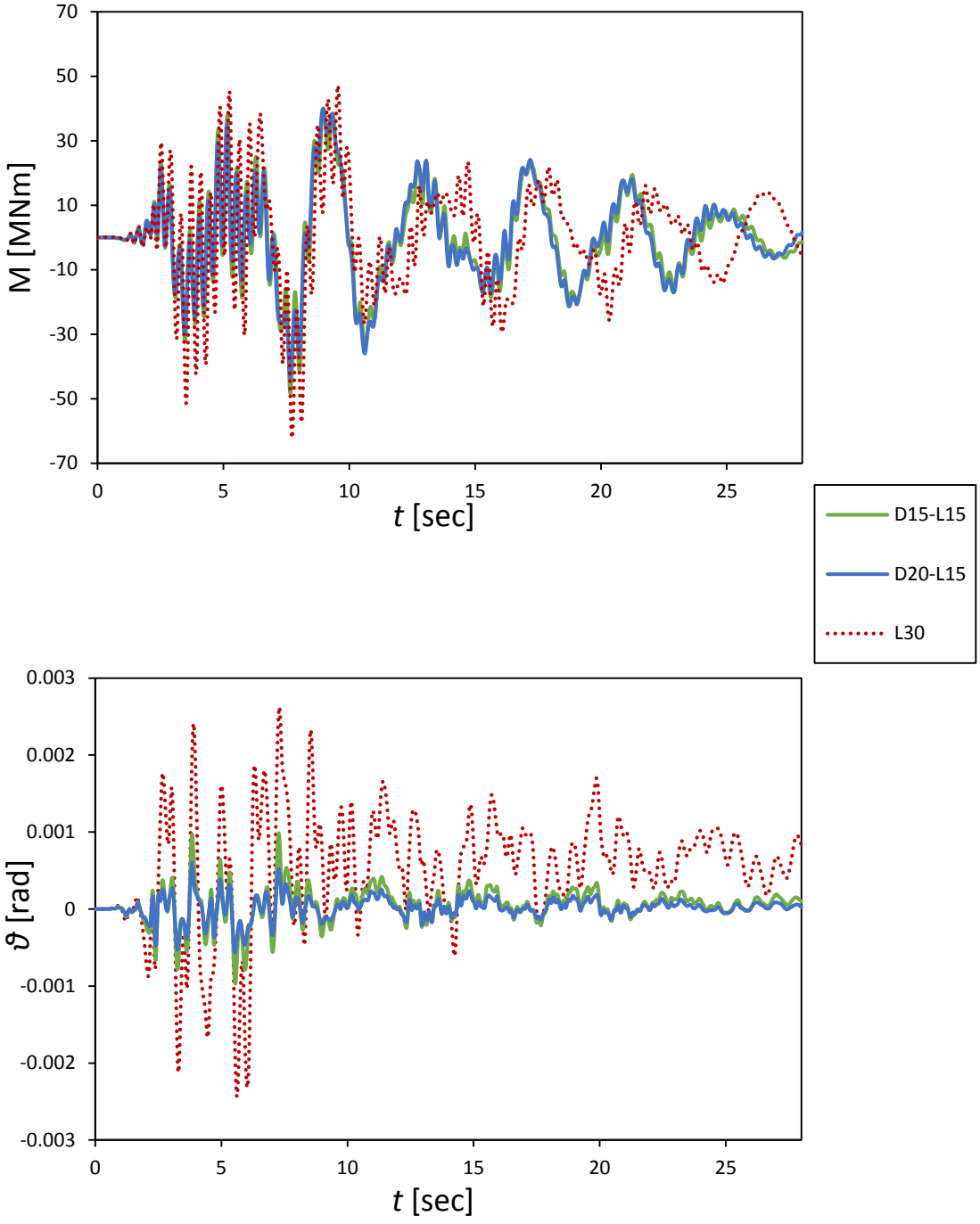

Figure 6.8. Top: Overturning moment time histories at tower base. Bottom: Rotation time histories at tower base. Seismic excitation without waves and wind acting.

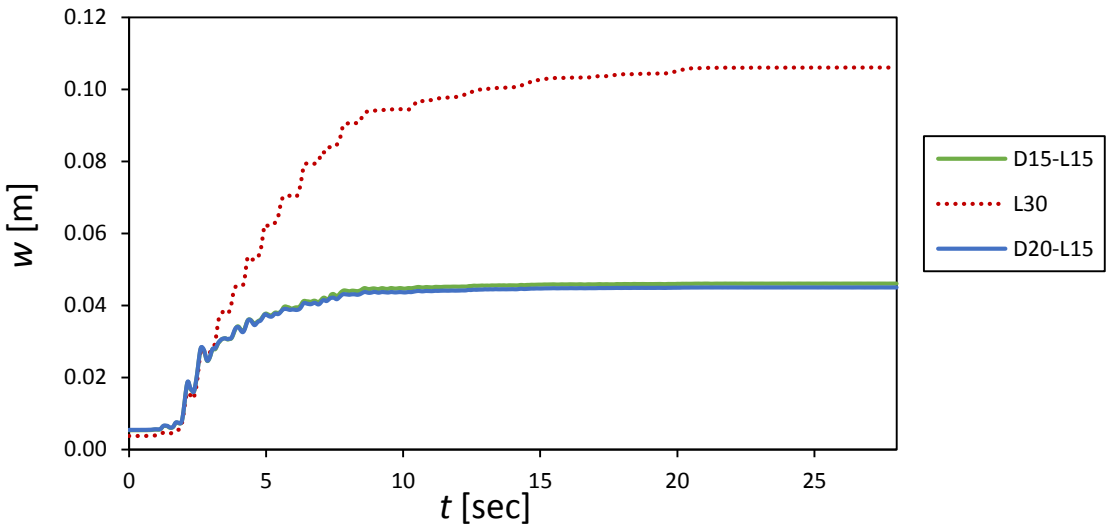

Figure 6.9. Settlement time histories for seismic excitation without waves and wind acting.

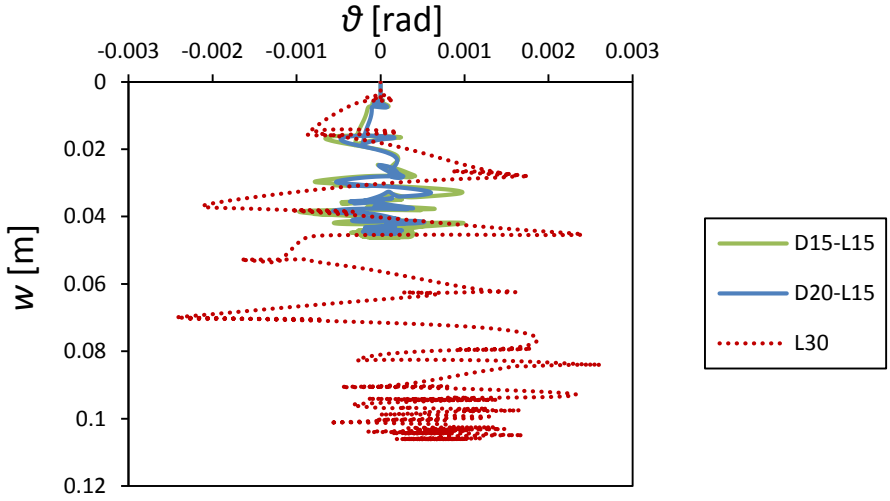

Figure 6.10. Settlement-rotation diagrams for seismic excitation without waves and wind acting.

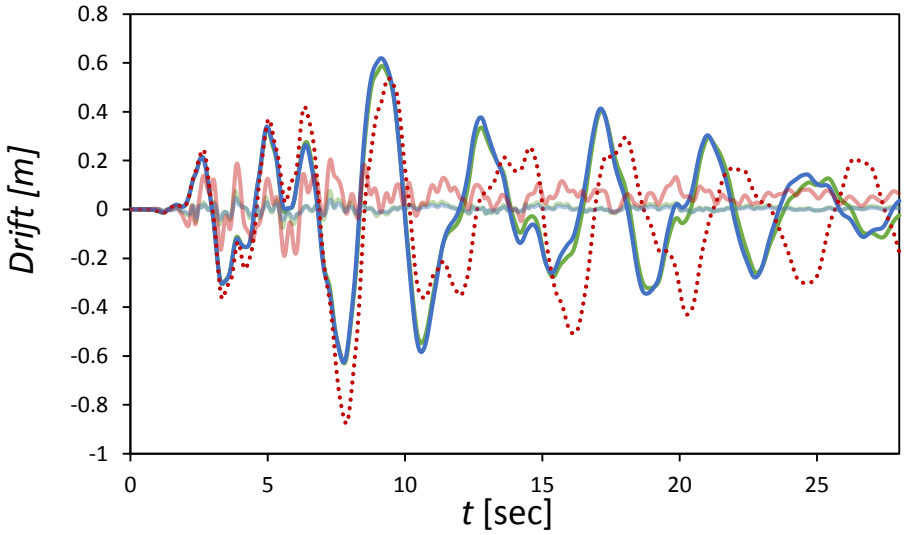

Figure 6.11. Total and rotational tower head drift time histories for seismic excitation without waves and wind acting.

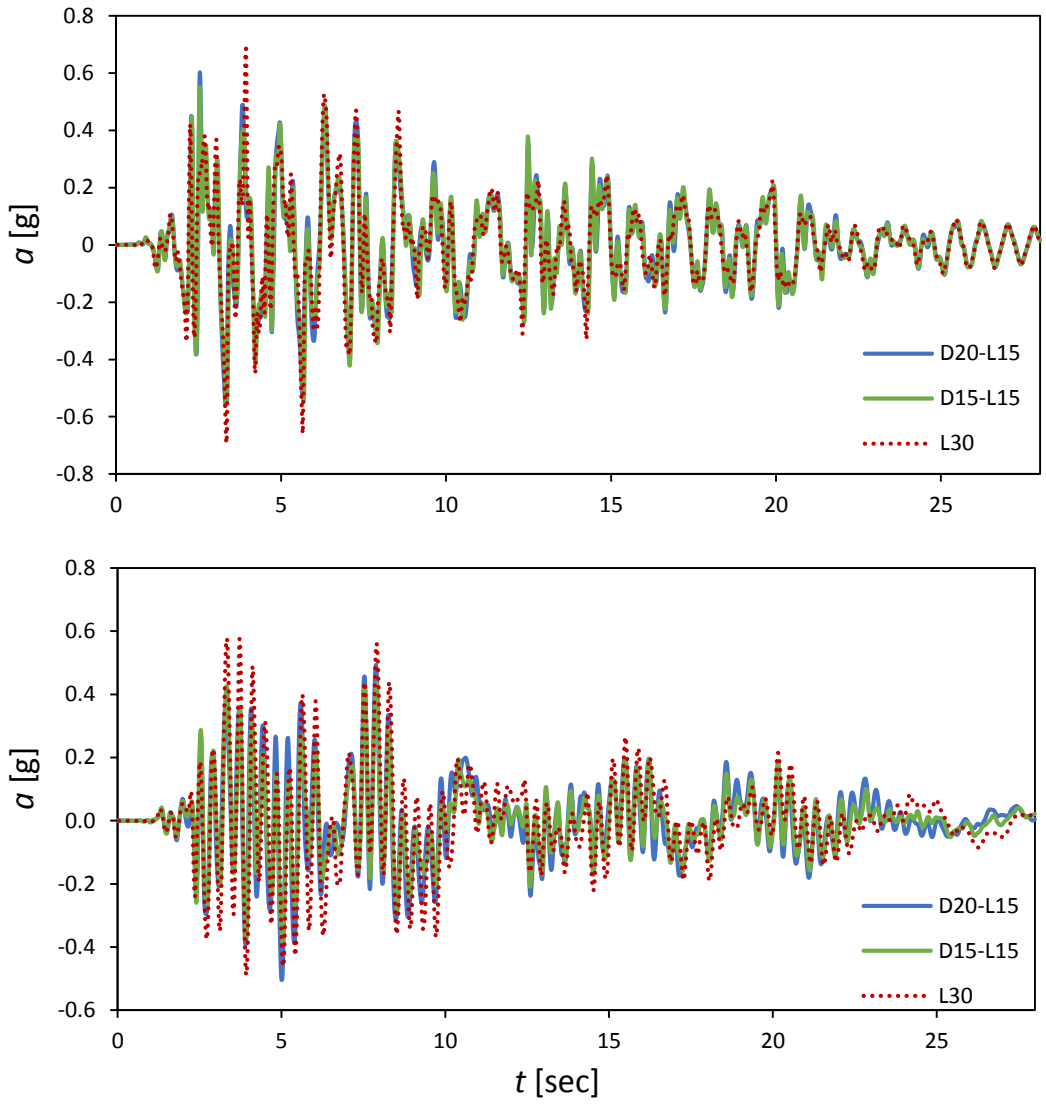

Figure 6.12. Top: Acceleration time histories at the foundation lid. Bottom: Acceleration time histories at the tower head. Earthquake excitation starts after monotonic wind and 9 cycles of cyclic wave loading.

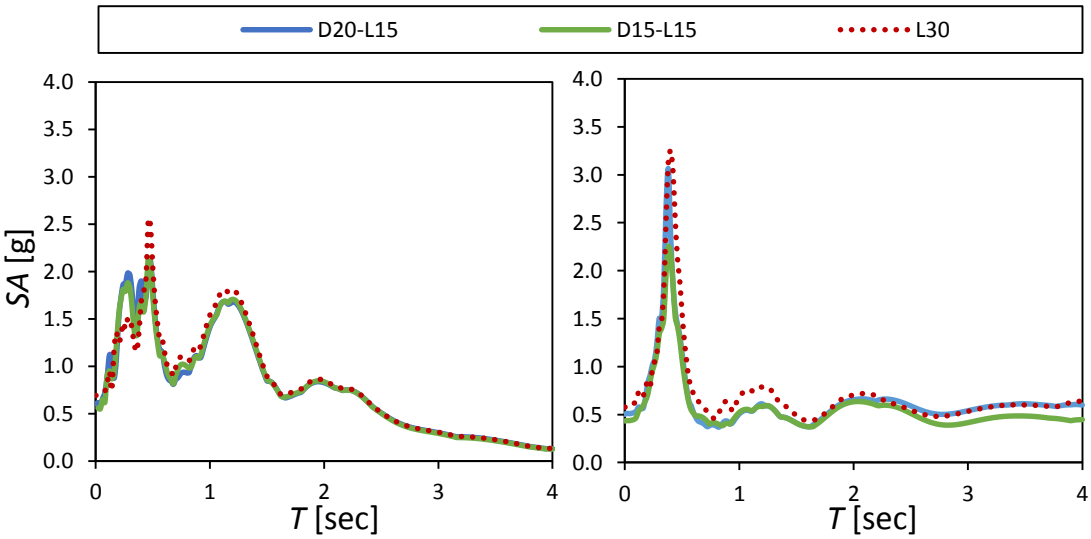

Figure 6.13. Left: Acceleration spectra at the foundation lid. Right: Acceleration spectra at the tower head. Earthquake excitation starts after monotonic wind and 9 cycles of cyclic wave loading.

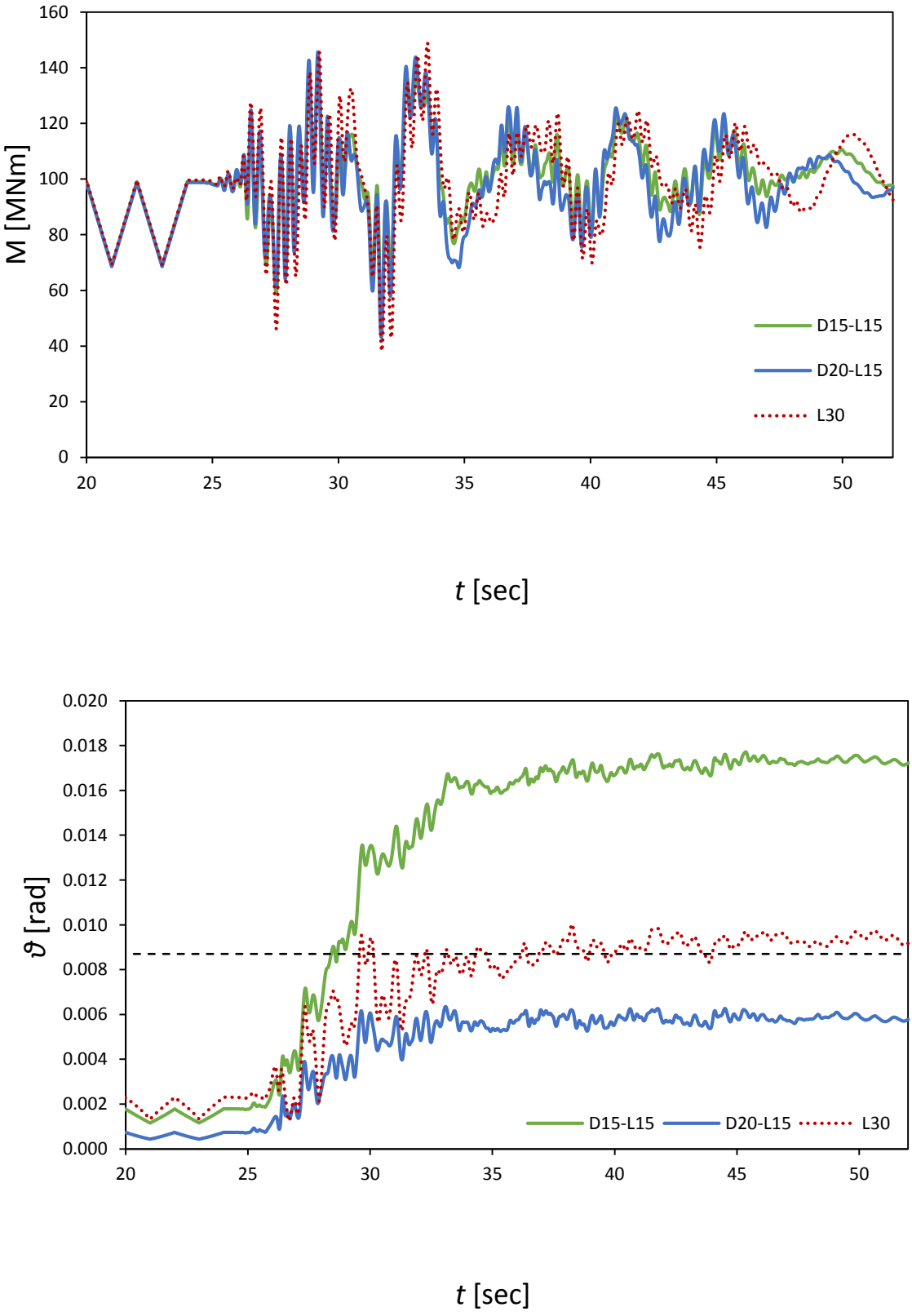

Figure 6.14. Top: Overturning moment time histories at the tower base. Bottom: Rotation time histories at the tower base. Earthquake excitation starts after monotonic wind and 9 cycles of cyclic wave loading.

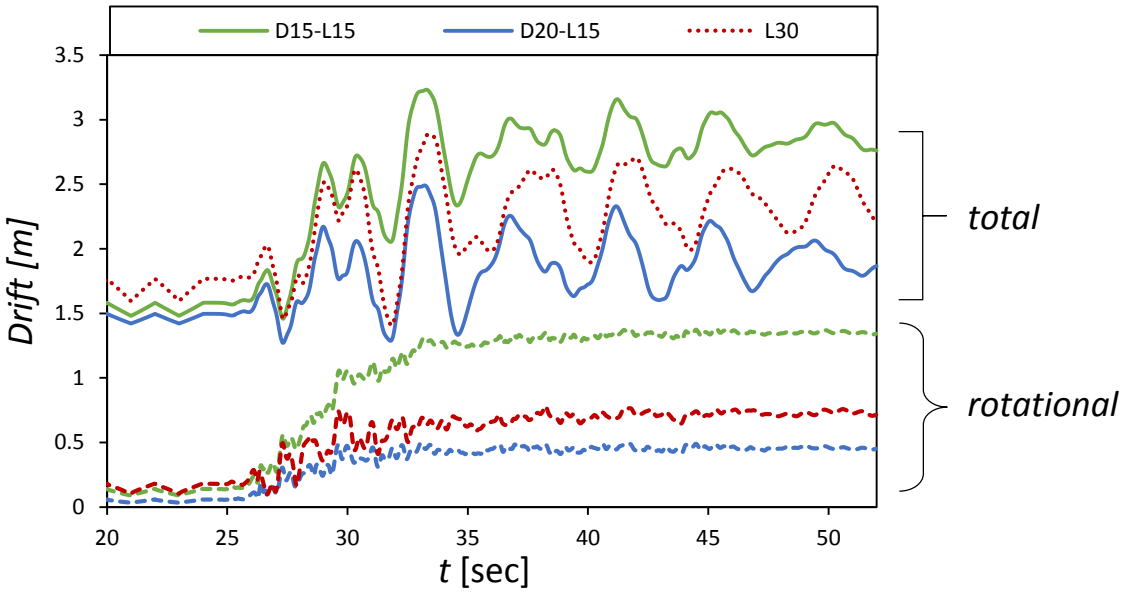

Figure 6.15. Total and rotational tower head drift time histories. Earthquake excitation starts after monotonic wind and 9 cycles of cyclic wave loading.

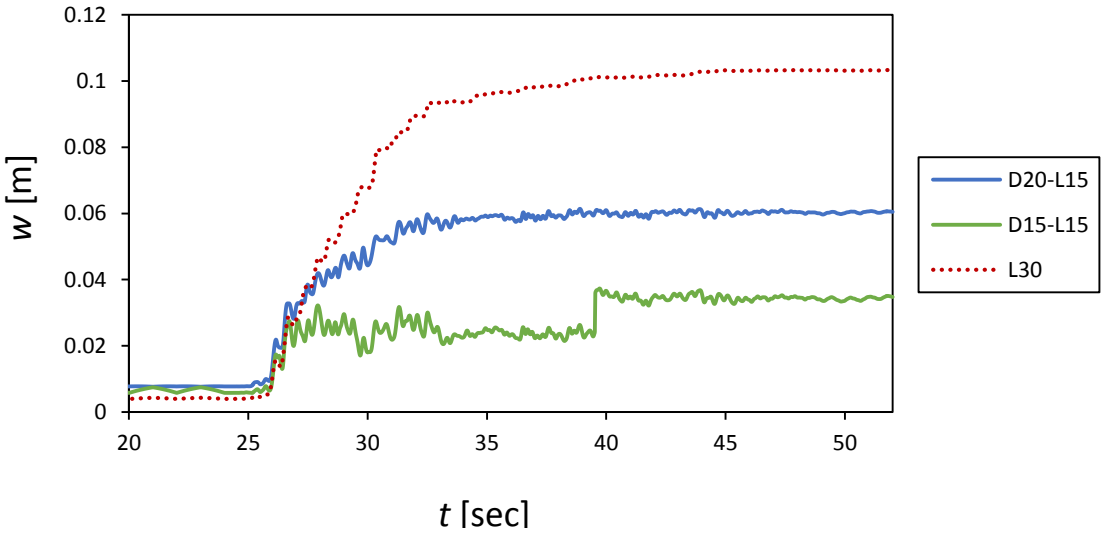

Figure 6.16. Settlement time histories. Earthquake excitation starts after monotonic wind and 9 cycles of cyclic wave loading.

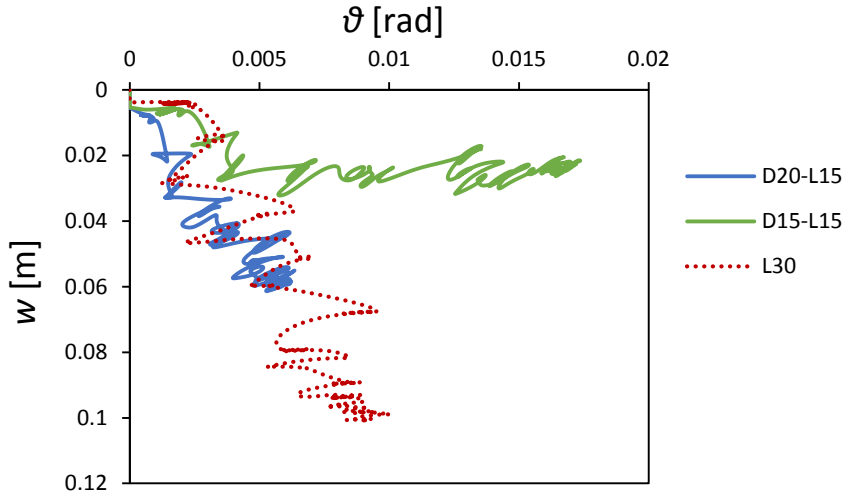

Figure 6.17. Settlement-rotation diagrams. Earthquake excitation starts after monotonic wind and 9 cycles of cyclic wave loading.

CHAPTER 7

Conclusions & Suggestions for Further Research

7.1 Conclusions of the Study
7.2 Suggestions for Further Research

7.1 Conclusions

The scope of the current study is the investigation of the performance of hybrid foundations supporting offshore wind turbines as viable alternatives to the widely applied foundation solution of the monopile. The hybrid foundation proposed is comprised of a monopile and a footing that are unconnected to each other in the vertical sense but share a common lateral response. A series of 3D numerical analyses were conducted, which deal with some of the geotechnical aspects of the problem. In the first part of the study, geometrical parameters such as the diameter of the footing D and embedment length of the pile L were correlated to fundamental geotechnical properties such as bearing capacity and stiffness. In the second part, three typical offshore wind turbine superstructures were introduced and the whole soil – foundation – superstructure systems were subjected to environmental loads such as wind, waves and an earthquake motion. Attention was drawn to comparison of the hybrid systems against typical monopiles that best suited each wind turbine. The current study concerns cohesive soils and the influence of soil heterogeneity was also examined. Effect of interface nonlinearities and P – δ effects was also pointed out and was found to be of great importance in some aspects of the study.

Overall, the results indicate that the proposed hybrid foundation can compare quite well against monopiles, especially in terms of lateral stiffness, which is a key aspect of the design of foundations for offshore wind turbines. Based on the findings of chapter 5, appropriate hybrid foundations were assigned to each of the wind turbines examined. It is noteworthy that all of the proposed hybrid foundation solutions outperform the corresponding monopiles. Some of the most important findings of this study are listed below:

- Hybrid monopile – footing foundations seem to be a very competitive solution for offshore wind turbines, compared to monopiles. The most important advantage they have to offer is **superior performance** in terms of moment – rotation, which can be achieved by implementing a pile shorter by up to 50 % compared to the corresponding monopile solution. Considering that driving of the pile is a determining factor in the overall installation cost, significant **cost reduction** (of the order of 7 % of the total cost) can be accomplished.
- Increasing the diameter of the footing significantly improves the lateral stiffness of the system, thus rotations can be reduced. Limitation of rotations is one of the main goals in the design of foundations for offshore wind turbines, which are quite sensitive to such deformations. On the other hand, increasing the embedment length of the pile has a direct influence on the system's moment capacity. The above indicate that hybrid foundations offer increased **flexibility in their design**. The designer can chose between hybrid systems with a short pile and large footing or systems with longer piles and smaller footings, depending on the specific parameters of each case (in – situ soil conditions, underlying rock etc.).
- For homogeneous cohesive soil profiles, diameter of the footing plays a major role in the overall response of the system under working loads, while the contribution of the length of the pile is relatively smaller. This is not the case for inhomogeneous soil profiles, where weaker superficial soil layers can significantly deteriorate the

efficiency of the footing. In that case, increasing the pile length can be highly beneficial. This is also indicative of the high **adaptability** of the hybrid foundation.

- Compared to monopiles that are generally quite long (L > 30 m), hybrid foundations present smaller ultimate moment capacity. However, ultimate capacity of the foundation is not likely to be mobilized during the operational lifetime of the project due to very strict deformation limits that are imposed by regulations. Therefore, emphasis should be given to stiffness of the foundation. It is proven in the current study that foundations with a stiffer initial response and smaller ultimate moment capacity can satisfy operational criteria significantly better than foundations with a softer initial response and higher ultimate moment capacity such as monopiles.
- The configuration adopted in the current study, where the footing is unconnected to the pile in the vertical sense, allows it to carry the total vertical load which is imposed by the superstructure. This is found to have a beneficial effect on the lateral resistance of the system as implied by the M – N and Q – N interaction diagrams.
- Settlements are found to be smaller for monopiles, as they have increased vertical stiffness. However, in violent events such as earthquakes, detachment of the pile's shaft can extremely deteriorate their vertical resistance, while hybrid foundations remain intact because the vertical loads are carried exclusively by the footing.
- The effect of earthquakes is far from negligible, especially when they act simultaneously to operational wind and wave loads, which is the most probable case.

7.2 Suggestions for Further Research

This study is a preliminary investigation of the performance of hybrid foundations composed of a monopile and a footing. While the first results seem quite indicative of the superiority of these systems compared to monopiles, further investigation is definitely required before hybrid foundations can be applied to offshore wind turbines. Some suggestions for further research are the following:

- This study only concerns numerical analysis of cohesive soils under undrained conditions. In order to obtain a better image of the viability of hybrid foundations, their performance should also be assessed in drained conditions and sands. Of course, experimental research is also necessary to validate the results of numerical analyses.
- The first results from this study indicate that dead loads play an important role on the lateral resistance of hybrid foundations. Further research should be conducted to support these findings.
- Design of the hybrid foundation is still in a very preliminary level and there is space for improvements. Skirts could be added to the footing, further increasing its lateral capacity. In addition, stoppers could be added in the monopile – footing connection, in order to limit the amount of settlements.
- The hybrid foundation should be compared to other types of foundations for offshore wind turbines such as suction caissons. Extensive comparative cost analysis should also be performed.

- Results concerning bearing capacity and stiffness derived from this study are qualitative and further parametrical investigation should be performed in order to produce closed – form expressions and design charts.

References

ABAQUS 6.11. (2011). Standard user's manual. Dassault Systèmes Simulia Corp., Providence, RI,
USA.

Anastasopoulos, I., Gazetas, G., Loli, M., Apostolou, M. and Gerolymos, N. (2010). “Soil Failure can be used for Seismic Protection of Structures”, Bulletin of Earthquake Engng, 8 (2), 309-326.

Anastasopoulos I., Gelagoti F., Kourkoulis R., Gazetas G. (2011). “Simplified Constitutive model for Simulation of Cyclic Response of Shallow Foundations: Validation against Laboratory Tests”, *Journal of Geotechnical and Geoenvironmental Engineering*, ASCE, Vol. 137, No. 12, pp. 1154–1168.

Anastasopoulos I., Kokkali P., Tsatsis A. (2011). “1-dof System Lying on Square Foundation: Monotonic and Cyclic Loading”.

Anastasopoulos I., Gazetas G., Loli M., Apostolou M., Gerolymos N. (2010). “Soil failure can be used for seismic protection of structures”. *Bulletin of Earthquake Engineering* 8, pp. 309-326.

Apostolou, M., Gazetas, G. [2007]. “Analytical modeling of footings under large overturning moment” In. Proc. 2nd Greece - Japan workshop: Seismic Design, Observation, and Retrofit of Foundations, Tokyo, 3-4 April, 165-184.

Arshi HS. (2011). “Structural behavior and performance of skirted hybrid monopile-footing foundations for offshore oil and gas facilities”. Proceedings of the Institution of Structural Engineers: Young Researchers Conference ‘11. London: IStructE Publications, 8.

Arshi HS. (2012). “A new design solution for increasing the lateral resistance of offshore pile foundations for wind turbines located in deep-water”. Proceedings of the Institution of Structural Engineers: Young Researchers Conference ‘12. London: IStructE Publications, 10.

Arshi HS, Stone KJL and Newson TA. (2011). “Numerical modelling on the degree of rigidity at pile head for offshore monopile-footing foundation systems”. 9th British Geotechnical Association Annual Conference, London.

Arshi HS and Stone KJL. (2011). “An investigation of a rock socketed
pile with an integral bearing plate founded over weak rock”. Proceedings of the 15th European Conference of Soil Mechanics and Geotechnical Engineering. Amsterdam: Ios Pr Inc, 705 – 711.

Arshi HS and Stone KJL. (2012). “Lateral resistance of hybrid monopile footing foundations in cohesionless soils for offshore wind turbines”. Proceedings of the 7th International Conference on
Offshore Site Investigation and Geotechnics. London: Society for Underwater Technology, 519 – 526.

Arshi H.S., Stone K.J.L., Vaziri M., Newson T.A., El - Marassi M., Taylor R.N., Goodey R.J. [2013]. "Modelling of monopile-footing foundation system for offshore wind turbines in cohesionless soils", Proceedings of the 18th International Conference on Soil Mechanics and Geotechnical Engineering, Paris 2013.

Bazeos, N., Hatzigeorgiou, G. D., Hondros, I. D., Karamaneas, H., Karabalis, D. L. and Beskos, D. E. [2002]. “Static, Seismic and Stability Analyses of a Prototype Wind Turbine Steel Tower”, Eng. Struct.; Vol. 24, 2002; 1015.

Bell, R. W. [1991]. "The analysis of offshore foundations subjected to combined loading", MSc thesis, University of Oxford, Oxford, U.K.

Bienen B., Dührkop J., Grabe J., Randolph M.F., White D.J. (2012). “Response of Piles with Wings to Monotonic and Cyclic Lateral Loading in Sand”, Journal of Geotechnical and Geoenvironmental Engineering, 138(3):364–375.

Bransby, M. F., Randolph, M. F. [1997]. “Shallow foundations subjected to combined loadings” Proc. 9th Int. Conf. on Comp. Methods and Advances in Geomechcs, Wuhan 3, 1947–1952.

Bransby M.F., Randolph M.F. [1998]. “Combined Loading of Skirted Foundations”, Geotechnique, 48 (5), 637−655.

Bransby, M. F., Randolph, M. F. [1999]. “The effect of embedment depth on the undrained response of skirted foundations to combined loading”, Soils Found. 39 (4), 19–33.

Bransby, M. F. and Yun, G. J. [2009]. “The undrained capacity of skirted strip foundations under combined loading”, Geotechnique, 59 (2), 115-125.

Broms BB. (1964). “Lateral resistance of piles in cohesionless soils”. ASCE Journal of the Soil Mechanics and Foundation Division. 90(SM3), 123-156.

Brinch Hansen, J. [1970]. "A revised and extended formula for bearing capacity." Bulletin No. 28, Danish Geotechnical Institute, Copenhagen, 5-11.

Butterfield, R. & Gottardi, G. [1994]. “A Complete Three Dimensional Failure Enveleope for Shallow Footings on Sand”, Geotechnique, 44, 181−184.

Byrne, B. Houlsby, G. [2003]. “Foundations for offshore wind turbines”. The Royal Society, 10.1098/rsta.2003.1286

Byrne, B. W., Houlsby, G. [2005]. “Assessing Novel Foundation Options for Offshore Wind Turbines”, University of Oxford, Oxford, U.K.

Byrne, B. [2011]. “Foundation design for offshore wind turbines”. *Géotechnique* Lecture 2011, British Geotechnical Association, Institution of Civil Engineers, 9/11/11.

Chakrabarti, S.K. [1987]. "Hydrodynamics of Offshore Structures", ISBN 0-905451-66-X Computational Mechanics Publications Southampton.

Davis, E. H. and Booker, J. R. [1973]. "The effect of increasing strength with depth on the bearing capacity of clays", Geotechnique, 23 (4), 551-563.

Davis, R. O. and Selvadurai, A. P. S. [2002]. "Plasticity and Geomechanics", Cambridge University Press.

Det Norske Veritas (DNV) [2001]. "Guidelines for Design of Wind Turbines", Copenhagen: Det Norske Veritas.

Doherty, J. P. and Deeks, A. J. [2003]. "Elastic response of circular footings embedded in a non-homogeneous half-space", Geotechnique, 53(8), 703-714.

Doherty, J.P. and Deeks, A.J. [2005], "Adaptive coupling of the finite-element and scaled boundary finite-element methods for non-linear analysis of unbounded media", Computers and Geotechnics, 32, 6, pp. 436-444.

Doherty, J. P., Houlsby, G. T. and Deeks, A. J. [2005]. "Stiffness of flexible caisson foundations embedded in nonhomogeneous elastic soil", Journal of Geotechnical and Geoenvironmental Engineering, ASCE, 131 (12), 1498-1508.

El - Marassi, (2011). "Investigation of hybrid monopile-footing foundation systems subjected to combined loading", PhD Thesis, University of Western Ontario.

El-Marassi M, Newson T, El-Naggar H and Stone KJL. (2008). “Numerical modelling of the performance of a hybrid monopiled footing Foundation”. Proceedings of the 61st Canadian Geotechnical Conference, GeoEdmonton 2008. Edmonton, (Paper No. 480), 97 – 104.

Elsabee, F. and Morray, J. P. [1977]. "Dynamic behavior of embedded foundations", Research Rep. R77-33, MIT.

Duncan JM, Evans LT and Ooi PS. (1994). “Lateral load analysis of single piles and drilled shafts”. ASCE Journal of Geotechnical Engineering. 120(6), 1018-1033.

Faccioli, E., Paolucci, R. and Vivero, G. [2001]. “Investigation of seismic soil – footing interaction by large scale cyclic tests and analytical models”, Proceedings of 4th International Conference on
Recent Advances in Geotechnical Earthquake Engineering and Soil Dynamics, S. Prakash (Ed.), Paper no. SPL-5, San Diego, CA.

FEMA 356, [2000]. “Prestandard and Commentary for the Seismic Rehabilitation of Buildings”, Federal Emergency Management Agency, Washington DC.

Fleming, K., Weltman, A., Randolph, M., Elson, K. [2009]. “Piling Engineering, third edition”.Published by Taylor & Francis.

Fuglsang, L. D. and Steensen-Bach, J. O. [1991]. "Breakout resistance of suction piles in clay", Proc.Int. Conf. On Centrifuge Modeling: Centrifuge 91, Boulder, Colorado, 163-159.

Gajan, S. & Kutter, B. L. [2008]. “Capacity, settlement, and energy dissipation of shallow footings subjected to rocking”, J. Geotechnical & Geoenv. Engng, ASCE, 134 (8), 1129-1141.

Gajan, S., Kutter, B.L., Phalen, J.D., Hutchinson, T.C. and Martin, G.R. [2005]. “Centrifuge modeling of load-deformation behavior of rocking shallow foundations”, Soil Dynamics and Earthquake Engineering, 25 (7-10), 773–783.

Gazetas, G. [1983]. "Analysis of machine foundation vibrations: state of the art", Soil Dynamics and Earthquake Engng, 2 (1), 2-42.

Gazetas, G. [1987]. “Simple physical methods for foundation impedances”, Dynamics of Foundations and Buried Structures, Benerjee PK and Butterfield R., editors, Elsevier Applied Science, Chapter 2, 44-90.

Gazetas, G. [1991]. “Formulas and charts for impedances of surface and embedded foundations”, Journal of Geotechnical Engineering, ASCE, 117 (9), 1129–1141.

Gazetas, G., Anastasopoulos, I. and Apostolou, M. [2007]. “Shallow and Deep Foundations under Fault Rupture or Strong Seismic Shaking”, Earthquake Geotechnical Engineering, Pitilakis K., Editor, Springer: Berlin, 185–210.

Gazetas, G., Apostolou, M. and Anastasopoulos, I. [2003]. “Seismic Uplifting of Foundations on Soft Soil with Examples from Adapazari (Izmit 1999, Earthquake)”, BGA International Conference on Foundation Innovations, Observations, Design & Practice, Univ. of Dundee, Scotland, September 25, 37–50.

Gazetas, G., Apostolou, M. [2004]. “Nonlinear soil-structure interaction : foundation uplifting and soil yielding”, Proceedings of the 3rd US–Japan Workshop on Soil-Structure Interaction, Menlo Park, California.

Gazetas G. & Hatzikostantinou E. (1988). "Elastic formulae for lateral displacement of arbitrarily-shaped embedded foundations", Géotechnique, 38, No 3, 439-444

Gazetas, G., Anastasopoulos, I., Adamidis, O., Kontoroupi, Th. [2013]. “Nonlinear rocking stiffness of foundations”. Soil Dynamics and Earthquake Engineering, 47 (2013), 83 – 91.

Gelagoti, F., Kourkoulis, R., Anastasopoulos, I. and Gazetas, G. [2011]. “Rocking Isolation of Frames on Isolated Footings: Design Insights and Limitations”, J. Earthquake Engineering (in print).

Gerolymos, N. and Gazetas, G. [2006]. “Static and Dynamic Response of Massive Caisson Foundations with Soil and Interface Nonlinearities-Validation and Results”, Soil Dynamics & Earthquake Engineering, 26 (5), 377-394.

Gottardi, G., Houlsby, G. T. & Butterfield, R. [1999]. "The plastic response of circular footings on sand under general planar loading", Geotechnique, 49 (4), 453–470.

Gourvenec, S. [2007]. "Failure envelopes for offshore shallow foundations under general loading", Geotechnique, 57 (9), 715-728.

Gourvenec, S. [2008]. "Effect of embedment on the undrained capacity of shallow foundations under general loading", Geotechnique, 58 (3), 177-185.

Gourvenec, S., Acosta-Martinez, H. E. and Randolph, M. F. [2009]. "Experimental study of uplift resistance of shallow skirted foundations in clay under transient and sustained concentric loading", Geotechnique, 59 (6), 525-537.

Gourvenec, S. and Randolph, M. F. [2003]. "Effect of strength non-homogeneity on the shape of failure envelopes for combined loading of strip and circular foundations on clay", Geotechnique, 53 (6), 575-586.

Green, A. P. [1954]. "The plastic yielding of metal junctions due to combined shear and pressure", J. Mech. Phys. Solids 2, No. 3, 197-211.

Haenler, M., Ritschel, U. and Warnke, I. [2006]. “Systematic Modeling of Wind Turbine Dynamics and Earthquake Loads on Wind Turbines”, European Wind Energy Conference and Exhibition, European Wind Energy Association, Athens, Greece, 2006; 1–6.

Hasselmann et al., [1973]. "Measurements of wind wave growth and swell decay during the Joint North Sea Wave Project", Deutsche Hydro. Zeitschr. Riehe, A8.

Houlsby, G. T., Kelly, R. B. and Byrne, B. W. [2005]. "The tensile capacity of suction caissons in sand under rapid loading", Frontiers in Offshore Geotechnics, Taylor & Francis Group, London, ISBN 0-415-39063-X.

Houlsby, G. T., Kelly, R. B., Huxtable, J. and Byrne, B. W. [2005]. "Field trials of suction caissons in clay for offshore wind turbine foundations", Geotechnique, 55 (4), 287-296.

Houlsby, G. T. and Martin, C. M. [2003]. "Undrained bearing capacity factors for conical footings on clay" Géotechnique, 53 (5), 513-520.

Houlsby GT and Puzrin AM. (1999). “The bearing capacity of a strip footing on clay under combined loading”. Proc. R. Soc. London Ser. A. 455, 893–916.

Houlsby, G. T. and Wroth, C. P. [1983]. "Calculation of stresses on shallow penetrometers and footings", Proc. IUTAM/IUGG Seabed Mechanics, Newcastle, pp. 107-112.

House, A. R. and Randolph, M. F. [2001]. "Installation and pull-out capacity of stiffened suction caissons in cohesive sediments", Proc. Eleventh (2001) Intl. Offshore and Polar Engng Conf., Vol. 2, ISBN 1-880653-2.

Kausel, E. and Ushijima, R. [1979]. "Vertical and torsional stiffness of cylindrical footings", Research Rep. R76-6, MIT.

Kelly, R. B., Houlsby, G. T. and Byrne, B. W. [2006]. "Transient vertical loading of model suction caissons in a pressure chamber", Geotechnique, 56 (10), 665-675.

Kim JB, Singh LP and Brungraber RJ. (1979). “Pile cap soil interaction from full scale lateral load tests”. ASCE Journal of Geotechnical Engineering. 105(5), 643-653.

Kourkoulis, R., Anastasopoulos, I., Gelagoti, F., Kokkali, P. [2012]. "Dimensional Analysis of SDOF Systems Rocking on Inelastic Soil", Journal of Earthquake Engineering (in press).

Kourkoulis, R., Gelagoti, F. and Kaynia, A. [2012]. "Seismic response of offshore wind turbine foundations", 15th WCEE, Lisbon, 2012.

Kühn, M., Bierbooms, W., van Bussel, G., Ferguson, M., Göransson, B., Cockerill, T., et al. (1998). *Opti-OWECS Final Report Vol. 0: Structural and Economic Optimisation of Bottom-Mounted Offshore Wind Energy Converters - Executive Summary.* Institute for Wind Energy. Delft: Delft University of Technology

Kutter, B. L., Martin, G., Hutchinson, T. C., Harden, C., Gajan, S., Phalen, J. D. [2003]. "Workshop on modeling of nonlinear cyclic load-deformation behavior of shallow foundations", Report of the PEER Workshop, University of California, Davis.

Lavassas, I., Nikolaidis, G., Zervas, P., Efthimiou, E., Doudoumis, I. N. and Baniotopoulos, C. C. [2003]. "Analysis and Design of the Prototype of a Steel 1-MW Wind Turbine Tower", Eng. Struct.; Vol. 25(8), 2003; 1097–1106.

Liingaard, M., Andersen, L. and Ibsen, L. B. [2007]. "Impedance of flexible suction caissons", Earthquake Engng Struct. Dyn. 2007; 36:2249-2271.

LeBlanc, C. (2009). *Design of Offshore Wind Turbine Support Structures.* Aalborg: Department of Civil Engineering, Faculty of Engineering, Aalborg University.

LeBlanc C., Houlsby G.T. & Byrne B.W. (2010). “Response of stiff piles in sand to long-term cyclic lateral loading”, Géotechnique, 60(2):79–90

Lombardi D., Bhattacharya S., Muir Wood D. (2013), “Dynamic soil–structure interaction of monopile supported wind turbines in cohesive soil”, Soil Dynamics and Earthquake Engineering, 49:165–180.

Luke, A. M., Rauch, A. F., Olson, R. E. and Mecham, E. C. [2005]. "Components of suction caisson capacity measured in axial pull-out tests", Ocean Engng, No. 32, 878-891.

Maharaj DK. (2003). “Load-deflection response of laterally loaded single pile by nonlinear finite element analysis”. EJEG.

Makris, N. and Roussos, Y. [2000]. “Rocking Response of rigid blocks under near source ground motions”, Geotechnique, 50 (3), 243-262.

Malhotra, S., [2011]. “Selection, design and construction of offshore wind turbine foundations”. Wind Turbines, Dr. Ibrahim Al-Bahadly (Ed.), ISBN: 978-953-307-221-0, InTech.

Martin, C. M. [1994]. "Physical and numerical modeling of offshore foundations under combined loads", D.Phil. thesis, Univ. of Oxford, UK.

Martin, C. M. & Houlsby, G. T. [2000]. "Combined loading of spudcan foundations on clay: laboratory tests", Geotechnique 50, No. 4, 325–338.

Martin, G. R. and Lam, I. P. [2000]. “Earthquake Resistant Design of Foundations: Retrofit of Existing Foundations”, Proc. GeoEng 2000 Conference, Melbourne.

Matlock H and Reese LC. [1960]. “Generalized solutions for laterally loaded piles”. ASCE Journal of Soil Mechanics and Foundations Division. 86(SM5), 63-91.

Meyerhof, G. G. [1951]. "The ultimate bearing capacity of foundations", Geotechnique, 2 (4), 301-332.

Meyerhof, G. G. [1953]. "The bearing capacity of foundations under eccentric and inclined loads" Proc. 3rd Int. Conf. Soil Mech. Fndn Engng, Vol.1, Zurich, 440-445.

Mokwa RL. [1999]. “Investigation of the Resistance of Pile Caps to Lateral Loading”. Ph.D Thesis. Virginia Polytechnic Institute, Blacksburg, Virginia.

Mokwa RL and Duncan JM. [2001]. “Experimental evaluation of lateralload resistance of pile caps”. ASCE Journal of Geotechnical and Geoenvironmental Engineering. 127(2), 185 - 192.

Mokwa RL and Duncan JM. [2003]. Rotational restraint of pile caps during lateral loading. ASCE Journal of Geotechnical and Geoenvironmental Engineering. 129(9), 829 - 837.

Morison, J.R., O'Brien, M. P., Johnson, J. W., Schaaf, S. A. (1950), "The force exerted by surface waves on piles", Petroleum Transactions (American Institute of Mining Engineers) 189: 149–154

Murff, J. D. [1994]. "Limit analysis of multi-footing foundation systems", Proc. 8th Int. Conf. Comput. Methods, Adv. Geomech., Morgantown 1, 440-445.

Nova, R., Montrasio, L. [1991]. “Settlement of shallow foundations on sand”, Geotechnique, 41 (2), 243-256.

Ntritsos, N. [2011]. "Inelastic response of embedded foundations", Diploma thesis, NTUA.

Paolucci, R., Shirato, M. and Yilmaz, M.T. [2008]. “Seismic behaviour of shallow foundations: Shaking table experiments vs numerical modelling”, Earthq Eng Struct Dyn, 37(4), 577–595.

Pecker, A. [1998]. “Capacity Design Principles For Shallow Foundations in Seismic Areas”, Proc. 11th European Conference on Earthquake Engineering, A.A. Balkema Publishing.

Pecker, A. [2003]. “A seismic foundation design process, lessons learned from two major projects: the Vasco de Gama and the Rion Antirion bridges”, ACI International Conference on Seismic Bridge Design and Retrofit, La Jolla.

Pierson, W. J., Moskowitz, L. A. [1964]. "A proposed spectral form of fully developed wind seas based on the similarity theory of S.A. Kitaigorodshii", J. Geopys. Res., Vol. 69.

Poulos, HG. [1971]. “Behavior of laterally loaded piles: Part I-single piles”. ASCE Journal of Soil Mechanics and Foundations Division. 97(SM5), 711-731.

Poulos, H. G. and Davis, E. H. [1974]. "Elastic solutions for soil and rock mechanics", published by John Wiley & Sons, Inc., New York, London, Sydney, Toronto.

Poulos, HG and Randolph, MF. [1983]. “Pile group analysis: a study of two methods”. ASCE Journal of Geotechnical Engineering. 109(3), 355-372.

Prandtl, L. [1921]. “Uber die Eindringungsfestigkeit (Harte) plastischer Baustoffe und die Festigkeit von Schneiden”, Zeitschrift fur angewandte Mathematik und Mechanik, 1 (1), 15–20.

Randolph MF. (1981). “The response of flexible piles to lateral loading”. Géotechnique. 31(2), 247-259.

Randolph, M. F. and Gourvenec, S. [2011]. "Offshore geotechnical engineering", published by Spon Press.

Randolph, M. F. and Puzrin, A. M. [2003]. "Upper bound limit analysis of circular foundations on clay under general loading", Geotechnique, 53 (9), 785-796.

Randolph, M. F. and House, A. R. [2002]. "Analysis of suction caisson capacity on clay", Proc. Annual Offshore Tech. Conf., Houston, Paper OTC 14236.

Randolph, M. F. and Puzrin, A. M. [2003]. "Upper bound limit analysis of circular foundations on clay under general loading", Geotechnique, 53 (9), 785-796.

Reese LC, Cox WR and Koop FD. (1974). “Analysis of laterally loaded piles in sand”. Offshore Technology Conference. Vol. II (Paper No. 2080), 473-484.

Reese, L. C., and Matlock, H. [1956]. "Non-dimensional solutions for laterally loaded piles with soil modulus assumed proportional to depth." *8th Texas Conf. on Soil Mech. And Foundation Engrg.*, Sep. 14.

Reese L. & Van Impe W.F., [2001]. “Single Piles and Pile Group Under Lateral Loading”

Ritschel, U., Warnke, I., Kirchner, J. and Meussen, B. [2003]. “Wind Turbines and Earthquakes”,Second World Wind Energy Conference, World Wind Energy Association, Cape Town, South Africa, 2003.

Ritschel, U., Warnke, I., Kirchner, J. and Meussen, B. [2003]. “Wind Turbines and Earthquakes”, Second World Wind Energy Conference, World Wind Energy Association, Cape Town, South Africa, 2003.

Roesset, J. M. [1980]. "Stiffness and damping coefficients of foundations", Dynamic Response of Foundations: Analytical Aspects, M.W. O' Neil and R. Dobry (eds), ASCE, 1-30.

Roesset J. M. [1980]. "The use of simple models in soil-structure interaction", Civil Engineering and Nuclear Power, ASCE, Vol. 1, 1-25.

Salgado, R., Lyamin, A. V., Sloan, S. W. and Yu, H. S. [2004]. “Two and three-dimensional bearing capacity of foundations in clay”, Geotechnique, 54 (5), 297–306.

Skempton, A. W. [1951]. "The bearing capacity of clays." Building Research Congress, London, Vol. 1, 180-189.

Stone KJL, Newson TA and Sandon J. (2007). An investigation of the performance of a ‘hybrid’ monopole-footing foundation for offshore structures. Proceedings of 6th International on Offshore Site Investigation and Geotechnics. London: SUT, 391-396.

Stone KJL, Newson T and El Marassi, M. (2010). An investigation of a monopiled-footing foundation. International Conference on Physical Modelling in Geotechnics, ICPMG2010. Rotterdam: Balkema, 829-833.

Taiebat, H. A. and Carter, J. P. [2000]. “Numerical studies of the bearing capacity of shallow foundations on cohesive soil subjected to combined loading”, Geotechnique, 50 (4), 409–418.

Taiebat, H. A. and Carter, J. P. [2002]. "Bearing Capacity of Strip and Circular Foundations on Undrained Clay Subjected to Eccentric Loads", Geotechnique, 52 (1), 61-64.

Tempel, J. van der, Zaaijer, M.B. and Subroto, H.[2004]. “The effects of scour on the design of offshore wind turbines”, Proceedings of the 3rd International Conference on Marine Renewable Energy Marec, 27-35. London, IMarest.

Taylor, P.W., Bartlett, P.E. and Wiessing, P.R. [1981]. “Foundation rocking under earthquake loading”, Proceedings of 10th International Conference on Soil Mechanics and Foundation Engineering, AA Balkema, Stockholm, Sweden, Rotterdam, Netherlands, 3, 313–322.

Terzaghi, K. [1943]. “Theoretical soil mechanics”, John Willey, London and New York.

Ukritchon, B., Whittle, A. J. and Sloan, S. W. [1998]. "Undrained limit analyses for combined loading of strip footings on clay", J. Geotech. Geoenviron. Eng., 124 (3), 265-276.

Van der Tempel, J. [2005]. "Design of support structures for offshore wind turbines", PhD thesis.

Vesic, A.S. [1975]. “Bearing capacity of shallow foundations”, Foundation Engineering Handbook, Eds Winterkorn & Fang, Van Nostrand Reinhold, New York, 121-147.

Watson, P. G. and Randolph, M. F. [1997a]. "Vertical capacity of suction caisson foundations in calcareous sediments", Proc. 7th Int. Offshore Polar Engng Conf. Honolulu 1, 784-790.

Watson, P. G., Randolph, M. F. and Bransby, M. F. [2000]. "Combined lateral and vertical loading of caisson foundations", Proc. Annual Offshore Tech. Conf., Houston, Paper OTC 12195.

Witcher, D. [2005]. “Seismic Analysis of Wind Turbines in the Time Domain”, Wind Energy; Vol. 8; p. 81.

Yun, G. and Bransby, M. F. [2007]. "The horizontal-moment capacity of embedded foundations in undrained soil" Can. Geotech. J., 44 (4), 409-424.

Zhang L, Silva F and Grismala R. (2005) “Ultimate lateral resistance of piles in cohesionless soils”. Journal of Geotechnical and Geoenvironmental Engineering. Vol. 131(1), 78–83.

Zhao, X. and Maisser, P. [2006]. "Seismic Response Analysis of Wind Turbine Towers Including Soil-Structure Interaction", Proceedings of the Institution of Mechanical Engineers, Part K: J. Multi-Body Dynamics; Vol. 220, 2006; p. 53.

Zohaib, S. [2011]. “Alternatives and modifications of Monopile foundation or its installation technique for noise mitigation”. Report commissioned by the North Sea Foundation, M.Sc. Thesis, TU Delft.

http://www.energy.eu/publications/a07.pdf - European Wind Energy Association – EWEA
www.bwea.com - British Wind Energy Association
http://ec.europa.eu/dgs/jrc - The European Commission – Joint Research Centre (Renewable
Energy Snapshots 2010)
http://ocsenergy.anl.gov/index.cfm - OCS Alternative Energy and Alternate Use Programmatic EIS
Information Center
http://offshorewind.net
www.inhabitat.com
http://en.wikipedia.org
http://www.4coffshore.com/offshorewind